AD-A044 203 AVCO LYCOMING DIV STRATFORD CONN F/G 21/5
IMPROVED RESISTANCE TO ENGINE BIRD INGESTION.(U)
MAR 77 H B KAEHLER
UNCLASSIFIED DOT-FA76WA-3806
FAA/RD-77-55
NL

1 OF 3
AD
A044203

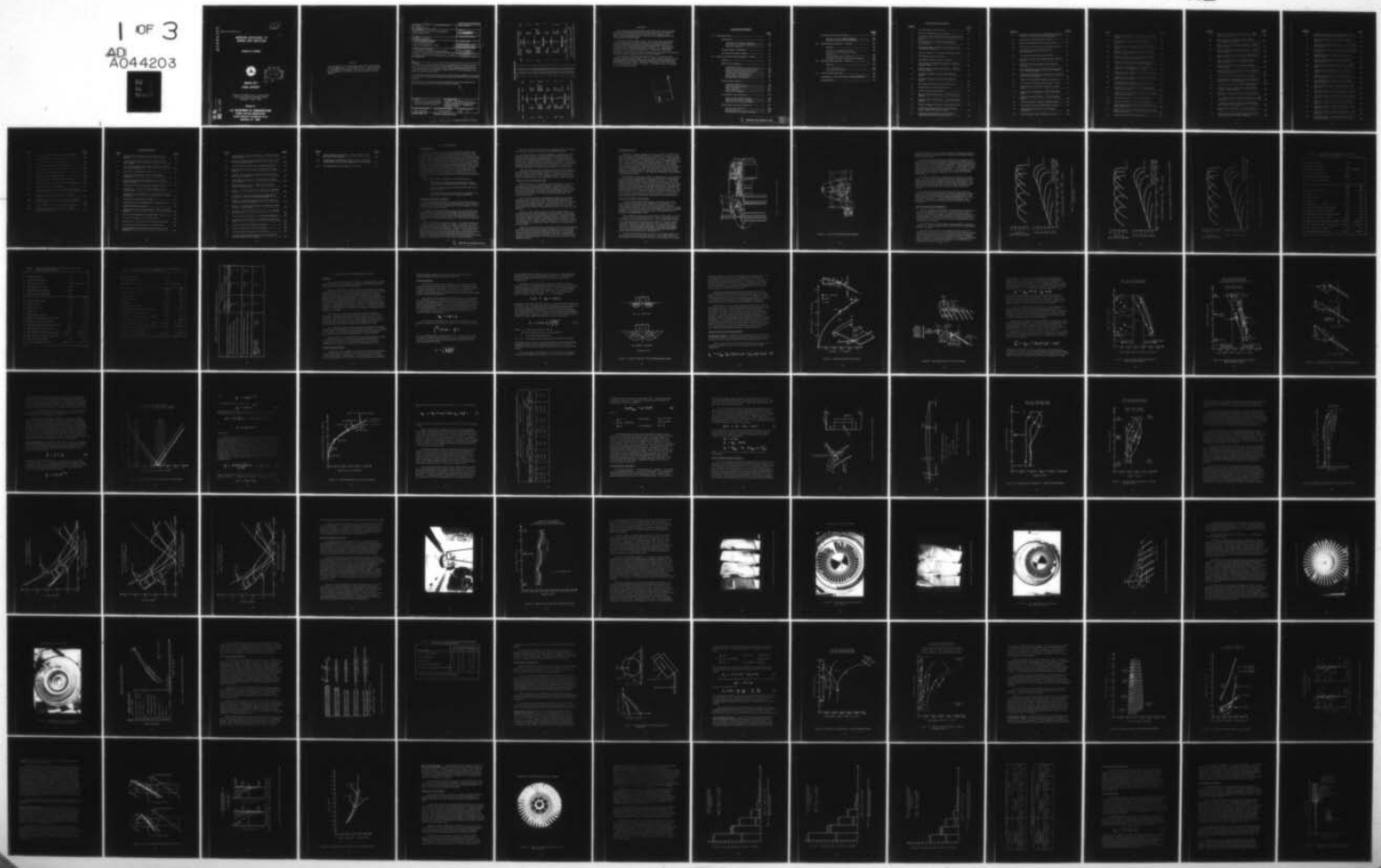

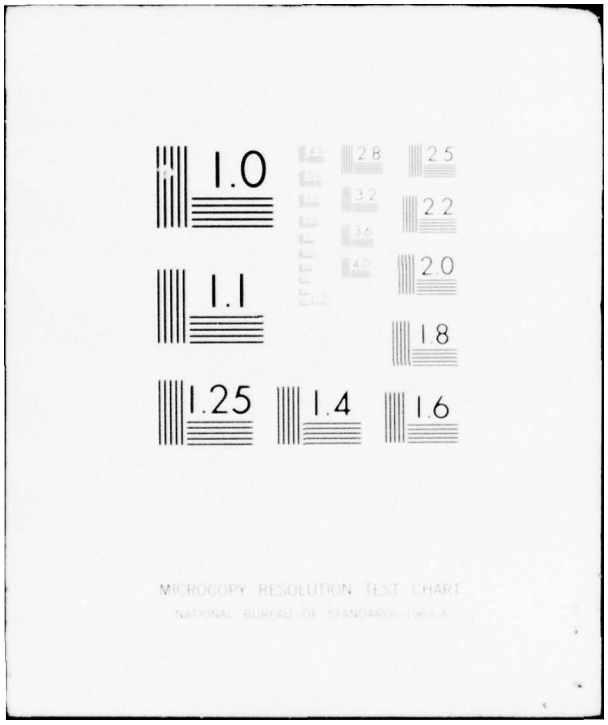
1.0
1.1
1.25
1.4
1.6
2.8
2.5
3.2
2.2
3.6
2.0
4.0
1.8
MICROCOPY RESOLUTION TEST CHART
NATIONAL BUREAU OF STANDARDS-1963-A

Report No. FAA-RD-77-55

IMPROVED RESISTANCE TO ENGINE BIRD INGESTION

Herbert B. Kaehler

MARCH 1977

FINAL REPORT

Prepared for

U.S. DEPARTMENT OF TRANSPORTATION
FEDERAL AVIATION ADMINISTRATION
Systems Research & Development Service
Washington, D.C. 20590

NOTICE

Technical Report Documentation Page

1. Report No.	2. Government Accession No.	3. Recipient's Catalog No.
FAA-RD-77-55		
4. Title and Subtitle		**5. Report Date**
IMPROVED RESISTANCE TO ENGINE BIRD INGESTION.		March 1977
		6. Performing Organization Code
		8. Performing Organization Report No.
7. Author(s)		
Herbert B. Kaehler		
9. Performing Organization Name and Address		**10. Work Unit No. (TRAIS)**
Avco Lycoming Division 550 South Main Street Stratford, Connecticut 06497		**11. Contract or Grant No.** DOT-FA76WA-3806
		13. Type of Report and Period Covered
12. Sponsoring Agency Name and Address		Final Report.
Department of Transportation, Federal Aviation Administration, Systems Research and Development Service, Washington, D. C. 20590		**14. Sponsoring Agency Code** 2330.

15. Supplementary Notes

16. Abstract

An analytical design method capable of quantitatively evaluating and ranking rotor blades for resistance to bird impact damage was investigated. This method was used to design blades having sufficient tolerance to meet the bird-ingestion requirements of FAR 33.77 for turbofan engines in the 6800 to 1600 lbf thrust class.

The design procedure was also used for the preliminary design of a damage-resistant boron/aluminum composite fan blade for the 6800 lbf thrust class engine.

In addition, two protective devices designed to prevent an ingested bird from striking sensitive engine parts were presented.

17. Key Words	18. Distribution Statement
Bird Ingestion, Foreign Object Damage, Composite Fan Blade, Turbofan Protective Devices	Document is available to the U.S. public through the National Technical Information Service, Springfield, Virginia 22161.

19. Security Classif. (of this report)	20. Security Classif. (of this page)	21. No. of Pages	22. Price
UNCLASSIFIED	UNCLASSIFIED	232	

Form DOT F 1700.7 (8-72) Reproduction of completed page authorized

213150

METRIC CONVERSION FACTORS

Approximate Conversions to Metric Measures

Symbol	When You Know	Multiply by	To Find	Symbol
		LENGTH		
in	inches	*2.5	centimeters	cm
ft	feet	30	centimeters	cm
yd	yards	0.9	meters	m
mi	miles	1.6	kilometers	km
		AREA		
in^2	square inches	6.5	square centimeters	cm^2
ft^2	square feet	0.09	square meters	m^2
yd^2	square yards	0.8	square meters	m^2
mi^2	square miles	2.6	square kilometers	km^2
	acres	0.4	hectares	ha
		MASS (weight)		
oz	ounces	28	grams	g
lb	pounds	0.45	kilograms	kg
	short tons (2000 lb)	0.9	tonnes	t
		VOLUME		
tsp	teaspoons	5	milliliters	ml
Tbsp	tablespoons	15	milliliters	ml
fl oz	fluid ounces	30	milliliters	ml
c	cups	0.24	liters	l
pt	pints	0.47	liters	l
qt	quarts	0.95	liters	l
gal	gallons	3.8	liters	l
ft^3	cubic feet	0.03	cubic meters	m^3
yd^3	cubic yards	0.76	cubic meters	m^3
		TEMPERATURE (exact)		
°F	Fahrenheit temperature	5/9 (after subtracting 32)	Celsius temperature	°C

*1 in = 2.54 (exactly). For other exact conversions and more detailed tables, see NBS Misc. Publ. 286, Units of Weights and Measures, Price $2.25, SD Catalog No. C13.10:286.

Approximate Conversions from Metric Measures

Symbol	When You Know	Multiply by	To Find	Symbol
		LENGTH		
mm	millimeters	0.04	inches	in
cm	centimeters	0.4	inches	in
m	meters	3.3	feet	ft
m	meters	1.1	yards	yd
km	kilometers	0.6	miles	mi
		AREA		
cm^2	square centimeters	0.16	square inches	in^2
m^2	square meters	1.2	square yards	yd^2
km^2	square kilometers	0.4	square miles	mi^2
ha	hectares (10,000 m^2)	2.5	acres	
		MASS (weight)		
g	grams	0.035	ounces	oz
kg	kilograms	2.2	pounds	lb
t	tonnes (1000 kg)	1.1	short tons	
		VOLUME		
ml	milliliters	0.03	fluid ounces	fl oz
l	liters	2.1	pints	pt
l	liters	1.06	quarts	qt
l	liters	0.26	gallons	gal
m^3	cubic meters	35	cubic feet	ft^3
m^3	cubic meters	1.3	cubic yards	yd^3
		TEMPERATURE (exact)		
°C	Celsius temperature	9/5 (then add 32)	Fahrenheit temperature	°F

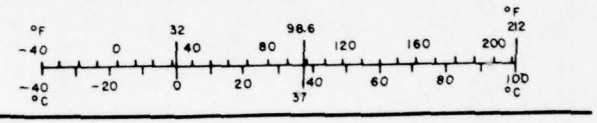

PREFACE

The study described herein was performed by the Avco Lycoming Division to develop practicable design techniques that would prevent or minimize bird-ingestion damage to gas turbine engines in the 6800 to 1600-pound thrust class. The work was conducted under FAA Contract DOT-FA76WA-3806.

The study comprises three tasks. Task I deals with the development and application of analytic procedures for designing and evaluating fan/compressor blading with sufficient damage resistance to satisfy the bird ingestion requirements of FAR 33.77. The objective of Task II was to extend the design methodology to evaluate damage-resistant blading of advanced materials - particularly composites. The intent of Task III was to derive a practicable bird-ingestion protection device suitable for engines in the lower thrust ranges.

This contract was technically supervised by T. G. Horeff of the Federal Aviation Administration. Mr. T. Dickey and H. Kaehler of Avco Lycoming Division were the Program Manager and Technical Director, respectively, for this study. Principal contributors to this effort were R. A. Ainsworth, D. Auth, L. Cernoch, J. O'Connor, and W. Schneider of Avco Lycoming Division.

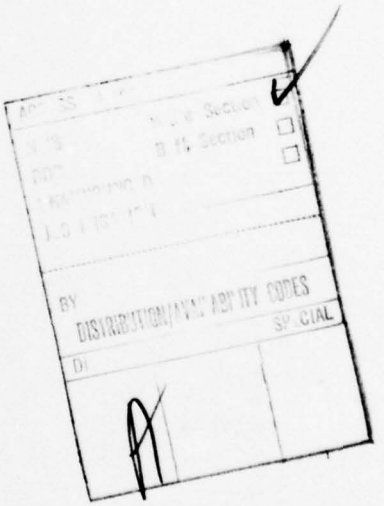

TABLE OF CONTENTS

LIST OF ILLUSTRATIONS

LIST OF TABLES

1.0 INTRODUCTION

BACKGROUND

Ingestion of birds is a major and well documented operating hazard affecting the structural integrity and survivability of gas turbine engines. (References 1 - 4). The U. S. Air Force, for example, reports approximately 1000 bird strikes per year, occurring mostly at low altitudes and in the immediate vicinity of an airfield. Bird-aircraft collisions cost the Air Force some 10 million dollars per year, with engine damage representing the largest dollar value. A typical large commercial operator will experience an average of one bird strike per day, with the cost of repairs alone reaching 3 million dollars per year. And, of course, the possibility of a catastrophic strike is always present, as evidenced by the recent loss of a jumbojet aircraft during takeoff from Kennedy International Airport.

The engine designer attempts to solve this problem by:

1. Strengthening existing engine components to absorb ingested material with acceptable tolerance to damage

2. Applying advanced material with improved impact properties, and/or

3. Installing protective devices to prevent or deflect bird debris from striking critical engine components.

Designing for Damage Tolerance

It is good design practice to use primary structures whenever possible to fulfill damage resistance requirements, since the use of any auxiliary device tends to add weight, cost, complexity, and reduces overall system reliability

Thickening of the low-pressure stage is the most simple and straight-forward approach. Local leading edge thickening is particularly effective in providing rugged, damage-tolerant blades to safely absorb impact shocks over the entire span and break-up the carcasses for subsequent safe ingestion by the following compressor stages.

Other modifications are also possible. Part-span shrouds, for example, have a major influence on impact resistance, since they provide added mass and stiffness to absorb and transmit direct impact shocks. On the other hand the shrouds act as stress risers, tending to promote local brittle-type fracture. The number and span-wise locations of the shrouds affect the bending response of the blade, while their chordwise placement affects its torsional response. The shroud's contact angle affects both bending and torsional reactions and the degree of load transfer to adjacent blades.

The root configuration may also be modified to alter the bending and torsional reactions of the blades and disk attachments.

An analytical damage criterion technique showing promise for determining the degree of damage resistance needed to meet safe ingestion requirements was studied here. The damage criterion relation was developed based on limit theory of structural analysis. Only the local contact region of the blade is considered. According to the model, damage increases with increasing values of the damage function, reaching a maximum at 1.0. In practice, a maximum allowable damage level is determined by tests in a running engine.

A second method, based on a transient finite-element analysis, was also used to study bending failure of a blade away from the impact site during, and just after, impact. This latter method also provides insight into the bird/blade impact process and assists the analyst in extending the criteria approach to new, untested designs.

Application of Advanced Materials

The fan section of a high-bypass ratio fan engine accounts for a large portion of the weight of the engine; consequently, engine manufacturers have made major efforts to reduce the weight of the fan. The total weight of the fan section is strongly influenced by the weight of the fan blades since their centrifugal loading defines the size of the disk which carries them and the attendant static and rotating structures.

As a result of the basic requirement of light weight and high-strength, production engines have generally employed fan blades fabricated from titanium forgings. Ti6Al-4V has been used in most cases, but some applications have involved Ti8AL-1Mo-1V, which has a somewhat higher modulus. These materials are relatively well understood, and their mechanical properties are available to the designer.

Because of the continuous drive to reduce engine weight, considerable effort has been expended in the development of composite fan blades using fiber reinforcement techniques. Composite blading offers the designer substantial savings in weight through the use of low-density, high-modulus, high-strength fibers to reinforce a soft, lightweight matrix. Industry-wide evaluation of such blades, however, has found them to be deficient in their resistance to foreign object damage (FOD).

Both of the analytical design procedures noted above were applied to the design and evaluation of damage-tolerant composite blading. For composite-damage evaluation, a modified form of the damage criterion relation was used to acoount for the fiber reinforcement. Equivalent isotropic material properties were used to illustrate the design of a boron/aluminum blade with improved resistance to bird-ingestion damage.

Protective Devices

In the past, engine manufacturers have provided a variety of devices to protect their engines from bird ingestion - typically by the use of permanent or retractable inlet grills or vanes. Over the years, these protective devices have generally proven to be impractical because of the complexities or performance penalties introduced by their use - often without providing the desired protection. The problem arises basically from the requirement that such protective devices must be strong enough to withstand very severe impact shocks without contributing fragments of their own, while at the same time eliminating any air blockage that may result from impact damage or from retention of bird carcasses. Anti-icing and maintenance requirements compound the problem.

Nevertheless, alternate concepts are continuously being reviewed since protective devices offer the only positive means of eliminating ingestion damage to the engines. (References 5 and 6.) Two inlet designs showing promise, particularly for small turbines, were considered during this study. The first protects only the thin, high-speed blade tips from direct impact by an unfragmented bird, relying on the greater damage tolerance of the thicker, lower-speed regions of the blades near the hub to safely absorb the remaining impact shock. The second approach is to prevent or minimize ingestion of birds into the core engine by positioning the fan stage sufficiently far upstream to permit centrifuging of bird debris away from the compressor inlet.

BASELINE ENGINE DEFINITIONS

Two basic fan engine configurations encompassing the 6800 lbf to 1600 lbf thrust range were considered for this study. The larger engine considered in this study is based on the ALF502 medium-thrust turbofan (6800 lbf), while the smaller engine is based on the ALF101 turbofan (1600 lbf class) (Figures 1 and 2). Throughout the study, the engine cycle was not varied, although the effect of scaling was independently studied.

The ALF502 turbofan engine is based on the T55 engine core and is rated at 6770 lbf SLS take-off thrust. The fan assembly consists of a single part-span shrouded fan stage, with a single supercharger stage located aft of the fan wheel and mounted on a conical support by means of thrust and roller bearings. The core engine is composed of a seven-stage axial/single-stage centrifugal compressor driven by a directly-coupled, two-stage, air-cooled axial turbine. A two-stage axial turbine drives the fan through the compressor shaft to the fan reduction gear. (Reference 7).

The ALF101 turbofan engine is based on the LTS101 engine core and is rated at 1575 lbf SLS take-off thrust. The single-stage unshrouded fan is driven through a planetary reduction gear by a single-

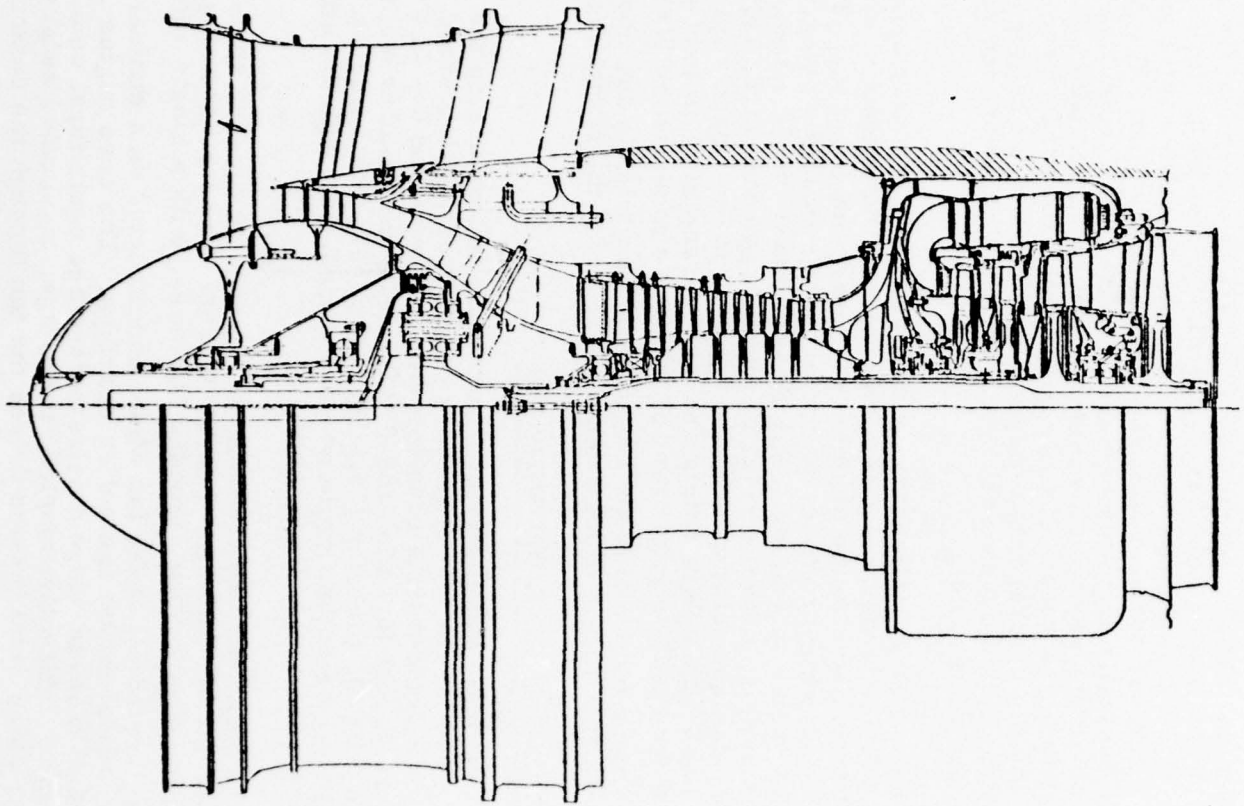

Figure 1. ALF 502 Engine Cross Section.

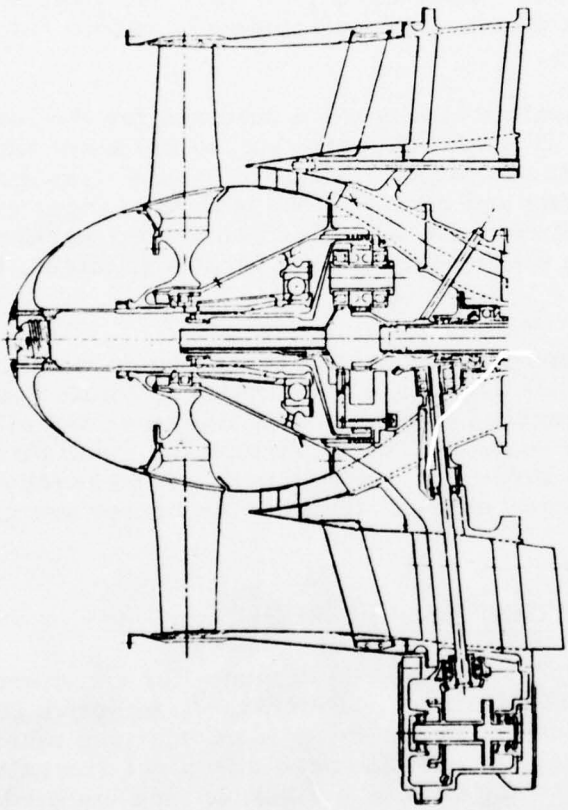

Figure 2. ALF 101 Fan Module Cross Section.

stage axial turbine. The core engine uses two axial and one centrifugal compressor stages driven by a single air-cooled axial turbine stage. (Reference 8).

The baseline blade configuration selected for the higher thrust range study was specially designed for the larger machine purely on the basis of weight and aerodynamic and performance considerations, without regard for bird-ingestion capabilities. This approach was taken to ensure a valid comparative base for evaluating the effects of "bird-proofing" on the final engine design. Accordingly, a mid-span shrouded, relatively high aspect ratio blade was specified, employing a thin multiple circular arc airfoil for good transonic performance.

Two baseline blades were selected for the lower thrust range study. The first was directly scaled in linear dimensions from the higher thrust machine. Midspan shrouds were specified for consistent scaling and comparisons with the larger size blading. The second baseline blade was based on a thin, unshrouded low aspect ratio design that would provide a more efficient, but heavier, machine.

Throughout the study, the engine cycle was not varied, but matching of all three baseline fans at optimum speeds and pressure ratios was carried out to provide maximum fan efficiencies. Fan performance maps for the three baseline configurations are shown in Figures 3 through 5. A summary of the aerodynamic and structural parameters describing the blades are given in Tables 1 through 3.

BIRD INGESTION REQUIREMENTS

The bird ingestion requiements for commercial certification by the FAA are specified in FAR 33.77, effective October 1974. Briefly, three different ingestion conditions must be considered: 1) small birds at lift-off speed of typical aircraft (up to sixteen 3 oz. birds, depending on intake size); 2) medium birds at initial climb speed (up to eight at 1-1/2 lb); and 3) up to one large bird (4.0 lb) at maximum climb speed.

For convenience, the pertinent FAR paragraphs are given in Appendix A. Corresponding military and CAA (U. K.) requirements are also provided.

Fan and aircraft speeds corresponding to FAR 33.77 bird-ingestion requirements are given in Table 4 for the baseline engines of this study. In this table, aircraft performance values appropiate to the 6800 lbf thrust class machine were taken as typical of a medium (24,000 lb) twin-turbofan transport. For the 1600 lbf thrust class application, performance values for a light (7800 lb) twin-turbofan executive aircraft were used.

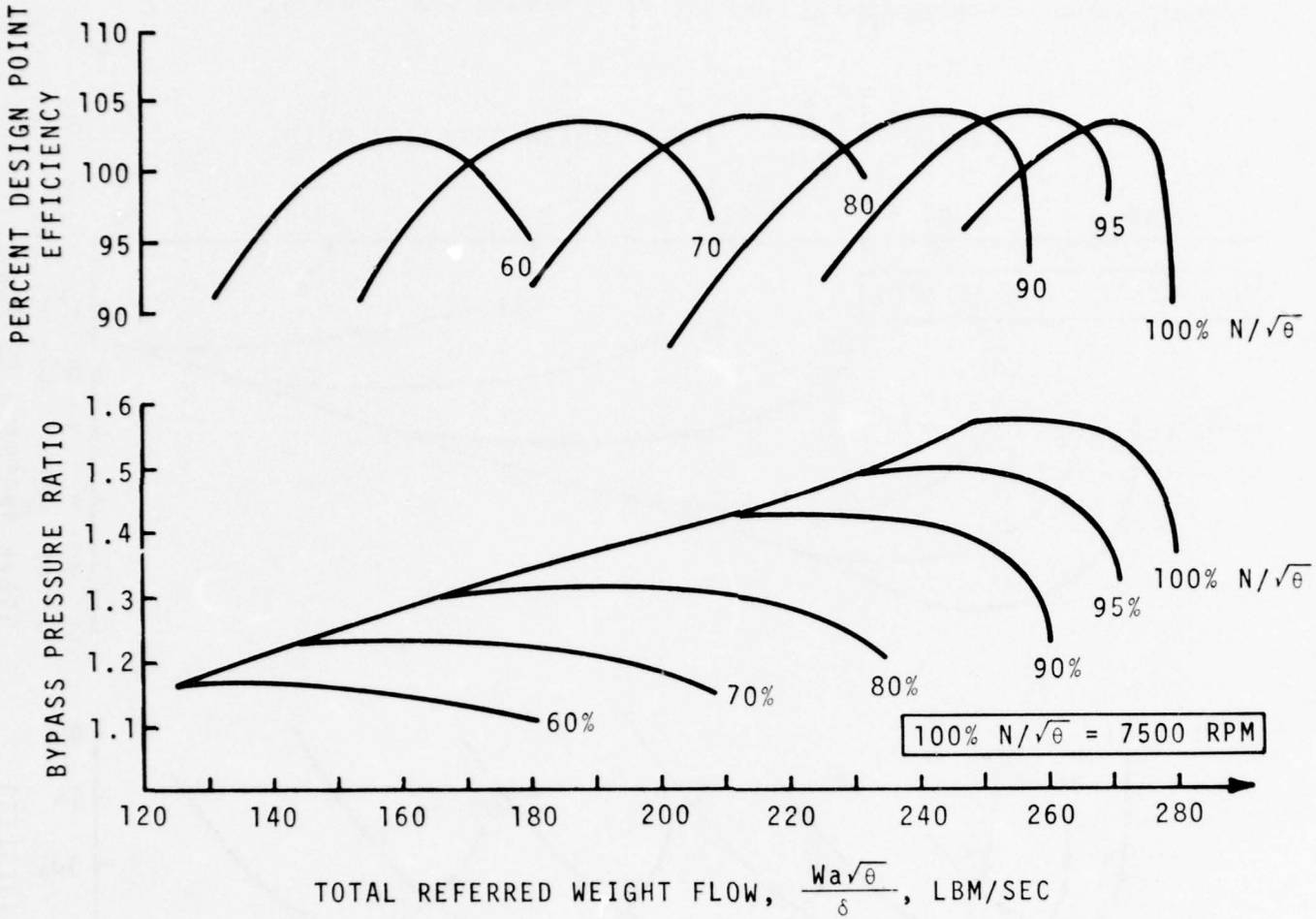

Figure 3. Fan Bypass Map, 6800 lbf Thrust Engine - Baseline Blades

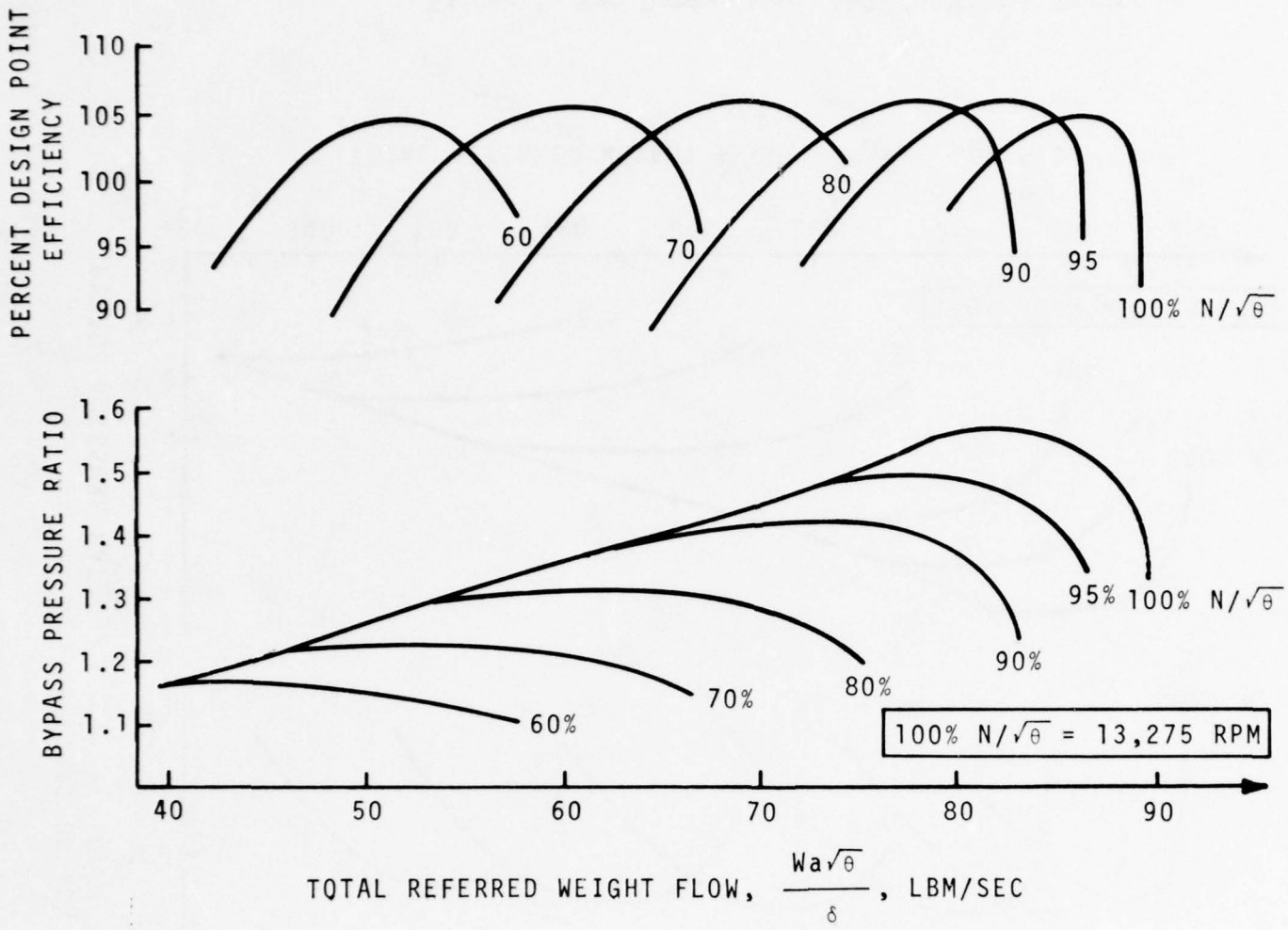

Figure 4. Fan Bypass Map, 1600 lbf Thrust Engine - Scaled Blades.

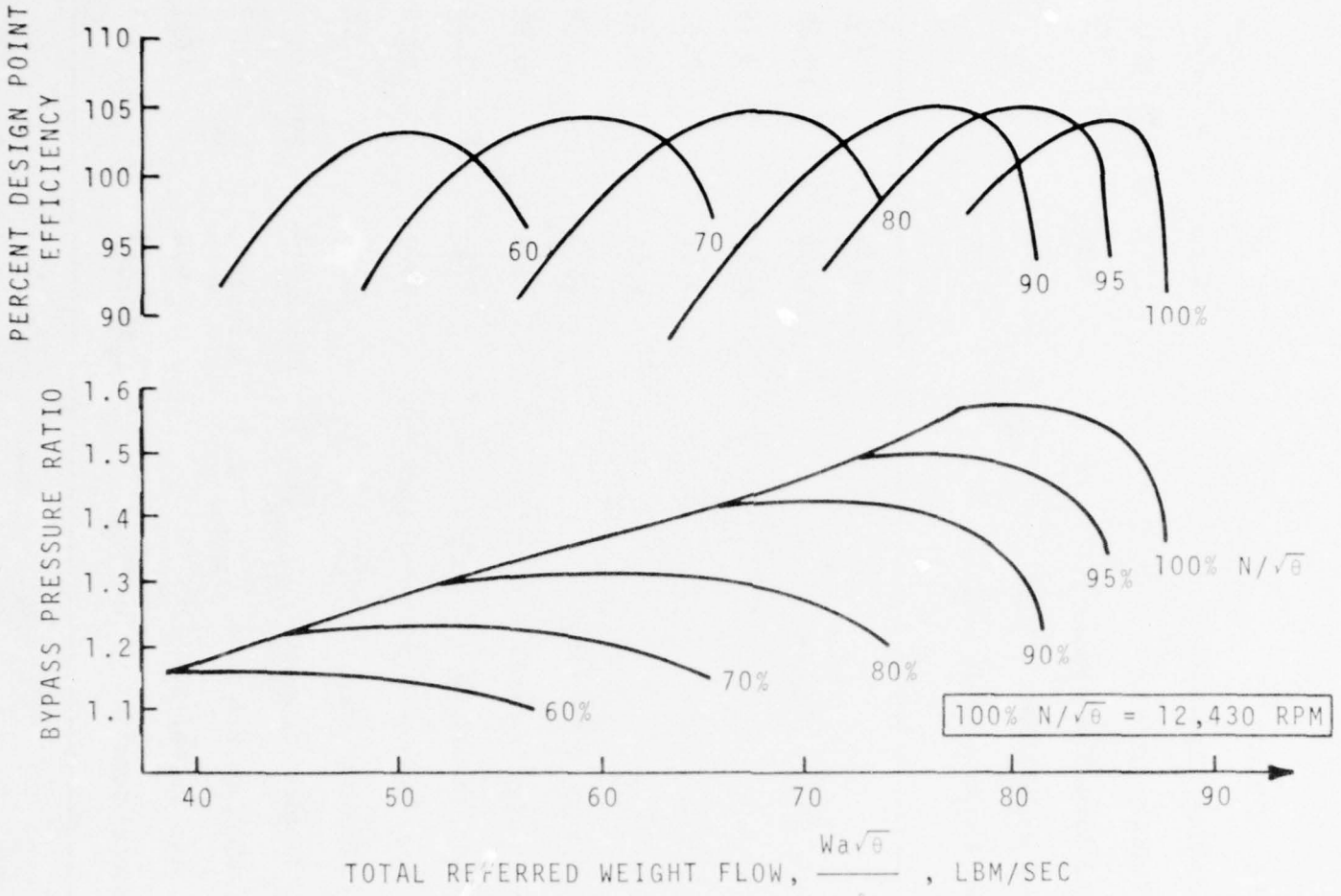

Figure 5. Fan Bypass Map, 1600 lbf Thrust Engine - Low Aspect Ratio Blades.

TABLE 1 - BASELINE BLADE DEFINITION, 6800 LBF THRUST CLASS ENGINE

Number of Blades	40	
Hub Radius/Tip Radius	0.46	
Tip Velocity (ft/sec)	1293.	@ 7500 rpm
Shroud Span/Blade Span	0.58	
Shroud Weight/Span Weight	0.0807	
Shroud Contact Angle (deg)	15.	

	Hub	Tip
Radius, @ CG. R (in.)	9.08	19.80
Chord, c (in.)	2.80	4.19
Aspect ratio, AR	3.81	2.55
Solidity, S	1.96	1.35
Wedge angle, θ_{LE} (deg)	11.3	3.0
Leading edge thickness/chord (%)	1.34	0.55
Maximum thickness/chord (%)	7.53	3.39
Maximum thickness position/chord (%)	48.0	72.0
Airfoil section area, A ($in.^2$)	0.439	0.386
Max. Moment of Inertia, $I_{max.}$ ($in.^4$)	$206.x10^{-3}$	$393.x10^{-3}$
Min. Moment of Inertia, $I_{min.}$ ($in.^4$)	$5.39x10^{-3}$	$0.49x10^{-3}$
Min. axis angle. ϕ (deg)	9.4	66.1
Torsional constant, K ($in.^4$)	$4.39x10^{-3}$	$1.60x10^{-3}$

TABLE 2 - SCALED BASELINE BLADE DEFINITION, 1600 LBF THRUST CLASS ENGINE

Number of blades	40	
Hub Radius/Tip Radius	0.46	
Tip Velocity (ft/sec)	1293. @ 13275 rpm	
Shroud Span/Blade Span	0.58	
Shroud Weight/Span Weight	0.0807	
Shroud Contact Angle (deg)	15.	
	Hub	Tip
Radius @ CG. R (in.)	5.13	11.2
Chord, c (in.)	1.58	2.37
Aspect ratio, AR	3.81	2.55
Solidity, S	1.96	1.35
Wedge angle, θ_{LE} (deg)	11.3	3.0
Thickness at leading edge/chord (%)	1.34	0.55
Maximum thickness/chord (%)	7.53	3.39
Maximum thickness position/chord (%)	48.0	72.0
Airfoil section area, A ($in.^2$)	0.140	0.123
Max. Moment of Inertia, $I_{max.}$ ($in.^4$)	21.0×10^{-3}	40.0×10^{-3}
Min. Moment of Inertia, $I_{min.}$ ($in.^4$)	0.547×10^{-3}	0.045×10^{-3}
Min. axis angle, ϕ (deg)	9.4	66.1
Torsional constant, K ($in.^4$)	0.447×10^{-3}	0.163×10^{-3}

TABLE 3 - LOW ASPECT RATIO BASELINE BLADE DEFINITION, 1600 LBF THRUST CLASS ENGINE

Number of Blades	24	
Hub Radius/Tip Radius	0.48	
Tip Velocity (ft/sec)	1233 @ 12430 rpm	
	Hub	Tip
Radius @ CG , R (in.)	5.48	11.40
Chord, c (in.)	2.80	4.10
Aspect ratio, AR	2.10	1.44
Solidity, S	1.95	1.37
Wedge angle, θ_{LE} (deg)	11.5	3.44
Thickness of leading edge/chord (%)	0.713	0.239
Maximum thickness/chord (%)	7.09	3.17
Maximum thickness position/chord (%)	47.5	56.0
Airfoil section area, A (in.^{2})	0.432	0.370
Max. Moment of Inertia, $I_{max.}$ (in.^{4})	$198.\times10^{-3}$	$382.\times10^{-3}$
Min. Moment of Inertia, $I_{min.}$ (in.^{4})	3.39×10^{-3}	0.392×10^{-3}
Min. axis angle, ϕ (deg)	9.4	63.1
Torsional constant, K (in.^{4})	3.90×10^{-3}	1.32×10^{-3}

TABLE 4 - FAN AND AIRCRAFT SPEEDS PER FAR 33.77

	Engine Thrust Class		
	6800 lbf	1600 lbf	
	Baseline Blade	Scaled Blade	Low AR Blade
Engine Take-Off Fan Speed (rpm)	6,880	10,940	10,290
Lift-Off Speed of Typical Aircraft (kt)	100	90	90
Initial Climb Speed of Typical Aircraft (kt)	120	115	115
Engine Maximum Cruise Fan Speed (rpm)	6,760	10,440	9,840
Maximum Climb Speed of Typical Aircraft (kt)	160	150	150
Number of Birds: 3 oz	16	8	9
Inlet area based 1.5 lb	3	2	2
on blade inlet tip 4.1b	1	1	1
radius			

2.0 BIRD-TOLERANT BLADE DESIGN - TASK I

GENERAL

The objective of this task was to develop analytical design methods capable of quantitatively evaluating, ranking, and modifying standard airfoil designs for resistance to bird impact.

Damage analyses were performed using a local damage criterion method that was used at Lycoming during the development of the ALF 502 turbofan engine. The intent of this criterion approach is to relate significant projectile and target parameters to the impact conditions producing critical damage in the blades. To ensure survivability in the damaged state, an acceptable damage level is determined by analysis of full-scale engine ingestion tests. Engine survivability with other blades or at other ingestion conditions may then be predicted with some confidence by application of the damage criterion. A description of the damage criterion approach and application to design of damage-tolerant blading are discussed.

The results of a follow-up analysis dealing with the dynamic behavior of the blades during and just after impact by a bird are also discussed. The intent of this work is to gain further insight into the bird/blade impact process with particular emphasis on gross failure of blades away from the impact region caused by excessive motion. A transient finite-element beam analysis was used for this work.

The aerodynamic/performance benefits and penalties of alternate fan configurations designed for improved damage resistance are evaluated in this section. An aerodynamic/performance analysis dealing with post-ingestion operation with damaged blades is also described.

The final effort in Task I was devoted to incorporating the results of the above work into developing blades capable of satisfying the requirements of FAR 33.77. Effects on engine size and weight, aerodynamic efficiencies, and performance and costs are shown.

BLADE LOCAL DAMAGE

At this time the complexity of the bird/blade collision phenomena has precluded rigorous analytical investigations of damage-tolerant design requirements. Accordingly, a criterion approach was sought to provide a simple, reliable method of assessing design requirements

and to provide a yardstick for comparing the damage severity of different engine designs and ingestion conditions.

Criterion Analysis

The criterion relation was developed from the observation that a metal sheet or plate will sustain maximum structural damage when struck by a projectile traveling at, or just above, that speed required to penetrate (Reference 9). As this "ballistic-limit velocity" is reached, the material shears immediately upon contact, offering little further resistance to penetration.

The requisite shear-penetration damage model can be developed by considering only the local contact region of the blade (treated as a thin plate) and neglecting both the elastic energy absorbed by the blade and the effects of blade support. If it is also assumed that the velocity of the impacting projectile decreases linearly during penetration of the material thickness, h, then the critical impact velocity, V_i, (that is, the minimum required to just reach the aft surface) fixes the critical duration for penetration as

$$t_p = 2h_i / V_i$$

The impulsive load imposed on the blade can be equated to the change in momentum of the impacting projectile of weight W according to

$$\int_0^{t_p} F(t)\,dt = \frac{W}{g} V_i$$

and, since experimentally obtained force-time records indicate that a triangular contact-pressure signature gives a reasonable approximation to actual high-speed impact conditions (Reference 10), the resulting integration yields

$$V_i = \sqrt{\frac{g h p_i}{(W/A)}}$$

for the ballistic limit velocity. Here, p_i is the peak impact pressure applied uniformly over the blade contact surface A. The parameter W/A is the projectile caliber density or weight per unit cross-sectional area.

During the very short impact interval, the bird may be considered to act as a rigid punch quasi-statically loading the surface with a uniform pressure over the contact surface. Limit analyses applied to punch/indentation problems have shown that the critical pressure required to plastically deform the surface of an elastic/perfectly plastic material of shear strength, τ_v, lies between

$$5.0\,\tau_Y \leq p_i \leq 5.8\,\tau_Y$$

depending on the cross-sectional shape of the (rigid) indentor (References 11 and 12). For a thin plate (thickness dimension small with respect to the contact area dimensions) of elastic/perfectly plastic material, permanent indentation by plastic flow of the material implies penetration of the plate (Figure 6). Using the lower bound plastic-flow indentation pressure as a conservative estimate of the critical impact pressure results in a shear-penetration damage criterion expressed as

$$D = 0.273\,V_i\sqrt{\frac{(W/A)}{h\,\tau_Y}} \qquad (1)$$

where V_i is the impact velocity, (ft/sec)

W/A is the projectile caliber density, ($lb/in.^2$)

h is the target thickness, (in.)

and τ_y is the shear yield strength of the target material (psi).

According to this criterion, maximum damage is sustained when plate penetration occurs, that is, when the damage level, D, reaches 1. In practice, the maximum allowable damage level must be determined by test.

In this relation, the parameter of most interest to the designer is seen to be the blade local thickness, since in practice the engine

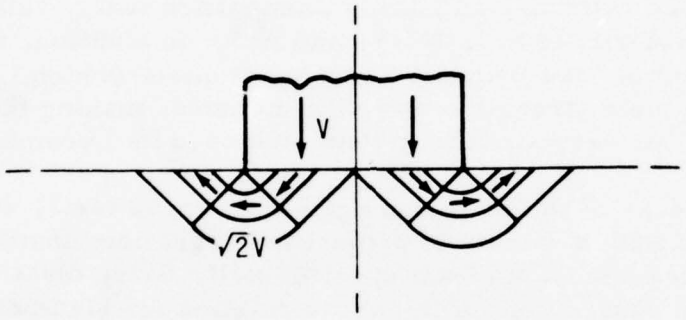

(A) HILL SOLUTION

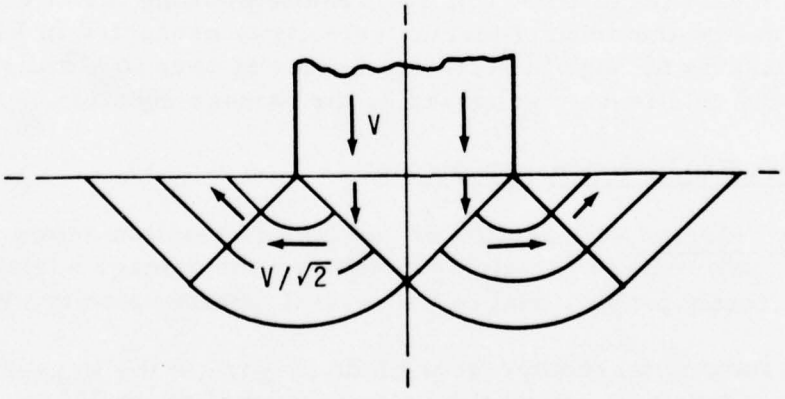

(B) PRANDTL SOLUTION

(Reference 12)

Figure 6. Velocity Fields for Two-Dimensional Flat Punch.

ingestion conditions and material strength are essentially fixed. The $h^{.5}$ relationship was found to correspond exactly to that derived empirically by McNaughton and Perfect (Reference 13) from tests of birds impacting engine intake structures. In addition, their design equation also indicated - within the range of tests performed - that the bird penetration velocity varied according to $W^{-.33}$ but with no account being made of bird contact areas.

Another empirical design equation, developed by Burch and Avery (Reference 14)from small arms ammunition tests, relates the ballistic limit velocity to $h^{.7}$, $W^{-.5}$, and $A^{.4}$. In addition, a target material parameter, the Brinnell Hardness Number (which is relatable to a material's yield strength), was also included, making their empirical equation very similar to that developed by Lycoming.

Initial checks of the criterion against in-house tests, which had been performed with a variety of projectile/target combinations, was sufficiently successful to warrant specific static firing tests to corroborate the square root of thickness relation for blade damage resistance. For these tests, titanium sheet stock specimens were designed to simulate the 6800 lbf thrust fan blade dimensions and material and the root and midspan shroud supports provided by a fully bladed disk. Two-inch diameter gelatin balls were used to simulate small-bird impact (Reference 15). The results showing the effect of plate thickness on the critical tearing velocity is presented in Figure 7. The curve passing through the torn specimens is seen to closely fit the theoretical relationship proposed by the damage equation.

Application to Fan/Compressor Blades

Bird Impact Velocity - Inspection of the damage relation shows that - for all other parameters remaining constant - the damage sustained by a blade is directly proportional to the normal impact velocity, V_N.

For a running fan/compressor blade (Figure 8) the impact velocity damaging the blade is taken as the velocity normal to the blade expressed as

$$V_N = (V_{FAN} + V_{F.O.} \sin\beta)\cos\phi - (V_{F.O.} \cos\beta)\sin\phi \quad (2)$$

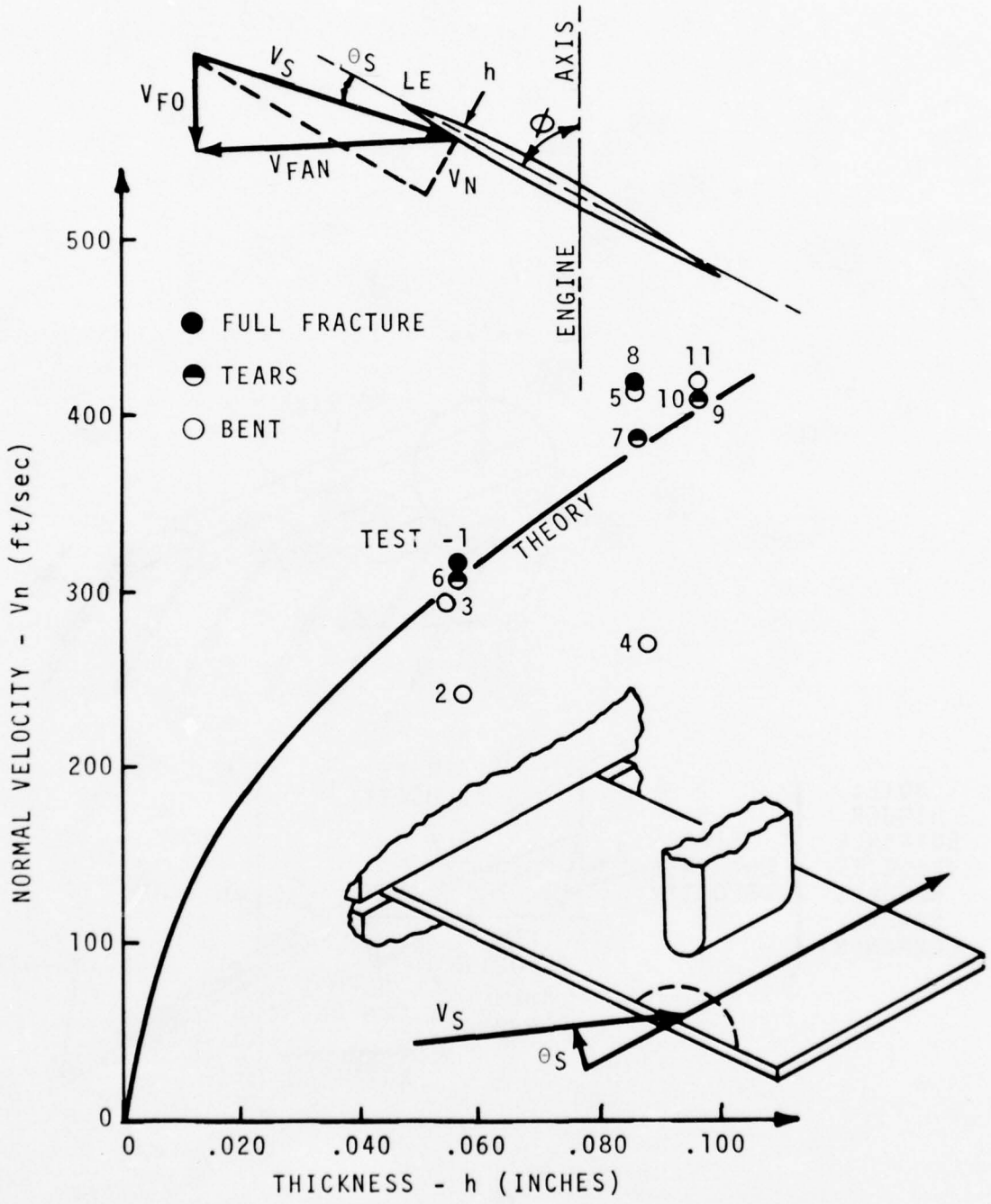

Figure 7. Flat Plate Impact Test Results.

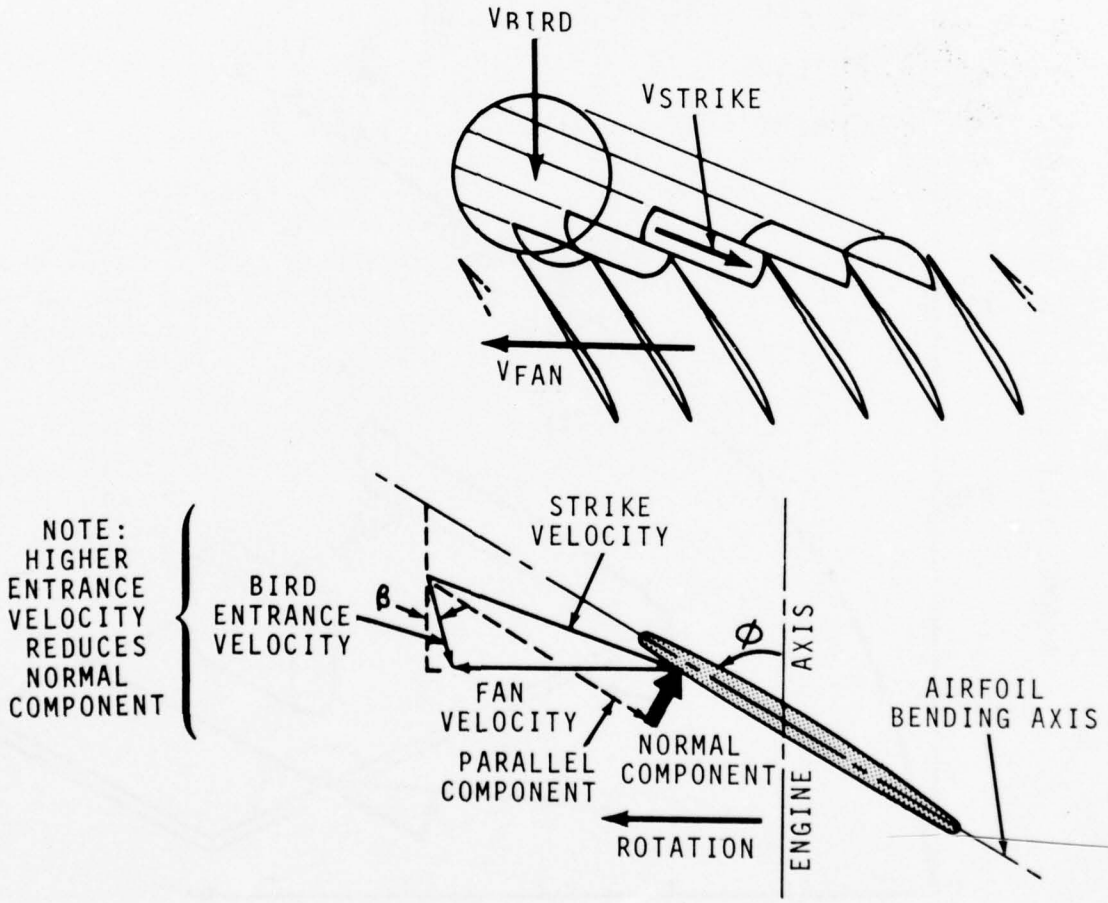

Figure 8. Bird/Blade Impact Velocity Triangles.

where V_{FAN} ($= R\ \omega$) is the rotational speed of the blade at the impact radius, R, and $V_{F.O.}$ is the velocity of the foreign object entering the stage at the angle β from the engine centerline. The surface that decelerates the bird mass is represented by the minimum axis of inertia of the airfoil section, oriented at the angle ϕ from the engine centerline. It is seen that for straight ingestion of a bird,

$$V_N = V_{FAN} \cos\phi - V_{F.O.} \sin\phi$$

so that the normal velocity increases linearly with fan speed and decreases linearly with entering velocity. Blade twist results in decreased normal velocity near the tip. Furthermore, typical blade section orientation tends to make the normal velocity insensitive to ingestion speed near the hub, most sensitive near the tip.

The normal impact velocity distribution over the blade span is shown in Figures 9 and 10 for the three baseline blades at the appropriate FAR conditions specified previously in Table 4. Maximum values are seen to occur just above the root and are greater for the smaller size birds. The figures also illustrate the maximum extent of (spherical) bird impacts over the blade span.

Inspection of the impact velocity equation also shows that, under take-off and climb conditions, the impact point is on the pressure face because the blade speed is typically much higher than that of the entering object. For example,when the aircraft is on the ground just prior to take-off, then $V_{F.O} \cong 0.$ and the impact velocity ($= V_{FAN} \cdot \cos\phi$) is at a maximum (detail a, Figure 11). As the entering speed of the object increases (due to increasing aircraft speed), the normal impact velocity decreases to zero. At this point, the foreign object/aircraft speed is

$$V^*_{F.O.} = V_{FAN} / (\tan\phi \cdot \cos\beta - \sin\beta)$$

See Figure 11, detail b. At this combination of speeds and blade orientation, the bird's center of mass impinges directly on the leading edge and so represents a pure slicing action, and the blade theoretically suffers no damage. In practice of course, some denting or buckling

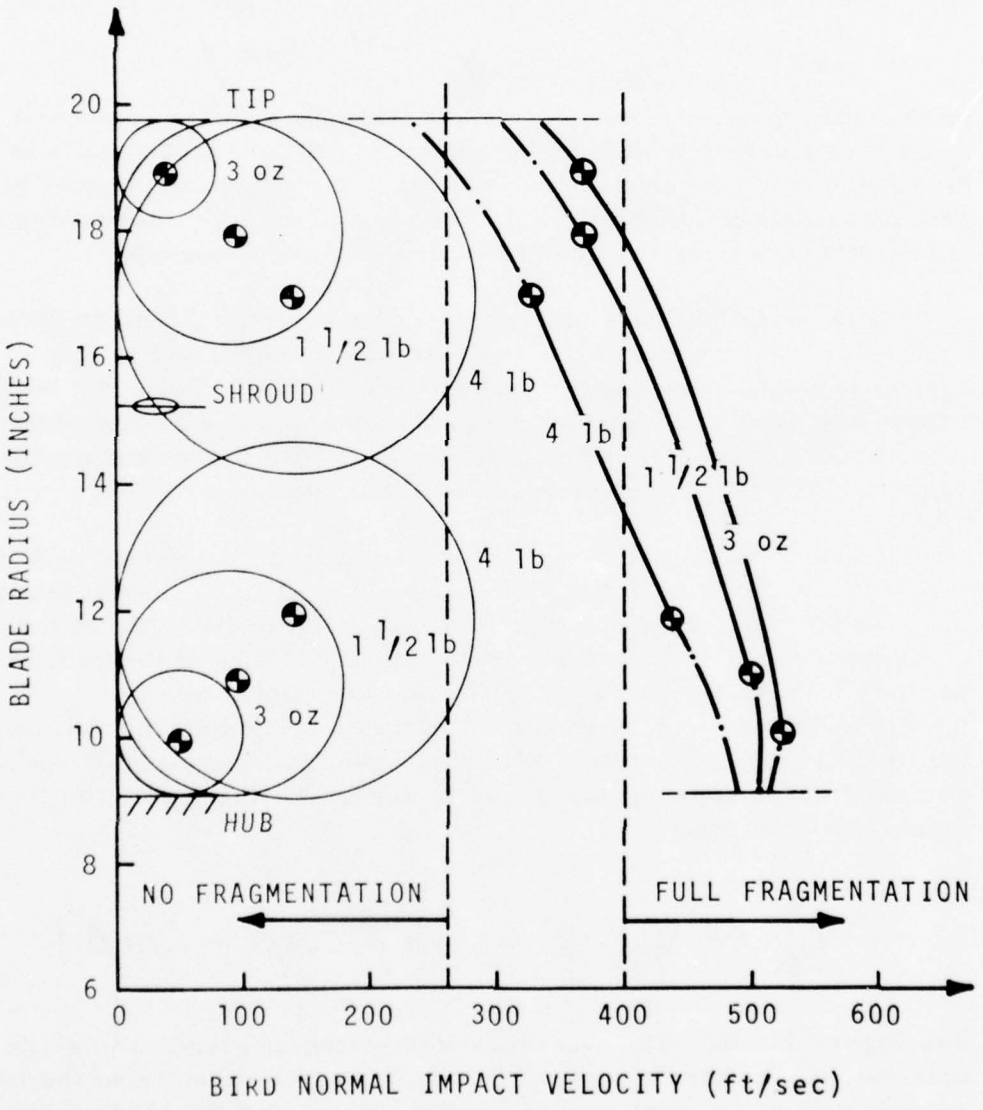

Figure 9. Normal Impact Velocity Distribution - 6800 lbf Baseline Blade.

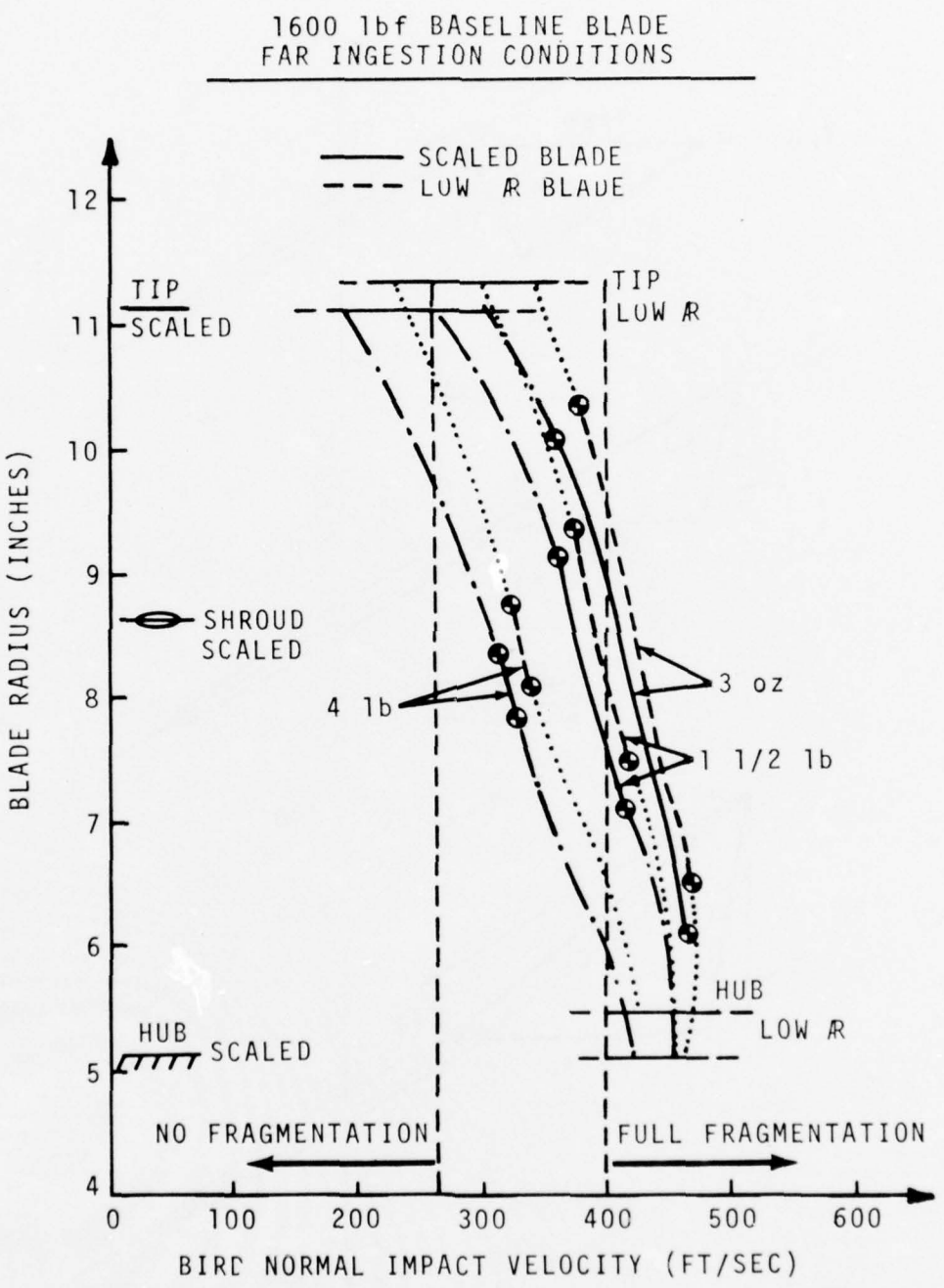

Figure 10. Normal Impact Velocity Distribution - 1600 lbf Baseline Blades.

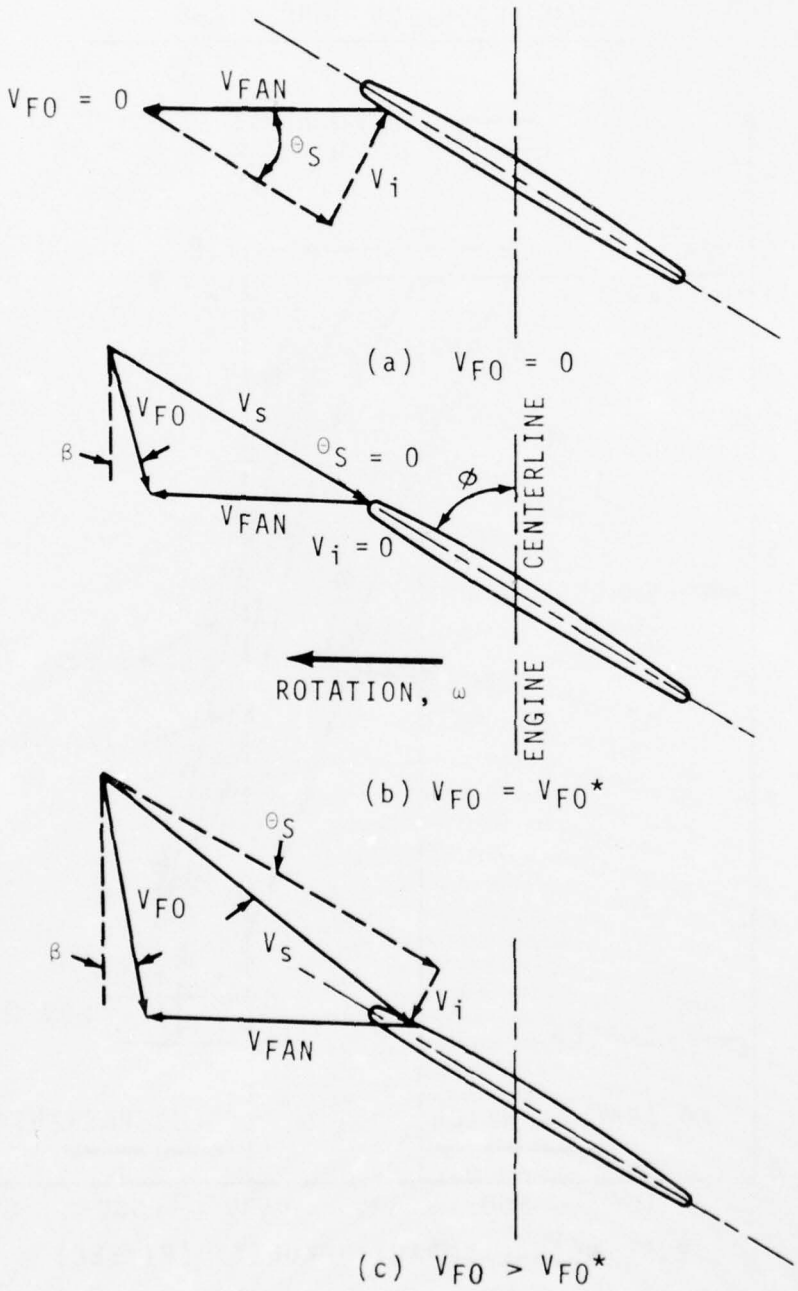

Figure 11. Variation of Impact Location With Ingestion Speed.

of a thin leading edge can be expected. Some damage would also be predicted by the criterion at radial stations just inboard or outboard of the bird center of mass resulting from the slightly different combinations of the blade speeds and orientations. It should also be noted that at this velocity a sufficiently small bird (small with respect to blade pitch) may pass directly through the fan stage without striking a blade.

As the flight speed increases beyond $V_{F.O.}$, the normal impact velocity increases in magnitude; but impact will then occur on the suction side of the blade (Figure 11, detail c).

A plot of the normal impact velocity as a function of foreign object entrance velocity is shown in Figure 12 for the three baseline engines, assuming a bird strike at the 80 percent span locations and with the fans operating at their maximum cruise rpms. Typical flight speeds are also shown and indicate that for the same size bird the take-off speed ranges impose the most severe impact velocity conditions on the fan blades. Pure slicing of the bird passing through the fan rotor is seen to occur in the 350-knot range, implying minimum damage not only to the fan blade but to the bird as well. This in turn implies that maximum damage to subsequent stages can be expected near 350 knots with less damage to subsequent stages at the lower flight speeds.

Bird Caliber Density - Inspection of the criterion equation also shows that for all other parameters remaining constant the damage sustained by a blade increases with increasing projectile caliber density, W/A. A caliber density relation applicable to (unfragmented) ice, birds, stones or steel spheres is

$$\frac{W}{A} = \frac{2}{3} \gamma d_Q \qquad (3)$$

where the respective densities, γ , may be taken as 0.035, 0.045, 0.10, and 0.28 lb/in.^{3}. For birds, the above caliber density relation is applicable only to full, unfragmented bird impact and can be calculated from an equivalent spherical bird diameter, d_Q, determined experimentally by Metcalf (Reference 6) as

$$d_Q = 3.50\, W^{0.30}$$

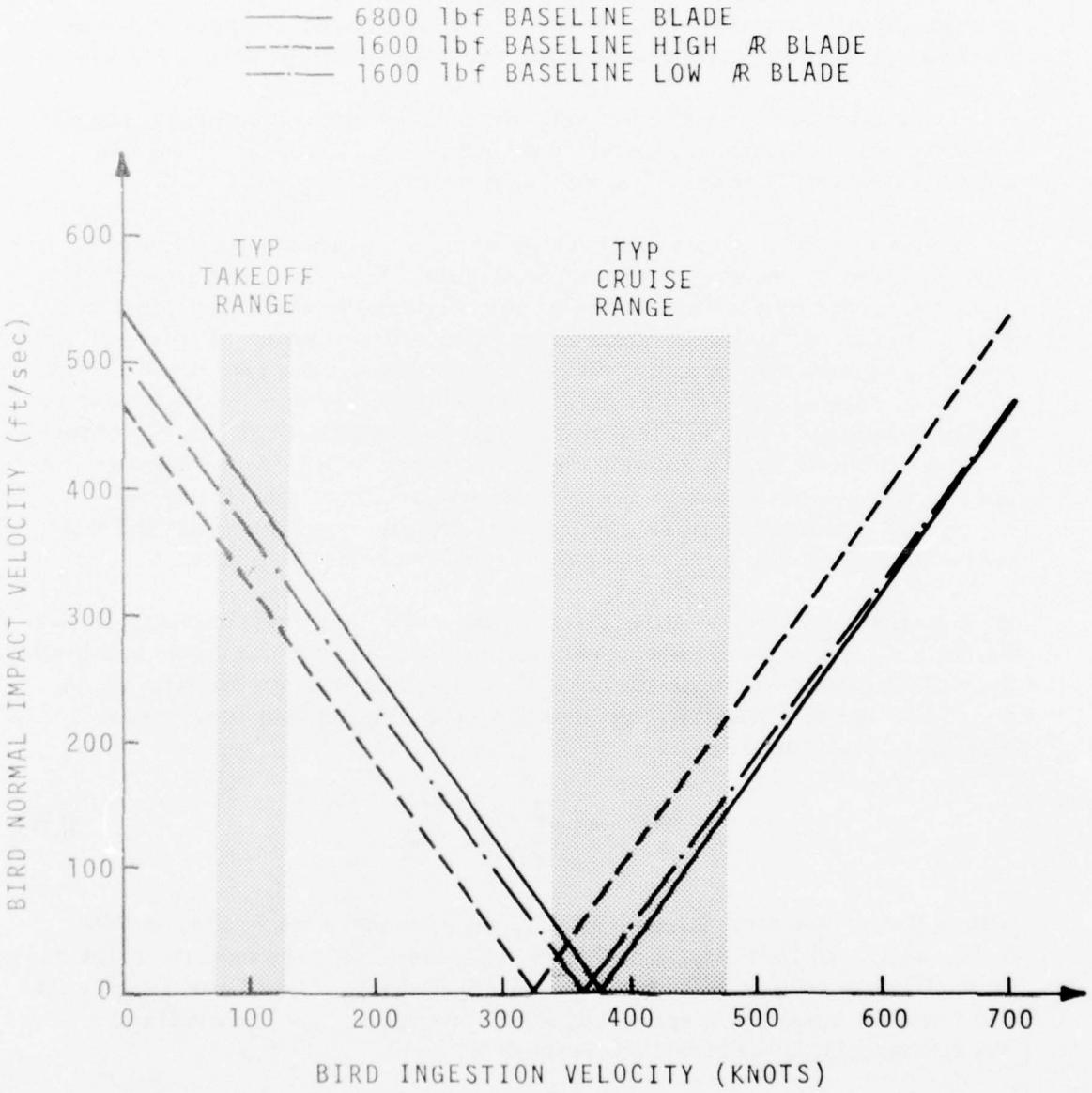

Figure 12. Variation of Impact Velocity With Ingestion Speed.

or by

$$d_Q = 3.76\, W^{0.35}$$

if the weight/size data for chickens is neglected, or by

$$d_Q = 3.48\, W^{0.33} \qquad (4)$$

which approximates the two (Figure 13). This latter equation is consistent with the above quoted bird density value, since for a sphere,

$$W = \gamma \pi d_Q^3 / 6 = \gamma \pi 3.48^3 W / 6$$

or

$$\gamma = 0.045\ lb/in.^3$$

and constant.

While the above caliber density relation could be used to predict the damage sustained by full impact of an entire bird on a single blade, two factors will influence the actual caliber density causing damage to a blade in a rotating fan stage. The first factor results from the slicing action of the moving blades passing across the front of the bird as it enters the stage. At sufficiently high entrance speeds, a small bird can be expected to enter the stage before being struck by an oncoming blade. The full-bird caliber density would, therefore, apply. At low entrance speeds, or for larger birds, several blades will strike the bird as it enters the stage. If blade deflection during impact is neglected, the caliber density relation for a central slice is approximately

$$\frac{W}{A} = \frac{\gamma w (\pi d_Q^2 / 4)}{w d_Q} = \frac{\pi}{4} \gamma d_Q \qquad (5)$$

which is some 18 percent greater than the full bird value. The width of the bird slice, w, depends on the number of blades struck and is

$$w = d_Q / n_B \qquad (6)$$

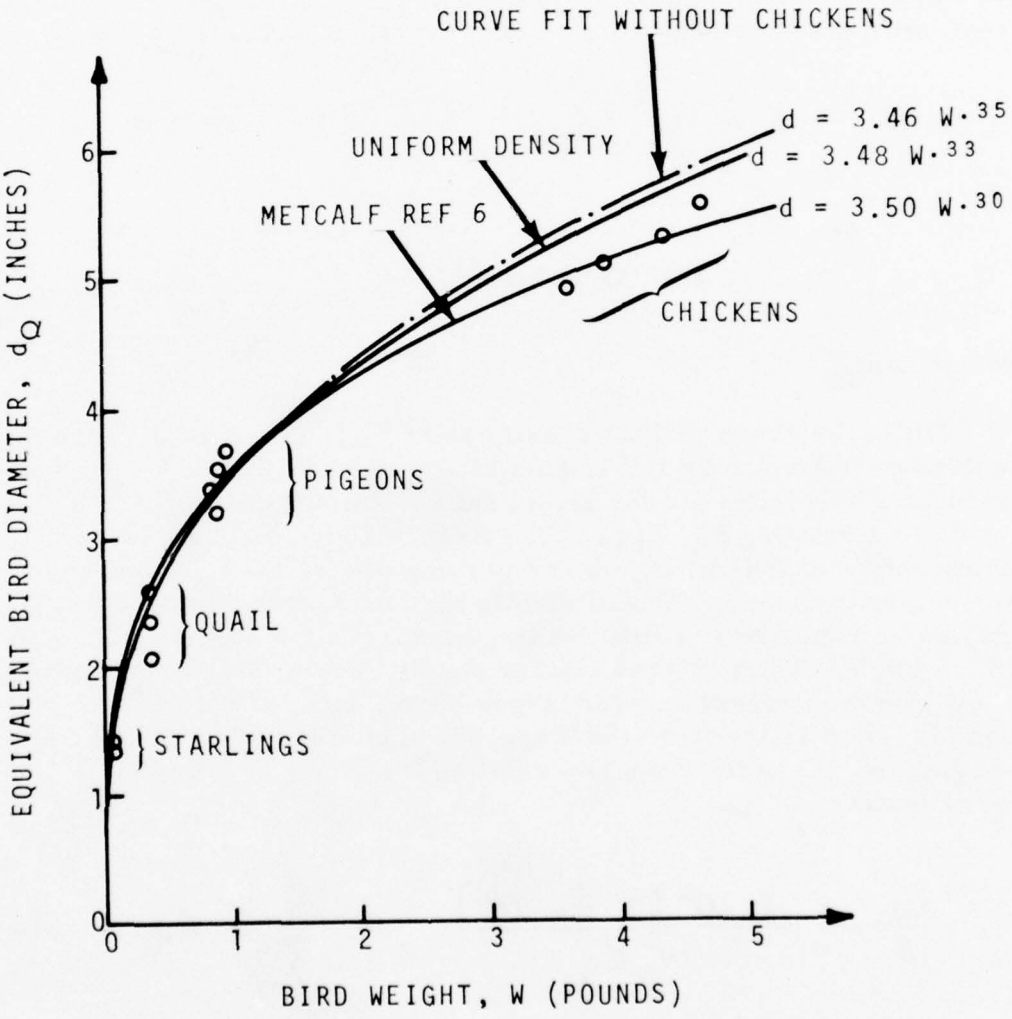

Figure 13. Equivalent Bird Size Versus Bird Weight.

where the number of blades striking the bird, n_B, can be estimated from

$$n_B = (N_B N d_Q)/(720 V_{F.O.} \cos\beta) \qquad (7)$$

Here, N_B is the number of blades in the stage, and N is the fan speed in rpm.

Note that the number of blades struck and the corresponding slice width are independent of the bird's point of impact along the span. The number of blades struck per bird for the baseline engines operating at the FAR ingestion conditions are listed in Table 5. The actual number of blades struck will vary somewhat, of course, depending upon the attitude of the (nonspherical) bird. In practice, the calculated number is expected to be slightly low since the wings may be extended and since the bird may be accelerated tangentially (and rotated) as it is sliced upon entering the stage.

Increasing ingestion velocity (or decreasing fan rpm) results in fewer but thicker bird slices impacting further back along the blade chord. This implies that at the lower flight speeds local contact damage is limited to the blade leading edges but can be severe and result in excessive distortion and tearing of many blades. At the higher flight speeds, local damage may be reduced, but because of the greater loads imposed per blade, large blade motions may result with possible gross failures occurring near support points.

The second factor affecting the caliber density relation results from bird fragmentation at the higher impact velocities. Tests by McNaughton and Perfect (Reference 13) show that birds remain whole for impact velocities up to 260 ft/sec, and are fully disintegrated by 400 ft/sec. In addition, Mitchell (References 16 and 17) estimated the impact force of a fully fragmented or "zero-stiffness" bird as

TABLE 5 - NUMBER OF BLADES STRUCK UNDER FAR INGESTION CONDITIONS

		6800 lbf Thrust Class		1600 lbf Thrust Class			
		Baseline Blade		Scaled Baseline Blade		Low Aspect Ratio Baseline Blade	
Bird Weight W	Equivalent Diameter dq	Slice Thickness, w	No. of Blades Struck, n_B	Slice Thickness w	No. of Blades Struck, n_B	Slice Thickness, w	No. of Blades Struck, n_B
3 oz	2.0	0.442	4-5	0.250	8-9	0.443	4-5
1.5 lb	4.0	0.530	7-8	0.320	12-13	0.566	7-8
4.0	5.5	0.720	7-8	0.437	12-13	0.722	7-8

one-quarter that of a whole or "semi-rigid" bird. The caliber density relation can, therefore, be adjusted to account for bird stiffness or fragmentation effects according to

$$(W/A)_{eff} = \eta\,(W/A) \qquad (8)$$

where

$$\eta = \begin{cases} 1.0 & \text{"semi-rigid"} \quad V_N \leq 260 \text{ ft/sec} \\ 2.40 - 0.0054\,V_N & \quad 260 < V_N < 400 \\ 0.25 & \text{"zero-stiffness"} \quad 400 \leq V_N \end{cases}$$

Bird fragmentation effects have an important influence on the damage function distribution along the span. Referring again to Figures 9 and 10, it is seen that near the hub, where the impact velocity is highest, the birds are predicted to disintegrate completely, thereby decreasing the impact force on the blade. Less fragmentation, hence greater loads, occur farther out along the span until, for the 4-pound bird at least, fragmentation ceases near the tip. This implies that the bird debris leaving the stage near the hub behaves somewhat as a liquid dispersed in the airstream and so tends to inflict little physical damage to the exit stators or to subsequent stages. Near the tip, however, the bird tends to remain whole (sliced but unfragmented) and so can be expected to leave the stage with essentially the same axial velocity - but probably picking up most of the blade tangential component - prior to impacting on the exit stators. Maximum damage to the fan exit stators can then be expected.

Fan Blade Impact Thickness

As noted previously, the damage criterion, equation 1, decreases with increasing blade thickness at the point of impact. For convenience, the impact thickness used in the design calculations is based on the blade's thickness at the center of the contact surface. For consistency

with the bird caliber density relation, these dimensions are set to directly match the projected area of the bird slice (Figure 14). This procedure also tends to account for the known shift of the center of pressure towards the leading edge.

To further facilitate the use of the numerical damage function in blade parameter studies, a convenient method of relating the impact site thickness with readily available design parameters is required. Of the various mathematical relations tried (exponentials, higher order polynomials, and trigonometric functions), a simple quadratic was found to give consistently best results in the impact region and was used throughout this report (Figure 15). That is, for sufficient accuracy in the forward region of the blade, the function

$$t(x) = A_0 + A_1 x + A_2 x^2 \qquad (9)$$

was fitted along the chord such that both the leading edge radius and wedge angle were satisfied at the leading edge, while the maximum thickness (but not slope) was forced at the appropriate chordwise location. Based on this procedure,

$$A_0 = 2 R_{LE}$$

$$A_1 = \Theta_{LE} \cdot chord$$

$$A_2 = (t_{max} - A_0 - A_1 x_{max}) / x_{max}^2$$

where x = s/chord, and s is the chordwise distance from the leading edge.

Baseline Blades Damage Evaluation

The numerical damages along the span have been computed for the 6800 lbf thrust baseline fan and the two 1600 lbf thrust baseline fans in accordance with the appropriate FAR 33.77 bird ingestion requirements and are shown in Figures 16 and 17. The calculated damage values tend to remain fairly constant over the inner region of the blades where the bird is fully disintegrated, with increasing damage predicted near the outboard regions where less fragmentation takes place. In using these curves, it should be remembered that the damage equation does not consider the local effects of tip, part-span and/or root shrouds and

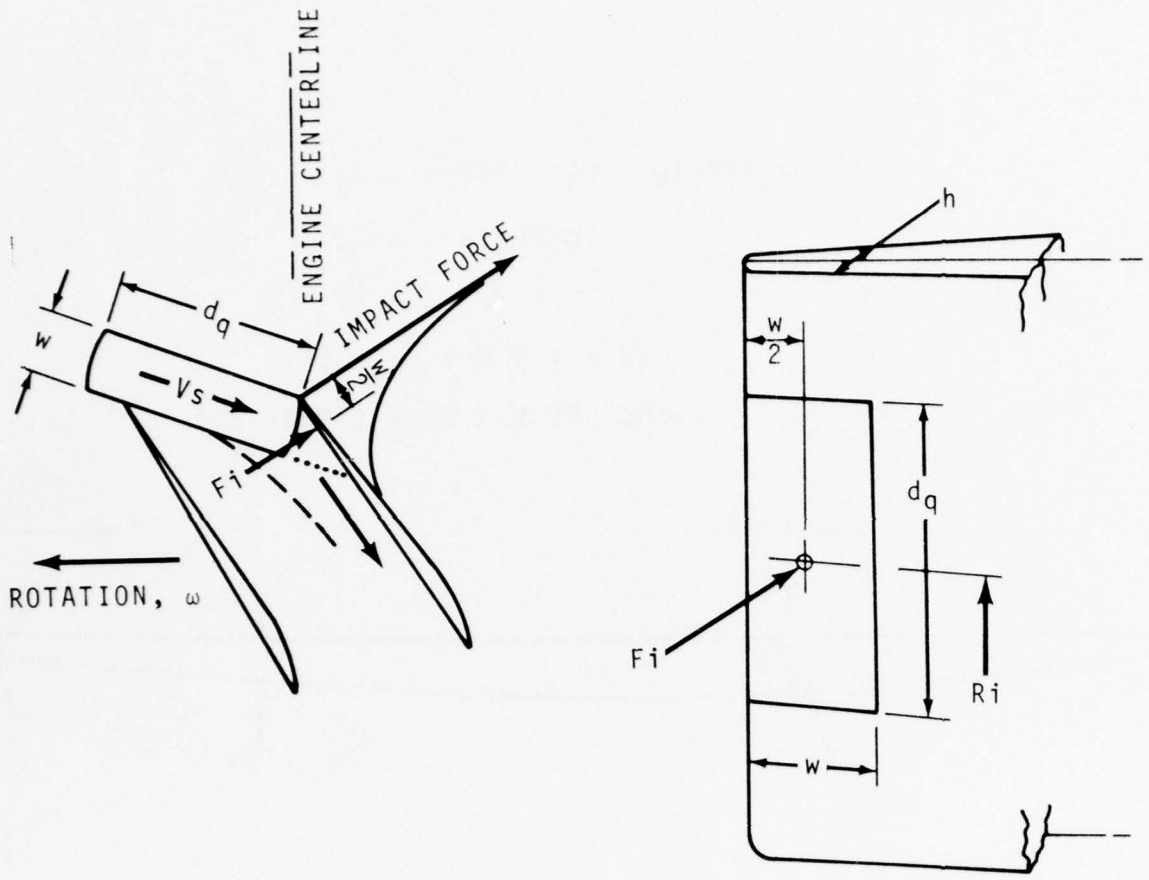

Figure 14. Blade Impact Surface and Thickness.

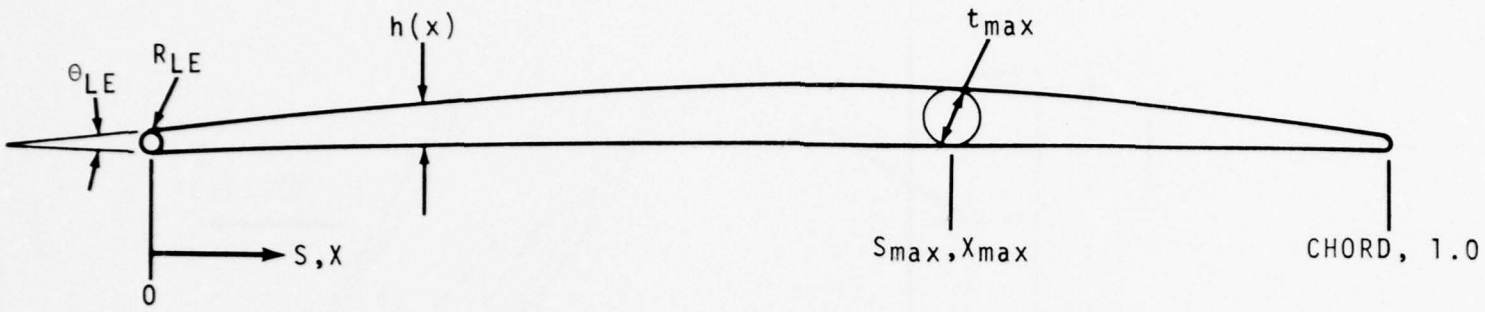

FOR IMPACT NEAR LEADING EDGE:

$$h(x) = A_0 + A_1 X + A_2 X^2$$

$$A_0 = 2\ R_{LE}$$

$$A_1 = \theta_{LE}\ \text{CHORD}$$

$$A_2 = (t_{max} - A_0 - A_1 X_{max})/X_{max}$$

Figure 15. Airfoil Thickness Parameters.

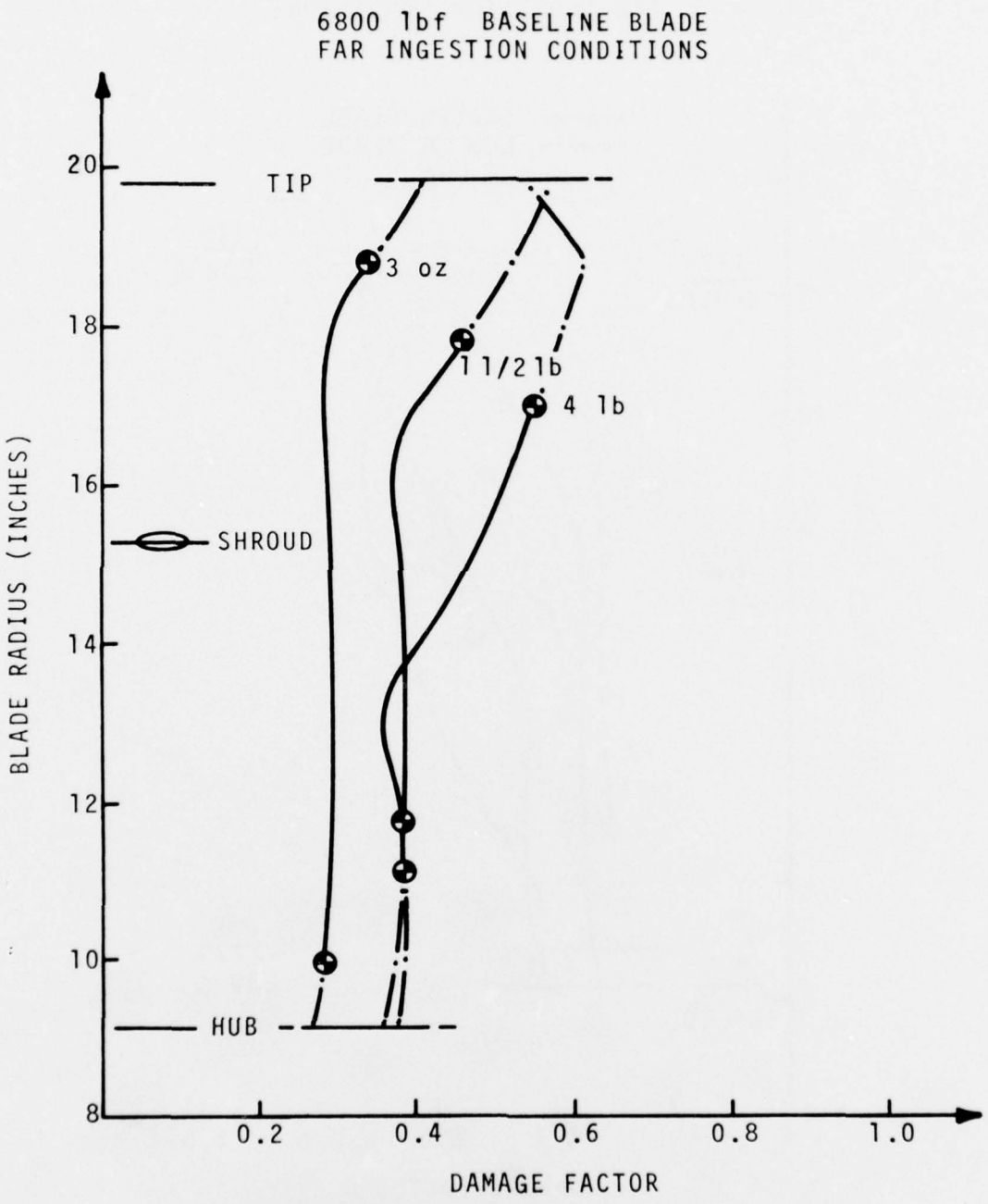

Figure 16. Damage Factor Distribution - 6800 lbf Baseline Blade.

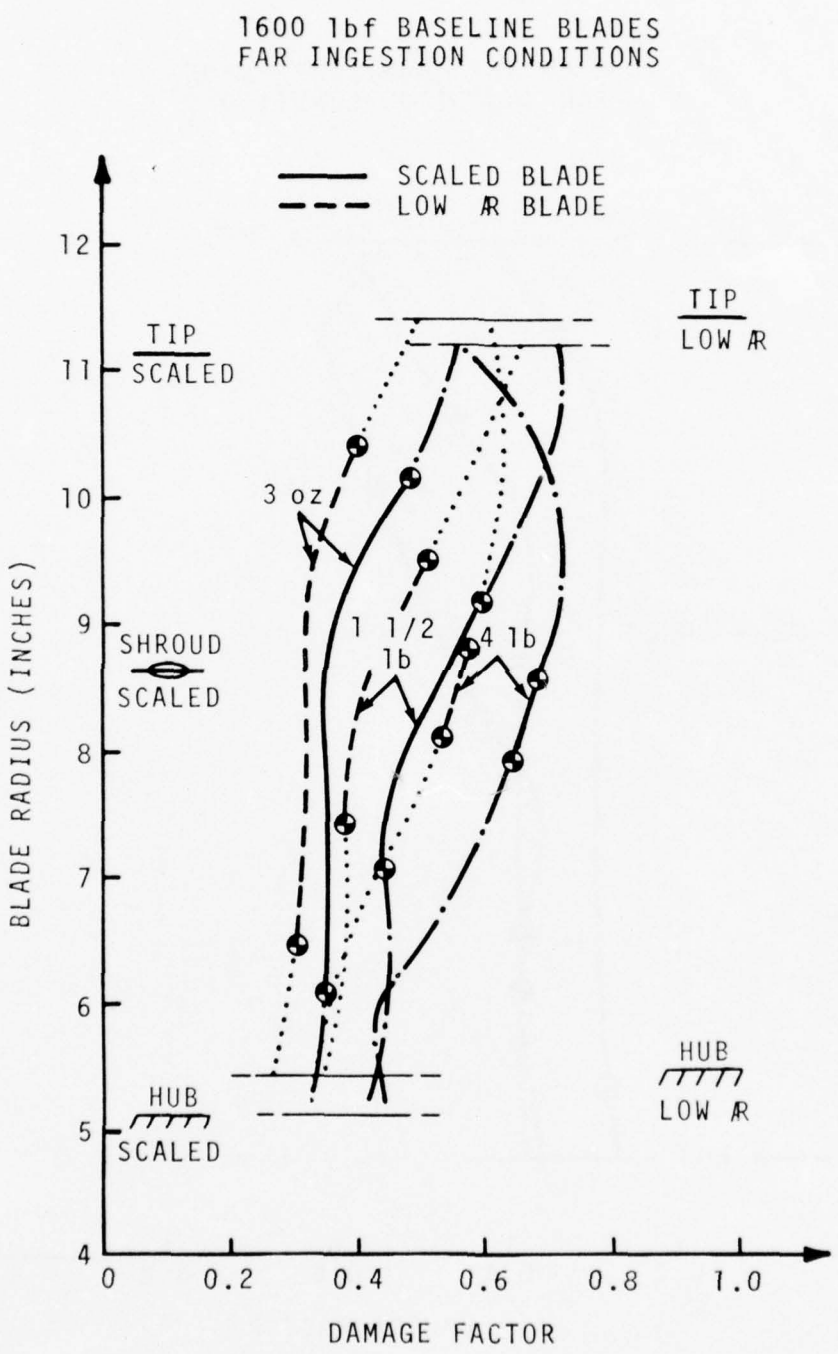

Figure 17. Damage Factor Distribution - 1600 lbf Baseline Blades.

support conditions, so that the calculated values do not account for these local stress concentrating effects. Experimentally obtained damage allowables must, therefore, be correlated with respect to span location.

From these curves it is also seen that fan blade damage is greater for the large size bird-ingestion conditions. However, the ingestion requirement corresponding to the 4-pound bird requires only that engine failure does not present a hazard to the aircraft, while an engine damaged from the small and medium size birds must still provide safe, 75 percent power operation. The 1.5 pound bird-ingestion condition that corresponds to the most hazardous aircraft condition, therefore, presents the structural designer with the most severe damage condition to be met.

The effect of blade size - or equivalently of engine thrust class - is shown in Figure 18 for the two midspan shrouded baseline blades and a third version scaled up for a 50,000 lbf thrust machine. Operating speeds and bird ingestion velocities were also adjusted to fit this very large engine size and its associated aircraft take-off conditions. The comparison clearly illustrates the difficulty in designing bird-tolerance into engines of the smaller thrust classes.

Note also that a short chord version of the 50,000 lbf thrust blade is still considerably more damage-resistant than the baseline 6800 lbf blade, implying that additional weight reductions can be obtained in the larger size machines and still provide comparable damage tolerance. On the other hand, for similar performance, the low-thrust machines tend to require lower aspect ratio blades to provide comparable damage tolerance. Additional weight penalties must then be absorbed by improved performance, obtainable for example, by removal of the shrouds.

It is of interest to see if the most hazardous ingestion speeds specified by FAR 33.77 also correspond to the ingestion speeds producing maximum calculated fan blade damage. The variation in damage with flight speed is shown in Figures 19, 20, and 21 for the baseline engines. Maximum damage speeds are seen to be somewhat higher than the FAR conditions, depending on the point of impact. The high calculated damage values shown at the very low ingestion velocities result from impacts very near the thin leading edges and typically do not represent as hazardous a condition to the engine or aircraft as would

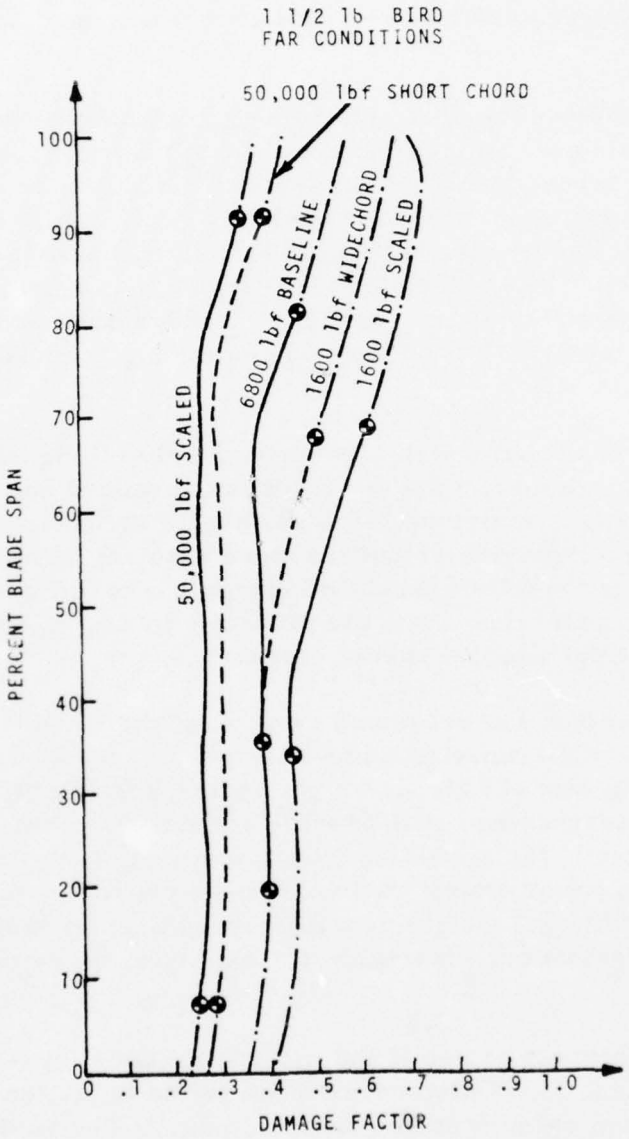

Figure 18. Effect of Engine Thrust Class on Damage Factor.

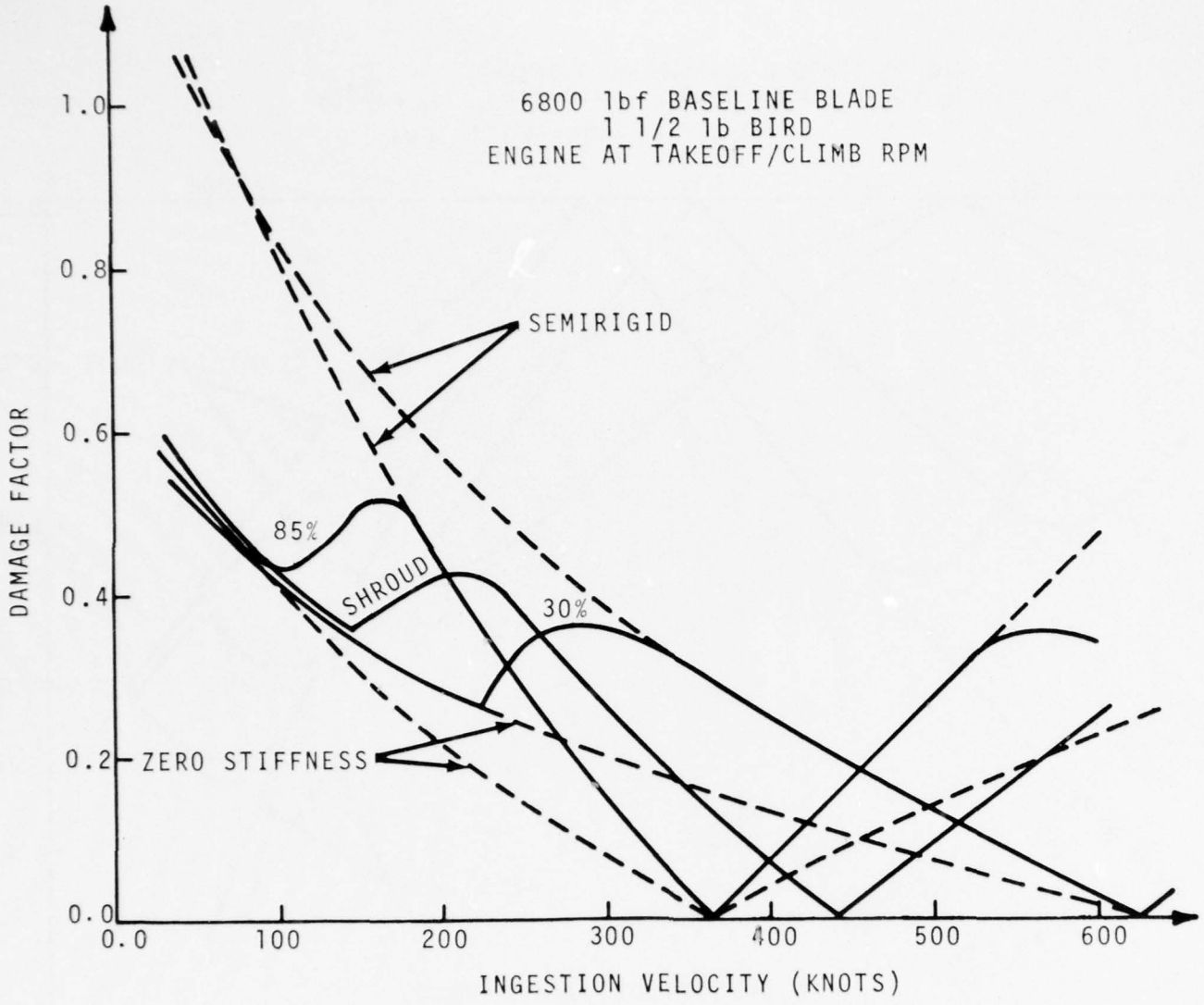

Figure 19. Variation in Damage Factor With Ingestion Speed - 6800 lbf Baseline Blade.

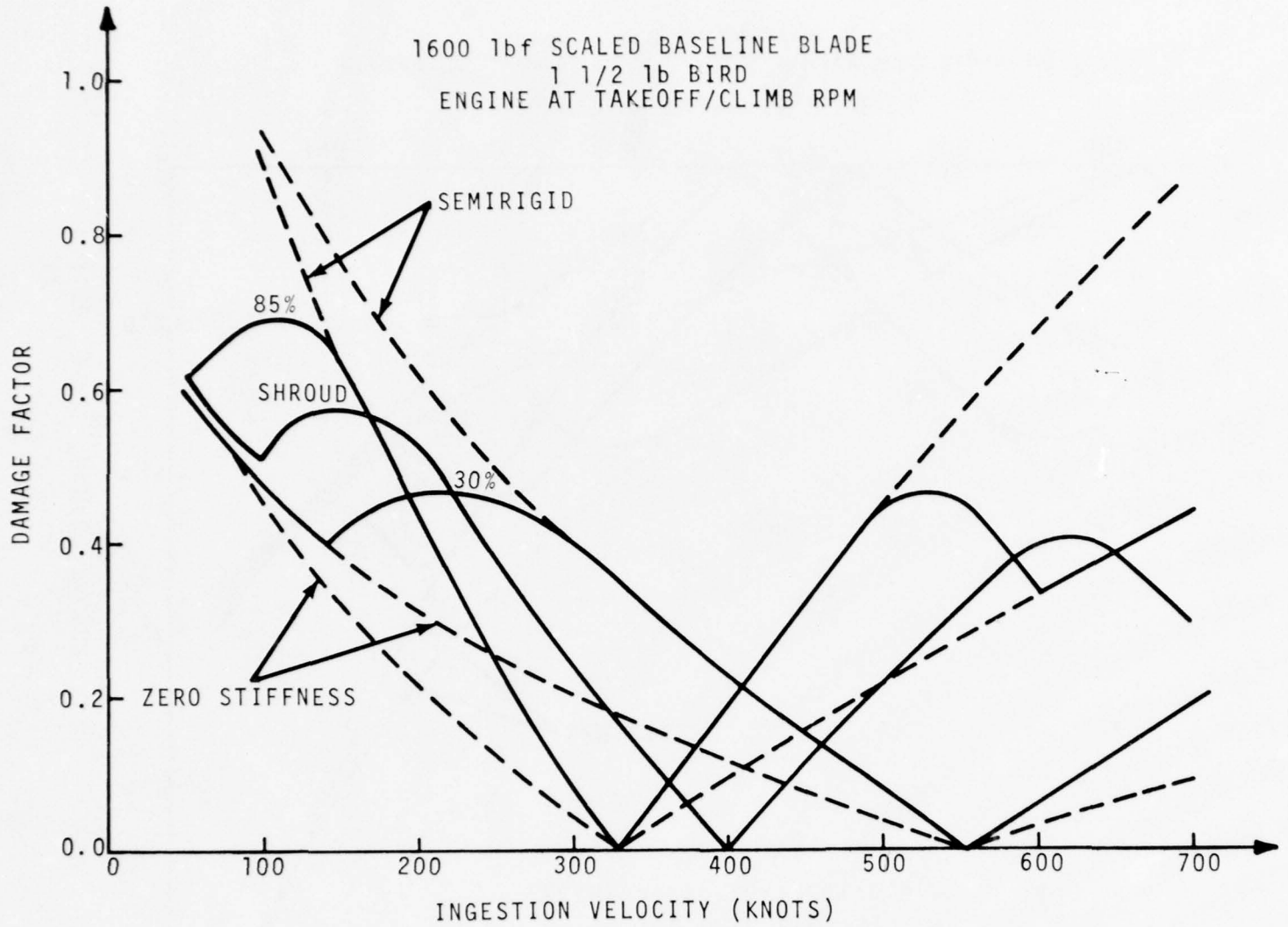

Figure 20. Variation in Damage Factor With Ingestion Speed-1600 lbf Scaled Baseline Blade.

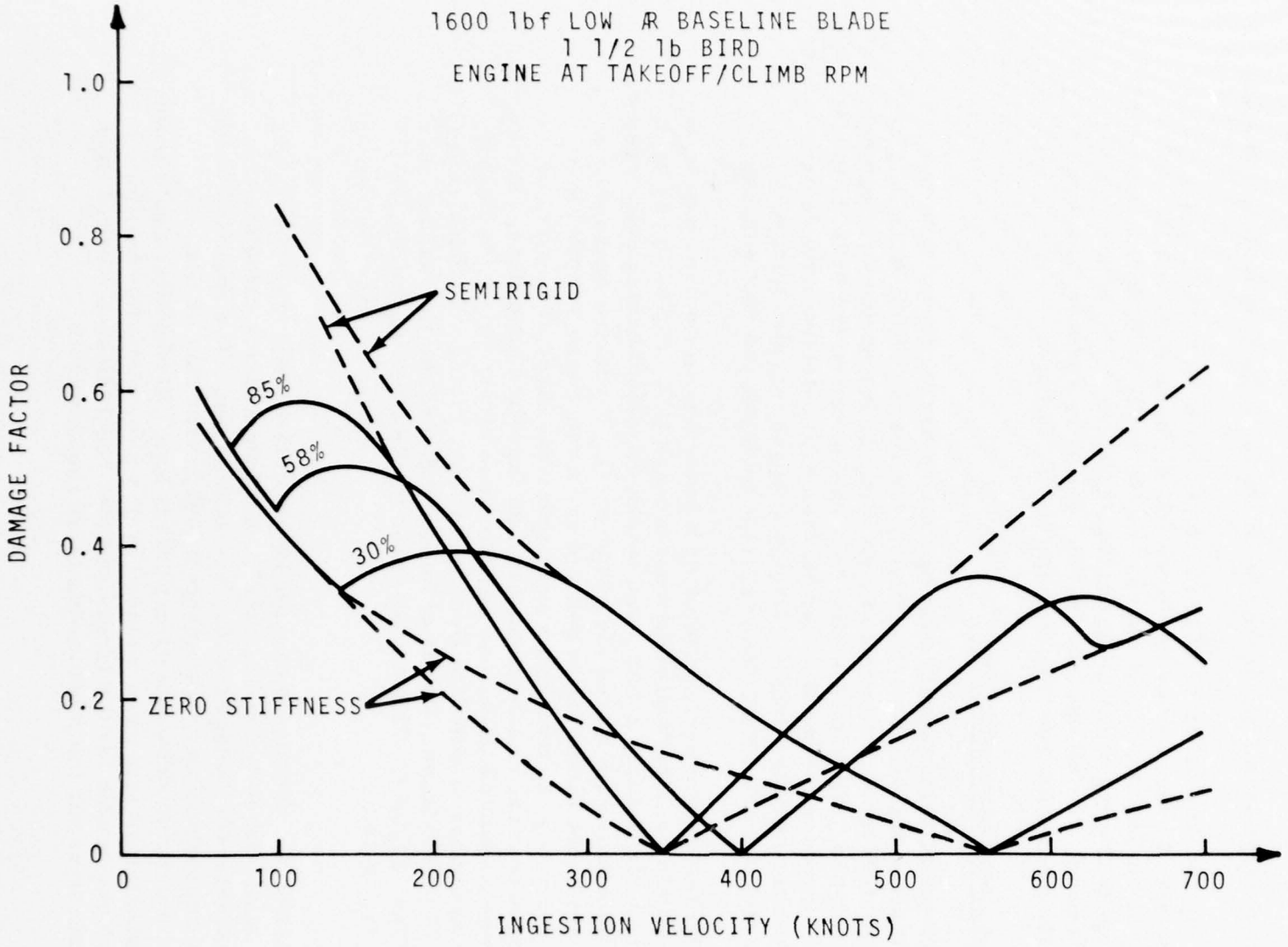

Figure 21. Variation in Damage Factor With Ingestion Speed - 1600 lbf Low Aspect Ratio Baseline Blade.

similar damage levels calculated for impacts farther back along the span.

The breakup behavior of the bird is also seen to have a large effect in these speed ranges - varying from full disintegration and low impact loading at the lower aircraft speeds to essentially no disintegration and high impact loading at the higher aircraft speeds. The points of maximum damage, as well as their values, will vary somewhat according to the fragmentation relation used in the calculations.

Damage Correlation with Test

In establishing physical damage limits to correspond with the numerical damage-factor calculations, the results of full-scale engine-bird ingestion tests performed at Lycoming during engine development were analyzed. All corroborative test data based on the 6800 lbf thrust machine included the baseline fan blades, a bird-tolerant fan design, and two intermediate designs. Design changes included thickened airfoil sections and detail changes to the midspan and root shrouds.

All tests were performed using a pneumatically driven ingestion gun consisting of a high-pressure air storage tank coupled to any of three firing barrels (1-inch, 2-inch, and 5-inch diameter) having quick response valves to release the stored air (Figure 22). Birds are encased in a styrofoam sabot within the barrel and are fired either wrapped in a strong nylon bag to maintain a tight spherical shape at impact, or unwrapped to more nearly simulate flight ingestion conditions. Firings have been conducted in various combinations either singly, in tandem, and/or in groups to simulate flock ingestion. Firing velocities ranged from 125 to 260 knots. Points of impact included the tip, shroud, hub, and spinner regions. Three high-speed movie cameras were used to record the tests.

Maximum calculated damage levels corresponding to successful engine tests are shown in Figure 23. Minimum values calculated from excessively damaged blades are also shown. The region between the two represents an as yet unknown region that may or may not provide a greater allowable damage limit line. Blade failure data from a 4.2-pound bird test were included in this plot, since the damage - although acceptable for the large-bird test requirements - would have been excessive for the medium-bird test requirements.

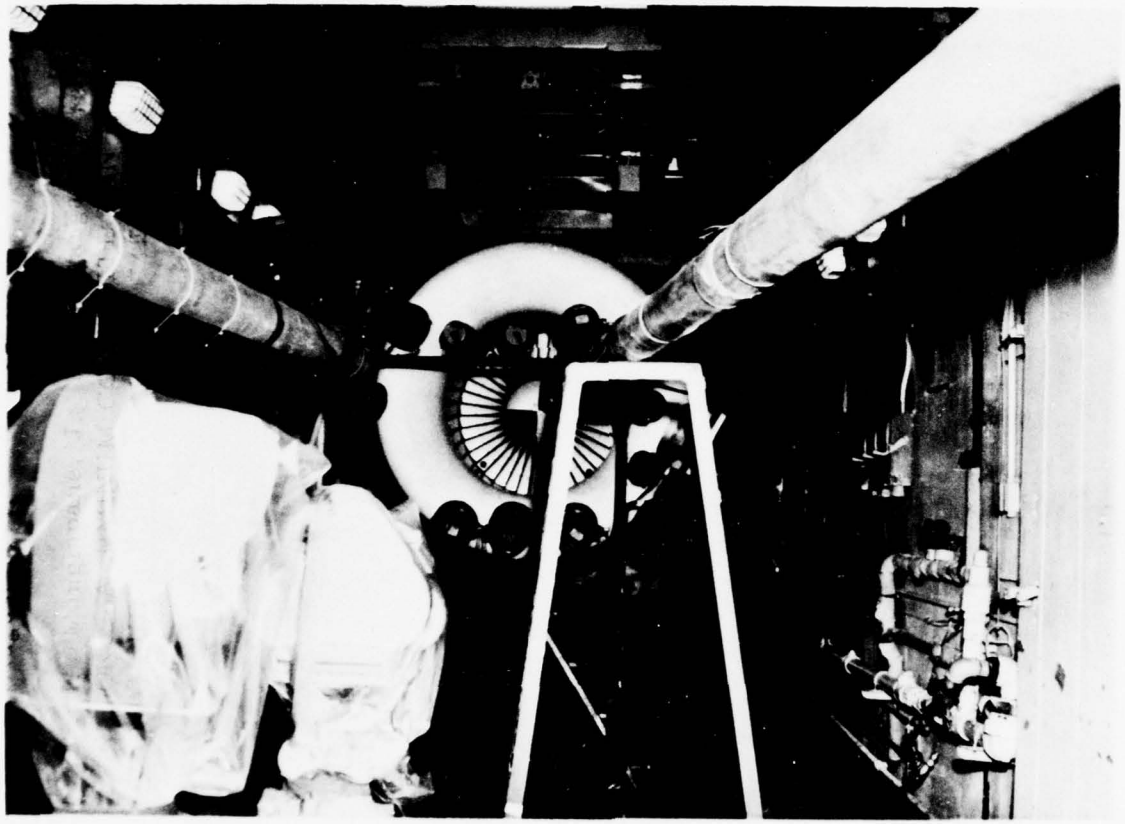

Figure 22. Lycoming Bird-Ingestion Test Facility.

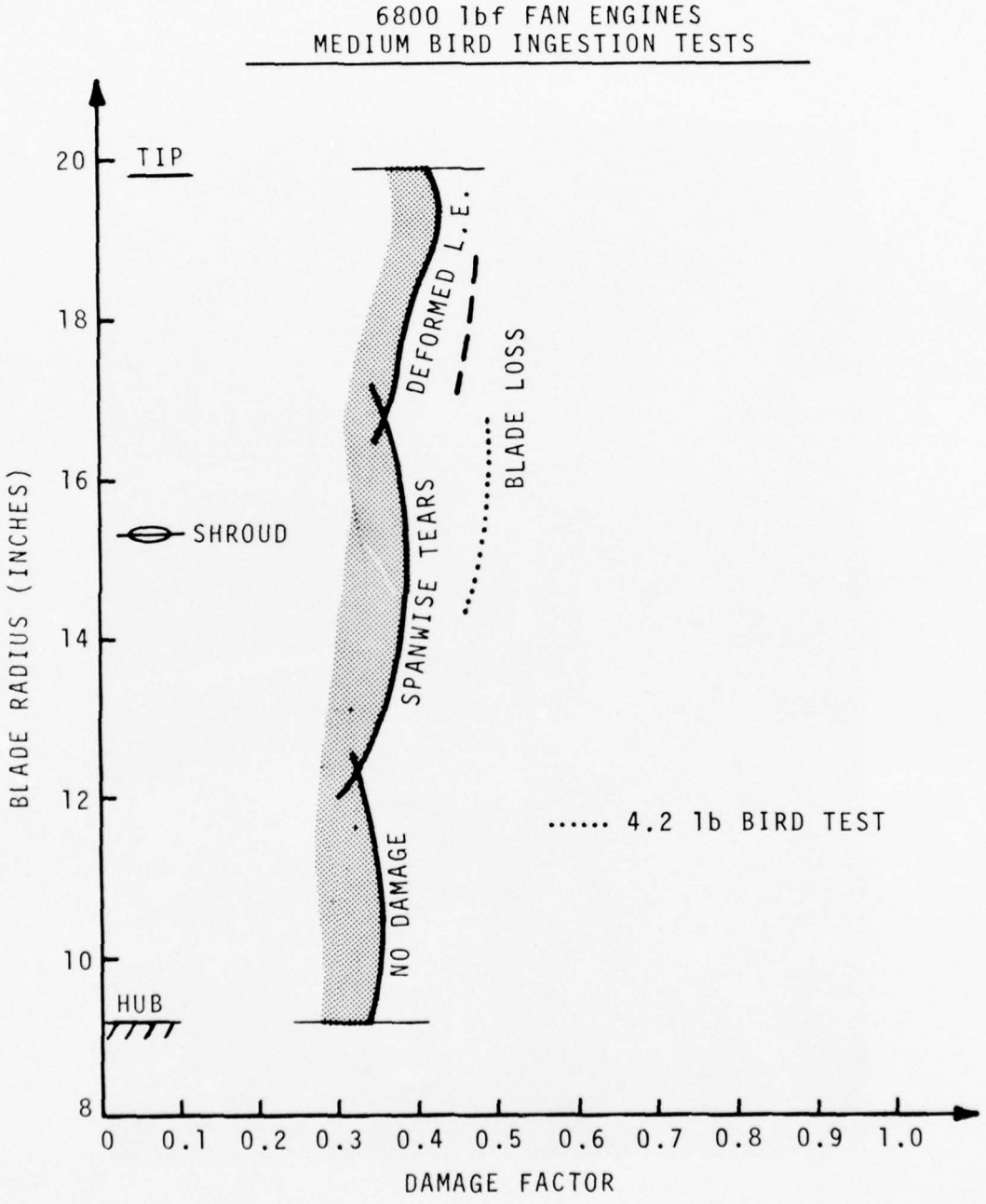

Figure 23. Medium-Bird Ingestion Test Damage Limits.

In evaluating the fan blade damage sustained in these tests, three general impact regions were considered based on the local support conditions: namely, the inboard region near the hub, the local shroud region, and the tip region outboard of the shroud. The use of separate criteria for the three different regions is consistent with the local damage criterion approach, since the relation used is independent of support conditions.

The first region, the inner blade span near the hub, was found to remain essentially undamaged throughout the test series so that the calculated limit line shown here ($D \cong 0.35$) is expected to be rather conservative. Apparently, a threshold damage level must be reached before permanent deformation can be obtained. This is consistent with the indentation pressure theory that first requires the development of a force sufficiently high to cause initial plastic deformation in the critical area under the punch and secondly is followed by penetration when the force is sufficiently high to cause all of the active material under the indentor to reach the flow limit.

Impacts in the second region (i. e. , the region near the midspan shroud) tend to roll back the leading edge and produce spanwise tears - apparently emanating from the shroud forward blend radius (Figure 24). Impact is seen to occur on the pressure face, tending to force the blade out against the incoming air and back against the direction of rotation. Shingling of some shrouds was noted on some tests. The failure damage line of approximately 0. 49 was drawn from a test where impact of a 4. 2-pound bird resulted in the loss of a blade just below the shroud (Figure 25). An adjacent blade was lost at the root approximately one-half revolution later, that is, somewhat after the bird had passed through the stage. The blades were contained and the engine was shutdown without incident.

In the third region, the tip region outboard of the shrouds, considerable leading edge distortion can be successfully sustained from a structural damage point of view (See Figure 26). The failure line for this region ($D \cong .46$) was determined from test conditions more severe than those specified by the FAR ingestion requirements (Figure 27). The failure pattern shown in this latter test indicates large blade motions occurred as the bird began impacting the blades, since they were apparently deflected outwards, protecting one of the following blades (Figure 28). The fifth tip - approximately 90° away - was subsequently lost many revolutions later by reingestion of one of the blade fragments.

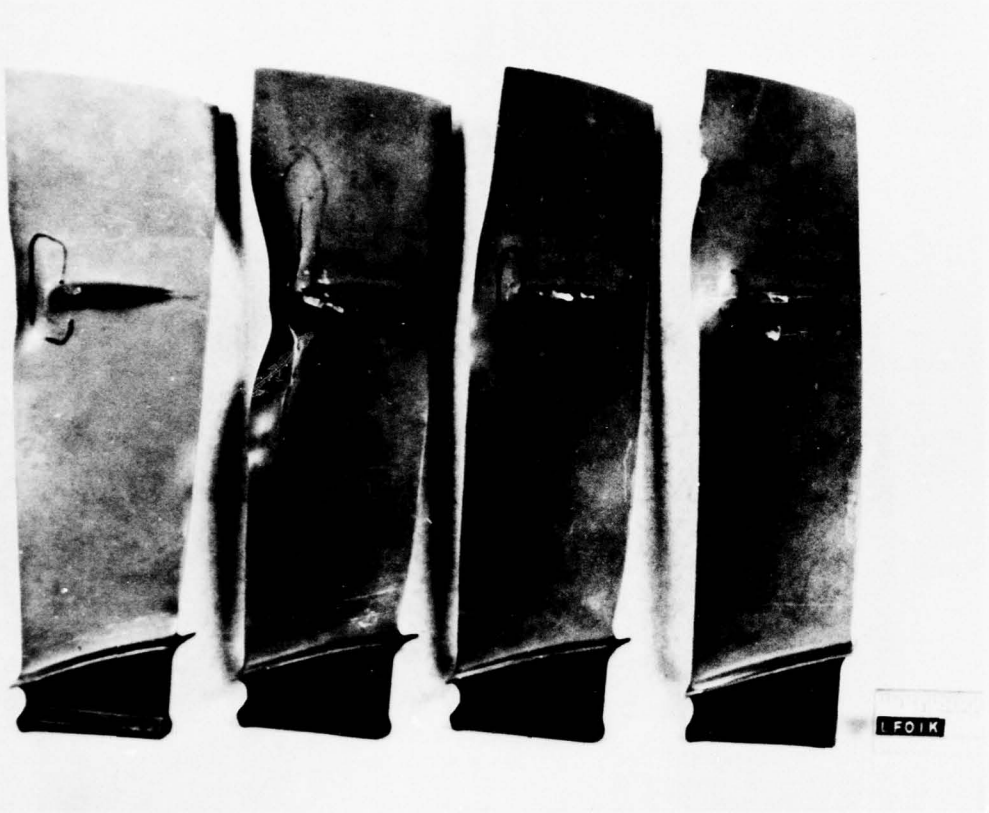

Figure 24. Shroud Region Damage After Bird-Ingestion Test.

Mid-Span Strike of 4.2 lb Bird

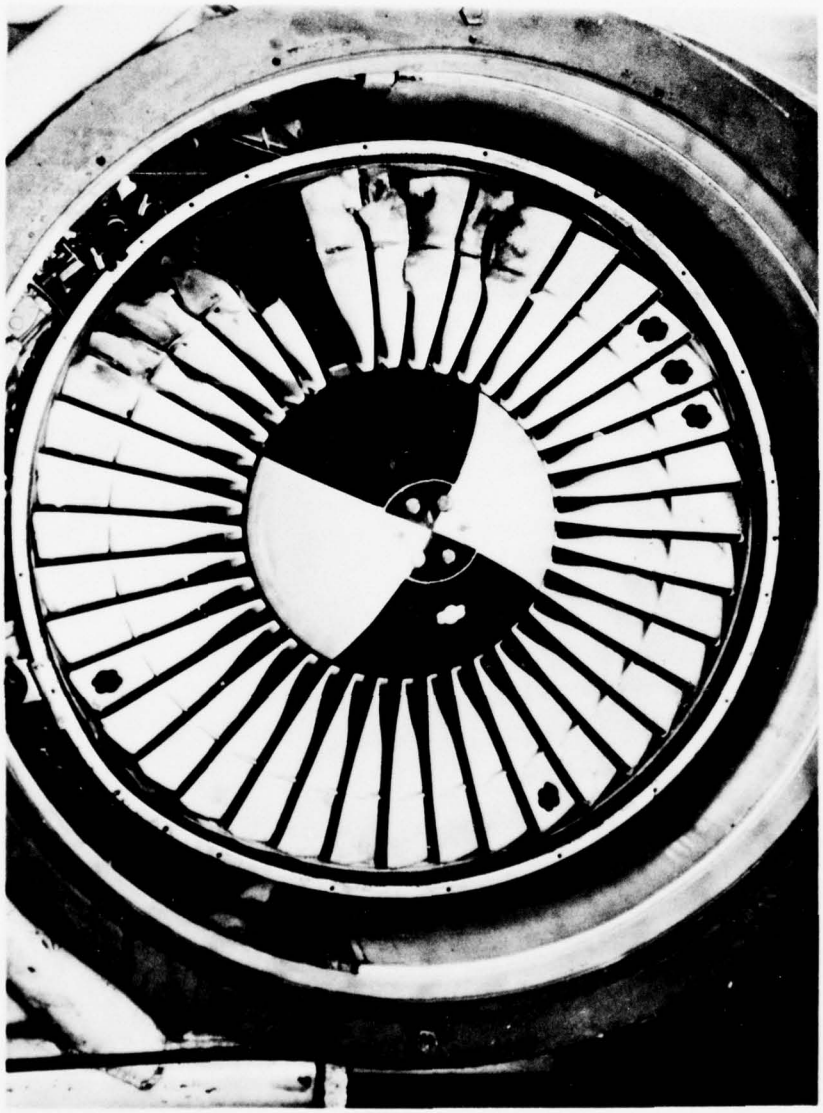

Figure 25. Fan After Large-Bird Ingestion Test, 6800 lbf.

Figure 26. Tip Damage After Bird-Ingestion Test.

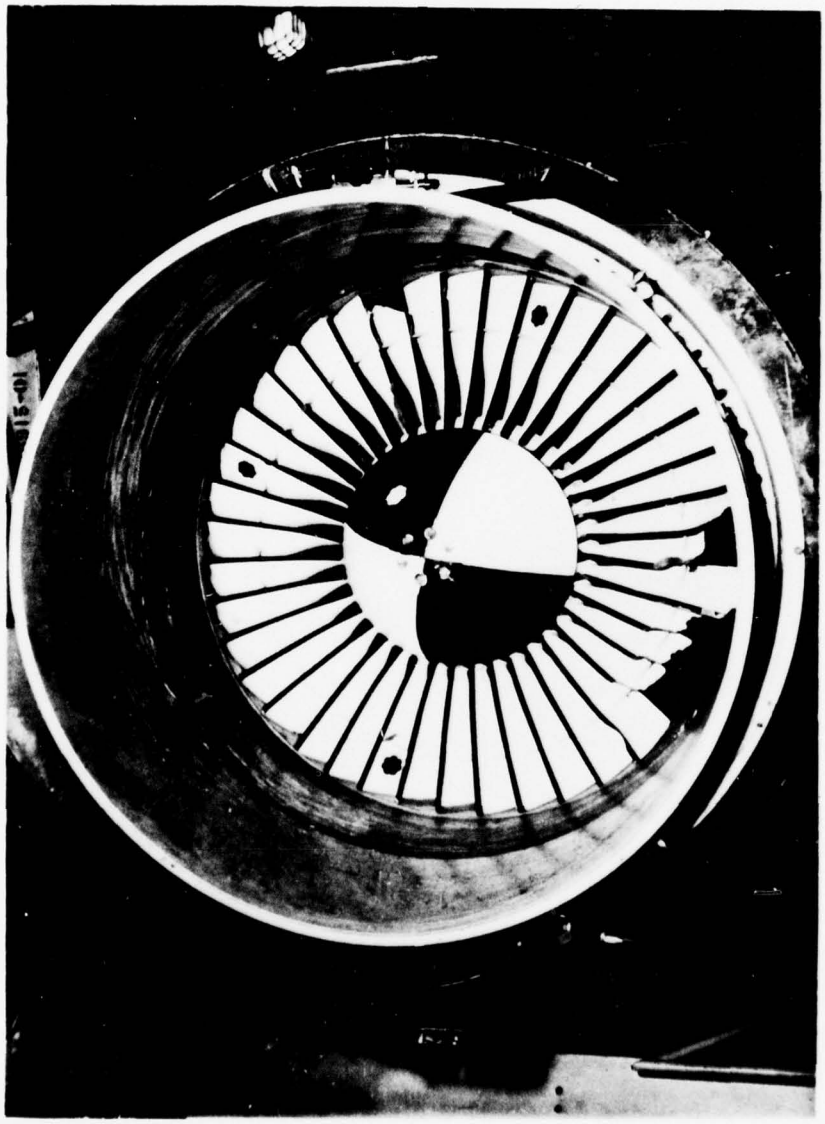

Figure 27. Fan After Medium-Bird Ingestion Test, 6800 lbf Engine.

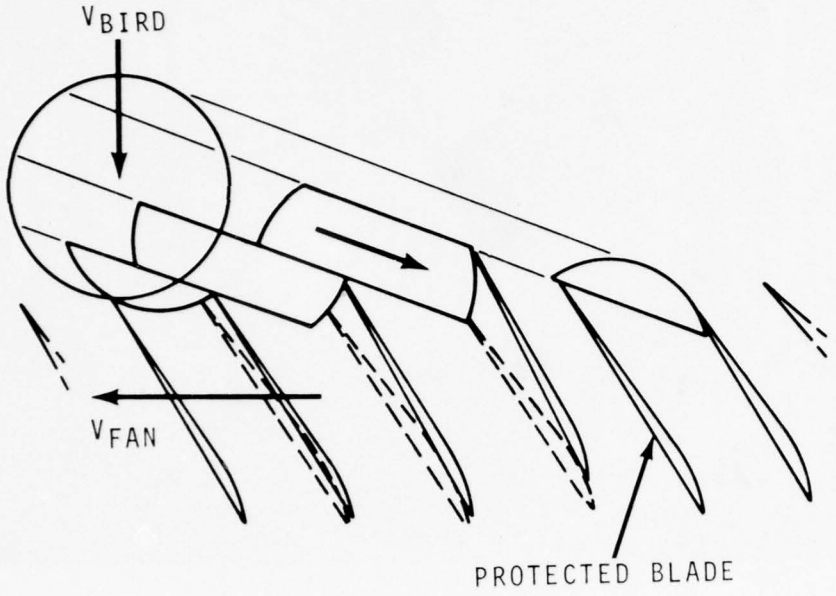

Figure 28. Blade Protection Resulting From Large Deflections.

A check of the trends towards less damage at higher ingestion velocities predicted by the analysis was made by comparing the above test - conducted at 175 knots ingestion velocity - with an identical test performed at 260 knots. (See Figure 29). Considerably less damage was sustained, as predicted.

In all the tests, the number of blades struck correlated well with the expected values.

Similarly, bird fragmentation seemed to follow the predicted behavior. Total disintegration was observed for impacts in the hub (and spinner) region, as predicted, and little or no damage was noted in the supercharger or core engine stages. Partial or no fragmentation was observed for shroud and tip strikes respectively, again as predicted. For these latter firings, local concentrated damage was noted in the exit stators behind the point of impact, confirming that little or no fragmentation occurred as the bird passed through this portion of the stage (see Figure 30).

Comparison of these failure levels with the baseline blades plotted in Figure 18 shows the original 6800 lbf blade would not adequately sustain a 1.5-pound bird strike outboard of the shroud at the FAR conditions. Scaling this blade to the 50,000 lbf thrust class machine shows the larger blade is exceptionally safe and even can be significantly lightened and still maintain adequate bird tolerance. Scaling to the 1600 lbf size, however, results in a totally unsafe blade. Even the heavier wide-chord design appears inadequate and will require further thickening for improved bird resistance. This comparison clearly illustrates the difficulty in designing bird tolerance into an engine of the small thrust classes. Redesign procedures for these blades were considered below as part of this task.

To further assist the designer in judging the safety of a given design/test combination, the observed damage was ranked according to an arbitrary damage severity code, ranging from zero for no damage to 10 for loss of a full blade (See Figure 31). The results correspond sufficiently well to permit reasonable predictions of the damage severity that can be expected in each of the three impact regions. More importantly, the chart can be used to set the airfoil thickness needed to reduce the damage to some prescribed lower level.

Shroud Strike and Outboard Strike of 1.5 lb Birds

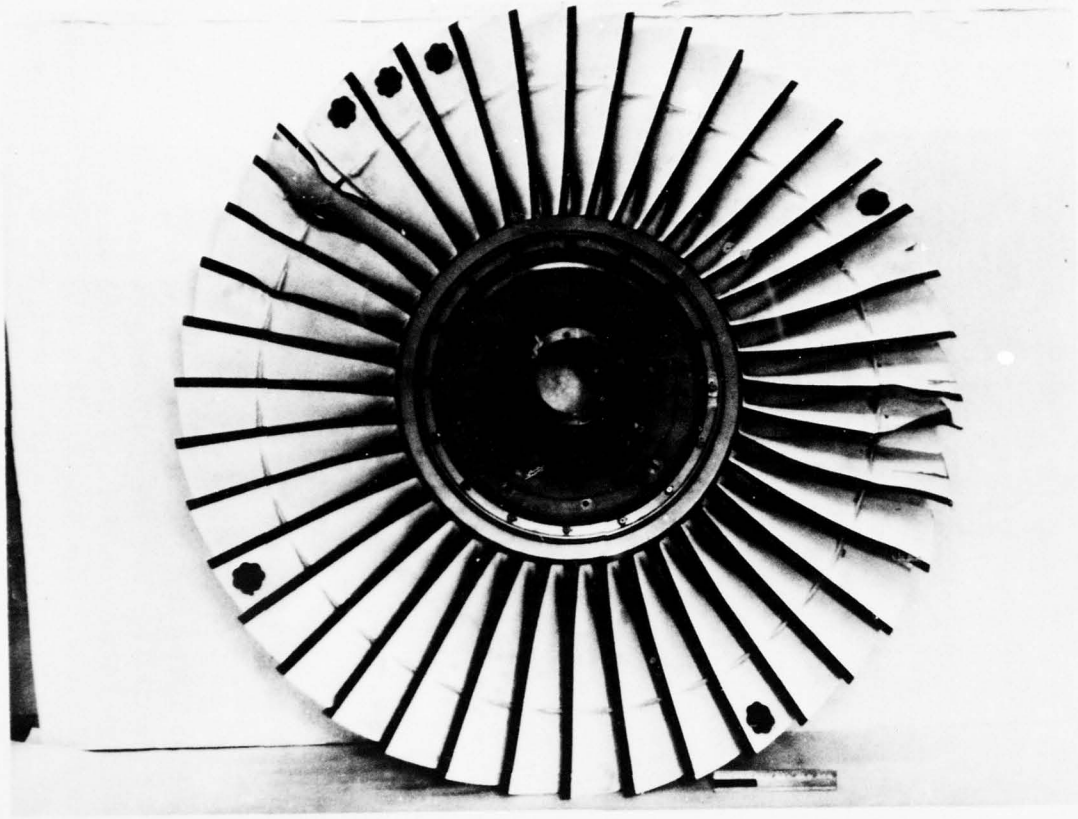

Figure 29. Fan After High-Velocity Medium-Bird Ingestion Test, 6800 lbf Engine.

Outboard Strikes of 1.5 lb Bird

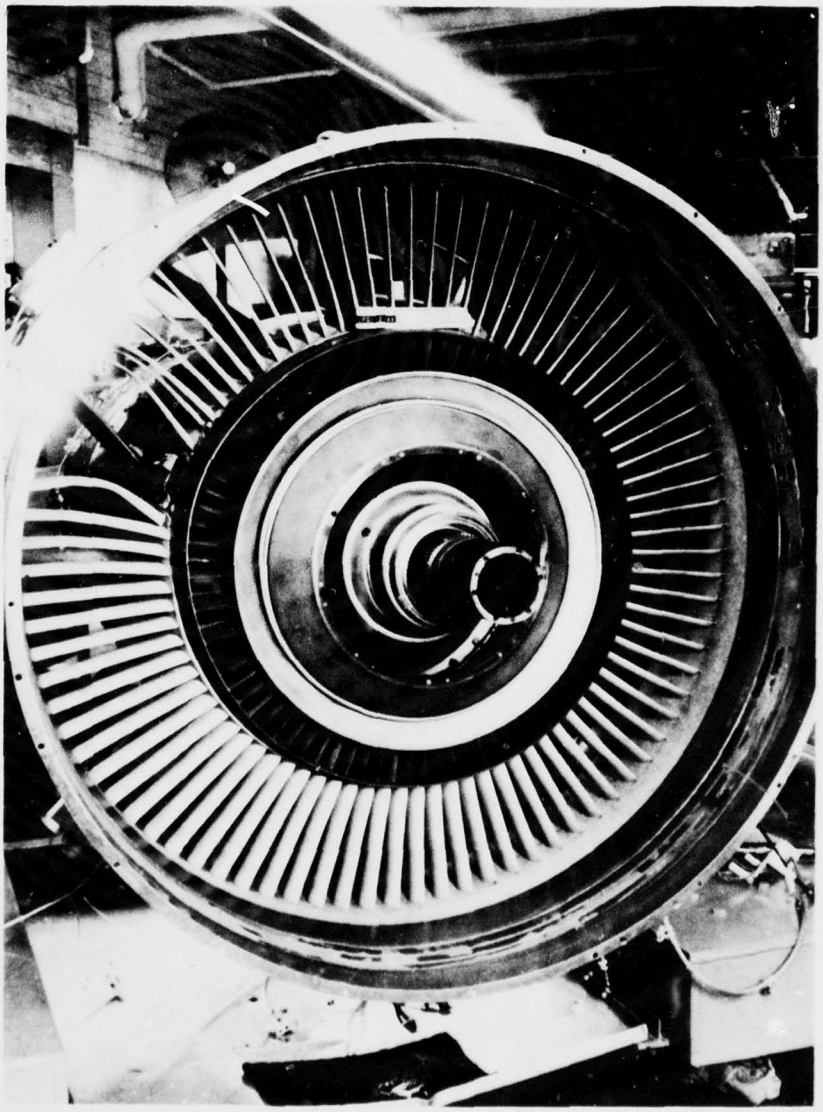

Figure 30. Damaged Fan Stator After High-Velocity Outboard Strike on Rotor Blades.

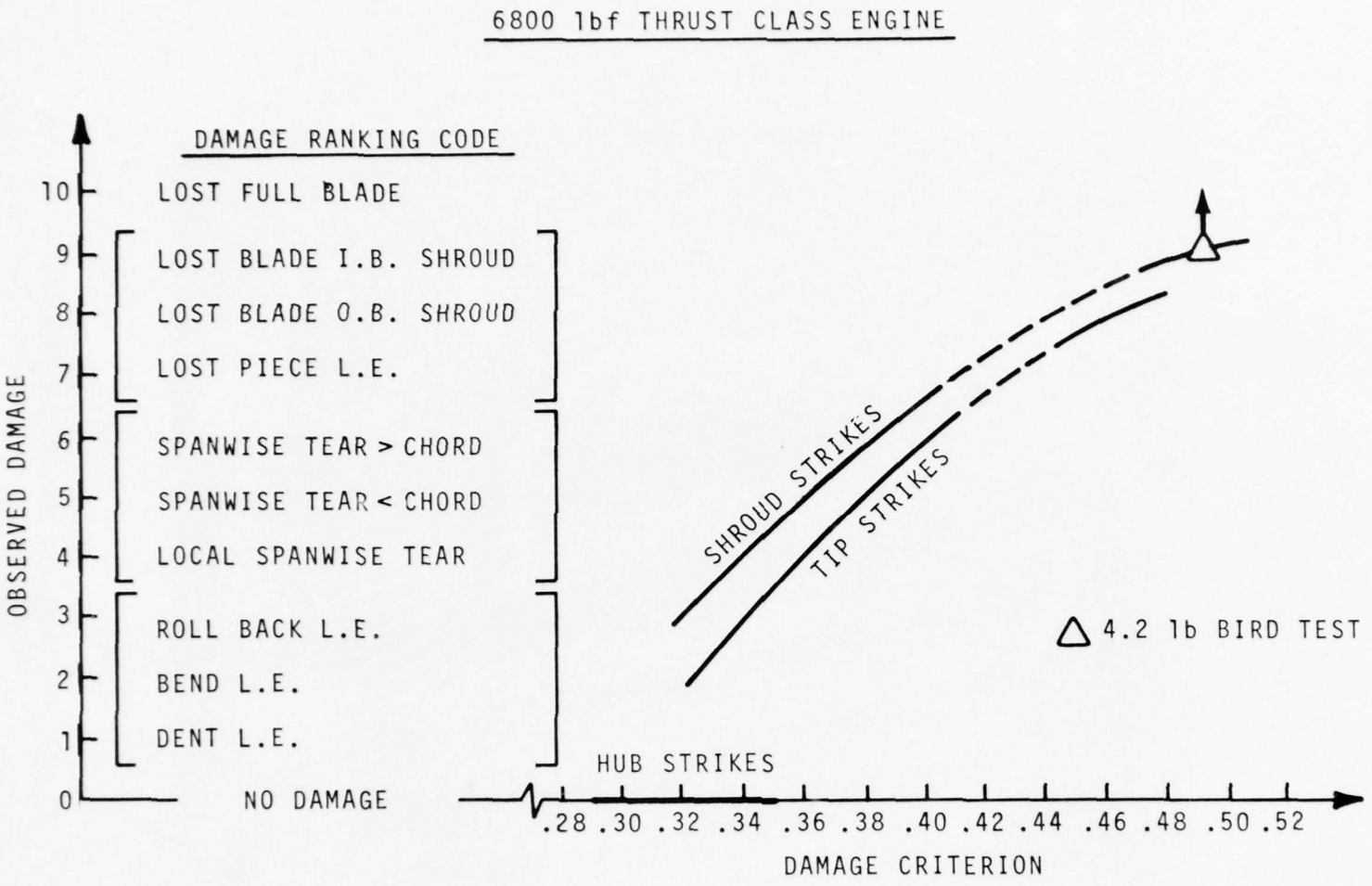

Figure 31. Medium-Bird Ingestion Damage Correlation.

It is also important to note that for similar calculated damage levels, shroud impact produced the greatest damage severity, implying that the local stress concentrating effects of the shroud more than offset the greater forces and deflections resulting from impacts near the tip. Local shroud redesign to minimize stress concentrations is indicated, as are proof-test firings aimed at the shroud region.

Airfoil Shape Considerations

The airfoils must be configured to produce the prescribed aerodynamics, to be structurally sound, and to avoid critical resonance and self-induced vibration at all running conditions, as well as being able to withstand bird ingestion damage. It should be recognized that in transonic blading, which encompasses most of the present state-of-the-art technology, the optimum aerodynamic blading is very thin and can only be increased in thickness at a cost in performance. Where damage tolerance is the prime consideration, subsonic airfoils that have a relatively thick leading edge and maximum thickness position well forward of midchord are best. Double circular arc designs are less desirable, while multiple circular arc designs with thin leading edges and maximum thickness positioned aft are least desirable from an ingestion viewpoint.

Procedures to thicken the baseline blades were studied based on the 1.5-pound bird-ingestion condition and considered separately the effects of maximum thickness, leading edge radius, chord length, and stage solidity in increments of 10 to 50 percent. Damage factor reductions were found to be essentially linear with respect to these incremental changes.

Reduction in the damage factor of almost 8 percent resulted from a 50-percent increase in maximum thickness (Figure 32). A decrease of almost 17 percent was realized with a simultaneous 50 percent increase in leading edge radius. An additional 50-percent increase in chord length (to recover the original airfoil shape) is beneficial only if the original solidity is also recovered. Very similar results were obtained regardless of position along the span.

These results point towards the use of thicker, lower aspect ratio fans of comparable solidity for improved local resistance to ingestion damage. This approach offers less performance loss - or even a performance gain if part-span shrouds can be eliminated - but will also involve increases in weight and engine length. Table 6 presents

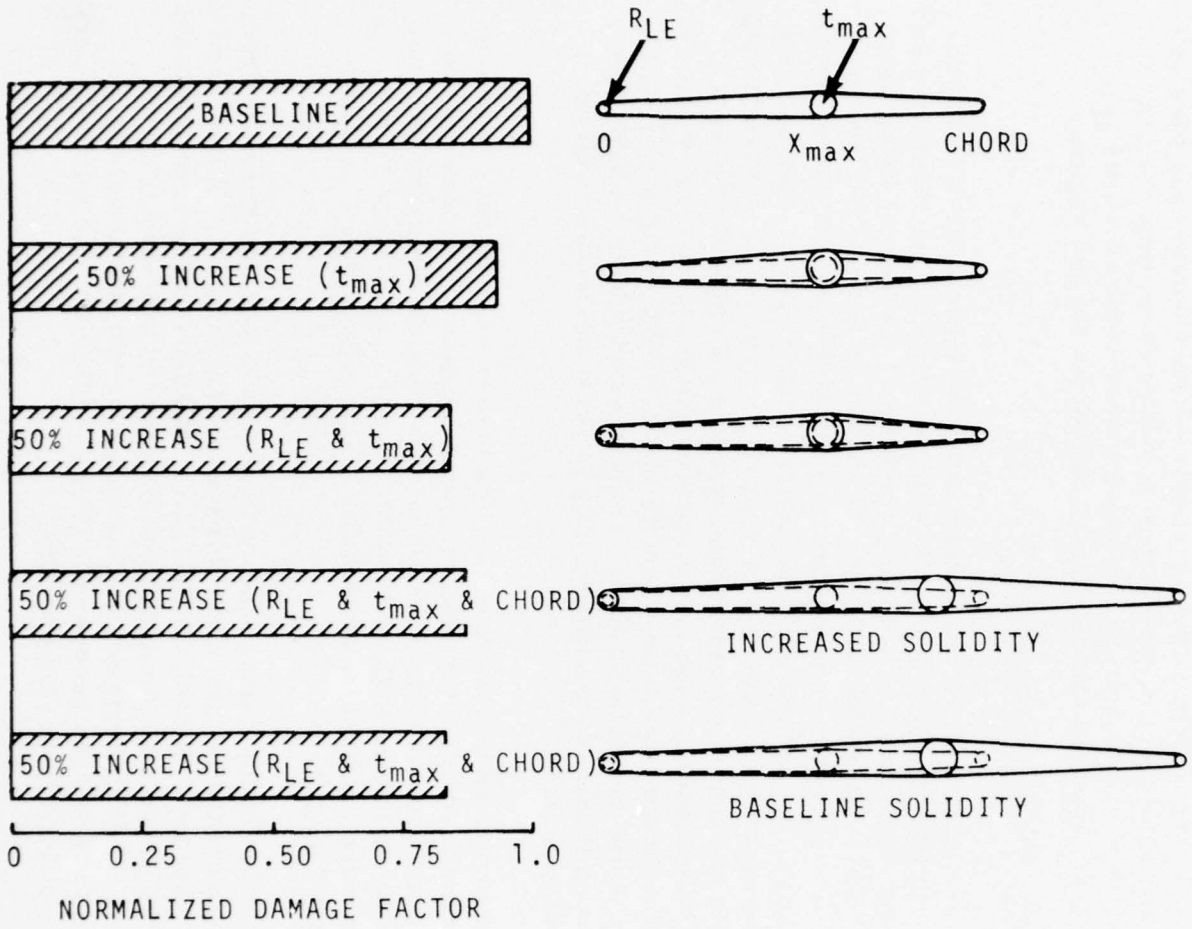

Figure 32. Results of Blade Thickness Parameter Study .

TABLE 6 - EFFECT OF VARYING BASELINE BLADE CHORD, 1600 LBF BASELINE ENGINE

Parameters	Chord Length Increase (%)		
	0	11	25
No. of Rotor Blades	40	36	32
Rotor Tip Chord	4.2	4.6	5.2
Aspect Ratio	2.9	2.6	2.3
Increased Fan Length (in.)	0	0.3	0.7
Fan Cruise Efficiency Increment* (%)	0	-0.2	-0.4

*Based on Part-Span Shroud For All Designs

a comparison of performance values for several alternate chord length designs.

It should also be noted that with fewer wide chord blades, each blade must absorb greater bird mass, possibly without benefit of midspan shroud support, so that their dynamic responses to impact may become a critical consideration. Blade dynamic response to the FAR ingestion conditions were considered below as part of this task.

Blade Support Considerations

Separate consideration was given to the design of the blade supports and constraints which are expected to play an important role in the blade's response to foreign-object impact, but whose effects were not included in the local shear-damage criterion analysis.

Much of the analyses on blade shroud constraints was performed using a standard Lycoming blade-design computer program which is based on a strength of materials approach that treats a blade as a twisted, rotating cantilevered beam with variable section properties and takes into account the steady-state shroud and aerodynamic forces and centrifugal restoring moments. Local (static) impact forces and moments can be applied at any section, and the resulting stress distributions and shroud and root reaction forces can be determined by this method.

The local impact sites and peak force levels imposed in these analyses were determined from the normal deceleration loads developed by a bird center slice in accordance with the appropriate FAR ingestion conditions.

The NASTRAN stress analysis program was also used to spot-check the trend results predicted by the blade design program and to more accurately assess local stress concentration effects. Reference 18.

Impact Force Analysis - The mass of a fully fragmented or zero-stiffness spherical bird striking a flat rigid wall is decelerated over the distance $d_s = d_q$ (Figure 33). If the bird doesn't fragment at all, i.e., a semi-rigid bird, the mass will be stopped in some smaller distance, $S = \beta \ d_s$, where β is taken as 0.25 consistent with the fragmentation behavior applied to the caliber density relation (Refer to Equation 8.) Here again, the tendency for birds to remain whole up to normal impact speeds of 260 ft/sec and to be fully disintegrated

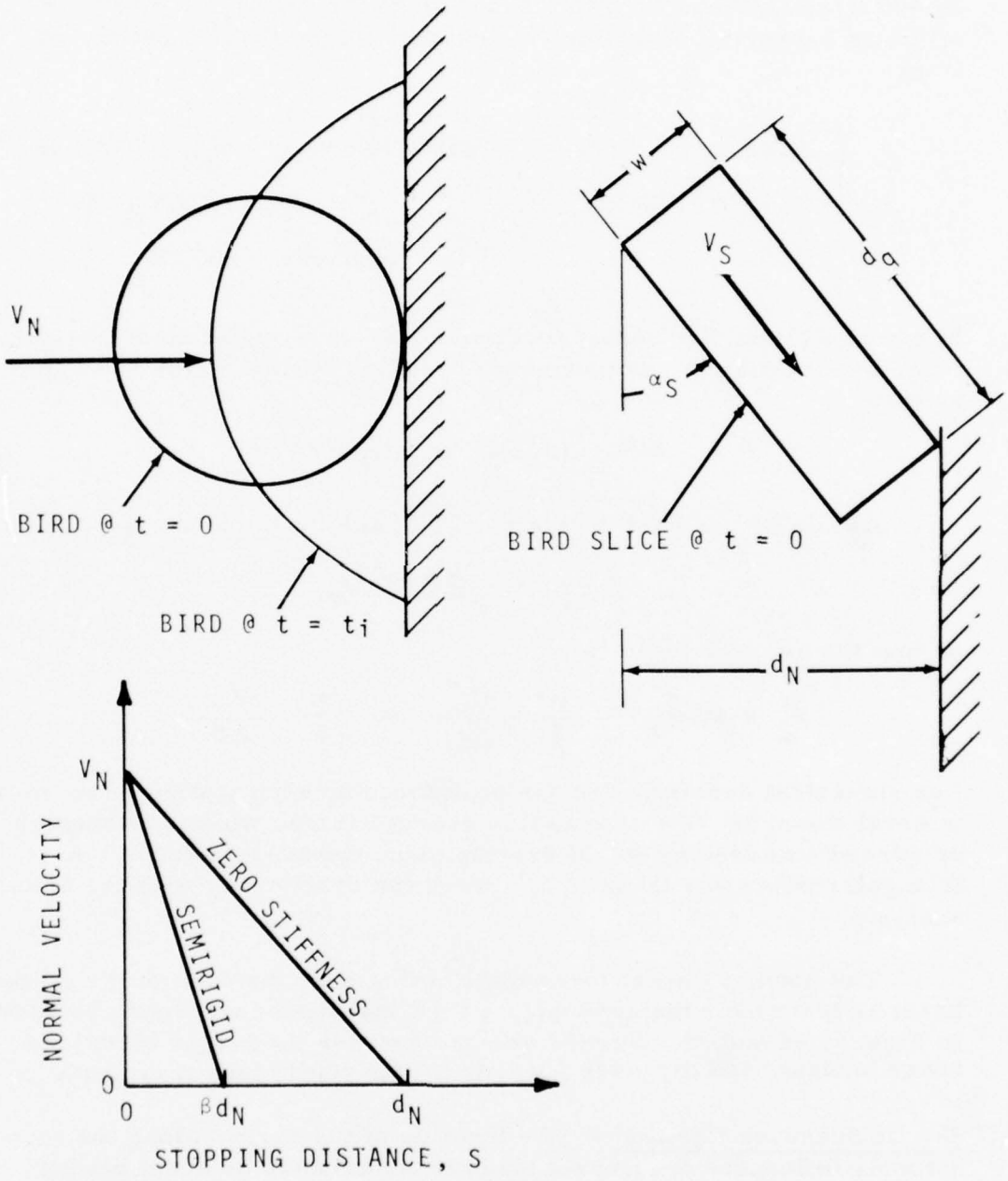

Figure 33. Decelaration of Bird Slice Normal to a Rigid Wall.

by 400 ft/sec may be used to fix the limits for semirigid and zero-stiffness behavior. The stopping distance S may then be estimated from

$$\beta = \begin{cases} 0.25 & \text{"semirigid"} \quad V_N \leq 260 \text{ ft/sec} \\ -1.15 + 0.0054\, V_N & 260 < V_N < 400 \\ 1.0 & \text{"zero stiffness"} \quad 400 \leq V_N \end{cases}$$

For a bird slice, the impact force imposed on a (rigid) blade results from decelerating the component of the slice normal to the surface, so that

$$d_N = w \cos\theta_s + d_Q \sin\theta_s \qquad (10)$$

Assuming constant deceleration, $\bar{a}$, the duration of impact becomes

$$\Delta t_i = 2S / V_N$$

so that the average force is

$$\bar{F}_N = m \bar{a}_N = \frac{W}{g} \frac{V_N}{\Delta t_i} = \frac{W}{g} \frac{V_N^2}{2S} \qquad (11)$$

For sinusoidal deceleration, the peak force developed during the impact interval would be $\pi/2$ times this average force, while a triangular or versed sine loading would develop twice the average force. A triangular pulse was taken in this work for consistency with the criteria analysis.

The normal impact force distribution over the span of the three baseline blades for the appropriate FAR ingestion conditions are shown in Figures 34 and 35. Forces are greatest for the larger birds (and fewer blades), and increase towards the tip where less fragmentation occurs.

Shroud Spanwise Position - The location of the shroud along the span strongly influences the impact loads transferred to adjacent blades and, consequently, the deflection behavior of the struck blade. For a (static) evaluation of the role played by the shroud position, the 6800 lbf baseline blade was investigated for two alternate shroud positions -

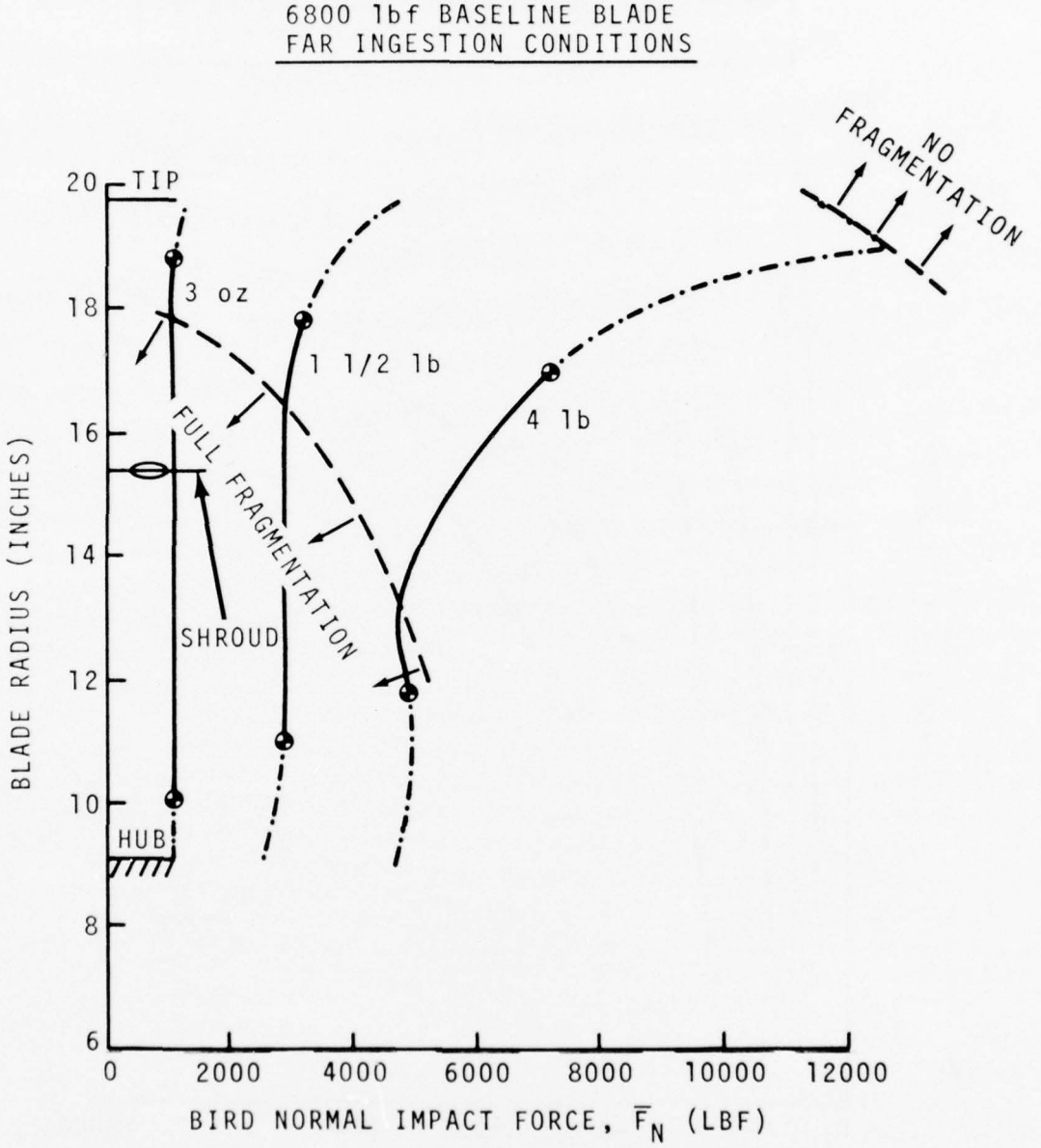

Figure 34. Impact Force Distribution - 6800 lbf Baseline Blade.

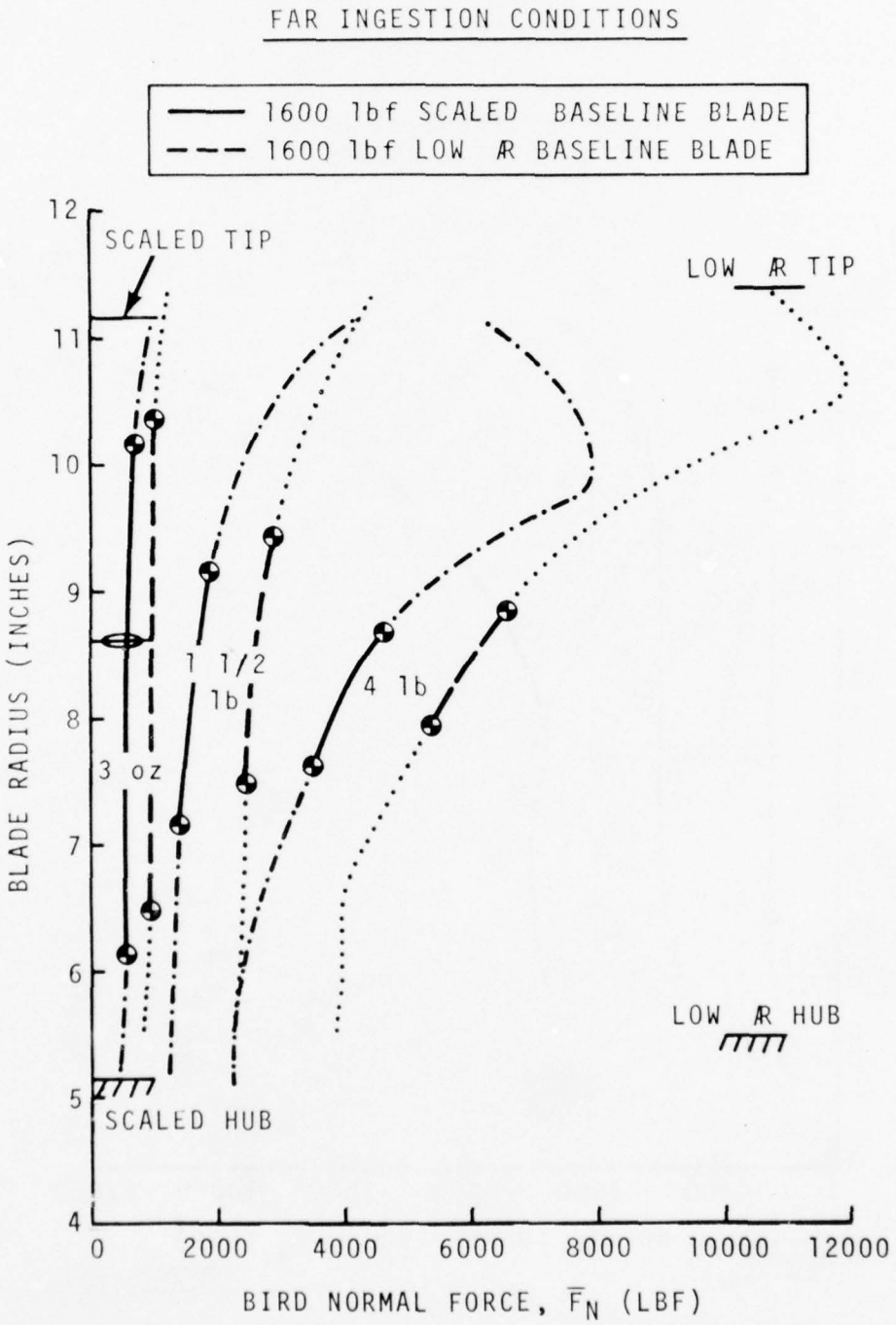

Figure 35. Impact Force Distribution - 1600 lbf Baseline Blades.

at 75 percent span and 100 percent span. Forces used in the analysis correspond to strikes near the tip (80% span) and hub (30% span) in accordance with the FAR 1.5-pound bird-ingestion requirements. In all cases, the shrouds were held fixed in the tangential and axial directions to simulate dynamic boundary constraints in effect during the short-duration impact pulse.

NASTRAN analyses were also performed to check the trends indicated by the standard blade design computer program. The 6800 lbf baseline blade was represented by the 204 triangular bending plate elements shown in Figure 36. Nodes along the hub were fully constrained to model a built-in root. Three nodes at each shroud location were fixed in the tangential and axial directions only, as in the beam program, to simulate the shroud constraint during the impact pulse.

The changes in maximum stresses for various combinations of shroud positions and impact sites are compared in Figure 37. The normalized stresses shown are based on the maximum free-beam root stresses calculated by the two methods. The trends predicted by the design program are seen to be in excellent agreement with the NASTRAN solutions.

The results show first that shrouds are beneficial in reducing the blade overall bending stress levels and second that the most detrimental strike location is near the tip.

Displacements of the blade elastic axis are shown in Figure 38 for the three shroud locations. The results confirm the intuitive expectation that minimum deflection of the struck blade - hence maximum load transfer to adjacent blades - takes place with shrouds at or just below the impact site. Further, since maximum impact forces, blade deflections, and root bending stresses occur for strikes near the tip, an optimum spanwise location of the shrouds would be 2 to 2.5 inches from the tip (to accommodate medium-to-large bird impact) or at 75 to 80-percent span for this blade.

Shroud Contact Angle - A study similar to the above was performed to investigate the influence of the shroud contact angle on the deflection and stresses in the struck blade. The same programs were used, but now the shroud boundary constraints were relaxed to permit the shrouds

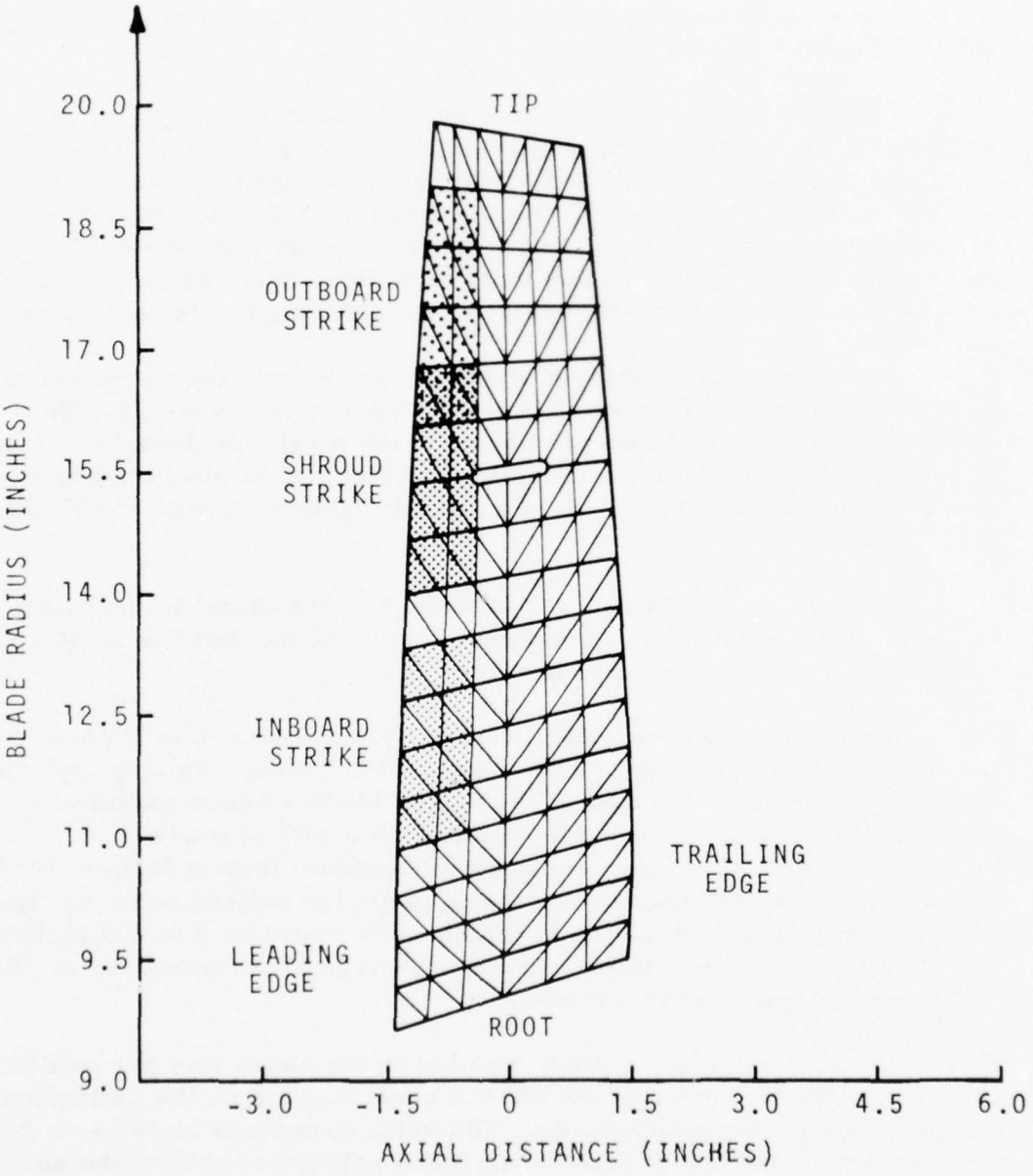

Figure 36. Element Breakup of 6800 lbf Baseline Blade.

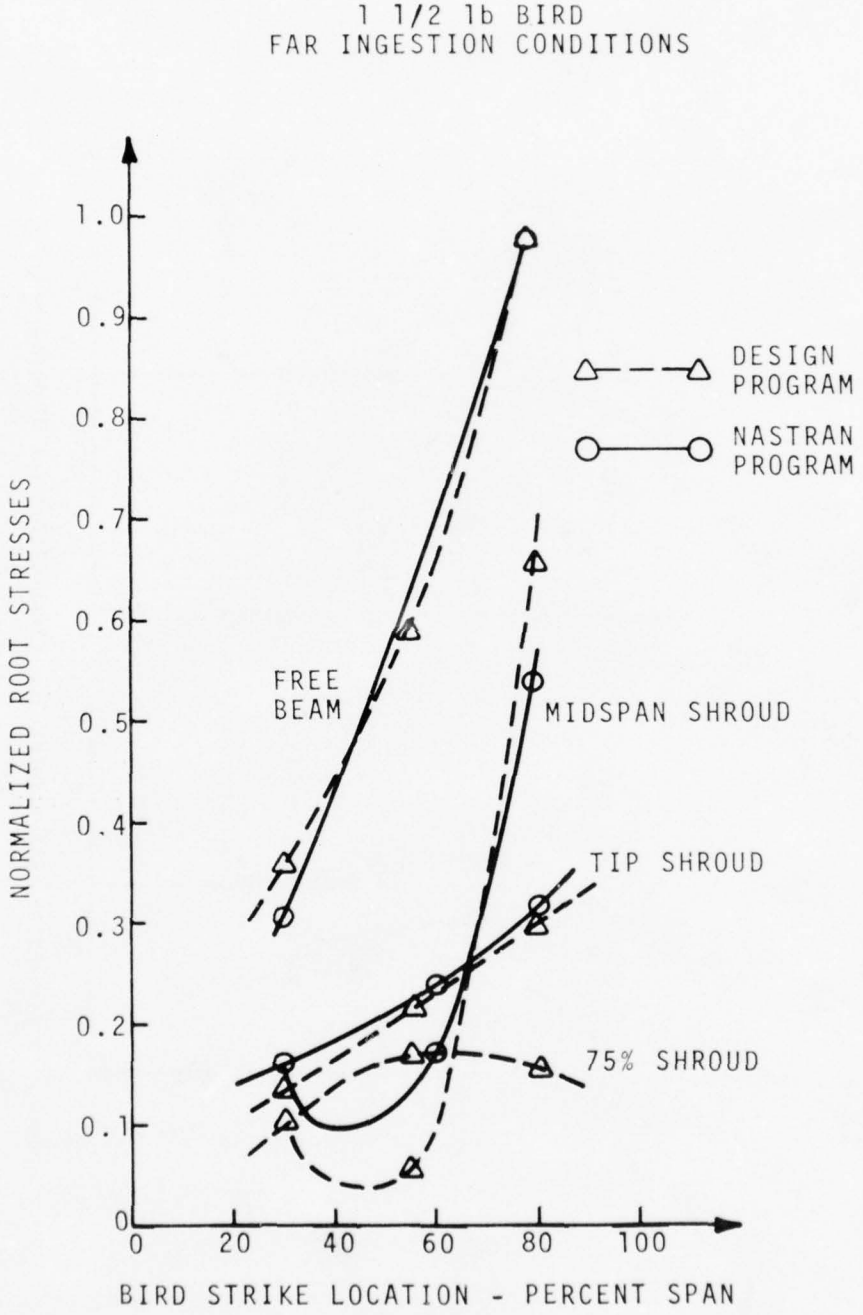

Figure 37. Root Stresses Versus Bird Strike Location.

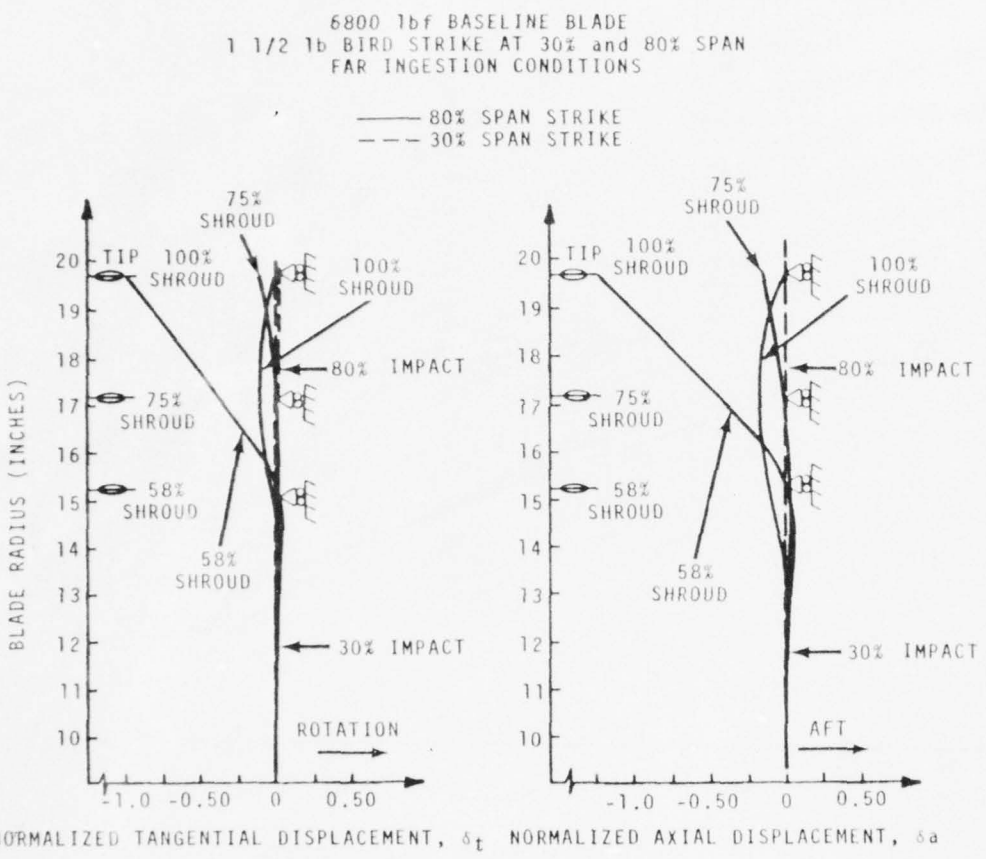

Figure 38. Blade Displacements for Various Shroud Locations.

to displace along the contact angle line, thereby approximating blade motion after impact (See Figure 39).

The displacements of the 6800 lbf baseline blade elastic axis are shown in Figure 40 for strikes at 80 and 30-percent span. Here again, the results have been normalized for the baseline tip displacements in the tangential direction. The increased flexibility provided by the larger contact angles is apparent. Mechanical assembly requirements limit the contact angle to approximately 40 degrees in practice, with vibration and flutter requirements being somewhat more restrictive, typically within 15 to 35 degrees. From these results, it is seen that the contact angle can provide the designer with some measure of controlling the deflection of the struck blade. For example, if tip impact causes blade loss above the shroud, the contact angle can be increased to provide greater flexibility at the shroud with correspondingly greater load transfer towards the root. For blade failures near the root, on the other hand, the shroud angle may be decreased in order to restrict overall blade motion, thereby transferring a larger portion of the load out through the shrouds.

As a design guide for maximum flexibility of the blade, the shroud contact angle should be normal to the minimum axis of the struck airfoil section.

Shroud Chordwise Position - The NASTRAN program was used to determine an optimum chordwise position for the shrouds in lieu of the blade design program, since the local stress patterns are of concern for this aspect of the shroud study. Here again, the 6800 lbf baseline blade was defined by the same triangular bending plate mesh, built-in rigidly at the hub, and fixed only in the tangential and axial directions at the shroud radii to simulate the short-time dynamic restraint conditions. Three shroud positions were considered, 33-percent chord, 50-percent chord, and 67-percent chord.

The maximum stresses in the blades, normalized with respect to the 50-percent chord results are shown in Figure 41. The midchord position resulted in the lowest peak stress for all strike locations studied, implying that the best chord position for the shroud is away from the impact site but near the section's maximum thickness point. The worst shroud location, especially for tip strikes, is forward near the thin leading edge.

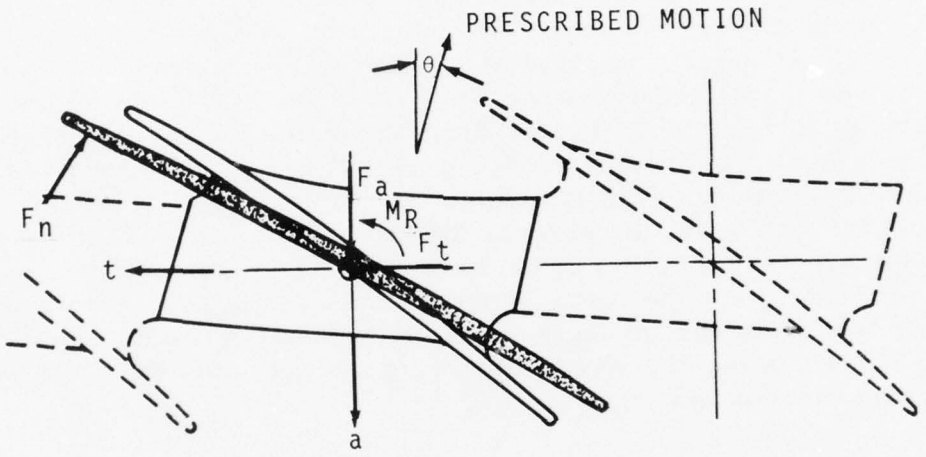

(a) 80% SPAN STRIKE

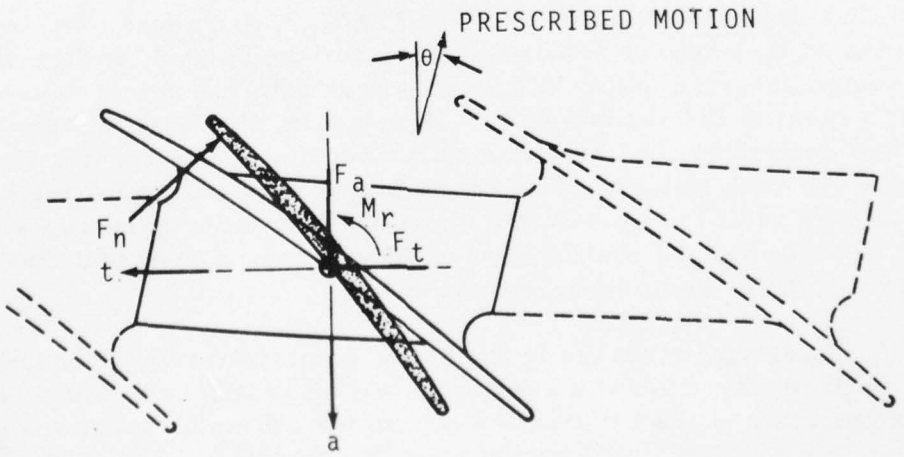

(b) 30% SPAN STRIKE

Figure 39. Shroud Contact Angle and Reaction Forces.

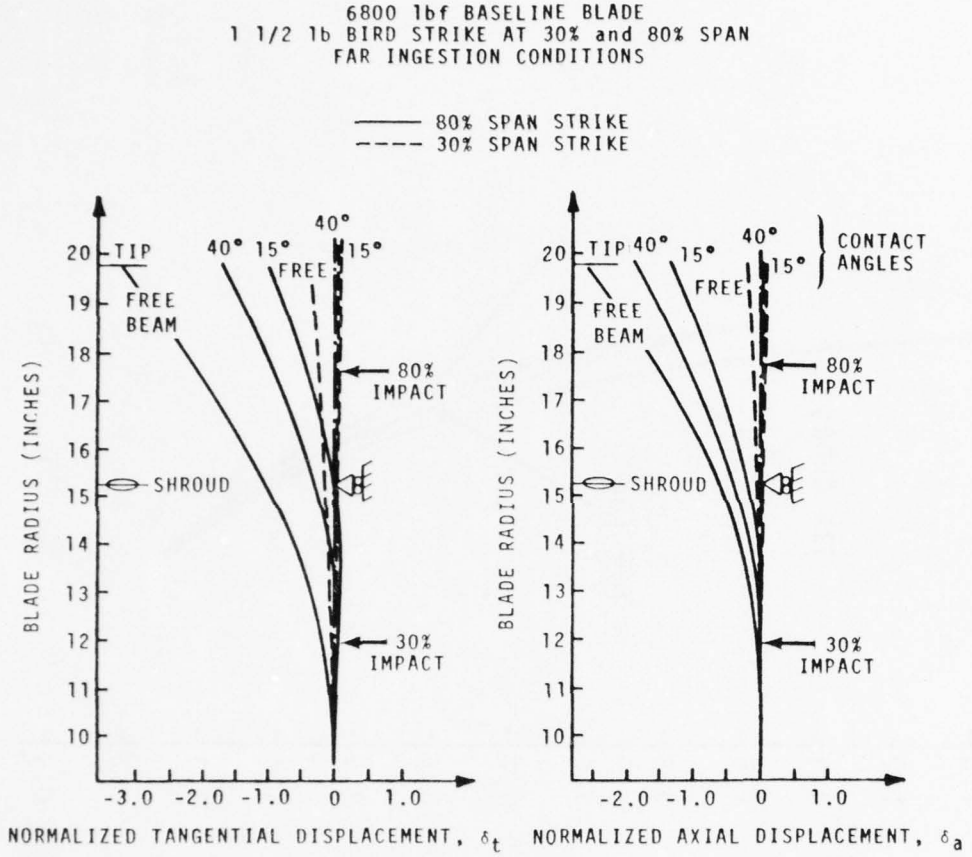

Figure 40. Blade Displacements for Various Shroud Contact Angles

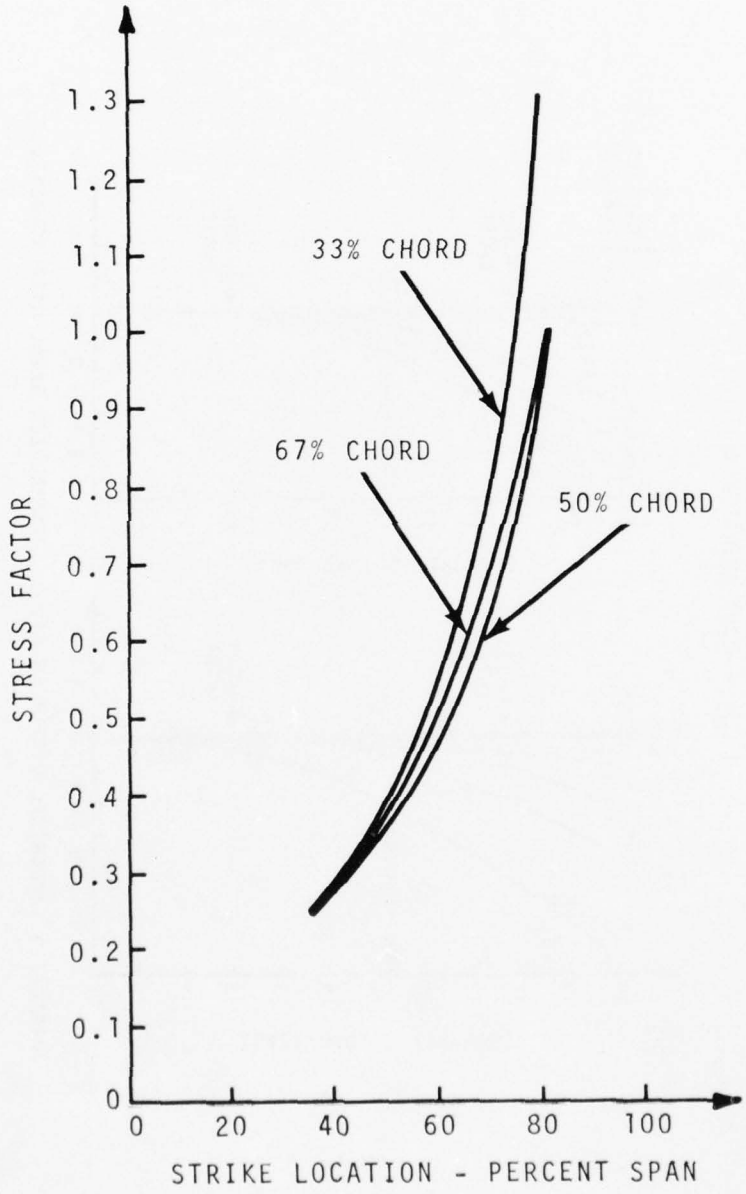

Figure 41. Blade Stresses Versus Shroud Chordwise Location.

Blade Root Cone Angle - A consideration also investigated through the use of the NASTRAN program was the effect of the root cone angle on the blade's behavior. An extreme case of zero degree root angle was run for comparison with the 18-degree angle prescribed for the baseline blade. The modified blade was represented by the same number of nodes and triangular bending plate elements; the same loading and boundary conditions were imposed.

The simulated bird strikes at the 30- and 80-percent span sites resulted in very minor changes in deflection and stresses between the two models, indicating this parameter has a negligible influence on a blade's resistance to bird-ingestion damage.

Multiple Strike Probability

The preceding damage analyses are based on a single impact on undamaged blades. These paragraphs discuss the possibility of a blade being struck more than once by successive birds entering the stage.

A local blade region that is permanently deformed by a bird strike will present a more unfavorable incidence angle to a subsequent impact, should it occur in the same location along the span. A greater damage intensity would therefore be expected from the second impact than from the first, which would then be superimposed over the previous damage. Leading edges torn by the first impact, for example, would be expected to separate entirely if struck again. Such damage has been noted in small-bird ingestion tests where sixteen 2 to 4 ounce birds were fired into the annular area between the hub and tip of the 6800 lbf thrust baseline fan. (See Figure 42.)

Shingling of blades should also be avoided, not only to maintain vibration/flutter control of the blades during post-ingestion operation, but also because the adjacent blades may no longer be supported adequately to absorb the possible impacts of successive birds.

Estimates of the probability of a blade sustaining multiple strikes when more than one bird is ingested were made using a numerical strike simulation program developed at Lycoming. Input to the analytical model consists of a frequency table describing the probabilities of a given integral number of blades being struck by a

Sixteen 2-4 oz Birds Fired Into Blade Annulus

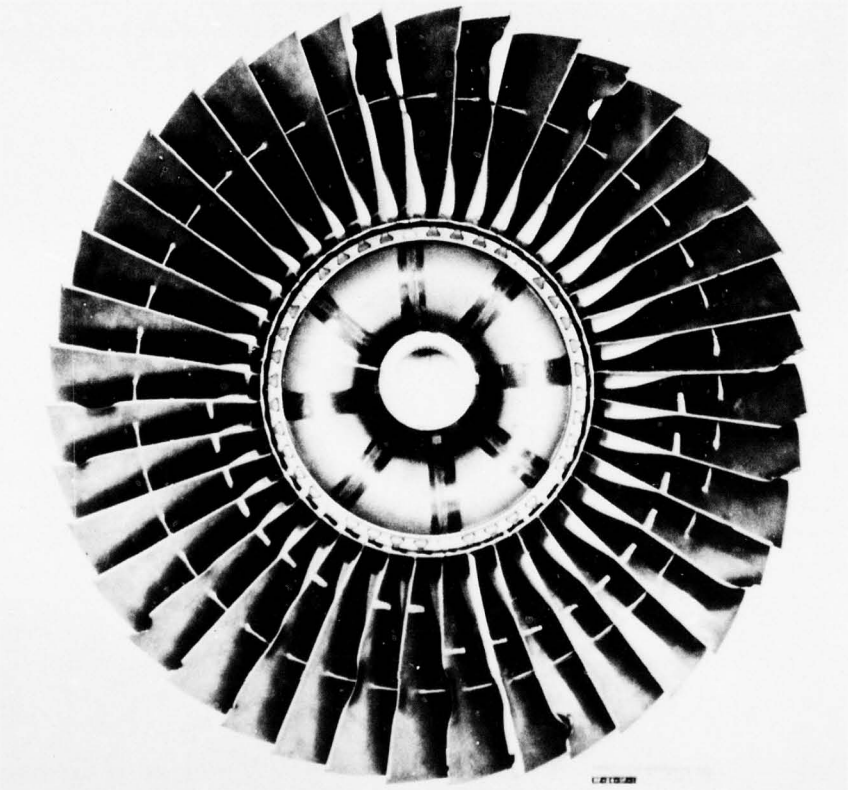

Figure 42. Fan After Small-Bird Ingestion Test, 6800 lbf Engine.

single bird (n_B of equation 7), the total number of birds being ingested (per FAR 33.77 requirements of Table 4), the total number of blades in the fan stage and the size of the spinner area with respect to the total inlet area. Two random numbers are generated to determine for each strike in the blade annulus the quantity of blades struck and a primary blade number or position in the fan. The position and each subsequent position for all struck blades in the stage are incremented by one, and the process repeated for the number of birds ingested. Each blade in the array is examined for the number of simulated strikes and the results tabulated. This tabulation is then repeated until a total of 100 simulated ingestion conditions are made. The results are an average of these 100 samples.

Histograms of the number of blades sustaining multiple strikes are shown in Figures 43 through 45 for the three baseline engines. These predictions imply that when the 6800 lbf fan ingests three 1.5-pound birds striking at random over the inlet area some 23 blades (out of 40) will not be struck at all, while 14 blades will be struck once. Another 2 blades are expected to be struck twice - although not necessarily in the same place along the span. It is also possible that on occasion one blade may be struck 3 times.

For the 1600 lbf thrust class engine, the low aspect ratio design suffers fewer multiple strikes than the shrouded blade design, even though one additional small bird must be ingested. Because of the smaller size blading, multiple impacts on a blade are now more likely to strike the same region. This is especially true for the case of the 1.5-pound bird since this size bird extends over most of the span.

Probability tables can be constructed from these results - and from the results of a similar analysis which considers also the impact area along the span - to show the probability of a blade sustaining multiple strikes and the probability of a blade sustaining multiple strikes in the same area. (Refer to Tables 7 and 8). These results show that a 6800 lbf thrust blade has only a 5.3-percent chance of being hit more than once by a 1.5-pound bird and only a 0.8-percent chance of being hit more than once in the same area. The chances of multiple impacts in the same area by 1.5-pound birds are from 2 to 3 percent for the smaller engine.

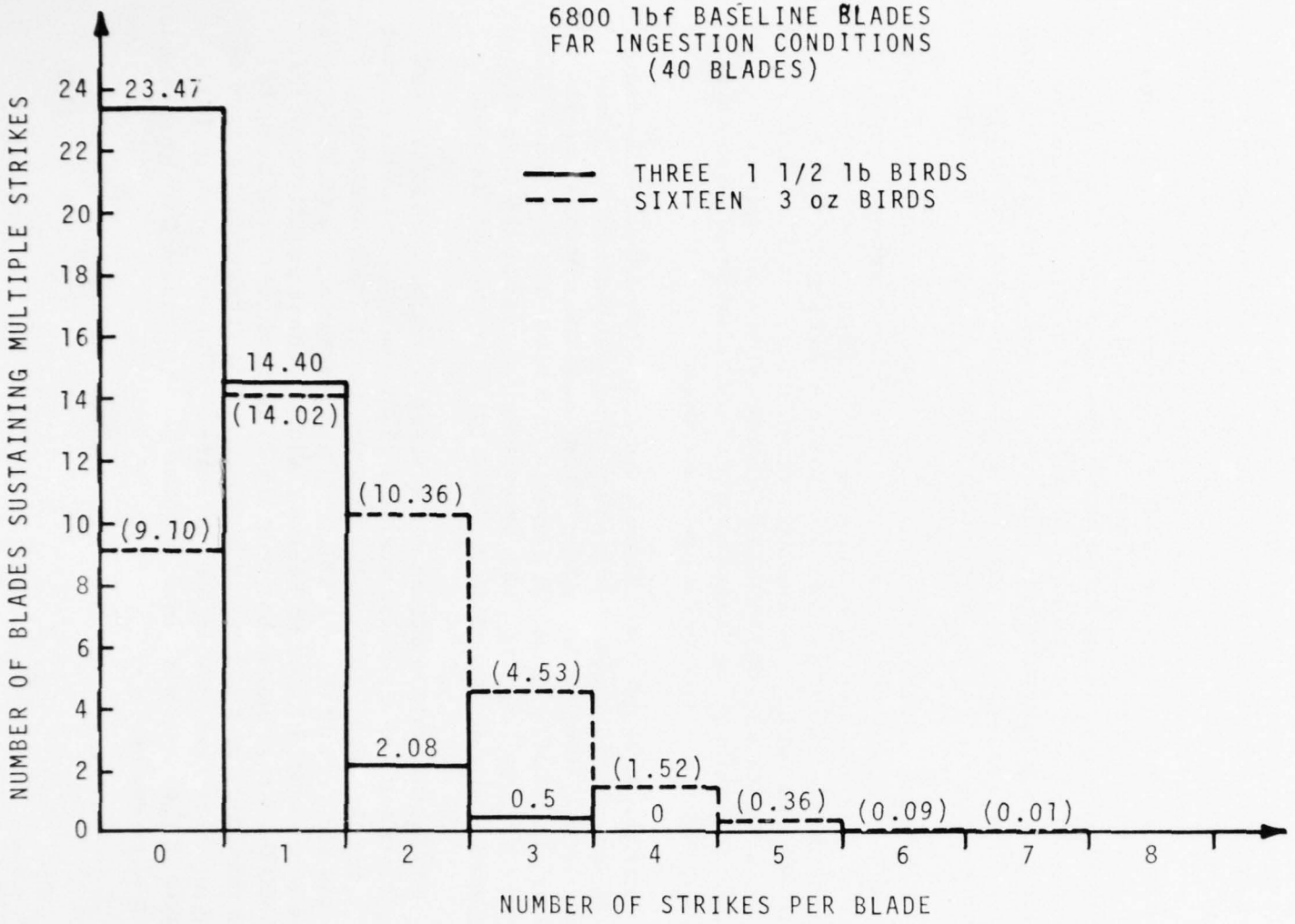

Figure 43. Number of Blades Sustaining Multiple Strikes - 6800 lbf Baseline Blades.

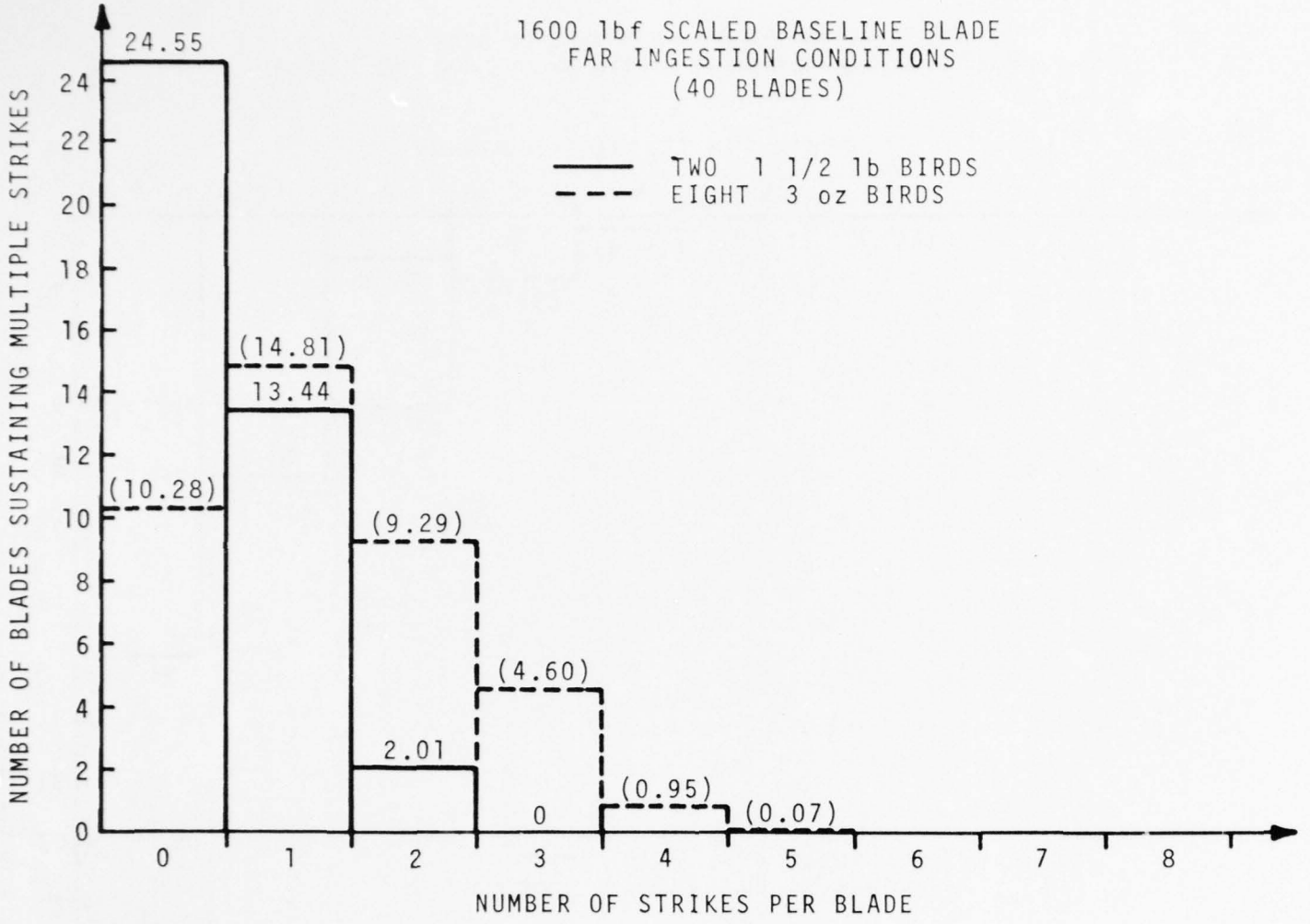

Figure 44. Number of Blades Sustaining Multiple Strikes - 1600 lbf Scaled Baseline Blades.

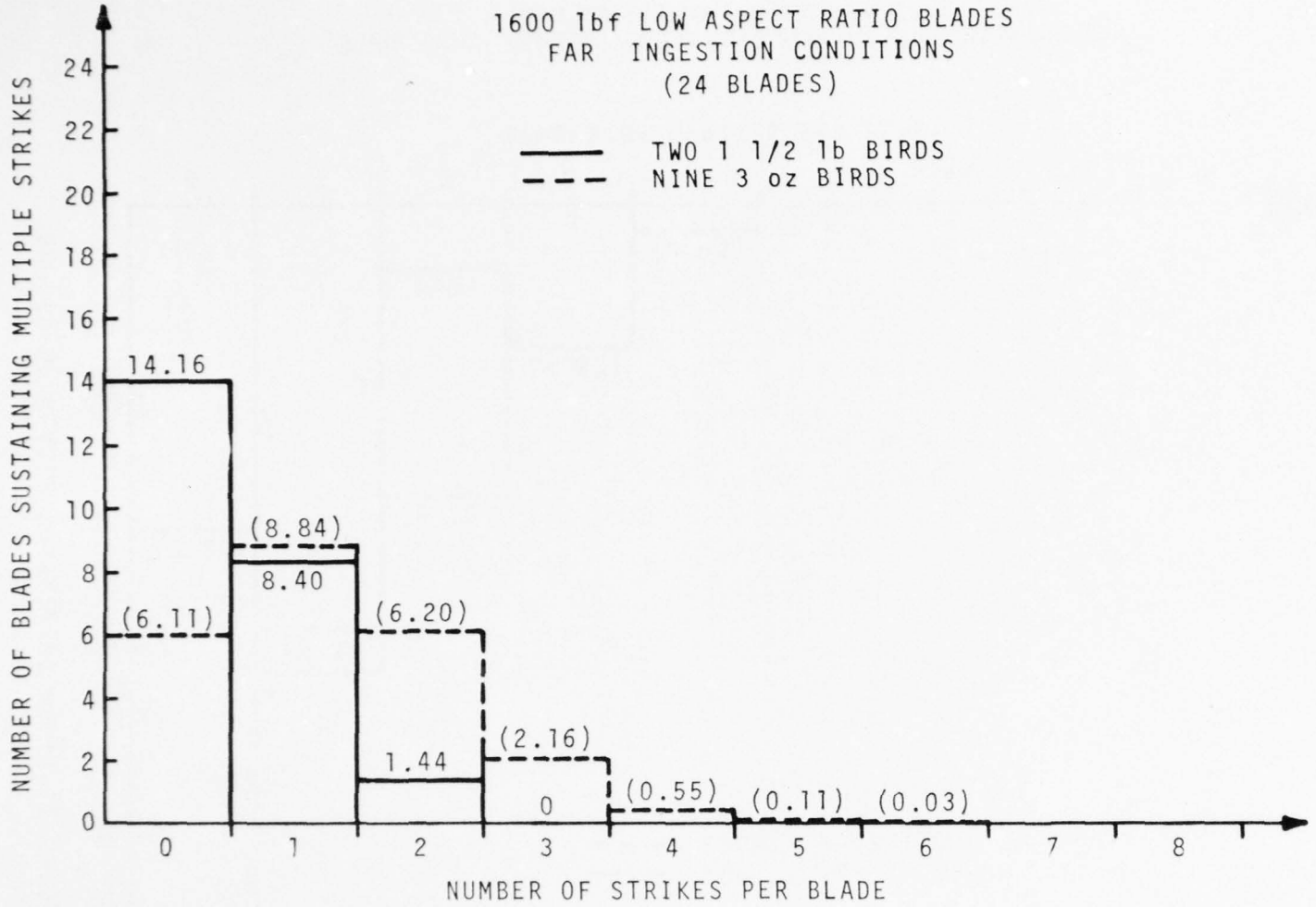

Figure 45. Number of Blades Sustaining Multiple Strikes - 1600 lbf Low Aspect Ratio Baseline Blades.

TABLE 7 - PROBABILITY OF A BLADE SUSTAINING MULTIPLE STRIKES

6800 lbf Engine		1600 lbf Engine			
Baseline Blade (40 Blades)		Scaled Baseline (40 Blades)		Low Aspect Ratio Baseline (24 Blades)	
Sixteen 3 oz	Three 1.5 lb	Eight 3 oz.	Two 1.5 lb	Nine 3 oz	Two 1.5 lb
0.422	0.053	0.373	0.050	0.377	0.060

TABLE 8 - PROBABILITY OF A BLADE SUSTAINING MULTIPLE STRIKES IN THE SAME AREA

6800 lbf Engine		1600 lbf Engine			
Baseline Blade (40 Blades)		Scaled Baseline (40 Blades)		Low Aspect Ratio Baseline (24 Blades)	
Sixteen 3 oz	Three 1.5 lb	Eight 3 oz	Two 1.5 lb	Nine 3 oz	Two 1.5 lb
0.029	0.008	0.066	0.022	0.067	0.028

BLADE DYNAMIC BEHAVIOR

The intent of the criterion approach described in the preceding section was to determine critical combinations of blade/bird ingestion conditions causing unacceptable levels of engine damage based on local bending or tearing damage in the forward parts of the blade. In this section, blade failure due to excessive bending motion is studied as an additional basis for determining unacceptable levels of engine damage. Further insight into methods for treating bird ingestion damage can also be gained with this latter approach, especially with respect to the roles played by centrifugal force, blade size and shroud/root restraints. Large displacement effects, and their influence on force generation can also be evaluated.

Transient Analysis

The transient response of fan blades to bird impact force excitation, in terms of displacement and stresses, was obtained by considering the struck blade as a series of small, multi-layered bending/shear beam elements. The theoretical analysis employed is based on an explicit incremental transient finite-element procedure described by Salus, Ip and Van Derlinden (Reference 19). The Lycoming developed computer program also accounts for centrifugal forces and large deformations. Built-in and/or pinned roller constraints were also made available for treating the root/shrouds boundary conditions.

The finite-element models used in these studies consisted of 19 elements over the span, each element being comprised of 10 layers of linearly elastic material. For simplicity, an equivalent beam thickness distribution over the span was used, based on the actual minimum moment of inertia and airfoil sectional area distributions according to

$$h_Q = \sqrt{12\, I_{min} / A} \qquad (12)$$

Essentially, this model defines the blade as untwisted and of rectangular section and is, therefore, somewhat more flexible than the actual undamaged blade. The effect of leading edge bending or rollback, which would typically tend to locally stiffen the blade, was not considered. Such local permanent deformation would be expected to reduce tip excursions but would also tend to concentrate the bending stress towards the airfoil section just inboard of the damage.

For all cases investigated, a 1.5-pound bird impact corresponding to the FAR ingestion condition was used, with the (sliced) bird mass assumed to be uniformly distributed over the outermost 4 inches of the blade. A triangular force pulse based on the rigid blade collision analysis discussed previously in the paragraph, Blade Support Considerations, was also assumed in every case. The duration of transient response studied was typically taken as approximately 6 times the impact pulse duration to ensure coverage of the full first deflection cycle.

Centrifugal Force Effects

An important feature of bird-tolerant fan blade design and analysis concerns the effect of centrifugal force on the bending behavior during and just after impact. In general, centrifugal loading will increase the blade's frequency while decreasing both deflections and stress levels, the magnitude of which will be dependent on the shape and extent of deformation in the impacted blades.

The calculated blade deformation patterns with and without the centrifugal force field are shown in Figure 46 for the 6800 lbf thrust baseline engine following ingestion of a medium bird at takeoff. Tip displacements are compared in Figure 47. It is seen that the centrifugal force has essentially no effect during the impact period. The rotating blade reaches its maximum displacement position earlier than the non-rotating blade and oscillates with a higher frequency. These effects are caused partly by the centrifugal forces acting to limit the bending excursion of the blade, and partly to the centrifugal stiffening effect that tends to increase the bending frequency, in this case, from 200 to 330 cps. These values, in fact, very nearly match the lowest natural frequencies of the actual baseline blade (205 and 310 cps).

For both running and static blades, the maximum bending stresses occur just outboard of the shroud. Also for both cases, the peak bending stress values occur at the peak displacement times, but the static blade value is 37 percent higher than the running blade (see Figure 48). The influence of the higher bending modes on the stress history is also seen in the figure.

Comparison of the centrifugal restoring force on the impact response of the 1600 lbf thrust baseline blades (scaled version) are shown in Figures 49 through 51. Note that for these smaller sized blades, a significant portion of the 1.5-pound bird impacts below the shroud. There are essentially no differences in displacements of the

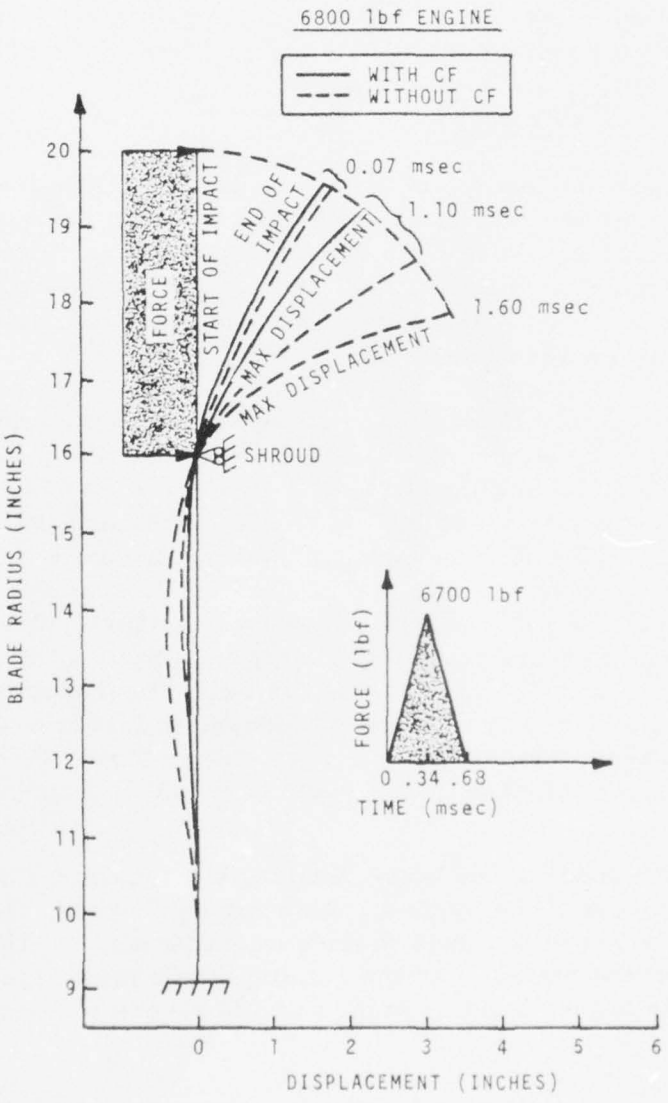

Figure 46. Centrifugal Force Effects on Transient Deformation - 6800 lbf Baseline Blade.

AD-A044 203 AVCO LYCOMING DIV STRATFORD CONN F/G 21/5
IMPROVED RESISTANCE TO ENGINE BIRD INGESTION.(U)
MAR 77 H B KAEHLER DOT-FA76WA-3806
UNCLASSIFIED FAA/RD-77-55 NL

2 OF 3
AD A044203

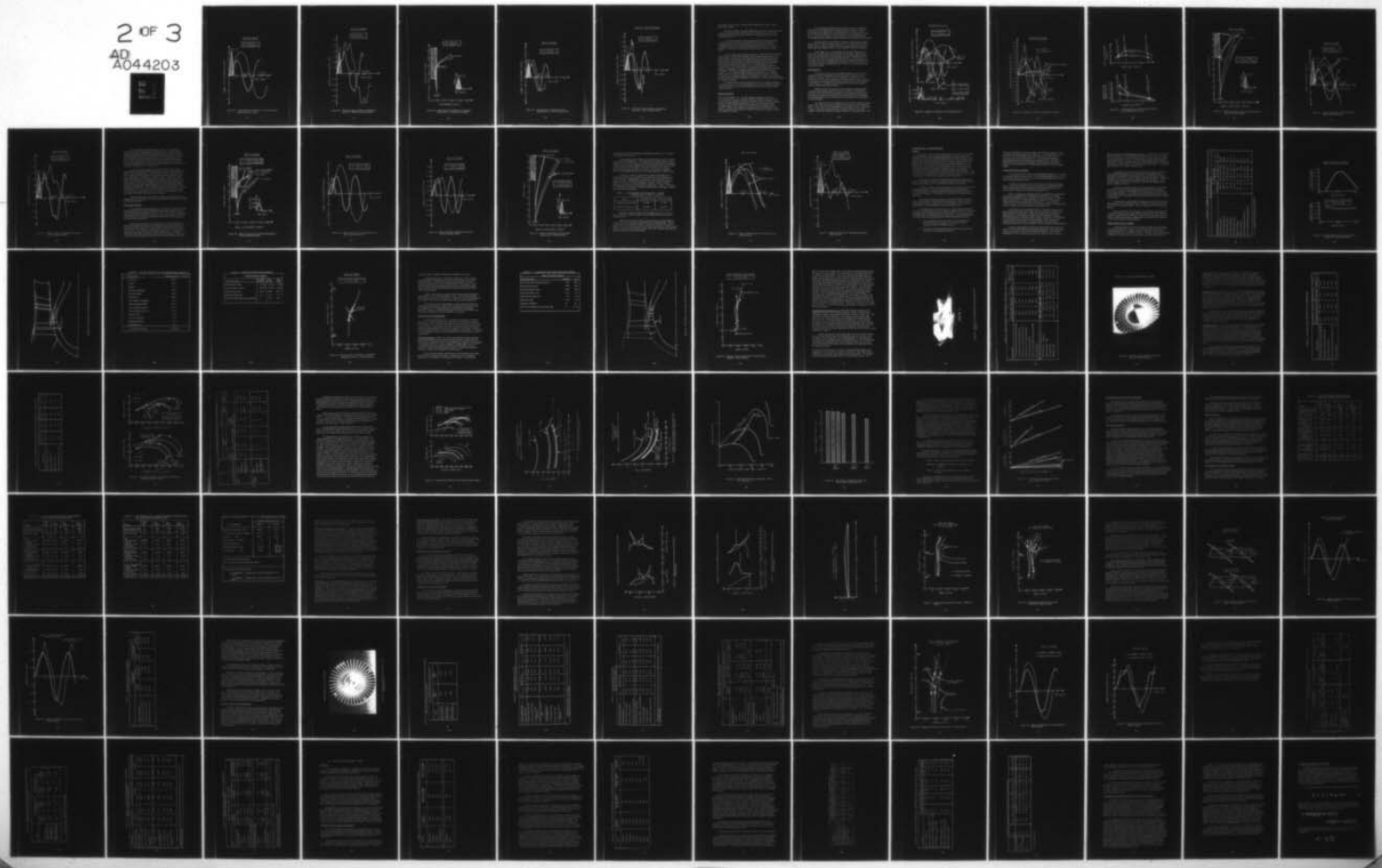

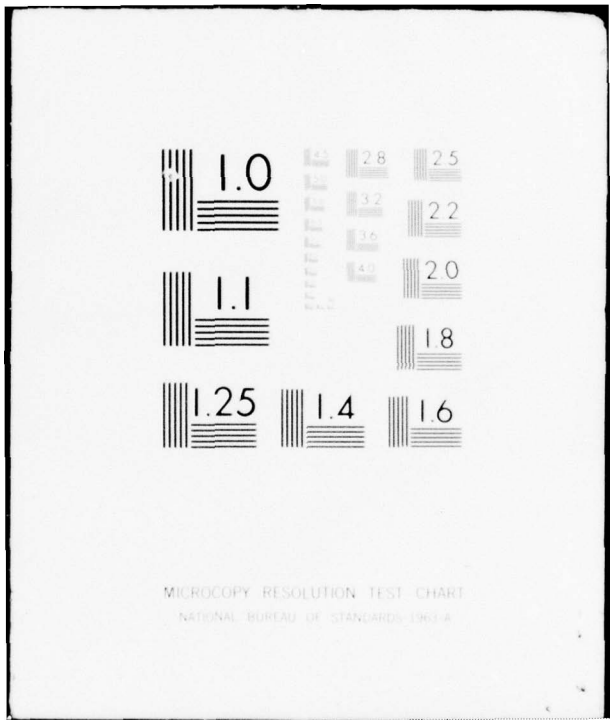
1.0
1.1
1.25
1.4
1.6
2.0
2.2
2.5
2.8
3.2
3.6
4.0
1.8
MICROCOPY RESOLUTION TEST CHART
NATIONAL BUREAU OF STANDARDS 1963-A

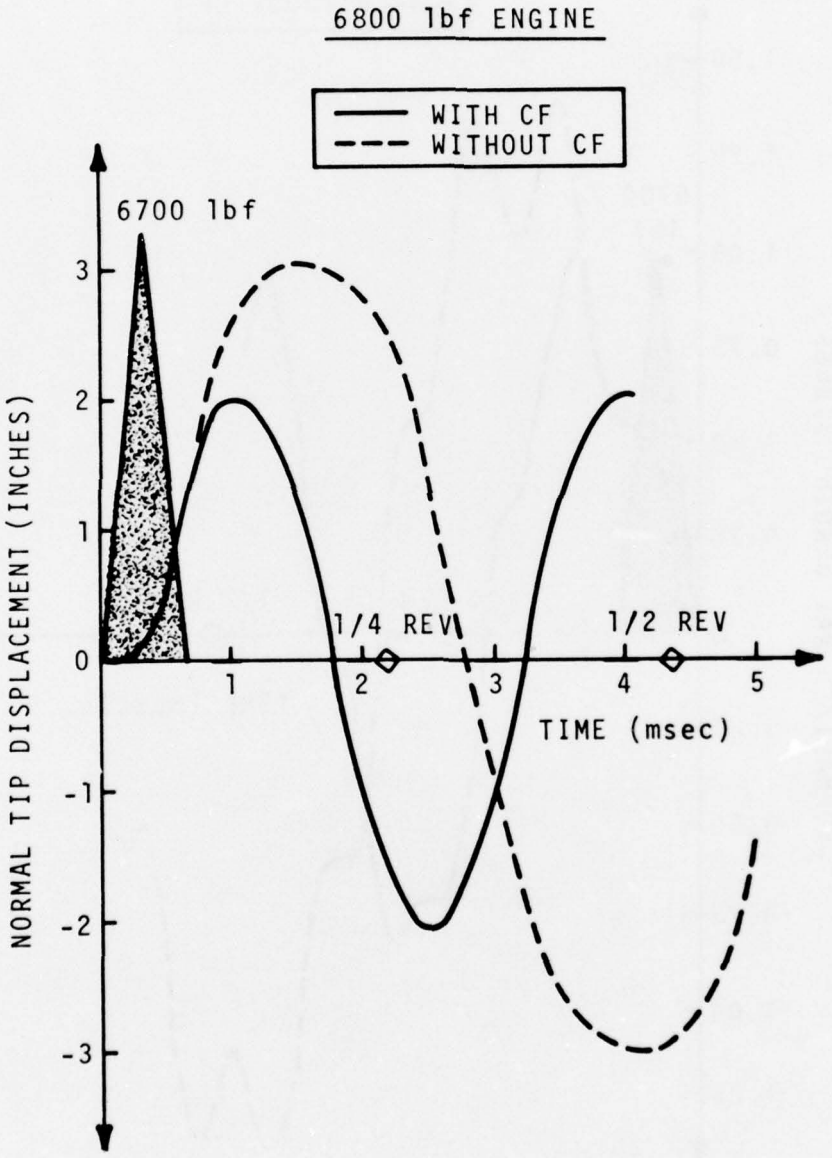

Figure 47. Centrifugal Force Effects on Tip Displacement - 6800 lbf Baseline Blade.

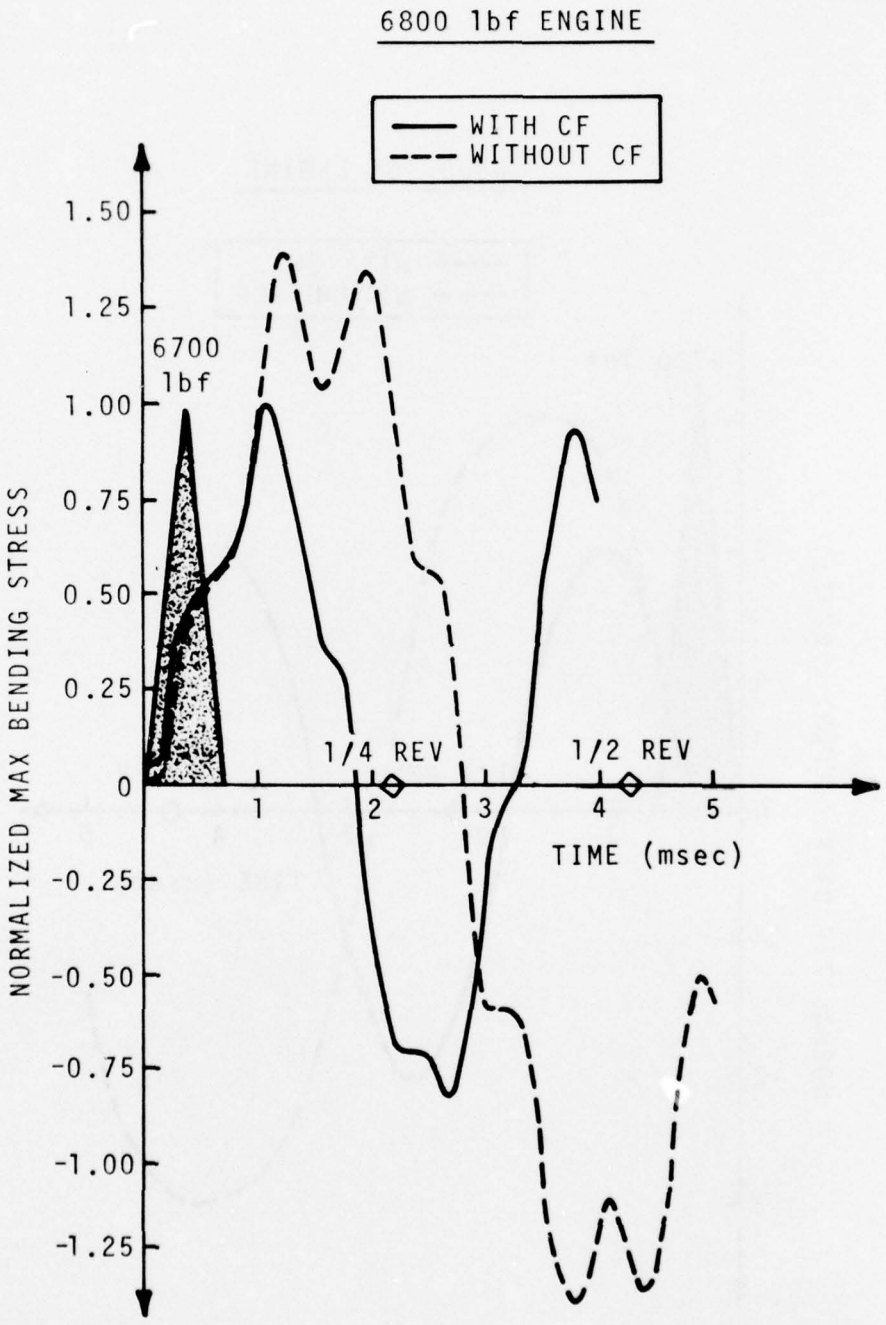

Figure 48. Centrifugal Force Effects on Maximum Stresses - 6800 lbf Baseline Blade.

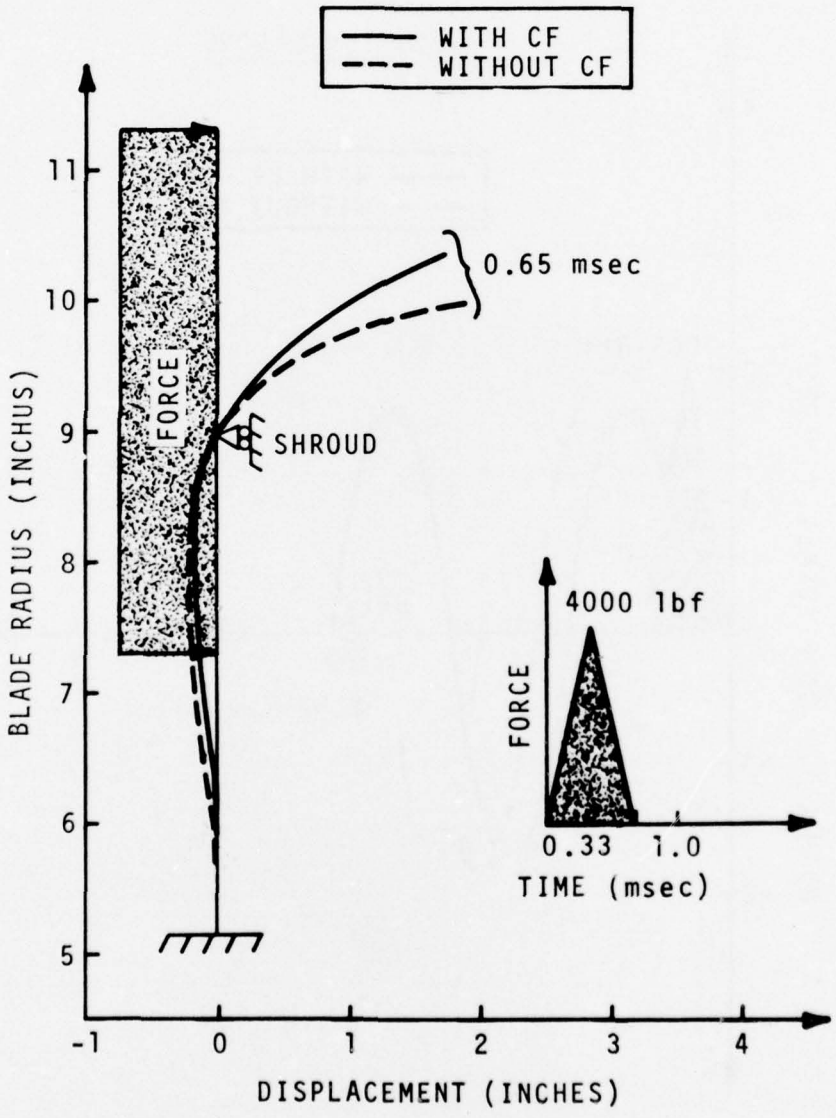

Figure 49. Centrifugal Force Effects on Transient Deformation - 1600 lbf Scaled Blade.

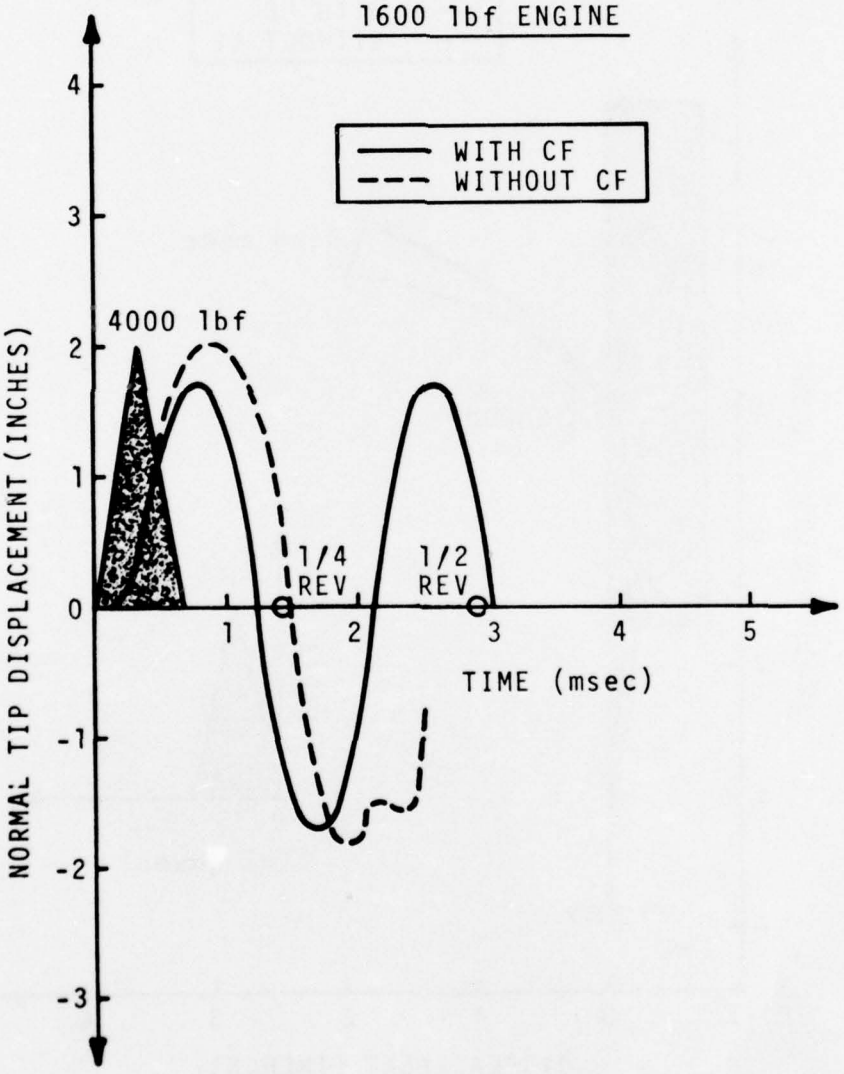

Figure 50. Centrifugal Force Effects on Tip Displacement - 1600 lbf Scaled Blade.

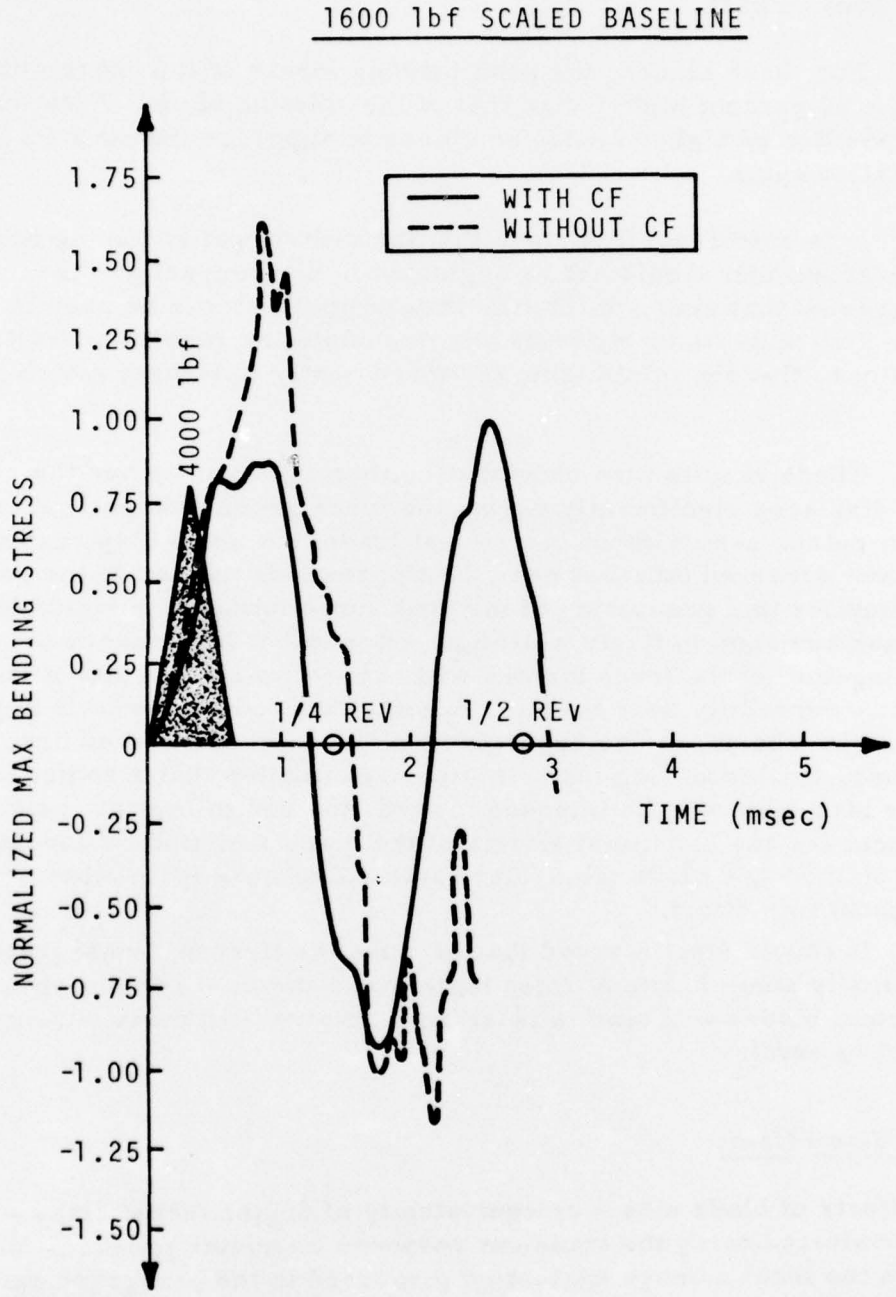

Figure 51. Centrigugal Force Effects on Maximum Stresses - 1600 lbf Scaled Blade.

two blades during impact, and very little additional motion of either blade after impact.

For these blades, the peak bending stress of the nonrotating blade is some 60 percent higher than that of the rotating blade. Note that superposition of higher modes combines to suppress the peak stress in the first cycle.

It is seen from this study that the centrifugal stiffening effect is significant and should not be neglected in bird impact studies. It is suggested that such nonrotating impact analyses can be used in conjunction with static rig tests to extrapolate the results to rotating conditions, thereby minimizing the more costly full-scale rotating tests.

These results also show that neither the 6800 lbf nor the 1600 lbf blade displaces significantly during the force generation portion of the impact pulse, even without centrifugal loads; but some displacement will have occurred (at least near the tip) towards the end of the pulse. This implies that generation of the peak force follows the rigid blade collision assumption fairly well; but a somewhat less severe or "trailing-off" of the force history will occur towards the end of the impact - especially near the tip. A somewhat reduced overall impulse load might therefore be expected than has been considered here. However, the increasing blade motion also implies that a somewhat larger bird slice will be imposed towards the end of impact, tending to cancel out any beneficial effects of the blade's motion. Calculations based on the rigid blade triangular force pulse were maintained accordingly throughout this effort.

It should also be noted that because the first torsional frequency is typically some 2.5 to 3 times higher than the first bending frequency, the actual blades will tend to twist back into the bird mass during the impact interval.

Blade Size Effects

The effects of blade size - or equivalently of engine thrust class - were evaluated using the transient response computer program, and, as with the local damage evaluation discussed in the paragraph entitled Baseline Blades Damage Evaluation, three directly scaled blades corresponding to 1600, 6800, and 50,000 lbf thrust engines were modeled. Medium bird-ingestion analyses were performed for both rotating and nonrotating blades to further illustrate the influence of the centrifugal force field.

The resulting tip deflections are shown in Figure 52, and the histories of the maximum stressed elements are shown in Figure 53. It is seen that the deflections, and especially the stresses, in the 50,000 lbf thrust blades are dramatically less than in either the 6800 lbf or 1600 lbf thrust blades, again pointing out the added difficulty in designing foreign object tolerance into the small thrust class machines.

The differences in tip deflection between these blades further illustrates the effects of engine size, since it is seen that the smaller blades tend to impact on adjacent blades causing additional damage, while the larger blades tend to remain isolated from their neighbors.

From Figure 54, it is seen that for the same size bird, the maximum tip deflections decrease both for the larger engine sizes (due to the greater blade mass) and for the smaller engine sizes (due to the greater influence of the part-span shroud). The maximum stresses, however, continually decrease with increasing engine size. The influence of the centrifugal force appears somewhat greater for the smaller blades, possibly due to the relatively greater distortions around the shroud.

Shroud Effects

The dynamic behavior of the 6800 lbf baseline blade was also compared with an unshrouded version using the transient analysis computer program. Here again, the response to impact by a 1.5-pound bird at FAR take-off conditions was considered, again assuming a triangular force pulse uniformly distributed over the outer 4 inches of both blades. The 6880 rpm centrifugal force field was included in the (large deformation) analysis.

Displacements and stresses in the shrouded and unshrouded versions of the baseline blade are shown in Figures 55 through 57. It is seen that removal of the part-span shroud results in very little difference in blade motion during the impact interval, but eventually the tip displacement of the free blade far exceeds that of the standard shrouded design.

The peak stress is also higher for the free beam and now occurs in the root, rather than just outboard of the shroud as in the standard blade. Thus, the free-standing blade is more likely to fail, and should it do so, would then impose greater imbalance loads on the rotor support structure and greater impact energies on the containment ring.

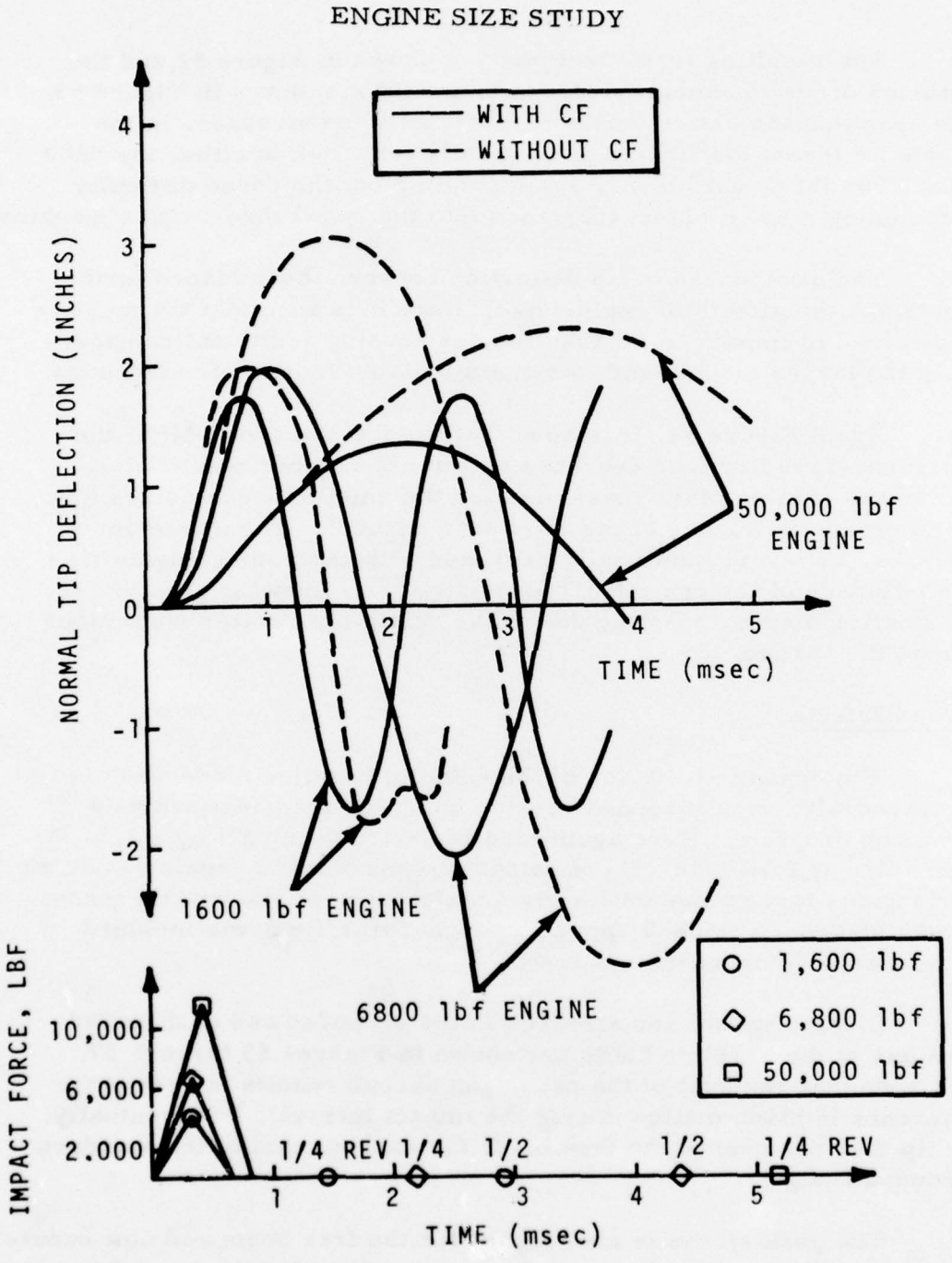

Figure 52. Engine Size Effects on Tip Displacements.

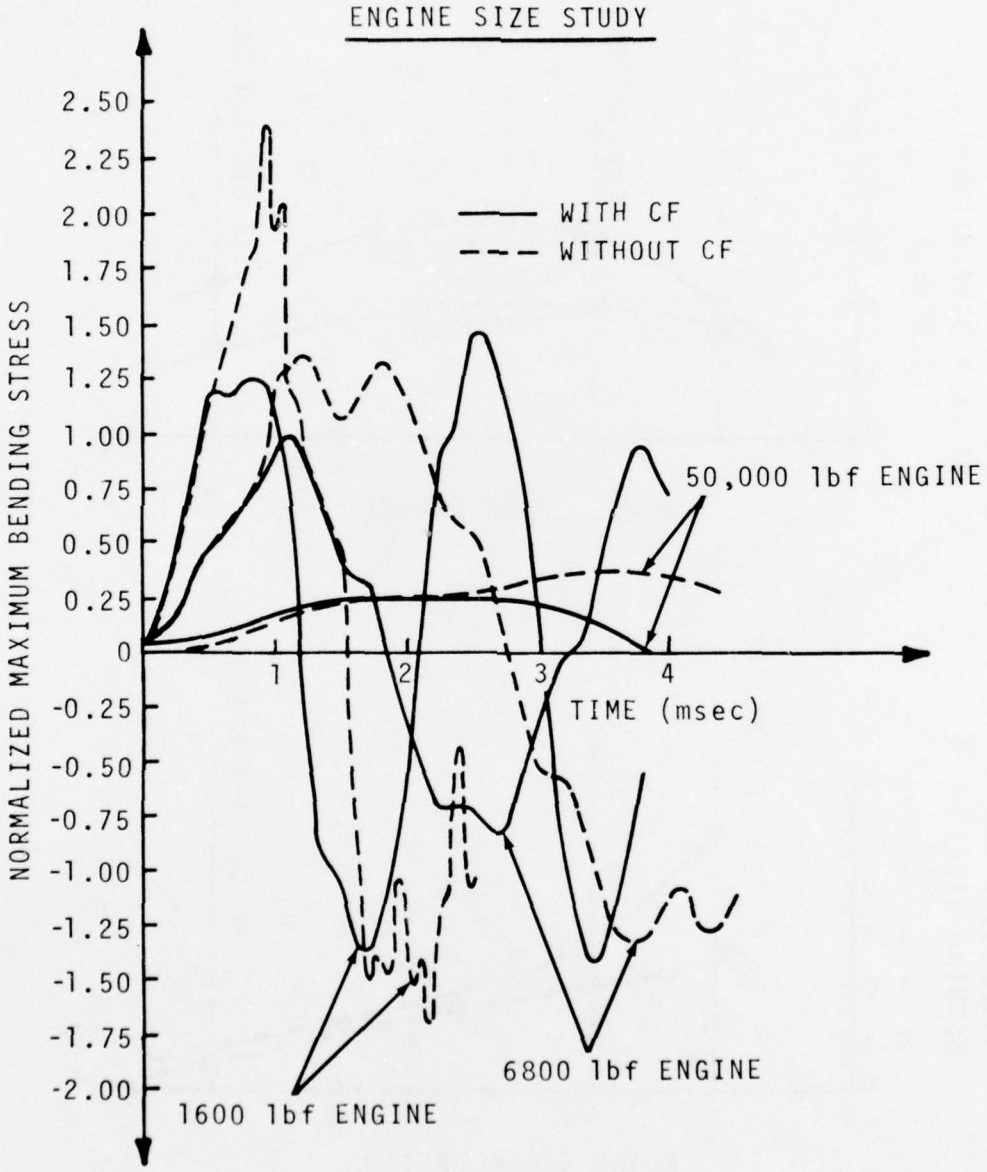

Figure 53. Engine Size Effects on Maximum Stresses.

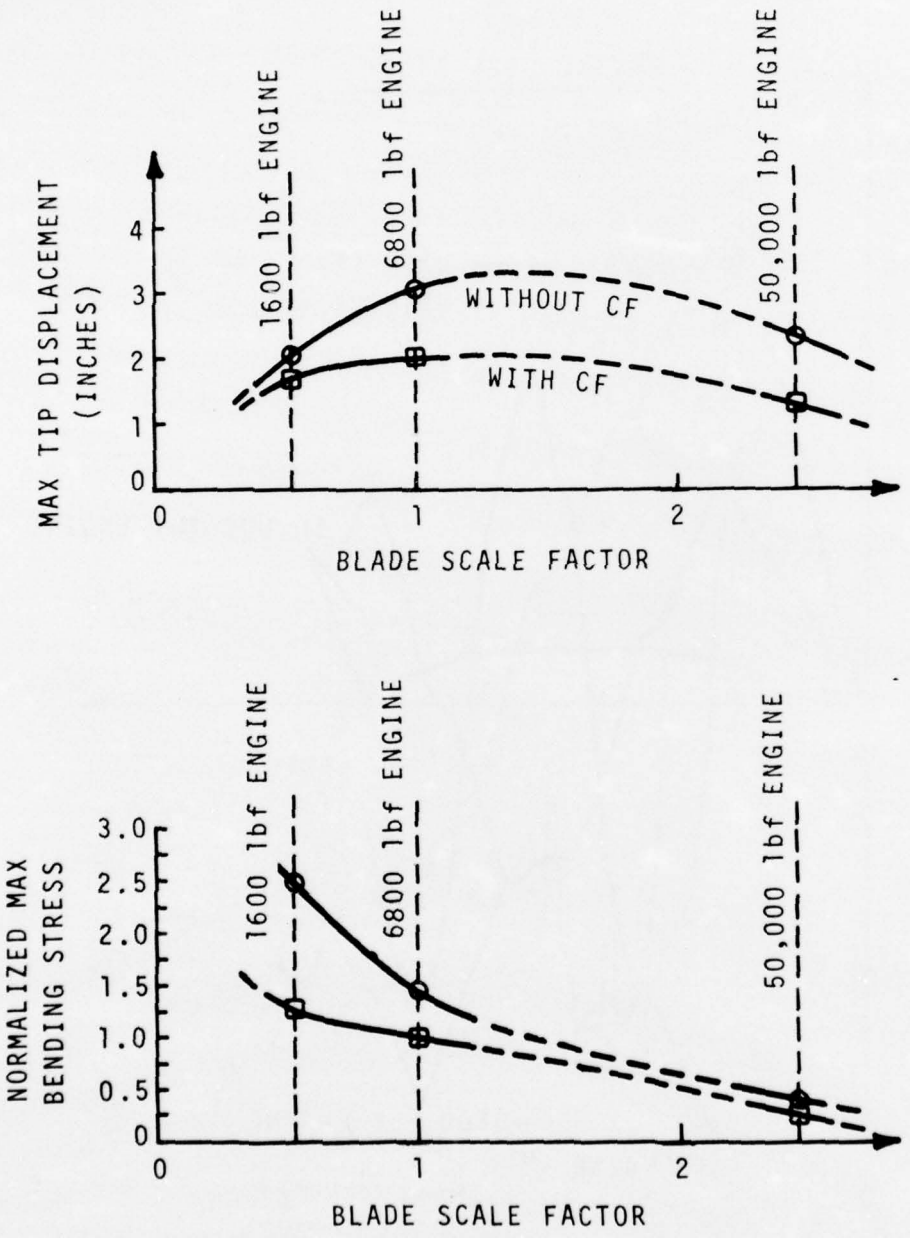

Figure 54. Tip Displacements and Maximum Stresses Versus Blade Scale Factor.

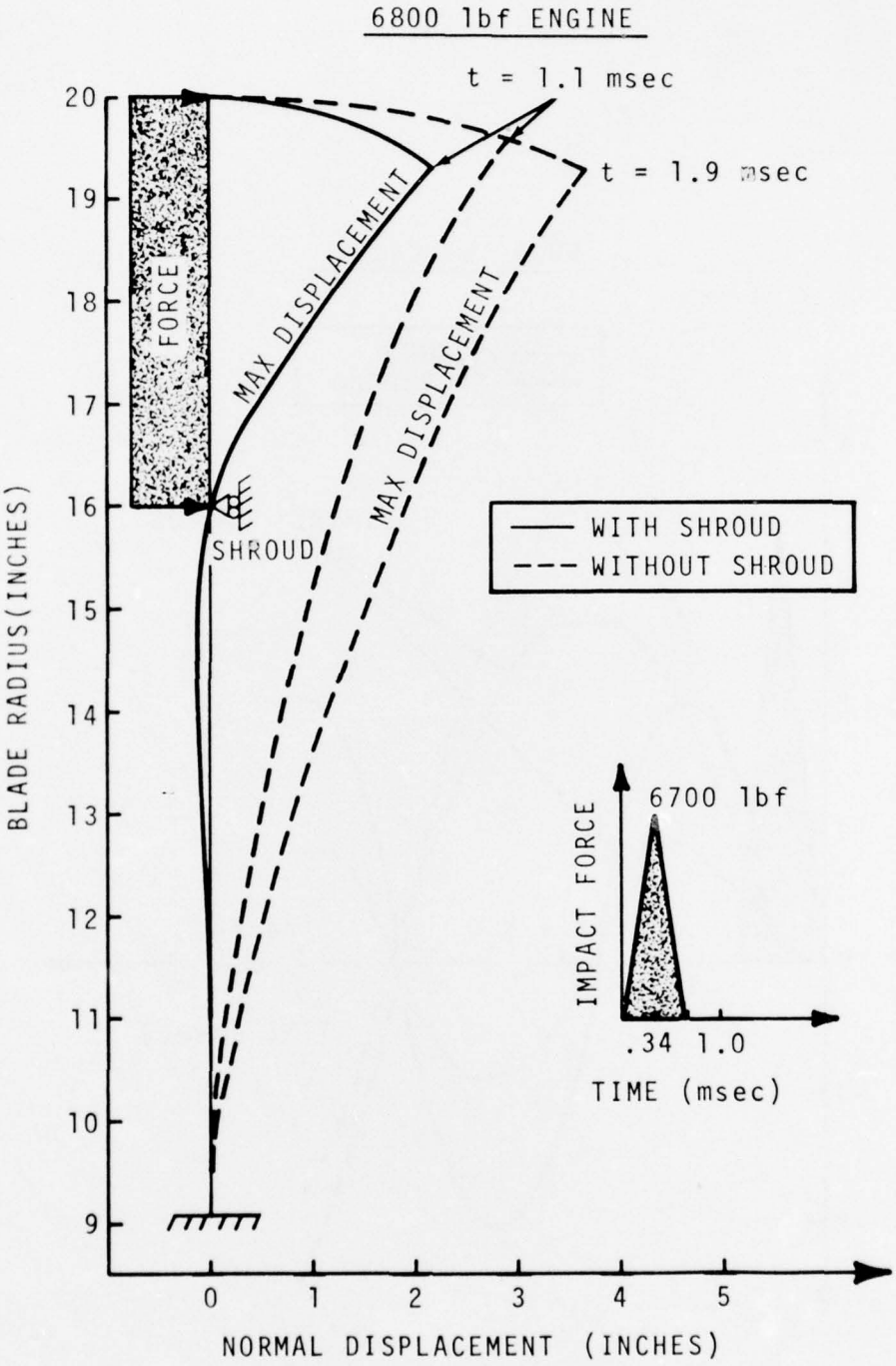

Figure 55. Effect of Shroud on Transient Deformation - 6800 lbf Baseline Blade.

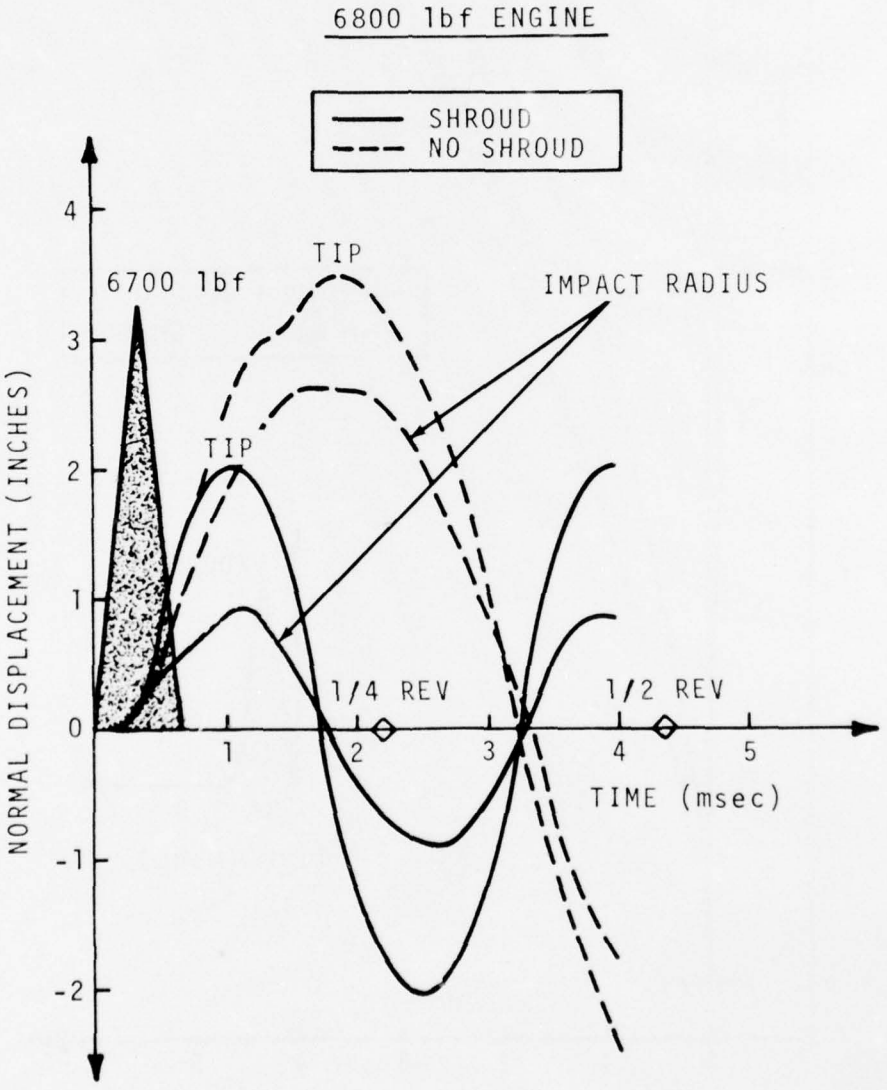

Figure 56. Effect of Shroud on Tip Displacement - 6800 lbf Baseline Blade.

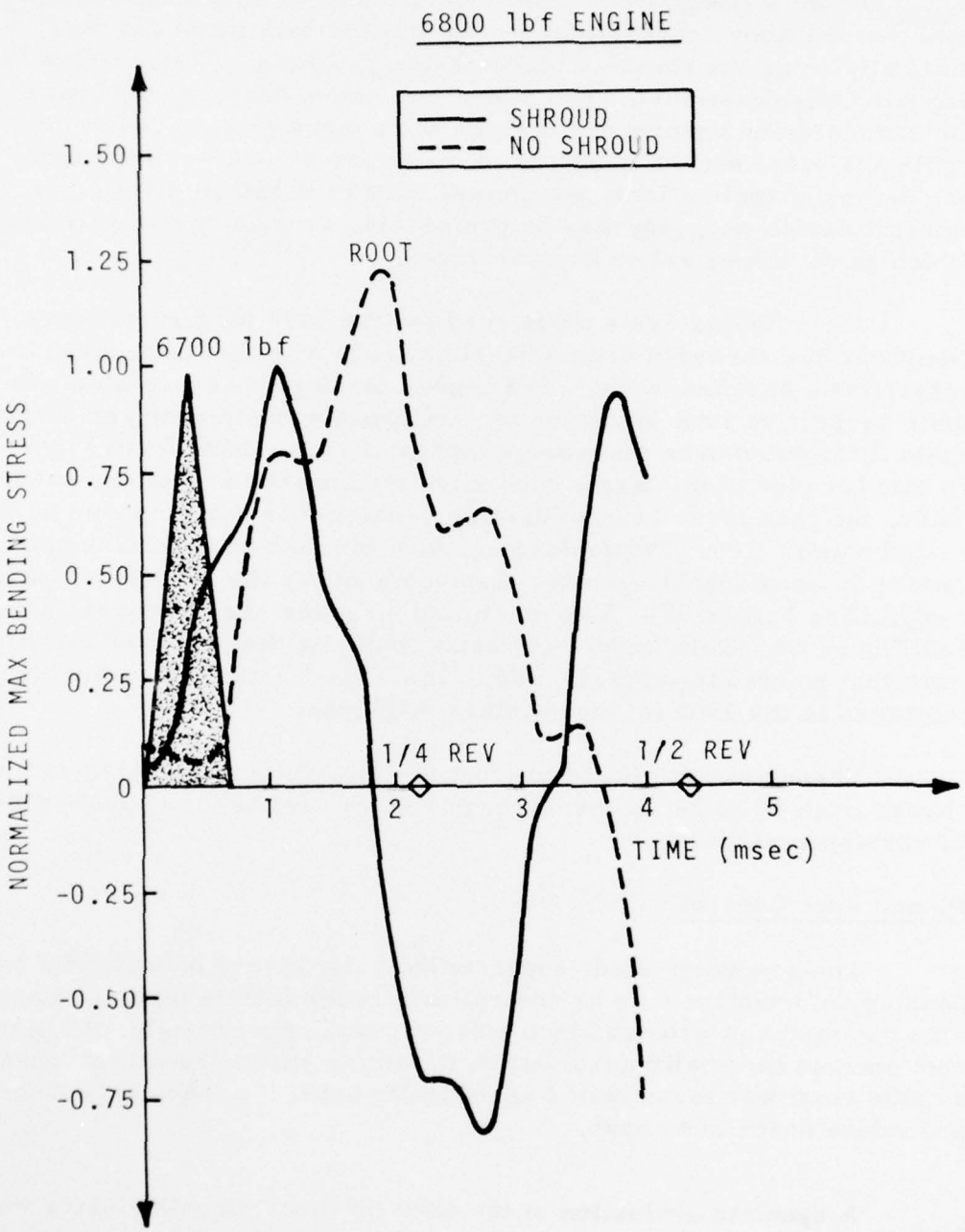

Figure 57. Effect of Shroud on Maximum Stresses - 6800 lbf Baseline Blade.

From a design methodology point of view, it is important to note that the above conclusions are consistent with those reached statically using the standard blade design program. (Refer to Blade Support Considerations). The maximum stress differences between the shrouded and unshrouded designs were more pronounced in the static analysis, but the locations of maximum stress were the same. So, for many applications, parameter studies based on the simple and fast design program may be preferable, especially if a wide variety of design variables are to be considered.

A similar analysis performed for the 1600 lbf thrust engine compared the shrouded scaled baseline blade with the unshrouded low-aspect ratio baseline blade. The impact force pulse associated with their respective FAR ingestion requirements were imposed on each, again distributed over the outer 4 inches of span. Note from Figure 58 that because of the larger bird slice striking the low aspect ratio blade, the peak force is considerably greater than that imposed on the scaled blade. This greater loading, plus the lack of shroud support, results in considerably greater displacement for the low aspect ratio design.(See Figure 59). The maximum stresses are, however, similar. See Figure 60. This important result confirms the previous analytic work that pointed towards the use of low aspect ratio blades for bird tolerance in the 1600 lbf thrust class machines.

These results also imply that the thickening associated with the change from 40 to 24 blades is roughly equivalent to the support provided by part-span shrouds.

Pinned-Root Concept

The preceding study suggests that, for blades of sufficient mass, bending deformation may be controlled through inertia effects rather than the restraint provided by a built-in root. Accordingly, the pinned-root concept (normally used only to minimize surge-induced stresses in a blade root) was investigated analytically using the transient-analysis procedure described above.

A dynamic evaluation of the 6800 lbf thrust baseline blade was performed considering that the root element was free to rotate about its minimum axis of inertia and the results compared with those of a built-in root. See Figure 61. Both blades were assumed unshrouded and operating at the FAR take-off speed of 6880 rpm. A triangular force pulse reaching a maximum value of 6700 lbf during a 0.68 m sec impact duration was again imposed and distributed uniformly over the

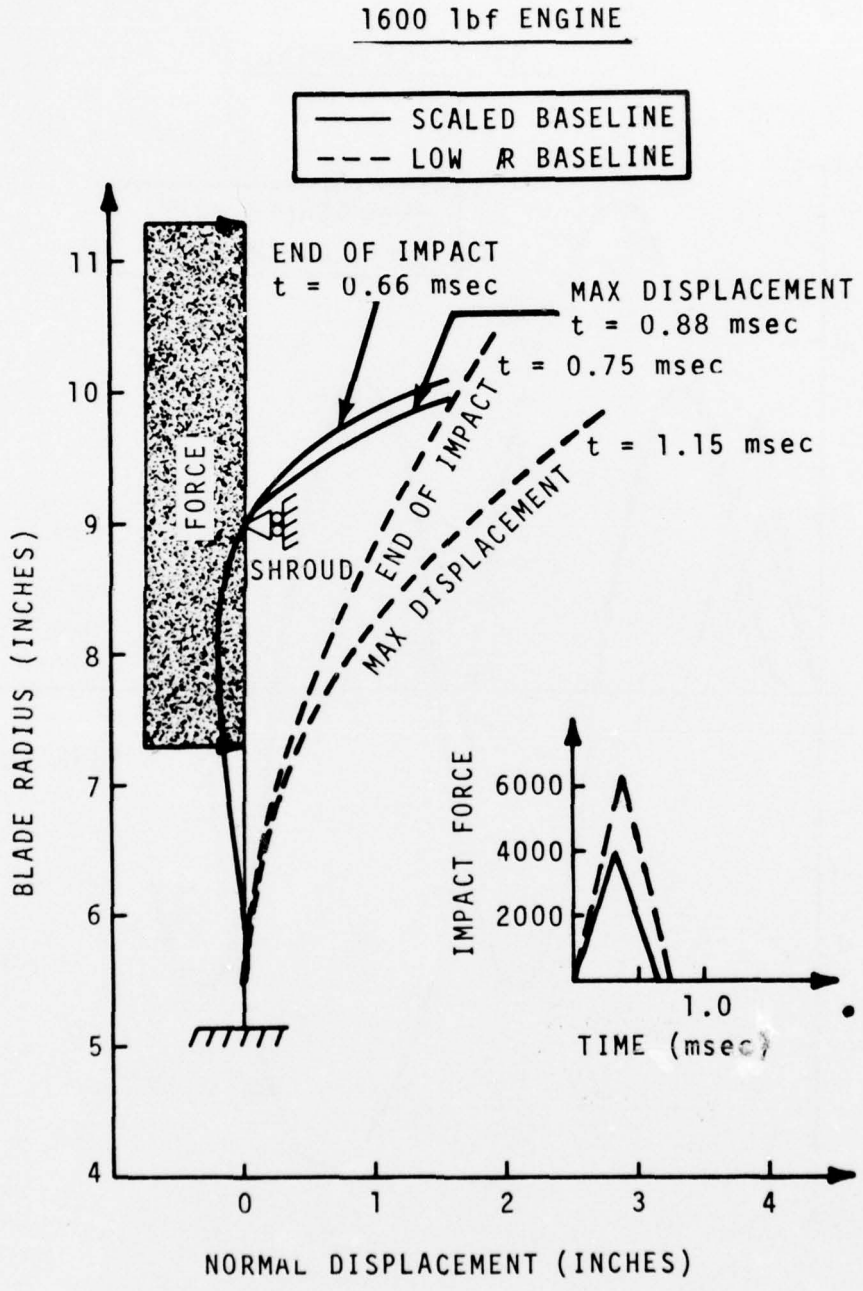

Figure 58. Effect of Shroud on Transient Deformation - 1600 lbf Baseline Blades.

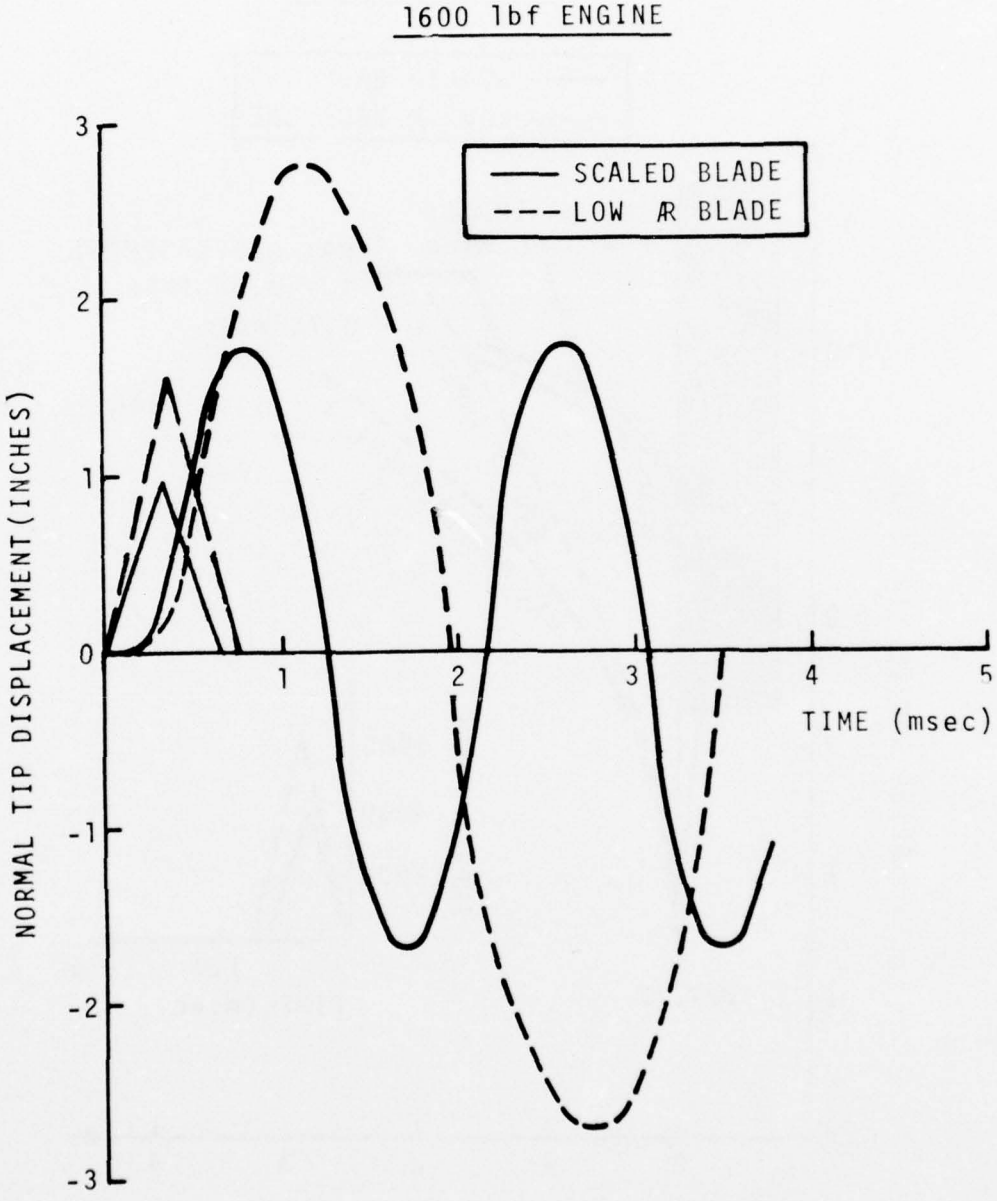

Figure 59. Effect of Shroud on Tip Displacements - 1600 lbf Baseline Blades.

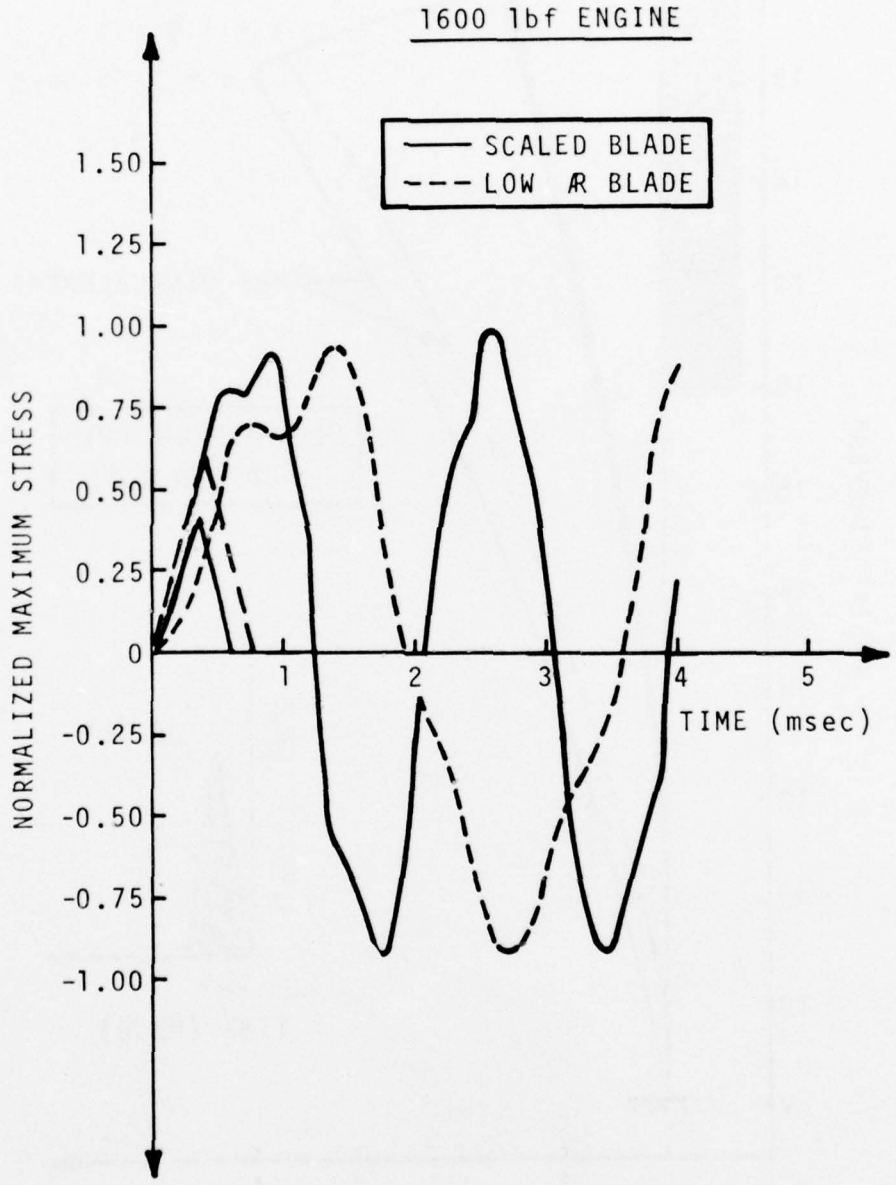

Figure 60. Effect of Shroud on Maximum Stresses - 1600 lbf Baseline Blades.

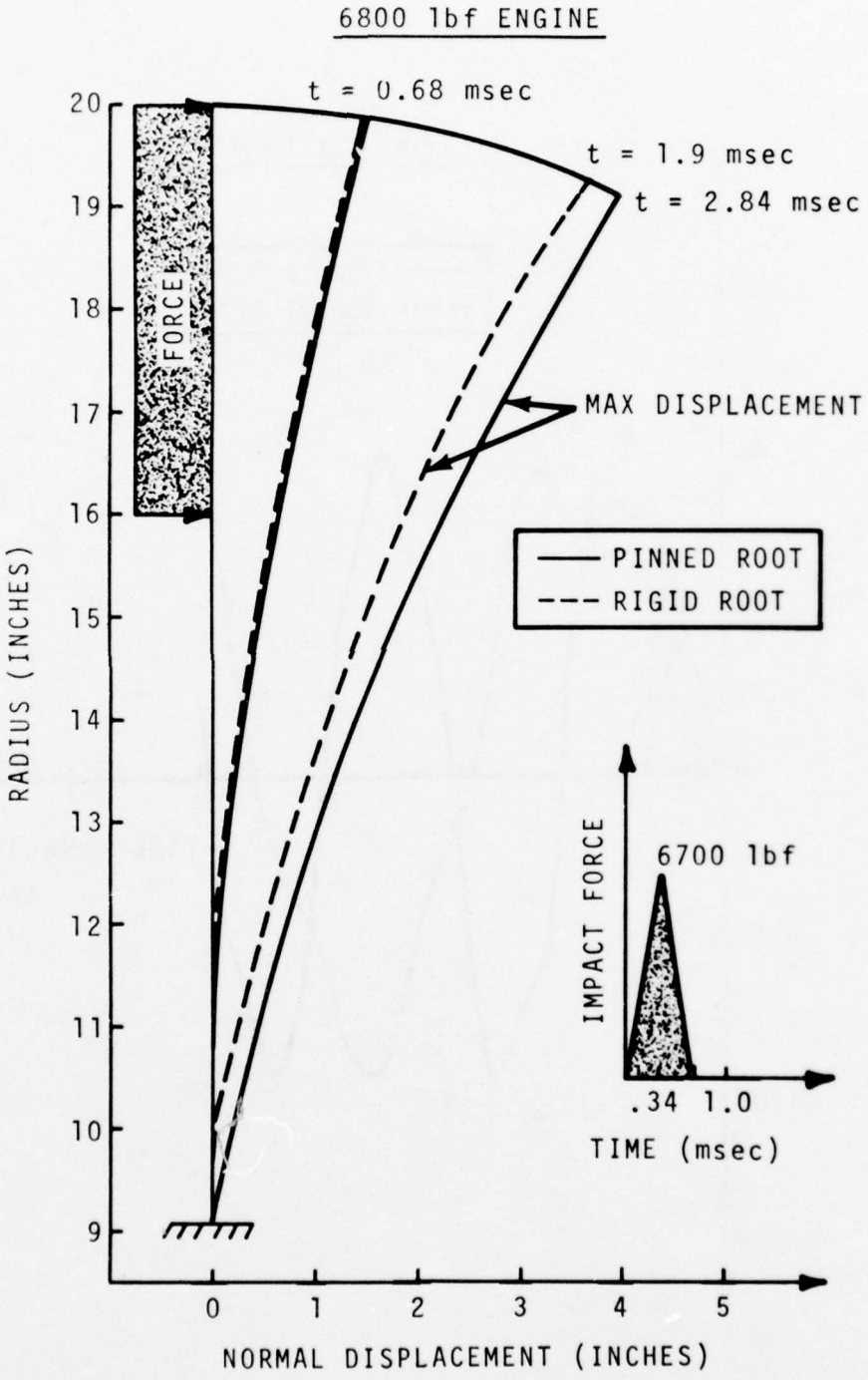

Figure 61. Effect of Pinned Root on Transient Deformation - 6800 lbf Blade.

outermost 4 inches of the blade to simulate the impact of a 1.5-pound bird ingested at 120 knots.

The displacement of blades at the tip and at the center of impact are compared in Figure 62. It is seen that the displacements during impact are essentially the same for both the pinned and built-in designs, implying the forces developed by the bird and transmitted to the blades are the same for either design. Since the behavior of the blades during the ingestion period are the same, no variation is expected either to local blade damage or to core engine damage or performance.

Figure 63, however, shows that stresses developed in the pinned-root design after ingestion are one-third that developed in the built-in design. Additionally, the location of the maximum stress region has now moved well outboard of the root to within 3 inches of the tip. Loss of a 3-inch tip fragment, should it occur, would be less serious than the loss of the entire blade span. Table 9 indicates the reduction in loading that would be realized on the bearings, supports, and containment structures.

TABLE 9 COMPARISON OF CANTILEVER VERSUS PINNED-ROOT LOADS AT FAILURE

Stress	Full-Span Loss	3-Inch Tip Loss
Imbalance Force (lbf)	15,000	4,600
Kinetic Energy (in. lbf)	112,000	42,700

Maximum rotation of the root is 24 degrees (at 2.2 m sec) so there should be no undue problem with providing adequate clearance at the disk rim.

Based on the above analysis, the pinned-root concept appears to be an attractive approach to bird-tolerant fan blade design. Further evaluation is still required, however, because the blade twist effects, (which were not considered here), will tend to inhibit pure rotation about the pin, so that for tip impacts at least, the blade response may approach that of a standard cantilevered blade.

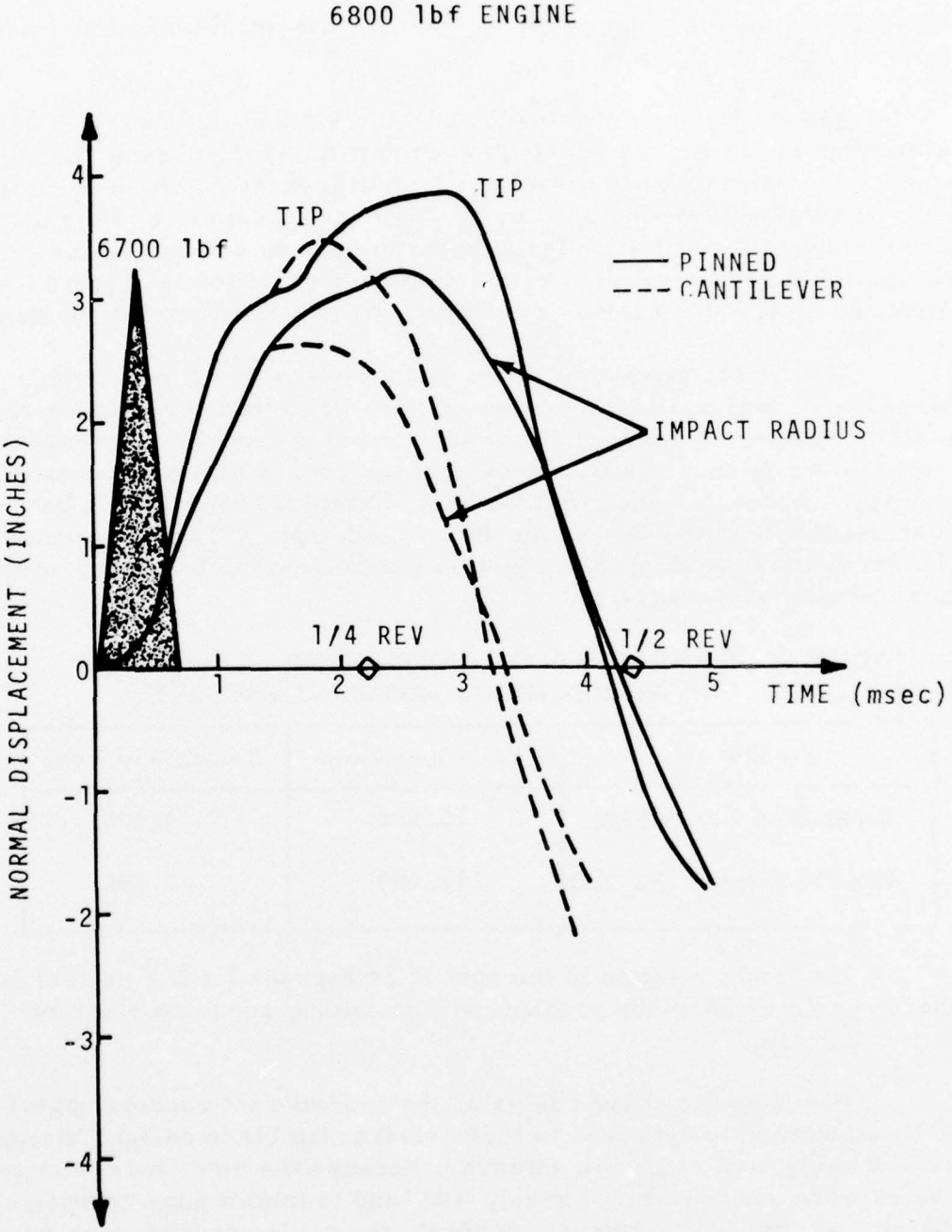

Figure 62. Effect of Pinned Root on Tip Displacement - 6800 lbf Blade.

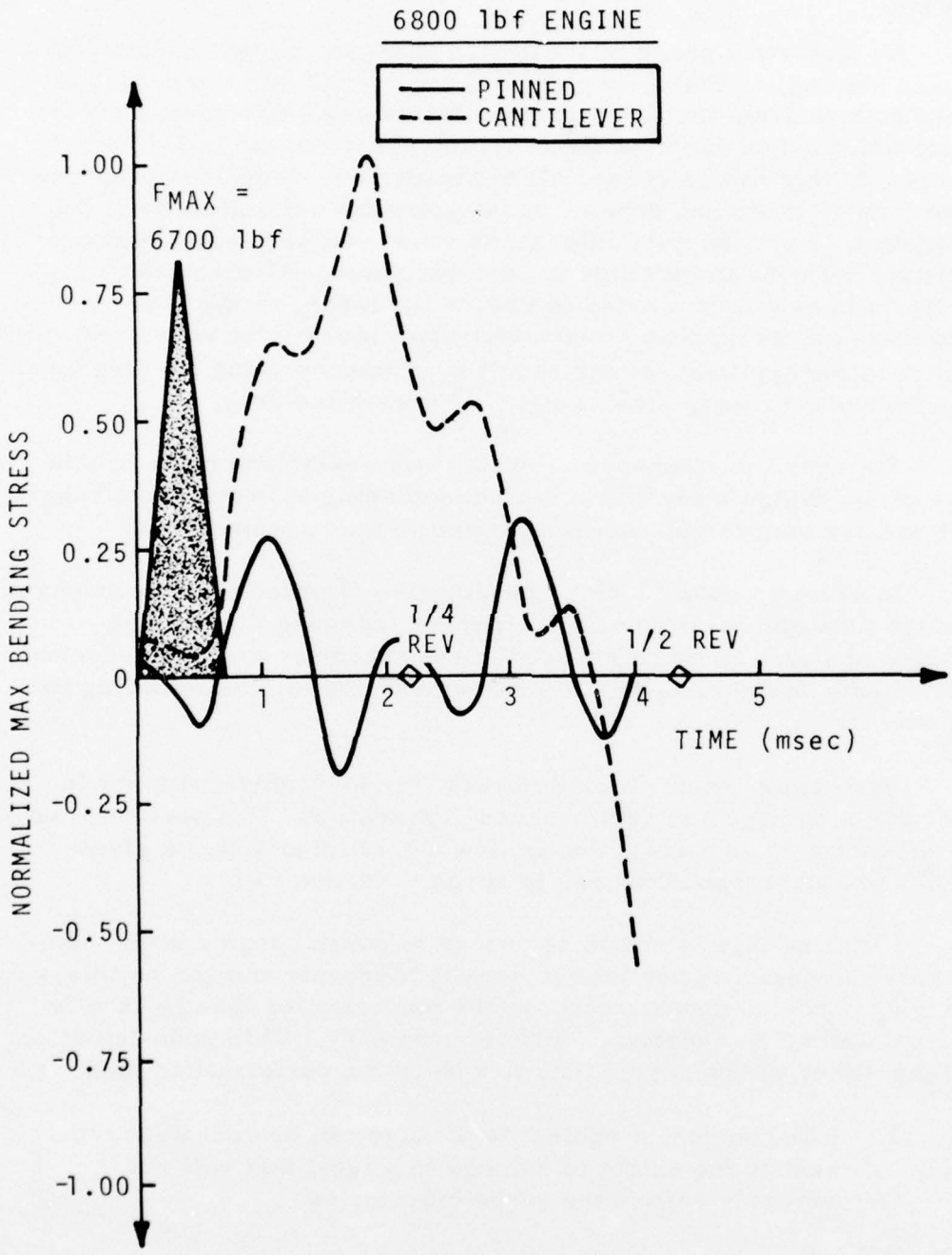

Figure 63. Effect of Pinned Root on Maximum Stresses 6800 lbf Blade.

AERODYNAMIC CONSIDERATIONS

General

An important phase of the design process, prior to selecting the detailed blading, is the aerodynamic design of the fan/compressor components wherein the flowpath geometries and blade speeds are set, both of which affect the ingestion characteristics of the individual components. In this design phase, all of the varying trades between size, performance, cost, and structural integrity and reliability must be considered. For example, inlet guide vanes can be used to improve efficiency but with an increase in cost and noise. Alternatively, the hub/tip ratio can be increased to reduce tip speed, or the blade orientation can be modified to accommodate lower inlet velocities. Both of these latter approaches may result in efficiency gains but also result in engines of increased size, weight, and installed drag.

Any inherent weakness resulting from decisions made in this phase of the design must be corrected by blading of increased strength; which factors tend to increase weight and reduce performance.

In order to obtain a clear perspective of practicable aerodynamic redesign procedures, studies were performed using the damage criterion analysis to weigh reduced wheel speed designs and reduced inlet velocity designs. The results are described in the following two sections.

Upon experiencing a bird impact, the fan/compressor could suffer some damage and performance degradation. The performance loss will show up as a reduction in flow and efficiency (for a given speed) and a corresponding loss in surge pressure ratio.

If the damage is not so severe as to cause surging of the compressor, the performance loss is usually moderate and can be tolerated. If surging of the component occurs, the performance loss is usually too great and some redesign would be necessary. This redesign effort can take either of two approaches to reduce the performance loss:

1. The component subject to damage can be redesigned to reduce the extent of damage to a level that will not severely reduce the surge margin, or

2. The engine can be rematched to provide increased surge margin for the damaged component.

The first approach will normally reduce the efficiency potential of the component and degrade engine performance. A weight penalty is also incurred. The second approach usually results in a basic loss of cycle pressure ratio and/or efficiency, consequently resulting in degraded performance throughout the operating range. An effort to determine the sensitivity of the engine to performance loss after ingestion is discussed below in the paragraph Operation with Damaged Blades.

Reduced Wheel Speed Designs

The reduction of fan wheel speed presents an alternative approach to reducing impact damage; in fact, reduced power takeoffs have become increasingly common since this practice can substantially extend life of the hot section (Reference 20).

An initial evaluation of the bird-resistance benefits stemming from a 10-percent reduction in take-off thrust for the 6800 lbf baseline engine showed only minor changes in fan speed (less than 4%) with even smaller changes in the calculated damage level.

Thus, aerodynamic redesign of the fan assembly was undertaken to evaluate the potential for increased bird tolerance in a machine specifically designed for up to 30-percent lower tip speed. The procedure pursued was to reduce the blade tip speed by moving up to a larger fan with an increased inlet hub-tip ratio. The meridional velocity levels were held constant, as was the fan blade hub wheel speed levels, in order to retain a constant hub loading level.

The preliminary fan design study was conducted using a computer program that calculates stage velocity triangles and subsequent blade losses and efficiencies. The loss system used is based on diffusion factor correlations modified from NASA testing, together with adjustments for end-wall, Mach number, clearance, and Reynolds number effects and has been correlated against both in-house and published performance data with good results. All performance estimates used in the study are based on this preliminary design program.

A series of designs varied the fan inlet hub/tip ratio from the 0.44 level of the 6800 lbf thrust baseline machine up to 0.6, which was felt to be as high as could be practically considered. The baseline blade geometry was modified to provide the required flow, pressure

ratio, and velocity triangles along the span. The characteristics of four alternate fans that were investigated are listed in Table 10. It is seen that the tip diameter of the fan increased by 5 inches, while the engine length increased by 7 inches. For the higher hub/tip ratio designs, a small gain in efficiency resulting from a lower Mach number is counterbalanced by a lower aspect ratio and increased duct length effects that tend to reduce the overall efficiency gain.

The changes in fan efficiency and damage resistance shown in Figure 64 point towards the 0.5 hub/tip ratio fan configuration as an excellent combination of fan performance and damage resistance - although at the cost of a larger, longer, and heavier engine. Figure 65 compares this configuration with the baseline fan assembly. A 10-percent weight increase is estimated for this design (approximately 46 lb). Refer to Table 11.

Preliminary design studies were also conducted to investigate the effects of varying the tip speed of the 1600 lbf thrust machine. In this case, however, the flowpath was held constant to maintain the same engine diameter. The rpm of the scaled version fan was varied ±5 percent to see if significant performance or bird-resistance changes would result.

A preliminary airfoil shape was designed to account for wheel-speed changes, but the blade number, thickness, and chord remained the same as the baseline blade. Table 12 compares the two alternate designs.

Figure 66 shows that the slower, more efficient version (C-1) resulted in a slightly less rugged blade because of the less favorable incidence angle for bird strikes at aircraft take-off speeds, while the faster version (C-2) shows a slightly better resistance to damage due to the more favorable incidence angle.

Reduced Inlet Velocity Designs

Impact damage also can be lessened by reducing the incidence angle of the blades with respect to an incoming bird. One means of accomplishing this is to design the fan for reduced axial velocity — ideally to match that of the bird. However, because the aircraft velocity at takeoff is low relative to the usual fan inlet axial velocity design

TABLE 10 - ALTERNATE LOW WHEEL SPEED DESIGNS

6800 lbf Baseline Engine					
		Alternate Fans			
Characteristics	Baseline	A-1	A-2	A-3	A-4
Design Speed (rpm)	7500	7000	6550	5850	5300
Take-Off Speed (rpm)*	6880	6420	6010	5370	4860
Tip Inlet Radius (in.)	20.0	20.4	20.8	21.6	22.5
Tip Relative Mach No.	1.32	1.27	1.22	1.16	1.11
Hub/Tip Radius Ratio	0.44	0.47	0.50	0.55	0.60
Number of Blades	40	42	46	52	57
Number of Vanes	85	92	97	106	114
Axial Length Increment (in.)	0	1.5	3.0	5.0	7.0
Fan Cruise Efficiency Increment %	0	+0.3	+0.5	+0.4	+0.1

* 1.5 - pound Bird FAR Ingestion Conditions

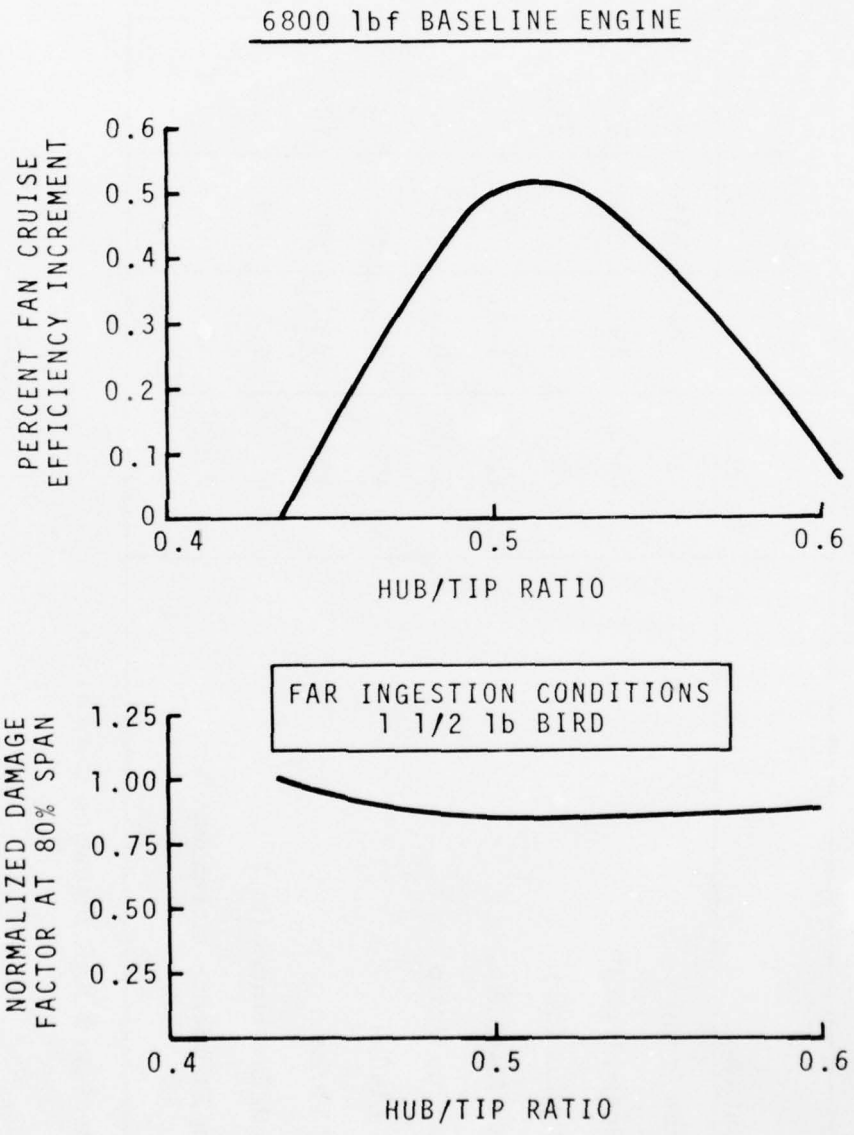

Figure 64. Cruise Efficiency and Damage Factor Changes Versus Hub/Tip Ratio.

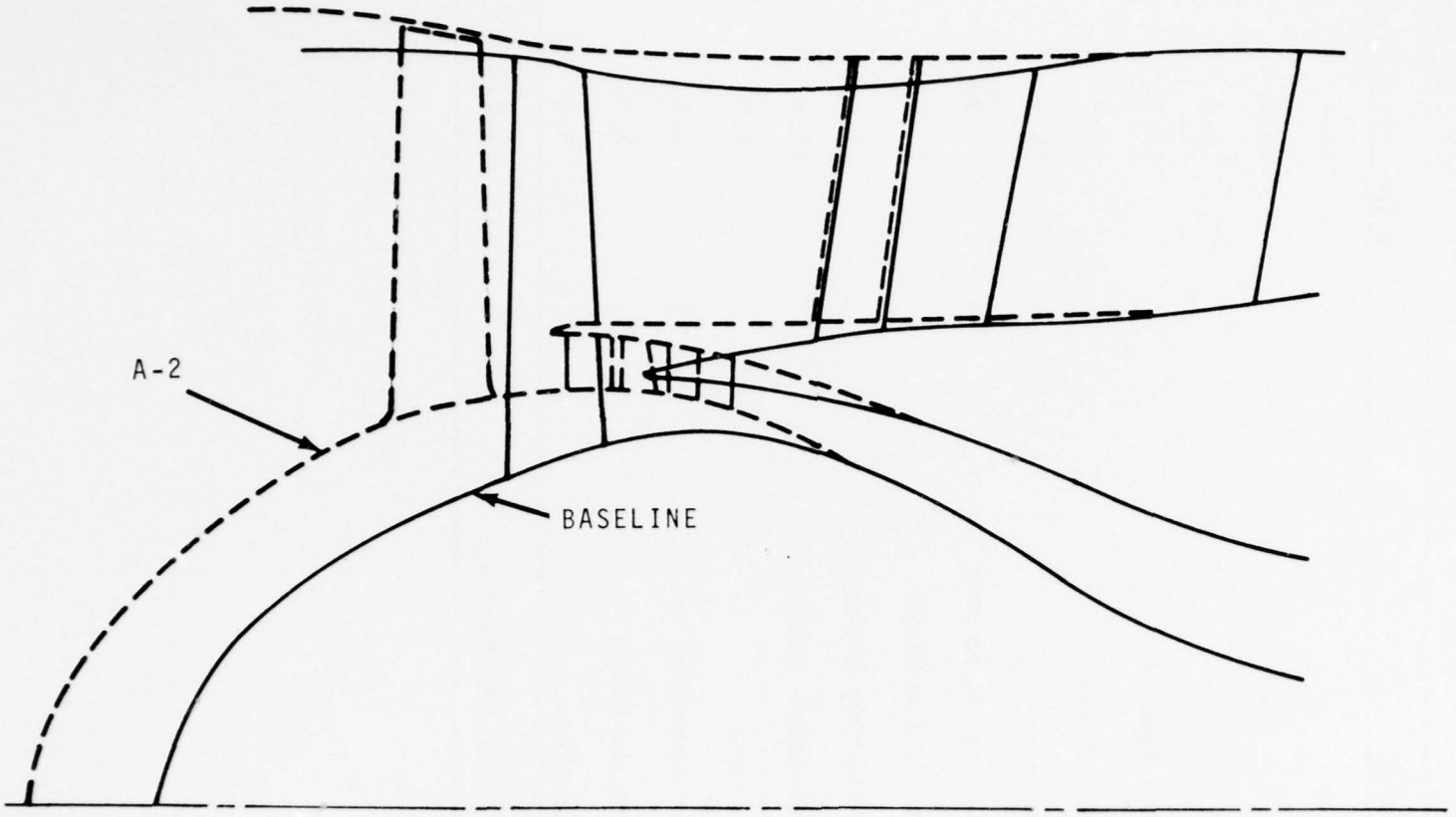

Figure 65. Flow Path of Low Wheelspeed Design (A-2).

TABLE 11 - WEIGHT PENALTY OF LOW WHEELSPEED DESIGN A-2

Component	Weight Increase - Percent
Fan Disk	18.0
Blades	12.8
Spinner	6.4
S/C Disk Assembly	10.5
Bearing Support	10.8
Fan Shroud	38.9
Cowl Support Assembly	9.5
Vane Assembly DEGV	13.6
Vane Assembly Stator 1	11.3
Vane Assembly Stator 2	11.8
Front Frame	6.8
Carrier Assembly	4.3
Containment Ring	2.0
Miscellaneous	3.0
Total Weight Increase	46.0 lb.

TABLE 12 - MODIFIED WHEELSPEED DESIGN

1600 lbf Baseline Engine

Characteristics	Baseline (Scaled)	C-1 (-5%)	C-2 (+5%)
Design Speed (rpm)	13,274	12,610	13,940
Take-off Speed (rpm)	10,940	10,393	11,489
Tip Speed (ft/sec)	1310.	1243	1374
Tip Inlet Radius (in.)	11.3	11.3	11.3
Fan Cruise Efficiency Increment (%)	0	+0.7	-0.6

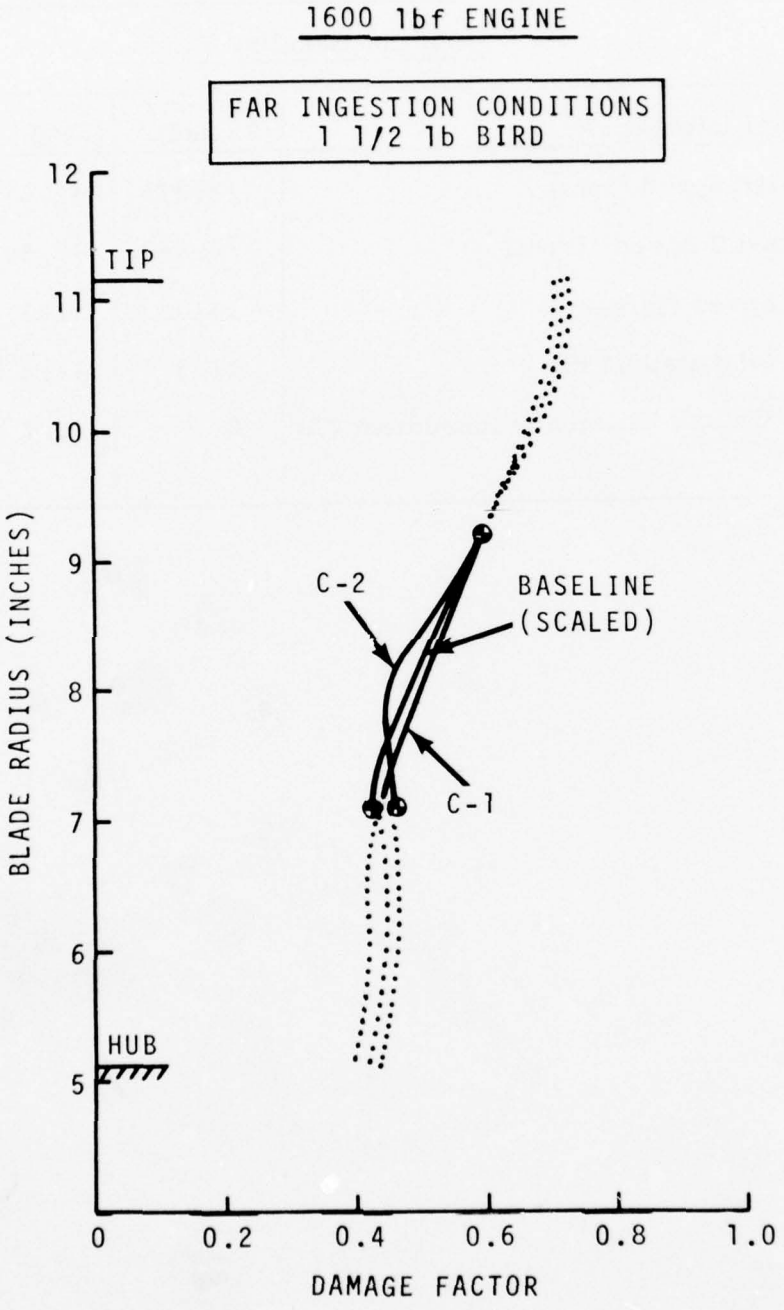

Figure 66. Damage Factor Comparison of Modified Wheelspeed Design - 1600 lbf Engine.

criterion, only a moderate reduction is possible in practice.

A design (B-1) with a 17-percent reduction in axial velocity was obtained by simultaneously increasing the annulus area of the 6800 lbf baseline engine by 15 percent and moving the tip radius outward to maintain the baseline hub/tip ratio. Here again, a preliminary airfoil shape was designed to provide the desired leading edge incidence angle with the necessary flow, pressure ratio, and core inlet conditions.

Table 13 presents a comparison of the significant aerodynamic parameters for this and the baseline design. The estimated design point efficiency level increased about 1.3 percent for this configuration but, again, at the cost of a larger and heavier machine (Figure 67).

The damage factor distributions for the two best aerodynamic redesigns are compared in Figure 68 and indicate that on balance the A-2 configuration is preferable when considering local damage tolerance, since it is substantially better near the tip and almost the same as the baseline over the remainder of the span.

Operation with Damaged Blades

These paragraphs discuss a method of predicting the reduced performance levels resulting from operation with various amounts of fan damage, based on damage severity levels and the flow area affected by the damage. The effects of damage on fan performance maps were estimated using engine test results as a guide. In all cases, since no visible damage occurred in the core compressor, combustor, or turbines, it was assumed that there was no deterioration in performance of these components.

Test Data Analysis - Data from three representative engine ingestion tests performed during the early development phases of the ALF 502 engine were analyzed to determine damaged fan (component) performance. The damage ranged from minor bending of leading edges as a result of ice ingestion tests that caused a change in local incidence only, to extensive rollback of leading edges caused by medium-bird ingestion tests that caused flow-blockage of the tip section.

Fan and supercharger performances were isolated from engine performance by using the test data in conjunction with a computer program that simulates the undamaged core engine. By fixing the

TABLE 13 - ALTERNATE LOW AXIAL VELOCITY DESIGN

6800 lbf Baseline Engine		
Characteristics	Baseline	B-1
Fan Inlet Axial Velocity (ft/sec)	605	500
Design Speed (rpm)	7500	6500
Take-Off Speed (rpm)	6880	5985
Tip Inlet Radius (in.)	20.0	21.8
Tip Relative Mach No.	1.30	1.22
Hub-Tip Ratio	0.44	0.44
Number of Blades	40	46
Fan Cruise Efficiency Increment (%)	0	+1.30

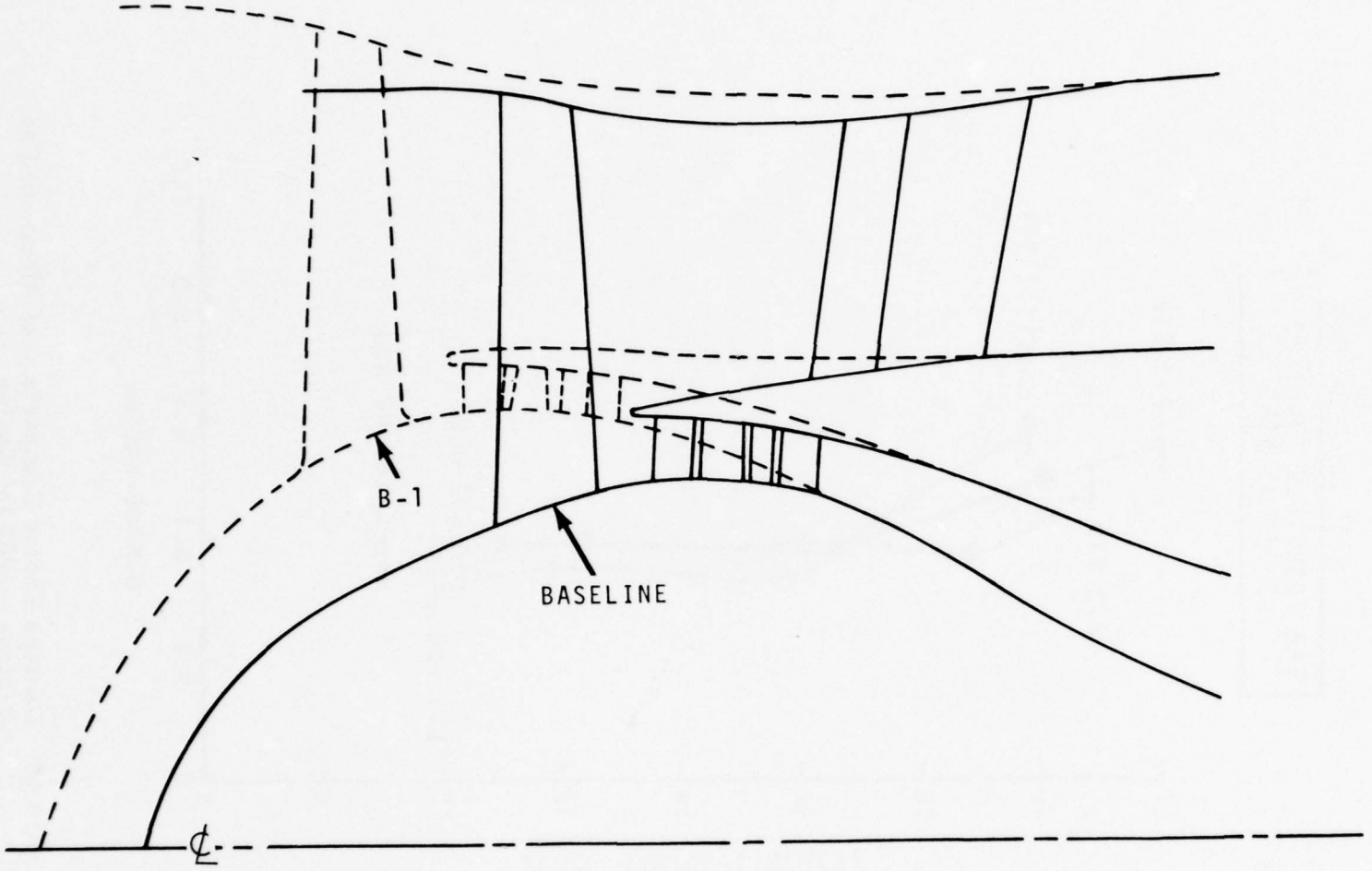

Figure 67. Flow Path of Low Axial Velocity Design (B-1).

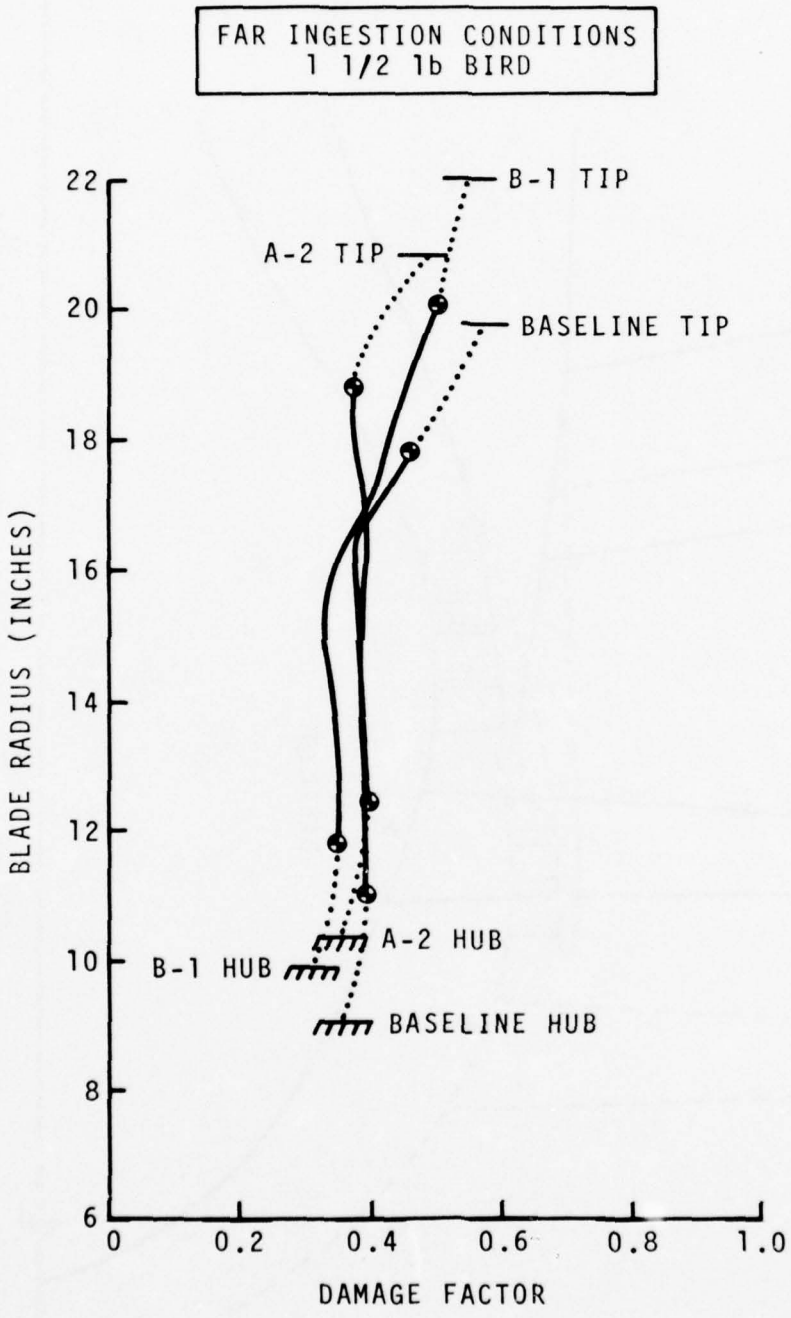

Figure 68. Damage Factor Comparison of Alternate Fan Designs - 6800 lbf Engine.

power turbine inlet temperature at the value measured during the test, the specific work available to the compressor can be determined from the turbine characteristics, and for a series of assumed high compressor inlet temperatures, the associated referred flow, referred speed, and compressor pressure ratio can be determined by satisfying continuity and energy balance between the compressor and turbines. If the high compressor inlet pressure is then adjusted to vary the core airflow until the fuel flow matches the tested values, the supercharger pressure ratio and temperature ratio will be known, and the supercharger efficiency can be calculated. The results may then be compared with the performance map representing the undamaged supercharger. Once the supercharger performance is established, the thermodynamic conditions throughout the core engine are known, and the power available for the fan bypass flow can be obtained along with the thrust from the hot exhaust gas. The thrust being provided by the bypass flow is then obtained from the difference between the measured net thrust and the hot exhaust thrust. These data, along with the nozzle characteristic, are used to determine the bypass flow, pressure ratio, and fan efficiency.

Ice Ingestion Test (Test No. 1) - Maximum damage resulting from ingestion of large 12 x 4 x 3/8-inch pieces of duct ice while demonstrating the engine icing protection system is shown in Figure 69. One blade (No. 11) was rolled back 1 1/4 inches at the tip leading edge, while six other blades suffered minor bending of the leading edge in the same area. Six bypass stators were also bent. Post-ingestion calibration runs were performed first with the total damage, next with fan blade No. 11 replaced, then with the six bent blades also replaced, and finally with the six bent stators also replaced. The pertinent measured test data for each calibration run are shown (at different power settings) in Table 14.

Using the procedure described above, the fan and supercharger were found to be operating at the conditions shown in the lower part of Table 14 which indicates that the supercharger was operating with no performance degradation due to the damaged fan. The total damage calibration run produced stall, but the test was made with an 8-percent reduced-area cold nozzle which caused the fan to operate closer to stall than normal.

Small Bird Test (Test No. 2) - Fan rotor blade damage sustained by ingestion of 16 small birds is shown in Figure 70. One blade tip was rolled back, and another tip suffered minor deformation. Two blades sustained rolled-back leading edges at the part-span shroud. The

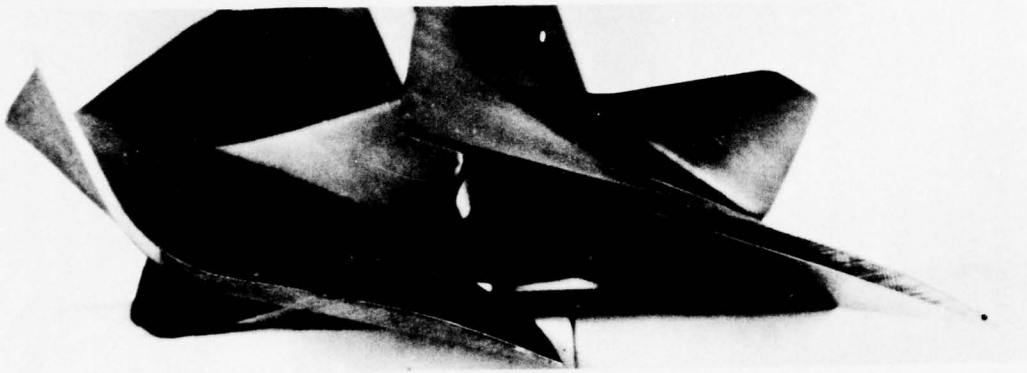

BLADE NO. 11

Figure 69. Maximum Tip Damage After Ice-Ingestion Test (No. 1).

TABLE 14 - DUCT ICE POST - INGESTION CALIBRATION TEST (No. 1)

Parameters	Total Damage After Ingestion	Blade No.11 Replaced	7 Blades Replaced	7 Blades, 6 Stators Replaced (Orig. Condition)
Fan/Supercharger Rotational Speed (%)	94.0	82.7	89.0	93.5
Compressor Rotational Speed (%)	94.0	91.4	94.7	96.8
Supercharger Exit Pressure (psia)	24.2	21.7	22.8	23.7
Compressor Exit Pressure (psia)	154.	135	155	170.
Fuel Flow Rate (lb/hr)	2409.	2024	2541.	2908.
Power Turbine Inlet Temperature (^{o}R)	1925.	1830.	1980.	2078.
Net Thrust (lbf)	5120.	4670.	5810.	6590.

	Fan	SC	Fan	SC	Fan	SC	Fan	SC
Referred Flow (lb/sec)	171.	34.4	168.	31.1	186.	34.5	197.	36.8
Referred Speed (%)	94.	94.	82.9	82.9	89.0	89.0	93.5	93.5
Pressure Ratio -	1.35	1.64	1.33	1.48	1.42	1.56	1.47	1.63
Efficiency (%)	68.4	84.2	77.9	84.0	80.0	83.1	81.6	83.0

Sixteen 2 -4 oz Birds Fired Into Blade Annulus

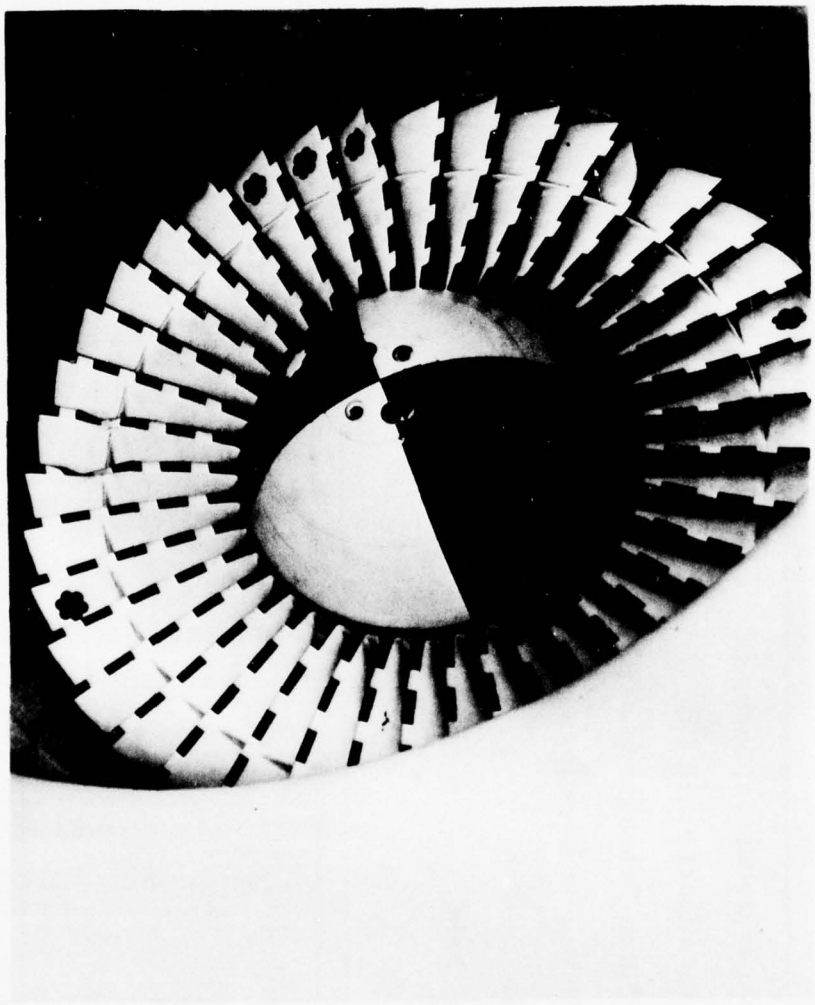

Figure 70. Fan After Small-Bird Ingestion Test (No. 2), 6800 lbf Engine.

pre- and post-ingestion test data of Table 15 show that for the same compressor speed, the fuel flow decreased, thereby indicating a decrease in compressor discharge pressure. The fan speed increased in order to pass sufficient flow to balance the power being provided by the power turbine. The overall supercharging pressure rise decreased 5 percent, while the efficiency decreased 3 percent from the undamaged condition. Damaged fan and supercharger operating conditions are given in Table 16.

Medium Bird Test (Test No. 3) - The third test selected for this study provided post-ingestion operation data for the most extensively damaged fan, resulting from the ingestion of three medium birds. See Figure 29. Rotor blade damage was limited to two areas, i. e., the tip region of four blades (especially bending of blade No. 27) and rollback of three leading edges at the midspan shrouds. Three bypass stators were dislodged and four adjacent vanes were bent. (See Figure 30). The supercharger inlet stators also exhibited some distortion. The supercharger rotor was not damaged.

In this case, the pre- and post-ingestion data shown in Tables 15 and 16 indicated that the fuel flow remained constant, while the fan speed increased some 5 percent to maintain the power balance. The performance analysis described above indicates that damage to the fan caused the supercharger to operate with a 7-percent reduction in pressure rise and efficiency.

Fan Performance - Fan maps reflecting the various degrees of damage were obtained by scaling the undamaged fan characteristics shown in Figure 71 for the 94 and 98 percent speed lines. Here, point A represents the rotating stall point for an undamaged fan at 94 percent speed, while point B represents the stalled point of the ice ingestion total damage run. The undamaged 94 percent speed line was scaled so it would collapse to a line starting at B. Lines AB and A'B' show the shift in the stall line with damage from test No. 1. The other speed characteristics were similarly scaled, as were the efficiency characteristics.

The small-bird ingestion test operating point is shown at C' and extended parallel to the stall line to D' at the 98 percent speed line of the undamaged fan. Scaling for the other degrees of damage were obtained in a similar manner, and the resulting reductions in flow, efficiency, and pressure rise are shown in Table 17.

TABLE 15 - PRE-AND POST-INGESTION TEST COMPARISONS

Parameters	Small Birds - Test No. 2		Medium Birds - Test No. 3	
	Undamaged	Damaged	Undamaged	Damaged
Fan/Supercharger Rotational Speed(%)	96. 7	98. 0	89. 3	94. 0
Compressor Rotational Speed (%)	96. 4	96. 4	93. 6	93. 6
Fuel Flow Rate (lb/hr)	3100.	2980.	2450	2450
Power Turbine Inlet Temperature (° R)	2140.	2110.	1952	1966
Net Thrust (lbf)	7350	6550	6120	5000

TABLE 16 - DAMAGED FAN AND SUPERCHARGER OPERATING CONDITIONS

Parameters	Small Birds - Test No. 2		Medium Birds - Test No. 3	
	Fan	SC	Fan	SC
Referred Flow (lb/sec)	204	37.1	176.	34.1
Referred Speed (%)	98.0	98.0	94.0	94.0
Pressure Ratio -	1.42	1.67	1.31	1.60
Polytropic Efficiency (%)	75.6	79.0	63.0	76.7

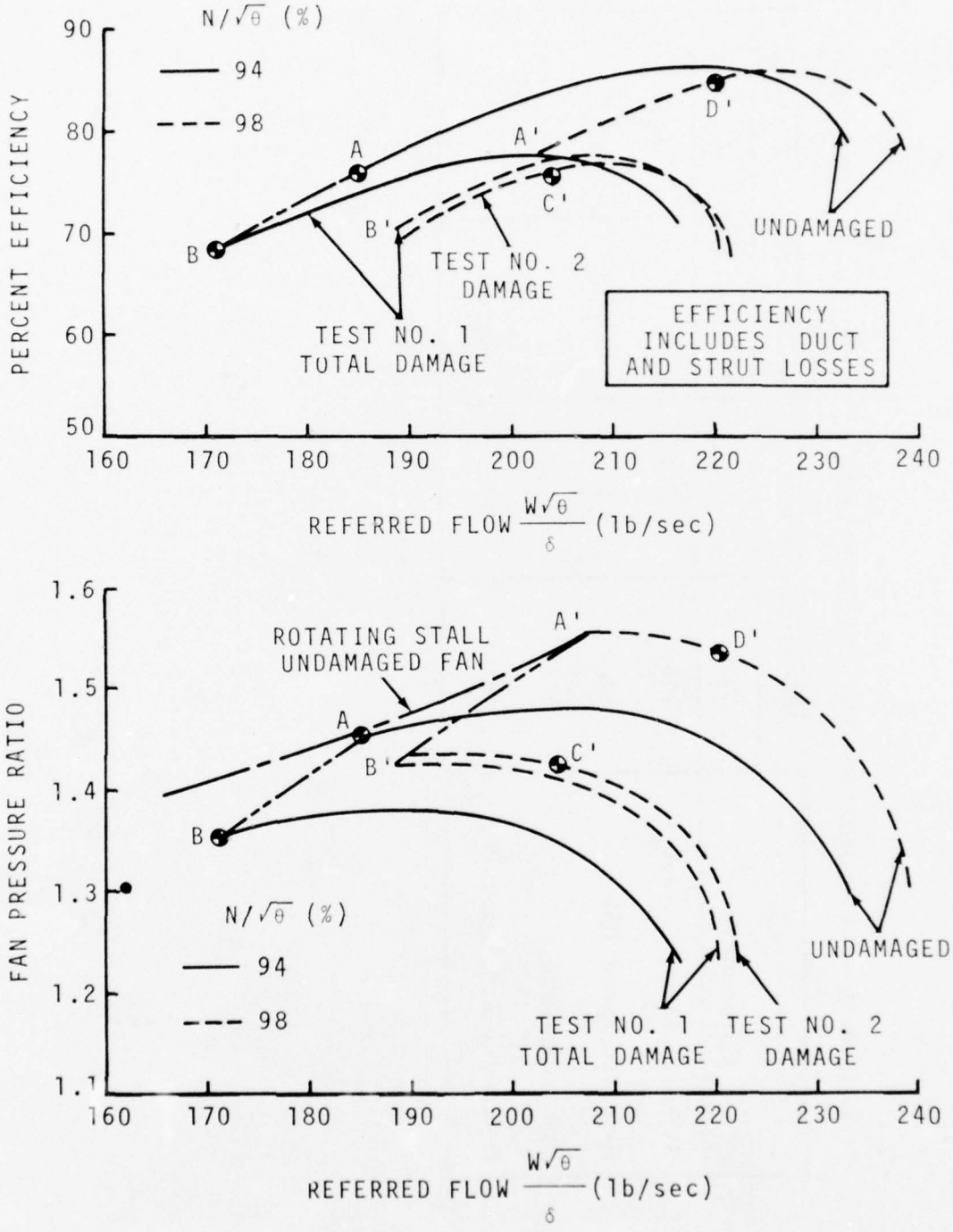

Figure 71. Scaling Procedure for Damaged Fan Efficiency and Pressure Ratio Maps.

TABLE 17 - FAN AND SUPERCHARGER PERFORMANCE DEGRADATION

Component	Reduction (%)	Fan Damage Levels					
		Test No. 1				Test No. 2	Test No. 3
		Total Damage After Ingestion	No. 11 Blade Replaced	7 Blades Replaced	7 Blades/ 6 Vanes Replaced (Orig. Cond.		
Fan	Flow	7.5	0.0	0.0	0.0	7.0	12.0
	Efficiency	10.2	2.6	1.2	0.0	11.0	23.0
	Pressure Rise (P_r -1)	21.3	0.0	0.0	0.0	20.0	35.0
Super-charger	Flow	0	0	0	0	0.0	1.0
	Efficiency	0	0	0	0	3.0	7.0
	Pressure Rise (P_r -1)	0	0	0	0	5.0	7.0

Damaged fan speed and efficiency characteristics are shown in the map of Figure 72 which was used in the engine performance computer program to estimate the thrust and flight performance that can be achieved at maximum rating for the different levels of damage. It should be noted, also, that the magnitudes of change in these fan characteristics are similar to that obtained from inlet distortion tests.

Engine performance for different damage levels is shown in Figure 73 for SLS standard day conditions and in Figure 74 for 25,000 ft, M = .7 cruise conditions. This performance is obtained with the nominal cold jet nozzle without any danger of stall; however, the stall margin for the test No. 3 damage (medium-bird test) reduces to 7 percent at take-off rating. (See Figure 75).

The percentage of undamaged take-off thrust achievable by each of the damaged configurations shown in the bar chart of Figure 76 points out that, in the worst cases, the engine could still maintain 84 percent of its thrust when operating at its maximum rating.

The degradation in fan performance does not increase in a simple proportion to the apparent damage. If a blade twists, the incidence changes and causes a change in local flow and work input for that section of the fan. However, if the blade incidence becomes too high, local separation occurs and the stall can affect adjacent passages; this is especially the case for severe rollback of the tip section. The adjacent blades, in the direction opposite to rotation, not only experience higher flow but more positive incidence. The adjacent blades in the direction of rotation experience flow with a negative incidence which causes them to unload. Due to the resulting work input variation, the flow must readjust to form an equilibrium. In the regions where the fan blades are severely rolled back, energy equivalent to the square of the tip speed is imparted to a fluid with negligible axial velocity and with a higher radial static pressure gradient necessary to sustain the higher centrifugal force field. Therefore, flow recirculation and mixing occur and this flow enters the stator vanes with high incidence, causing higher losses within the vanes, but does not experience a static pressure rise in the vanes proportional to the energy it absorbed. It would seem that the reduction in performance would not be as severe if the rolled-back leading edge of the rotor was broken off because the blockage would be reduced.

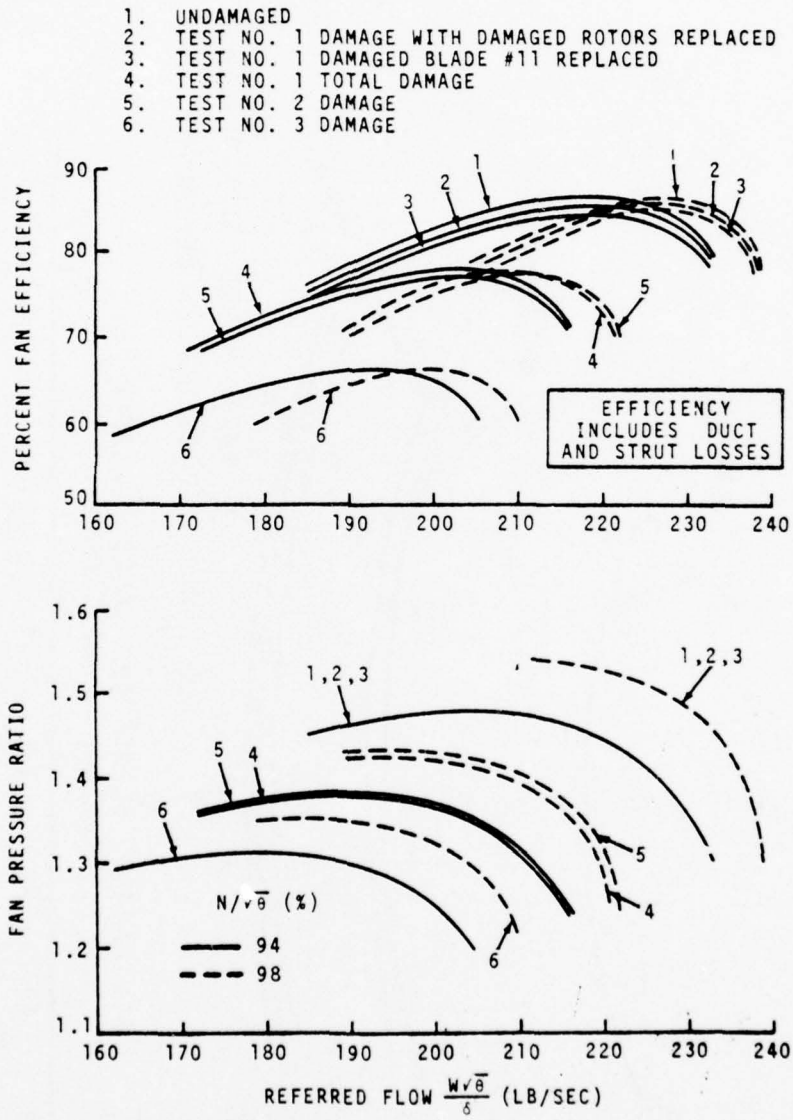

Figure 72. Damaged Fan Efficiency and Pressure Ratio Maps.

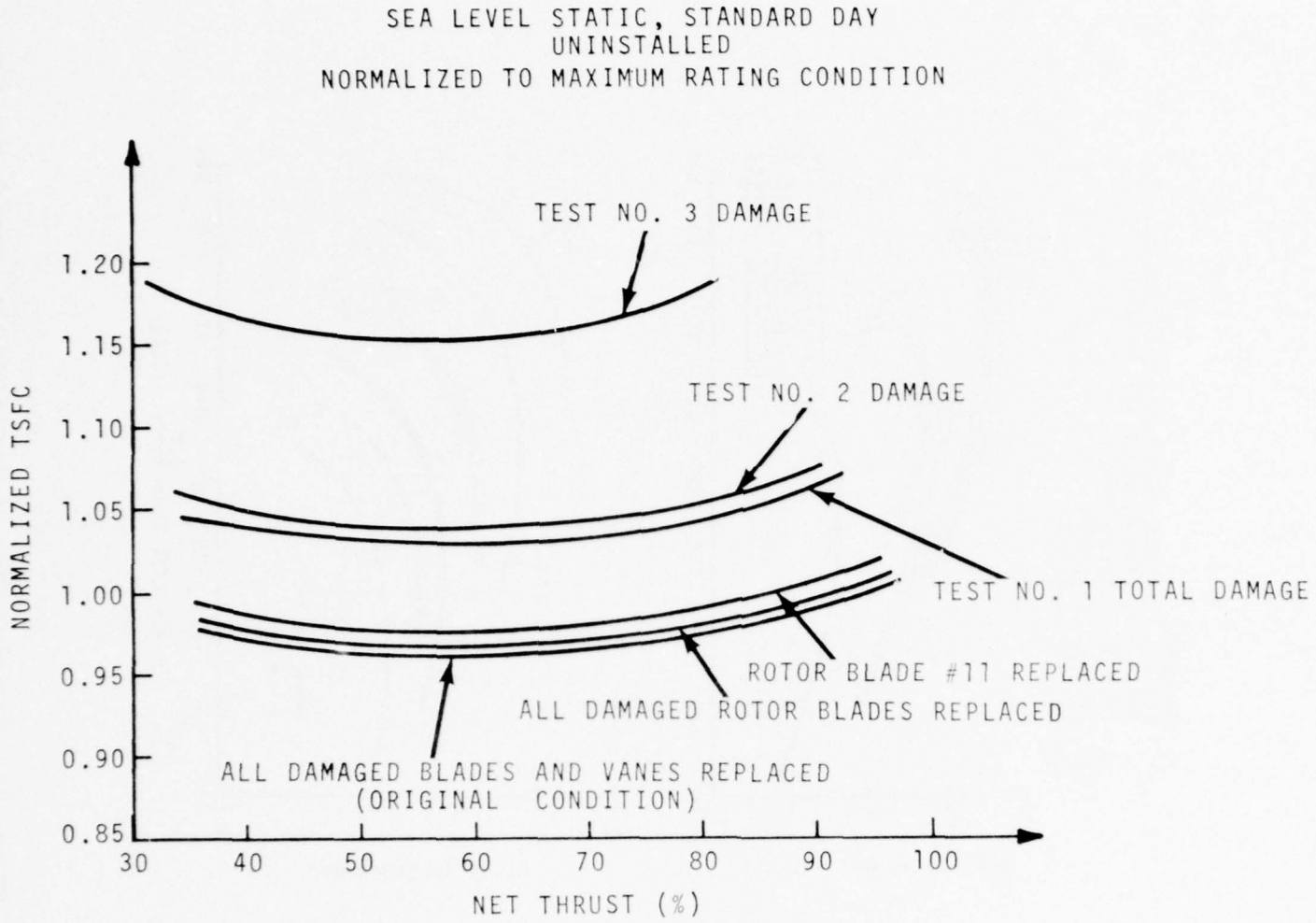

Figure 73. Specific Fuel Consumption Versus Net Thrust - Sea Level Standard, Static Conditions.

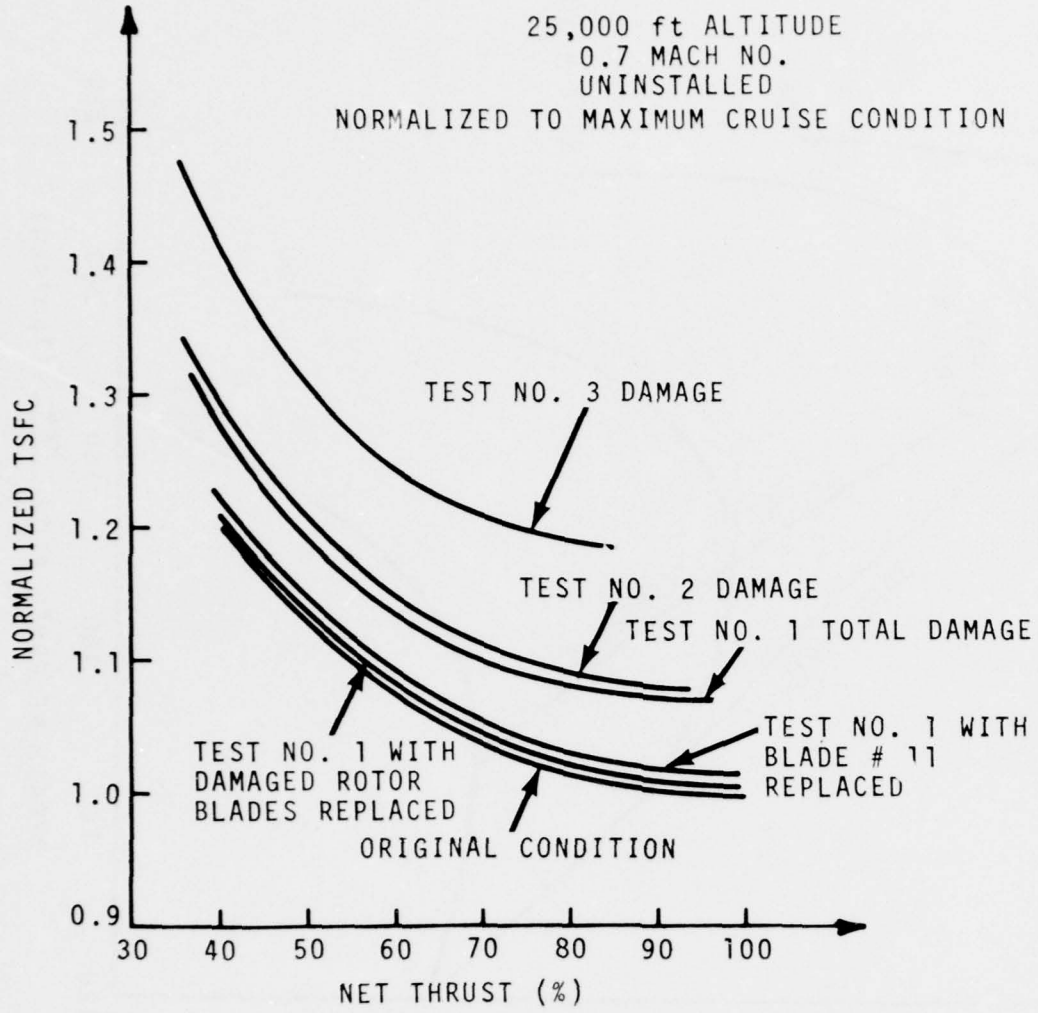

Figure 74. Specific Fuel Consumption Versus Net Thrust - 25,000 Feet Altitude and 0.7 Mach No.

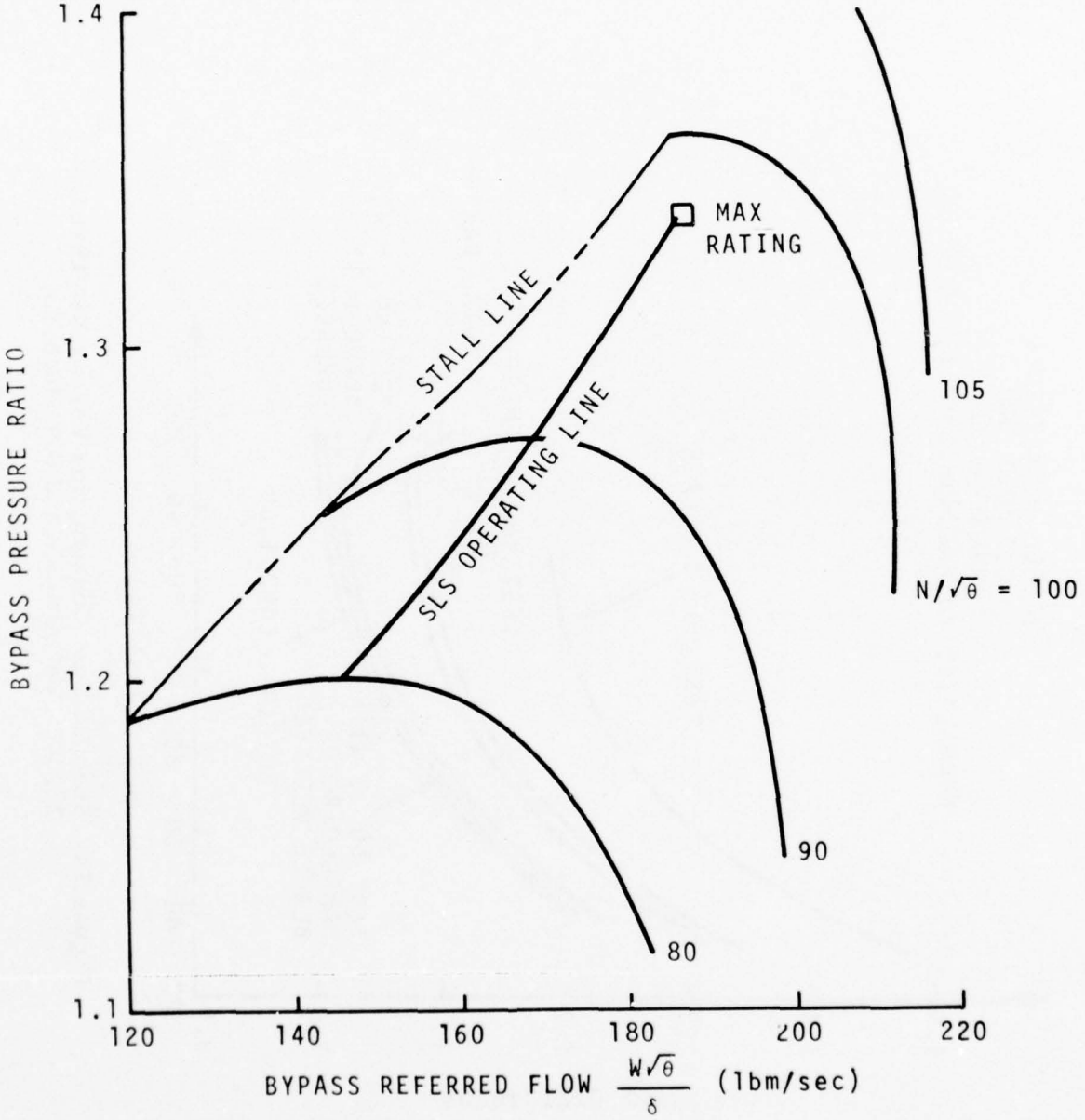

Figure 75. Estimated Fan Bypass Flow Map - Test No. 3 Damage.

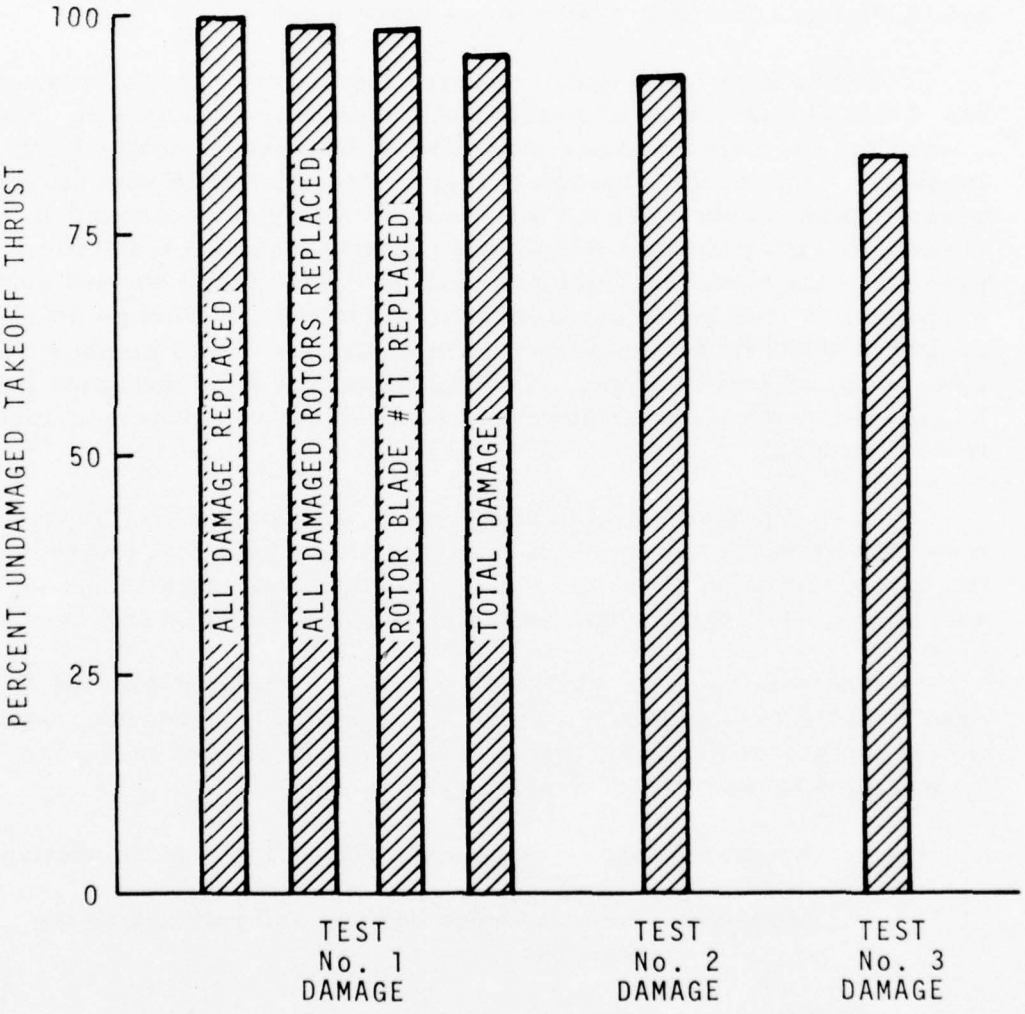

Figure 76. Percentage of Undamaged Take-Off Thrust Versus Damage Level.

As an interesting result of this study, the tip section of rotor blade No. 11, extensively rolled-back during Test No. 1, caused nearly all of the loss in performance of this engine. The remaining six damaged blades and six damaged bypass vanes only accounted for a 2 1/2 percent reduction in fan efficiency. Blade No. 11 not only caused a reduction in efficiency but it also caused a collapse of the fan speed characteristics in flow and pressure rise.

It was also found that the losses for the damaged fan used in Test No. 1 are almost identical to those of the damaged fan used in Test No. 2 when the performances are evaluated with the same nozzle area loading. The results also imply that no degradation in supercharger performance occurs when all the damage takes place outboard of the shroud, possibly because the shroud tends to maintain the static pressure rise along the blade hub section. Test No. 2 showed some performance loss in the supercharger due to the fan damage which occurred at the mid-span shroud even though there was no physical damage to the supercharger. The supercharger's performance loss in Test No. 3 was higher; however, some of the supercharger vanes were distorted.

It is expected that adjusting the performance maps (as was done here) does not apply for the entire range of the fan; however, the upper portion of the map is the most important when trying to assess the maximum thrust available from the damaged engine.

The data appearing in Table 17 were correlated with the flow area affected by the damage to provide a method of estimating degradation in fan performance. This correlation is presented in Figure 77. The various types of rotor damage classified are:

Major - Severe leading-edge rollback at the tip section

Moderate - Leading-edge bending and rollback at the shrouds

Minor - Leading-edge bending causing a change in incidence

The major and moderate rotor damages had an effect on the fan's capability to produce pressure rise and flow, whereas the minor rotor damage and the stator damage produced only a deterioration in fan efficiency.

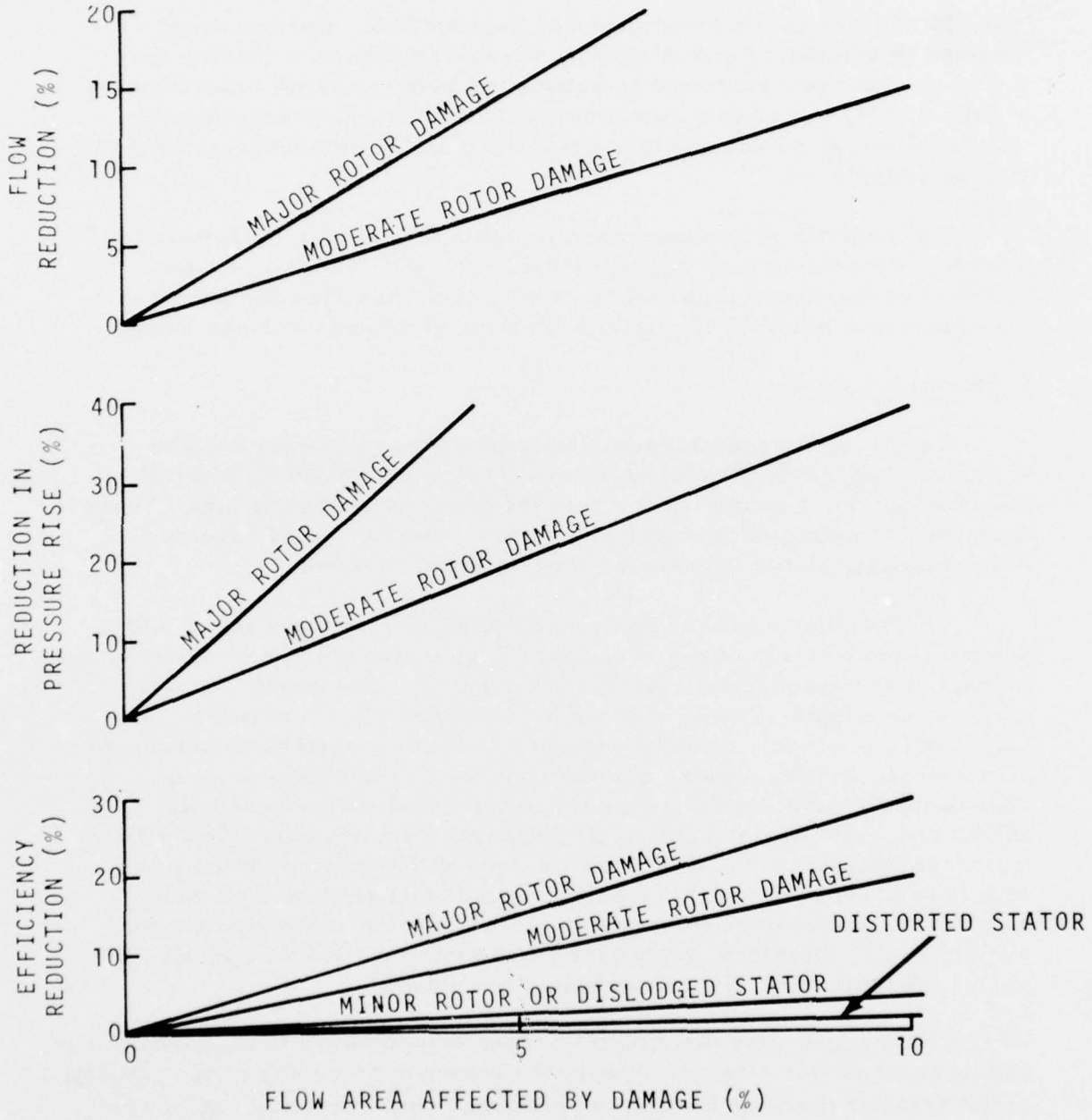

Figure 77. Performance Changes Versus Flow Area Affected by Damage.

PERFORMANCE AND COSTS ANALYSES

In addition to the structural and aerodynamic considerations involved in evaluating and modifying the fan/compressor blading for sufficient damage-resistance to satisfy the bird ingestion requirements of FAR 33.77, the effects on engine performance, aircraft operation characteristics and acquisition, operation, and maintenance costs must also be considered.

The analytic procedures used to determine engine performance, mission characteristics, and costs data are described below. Comparisons of damage-tolerant engines with their baseline designs are also presented below in the paragraph Damage-Tolerant Blade Design.

Performance Analysis

The performance characteristics of the two turbofan engines encompassing the 6800 to 1600 lbf sea level standard (SLS) take-off thrust range were evaluated for both the baseline configurations (those designed for optimum performance without regard to bird-ingestion requirements)and the redesigned bird-tolerant versions.

The baseline configurations fulfill the primary mechanical and performance criteria of the respective engine applications. Mathematical models of the aerodynamic and thermodynamic characteristics of the major components of these engines are combined in a computer program to produce a detailed aerothermodynamic mathematical model of the entire engine. These models consist of collections of aerodynamic component performance maps, duct and mechanical loss definitions, and turbine cooling air labyrinth descriptions. The performance analysis computer program uses an iterative solution procedure to provide internal component speeds and airflows, as well as external engine performance data. The results of the studies are used to scale and match component representations and to optimize the engines for specified aircraft operating conditions.

The math models defining the larger engines have been substantiated with measured test data, while only the core engine performance predictions of the smaller machine have been confirmed with operating engine tests. Scaling procedures were used to define the fan characteristics of both of the smaller baseline engines.

The performance information generated from these techniques for the baseline engines are presented in Tables 18, 19, and 20.

During the course of this study, the models were modified to simulate changes in airfoil design, shroud thickness or locations, hub/tip radius ratios, etc., as specified by the damage-tolerant redesign requirements . In most cases, rematching of components was so minor as to have negligible effect.

Mission Analysis

Mission analyses were performed for both thrust class of engines to determine differences in flight performance and costs brought about by incorporating damage-tolerant blading in the baseline engines. A medium-weight twin-turbofan transport was selected as representative of the 6800 lbf thrust class engines. For the 1600 lbf thrust class engines, a 6 to 8 place twin-turbofan general aviation aircraft was chosen. Particulars of the two aircraft are given in Table 21

In each case, a mission was defined by a full takeoff gross weight at rated cycle temperature (including ground run, acceleration in ground effect, and climb to clear an obstacle), an optimum climb to cruise altitude, and an acceleration to cruise Mach number. Normal cruise speed is then maintained (by gradual reduction of the turbine inlet temperature) until all available fuel has been consumed.

For the larger aircraft, two cruise altitudes (20,000 and 35,000 feet) and three cruise Mach numbers (0.6, 0.7, and 0.8) were examined. For the smaller aircraft, a cruise altitude of 25,000 feet and Mach numbers of 0.60 and 0.65 were chosen for study.

Aircraft performance characteristics including range and flight time were determined by a standard Lycoming mission analysis computer program for the baseline engines and the damage-tolerant versions.

Cost Analysis of Alternate Designs

A cost analysis of alternate engine designs was made to assess the economic penalties incurred in satisfying the bird-ingestion requirements of FAR 33.77. Many of the standard life-cycle cost elements (for example, spare engines and powerplants, facilities and support equipment) were assumed to be equivalent for the engine alternatives. The cost

TABLE 18 - BASELINE ENGINE PERFORMANCE,
6800 LBF THRUST CONFIGURATION

Rating	SLS Take-off	Initial Climb	Max. Climb	Max. Cruise
STD Altitude (feet)	-0-	100	2000	35,000
Flight Velocity(kt)	-0-	120	160	400
Net Thrust (lb)	6770	5480	4960	1432
Fan:				
Referred Speed (rpm)	6870	6870	6770	7690
Referred Airflow (lb/sec)	215.	216.	214.	241.
Pressure Ratio	1.44	1.43	1.42	1.53
Supercharger:				
Referred Speed (rpm)	6870	6870	6770	7690
Referred Airflow (lb/sec.)	36.26	36.11	35.26	39.77
Pressure Ratio	1.64	1.64	1.62	1.76
Core Compressor:				
Referred Speed- (rpm)	17,420.	17,390	17,300.	17,900
Referred Airflow- (lb/sec.)	24.09	23.98	23.74	25.07
Pressure Ratio	6.09	6.93	6.81	7.57
Bypass Ratio	5.91	5.98	6.07	6.05

TABLE 19 - SCALED BASELINE ENGINE PERFORMANCE
1600 LBF THRUST CONFIGURATION

Rating	SLS Take-Off	Initial Climb	Max. Climb	Max. Cruise
STD Altitude (feet)	-0-	100	2000	25000
Flight Velocity (kit)	-0-	115	150	350
Net Thrust (lb)	1550	1225	1000	435
Fan:				
Referred Speed (rpm)	10920.	10,910	10430	11720
Referred Airflow (lb/sec.)	59.75	60.60	59.63	69.63
Pressure Ratio	1.33	1.33	1.31	1.38
Supercharger:				
Referred Speed (rpm)	10920	10910	10430	11720
Referred Airflow (lb/sec)	7.17	7.13	6.86	7.61
Pressure Ratio	1.28	1.28	1.26	1.33
Core Compressor:				
Referred Speed (rpm)	43780	43550	42350	44240
Referred Airflow (lb/sec)	5.85	5.82	5.67	6.03
Pressure Ratio	9.30	9.22	8.91	9.86
Bypass Ratio	8.34	8.50	8.69	9.15

TABLE 20 - LOW ASPECT RATIO BASELINE ENGINE PERFORMANCE, 1600 LBF THRUST CONFIGURATION

Rating	SLS Take-Off	Initial Climb	Max. Climb	Max. Cruise
STD Alitiude (feet)	-0-	100	2,000	25,000
Flight Velocity (kt)	-0-	115	150	350
Net Thrust (lb)	1575	1247	1018	444
Fan:				
Referred Speed (rpm)	10290	10260	9860	11000
Referred Airflow (lb/sec)	60.35	61.16	60.66	70.15
Pressure Ratio	1.35	1.33	1.32	1.39
Supercharger:				
Referred Speed (rpm)	10290	10260	9860	11000
Referred Airflow (lb/sec)	7.27	7.14	6.95	7.62
Pressure Ratio	1.29	1,28	1.27	1.33
Core Compressor:				
Referred Speed (rpm)	41000	40710	39470	41240
Referred Airflow (lb/sec)	5.89	5.80	5.69	6.02
Pressure Ratio	9.38	9.19	8.96	9.83
Bypass Ratio	8.40	9.56	8.72	9.20

TABLE 21 - TWIN-TURBOFAN AIRCRAFT USED IN MISSION ANALYSIS

PARAMETERS	ENGINE THRUST CLASS	
	6800 lbf	1600 lbf
Design Gross Weight (lb)	24000	7800
Accommodation (max. seating)	24 - 32	6-8
Payload * (lb)	2200	1200
Wing Loading (lb/ft^2)	62	47
Wing Aspect Ratio	7.5	8
Total Fuel Weight (lb)	10,500	2300 (1) 2273 (2)
Fuel Reserve (lb)	1,000	405 (1) 399 (2)

(1) Scaled Fan Baseline Engine

(2) Low Aspect Ratio Fan Baseline Engine

* Long range missions based on:

12 passengers + baggage and 3 crew for 24000 lb G. W. aircraft

4 passengers + baggage and 2 crew for 7800 lb G. W. aircraft.

elements that were considered to be of significance are the investment in engines and airframe, the fuel costs per flight hour, and the direct maintenance costs per flight hour.

Investment in Engines and Airframe - Detailed designs and subsequent pricing by conventional methods are not always available or feasible for studies of this type. Estimates of the engine prices were, therefore, made by Maurer's parametric cost estimating relationships (C.E.R.), which is especially suited to this task because of its ease and ability to show relative cost differences. (Reference 21). By this method, engine production costs are estimated by linear interpolation of a relationship describing historical production costs for advanced technology aircraft engines and a material index factor (MIF). This factor is based on the summation of the products of engine parts weights (taken from a bill of material) and a material type factor (MTF). This material-type factor, in turn, is the product of a relative cost factor and a relative machinability factor for each type of material used.

Since only differences in costs were of interest in this study, the effects of various blade designs on engine cost were considered to be only a function of weight and material differences. A change in one pound of weight was considered to result in a specified dollar change in the acquisition price of the engine. Furthermore, since engine acquisition costs are approximately 25 percent of total aircraft costs, the weight differences in engine designs and, therefore, costs were assumed to affect airframe costs by a factor of 3.

Amortization of total acquisition costs in dollars per operating hour were based on a 10-percent residual over 15 years at a utilization of 2000 hours per year.

Fuel Costs - Fuel consumption figures were obtained from the computerized performance and mission simulations described above for the various alternate designs. Of the various missions evaluated, one was arbitrarily chosen as a "standard" to be used in the cost study for each engine size. The standard mission for the 6800 lbf thrust class engines was taken as a long-range flight of approximately 2500 NM cruising at Mach 0.8, and 35,000 feet. For the 1600 lbf thrust class engines, an approximately 1200 NM range cruise at Mach 0.65 and 25,000 feet was taken as the standard mission. Fuel costs in dollars per hour were based on pounds of fuel consumed and flight time using a weight of 6.5 pounds per gallon and a price of 46 cents per gallon.

Direct Maintenance Costs - Many of the alternate engine design items normally considered under direct maintenance costs were assumed to have negligible differences and, therefore, were not included in the analyses. Scheduled inspection intervals and times, for example, would not change with the slight differences in fan blade configurations. Also, the improvements in reliability and repairability of the blades and, therefore, the mean time-to-failure and man-hours to repair and/or replace them would probably not be measurable.

In this study, direct maintenance costs were determined solely by the engine operating characteristics and their effects on engine mean time-between-removal (MTBR). The parametric cost estimating relationships suggested by Sallee (Reference 22) were used to estimate the differences in MTBR and maintenance costs based on turbine inlet temperature and flight duration.

DAMAGE-TOLERANT BLADE DESIGN

The results of the preceding analyses and tests were used to design blading with sufficient damage resistance to successfully meet the bird-ingestion requirements of FAR 33.77. The approach selected was to thicken the airfoil sections of the baseline blades of both engines. For the 6800 lbf engine, particular attention was paid to the midspan region and to the mechanical design of the shroud. For the 1600 lbf machine, the final damage-tolerant configuration was based on the low aspect ratio baseline blade rather than the shrouded baseline design.

For both cases, an iterative procedure was required to optimize the design structurally and aerodynamically. The results of a bird-ingestion test performed on the damage-tolerant 6800 lbf engine was used to confirm the redesign procedure. Finally, performance and cost penalties were evaluated for both engine classes based on typical missions in representative aircraft.

Damage Tolerant 6800 lbf Blading

The damage-criterion distribution along the span of the baseline blade for the 1.5-pound bird FAR ingestion conditions, when compared with the ingestion test program results, defines the thickness requirements (at least at the impact sites aft of the leading edge) for an acceptable bird-resistant blade design.

To obtain the necessary thickness distribution over the span, the baseline blade section profiles were thickened by simultaneously increasing t_{max} and the leading-edge radius. Additionally, the location of t_{max} was shifted forward and the leading edge wedge angle was increased, both of which combine to form a still heavier, blunter, forward region. These changes shown in Figures 78 and 79 point out the extra thickening incorporated in the shroud area.

The high design Mach number levels that dictated a multiple circular arc airfoil section were compromised somewhat by choosing sections with definitions closer to that of a double circular arc. A representative streamline section of the two blades is shown in Figure 80. The result of these changes is an overacceleration of flow on the suction surface and a higher shock Mach number level than would otherwise be obtainable. The penalty in bypass efficiency resulting from these changes and the associated incidence increases required to maintain the cascade throat area were estimated to be one percent for SLS takeoff and 1.6-percent for cruise.

The resulting damage criterion distribution along the span is compared with the baseline blade and test program values in Figure 81. It is seen from the figure that a generous margin of safety was incorporated at the shroud region over that provided by the baseline blade. This was done to minimize tearing in this region and to guard against blade failure below the shroud, with the consequent loss of midspan support for the adjacent (high aspect ratio) blades.

Additional tolerance was also incorporated out towards the tip to inhibit tip rollback. The outermost 3/4 inch slightly exceeds the known limits of the acceptable damage range, but full impact by a (spherical) 1.5-pound bird is not possible within 2 inches of the tip in any case.

It is also seen that the damage criterion just outboard of the root region slightly exceeds the known acceptable damage line, but since no damage of any kind had ever been observed in this region, the thickness here is expected to provide more than adequate damage tolerance.

Comparisons of the predicted damage levels between the damage-tolerant blade and the baseline are shown in Figure 82 for the three bird sizes of FAR 33.77. Although a slight improvement is noted between the hub and the 13-inch radius, the major improvement was obtained between the 13- and 18-inch radii that reflects the design concerns for the outboard region near the shroud.

REDESIGN THICKENING PARAMETERS FOR FOD TOLERANCE

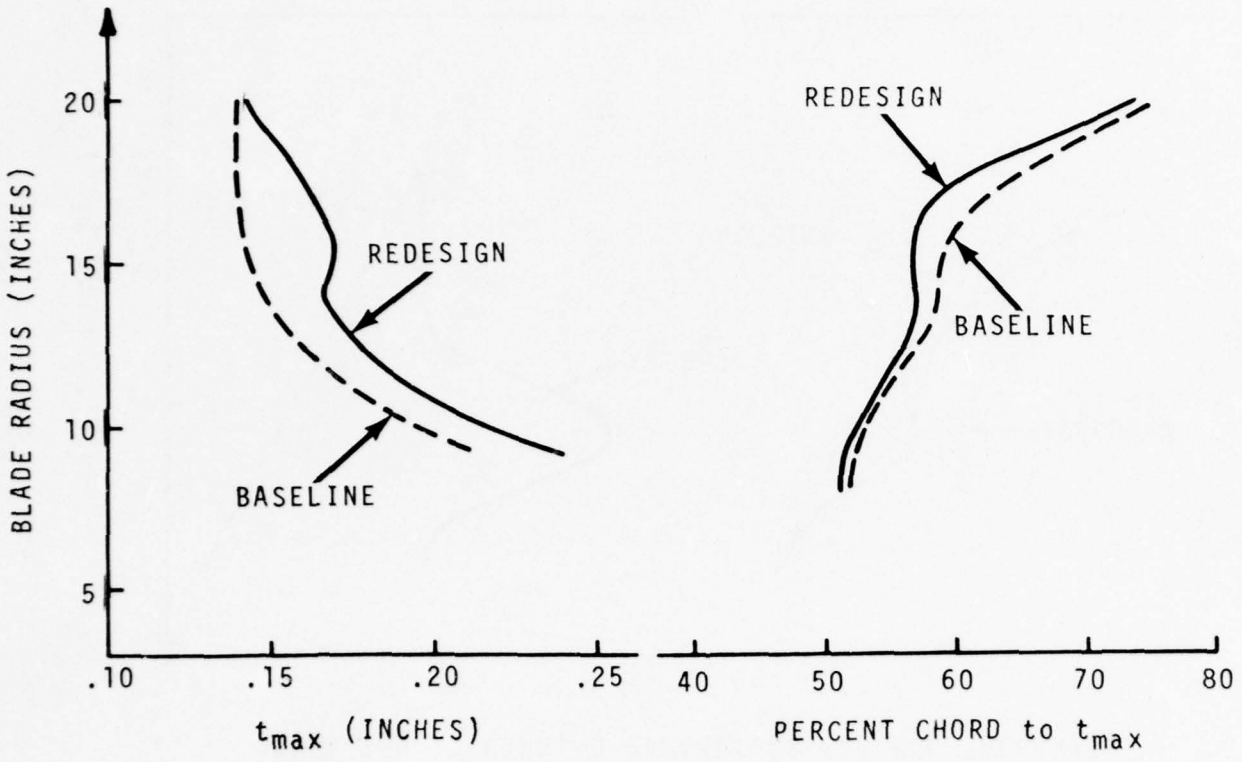

Figure 78. Redesign of Maximum Thickness Distribution - 6800 lbf Blade.

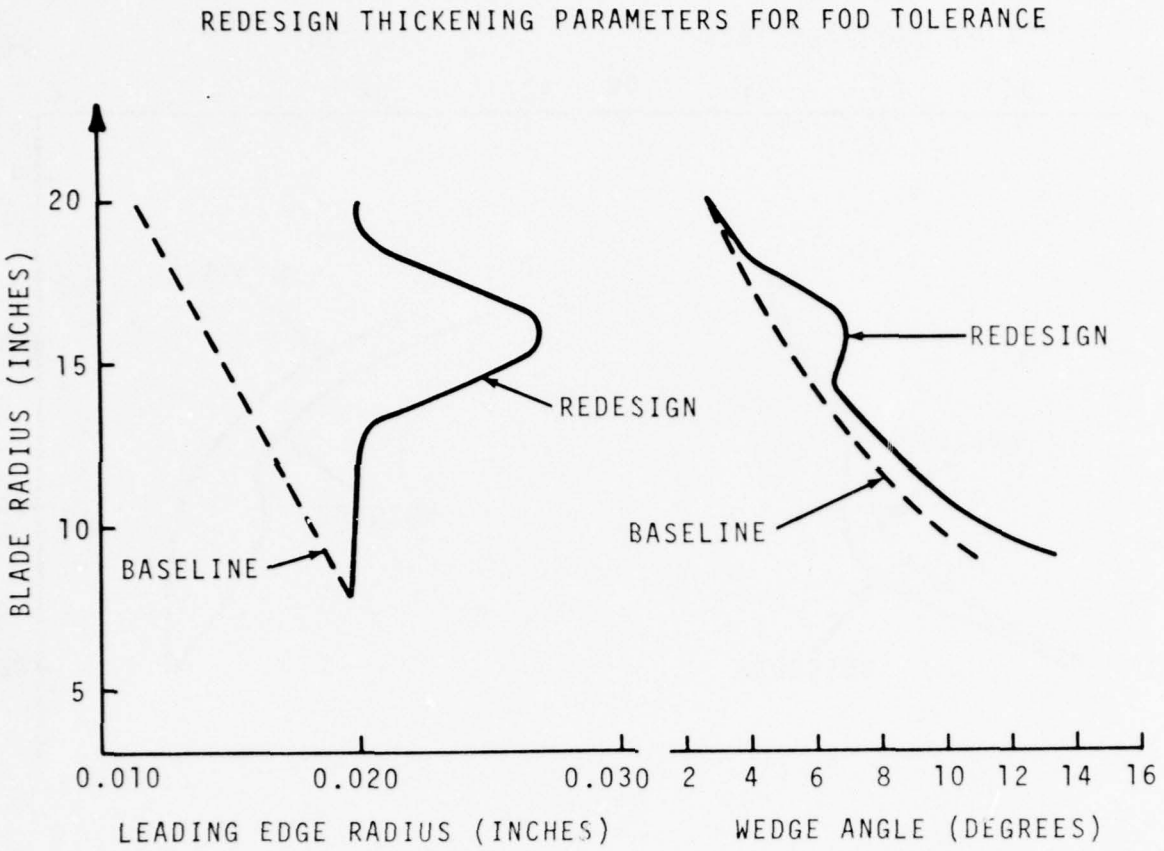

Figure 79. Redesign of Leading Edge Radius Distribution - 6800 lbf Blade.

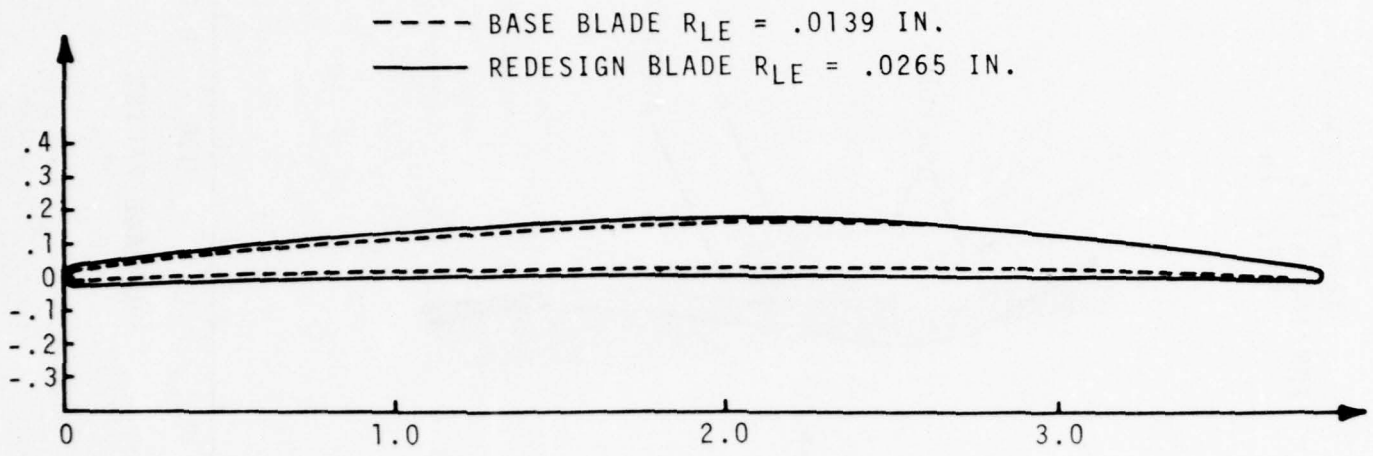

Figure 80. Redesign Airfoil Section Distribution - 6800 lbf Blade.

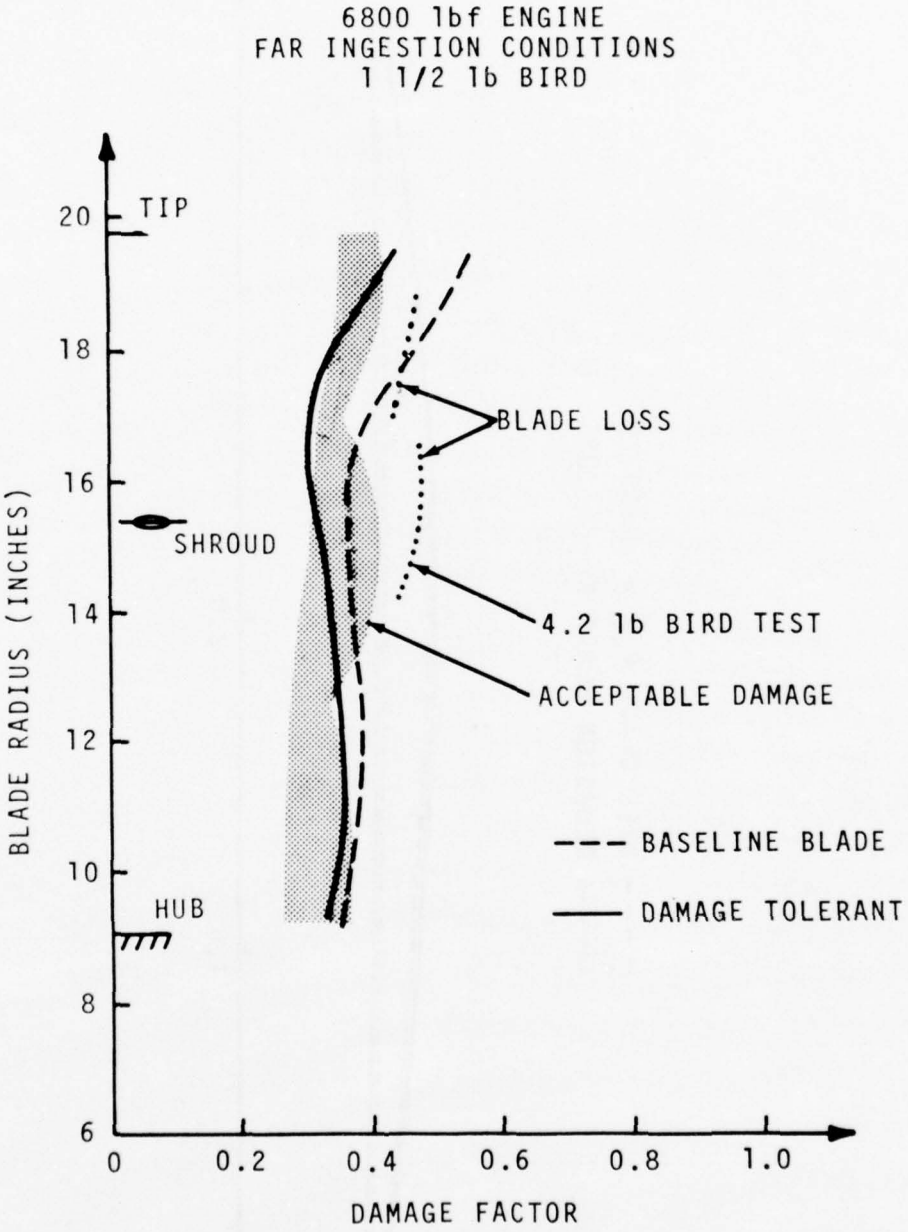

Figure 81. Redesign Damage Factor Limits - 6800 lbf Blade.

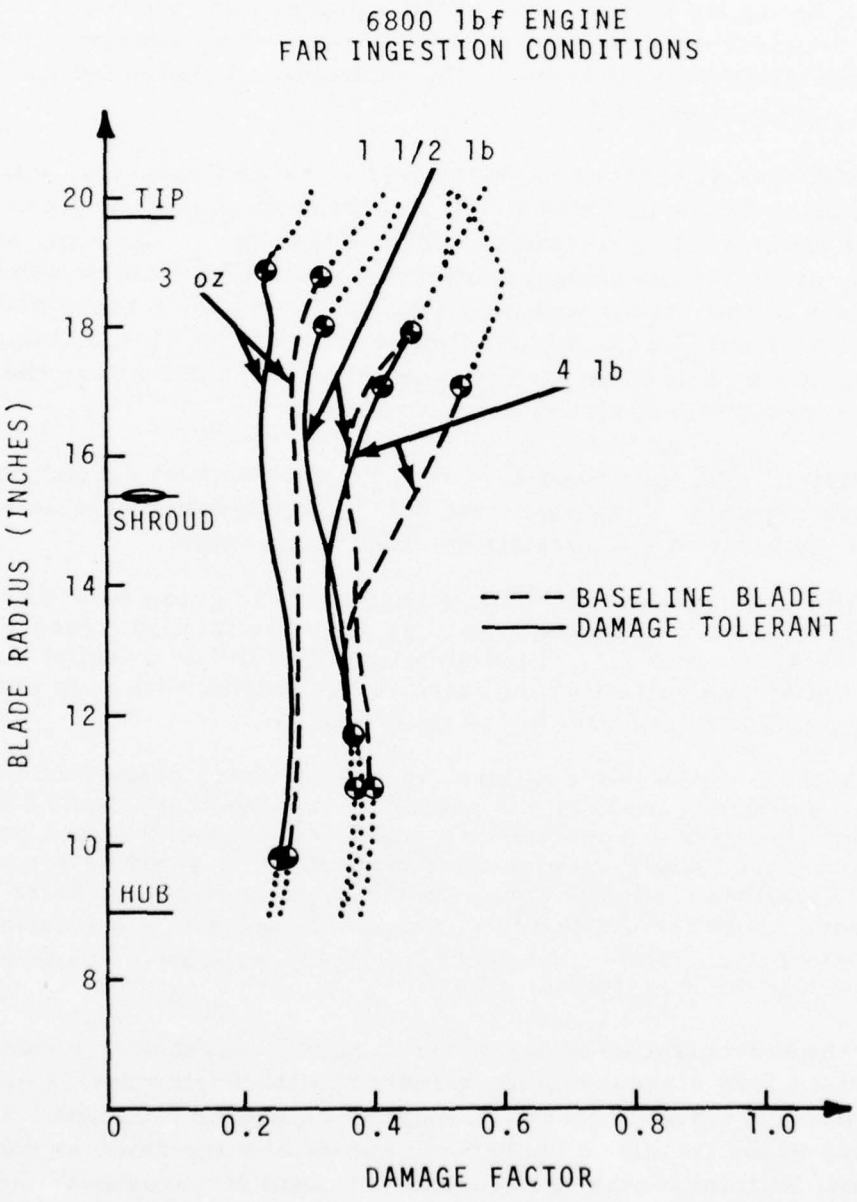

Figure 82. Redesign Damage Factor for FAR Conditions - 6800 lbf Blade.

In addition to thickening the airfoil, the shroud was positioned further out towards the tip (from 58 to 63 percent of the span) for better support during tip impact, while still satisfying the vibration and flutter requirements of the new blade design. This change was additionally beneficial in that it reduced the cantilevered region outboard of the shroud by 11 percent.

Mechanical changes to the shroud were also incorporated. (See Figure 83). These included first, an increased contact angle to provide greater blade bending flexibility and load transfer to the root, and second, an increased shroud contact area to further inhibit shingling. The shape of the shroud was also changed to provide a more blunt surface to impact on the adjacent blade if shingling should occur. Greater blend radii were also incorporated, especially near the leading edge, to reduce local stress concentrations.

Reinforcing tabs were also added under the root shroud contact surfaces to inhibit shingling in the hub region and the possible resultant loss of the blade in the dovetail or disk tenon region.

The damage-tolerant blade's resistance to gross bending failure was also evaluated using the transient response method. (See Figures 84 and 85.) The maximum tip displacement of the new design and the maximum stress value just outboard of the shroud were both reduced by 30 percent compared with the baseline blade.

In the event of blade failure, the new heavier blade would impose greater imbalance loads on the shaft bearings and associated support structure and also impose greater impacting kinetic energies on the containment ring. These results are summarized in Table 22 for various failure locations along the span. Redesign to accomodate these greater imbalance loads results in minor weight increases in the rotating and static support structures but requires an approximately 20-percent weight increase for the containment ring.

The structural integrity of the impact-tolerant design was checked for satisfactory steady-running stresses at the engine design operational speed using the NASTRAN finite-element computer program. The stresses in the thickened blade were essentially the same as for the baseline, with increases in the maximum span stresses near the root and in the shroud region of less than 5 percent. The maximum root reaction forces increased by 20-percent. A rotor disc weight increase of approximately 15 percent was required to carry the heavier blades.

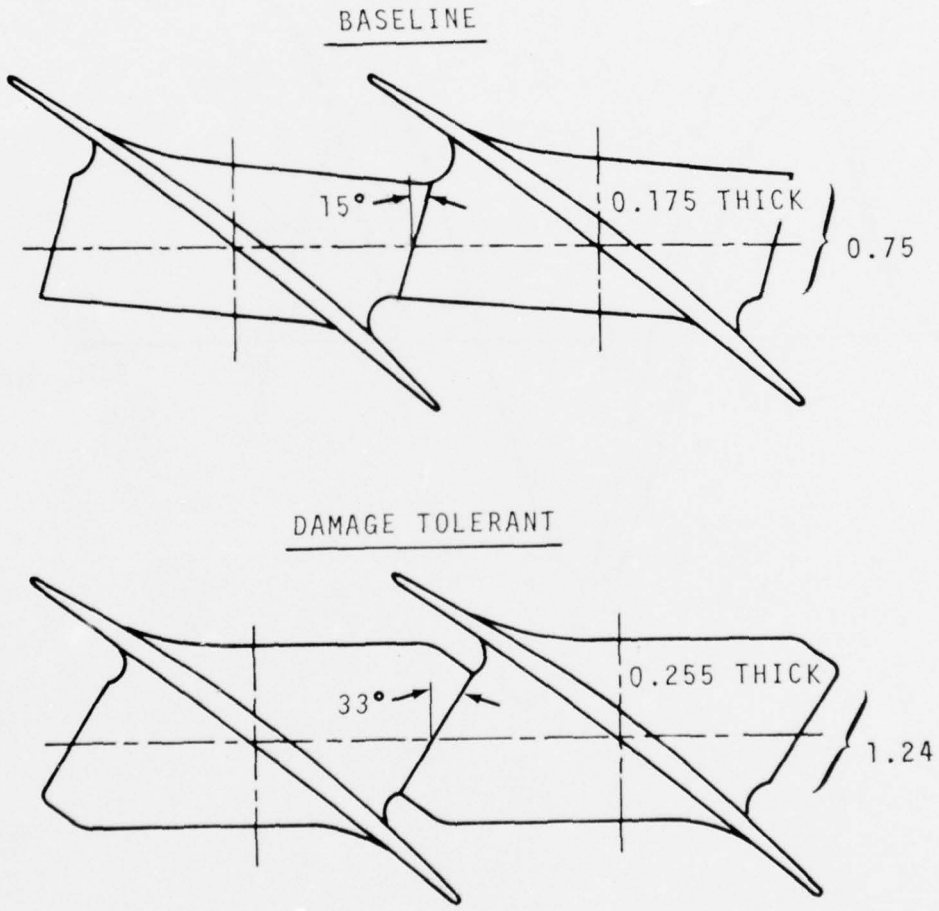

Figure 83. Shroud Redesign for Damage Tolerant Blade - 6800 lbf Blade.

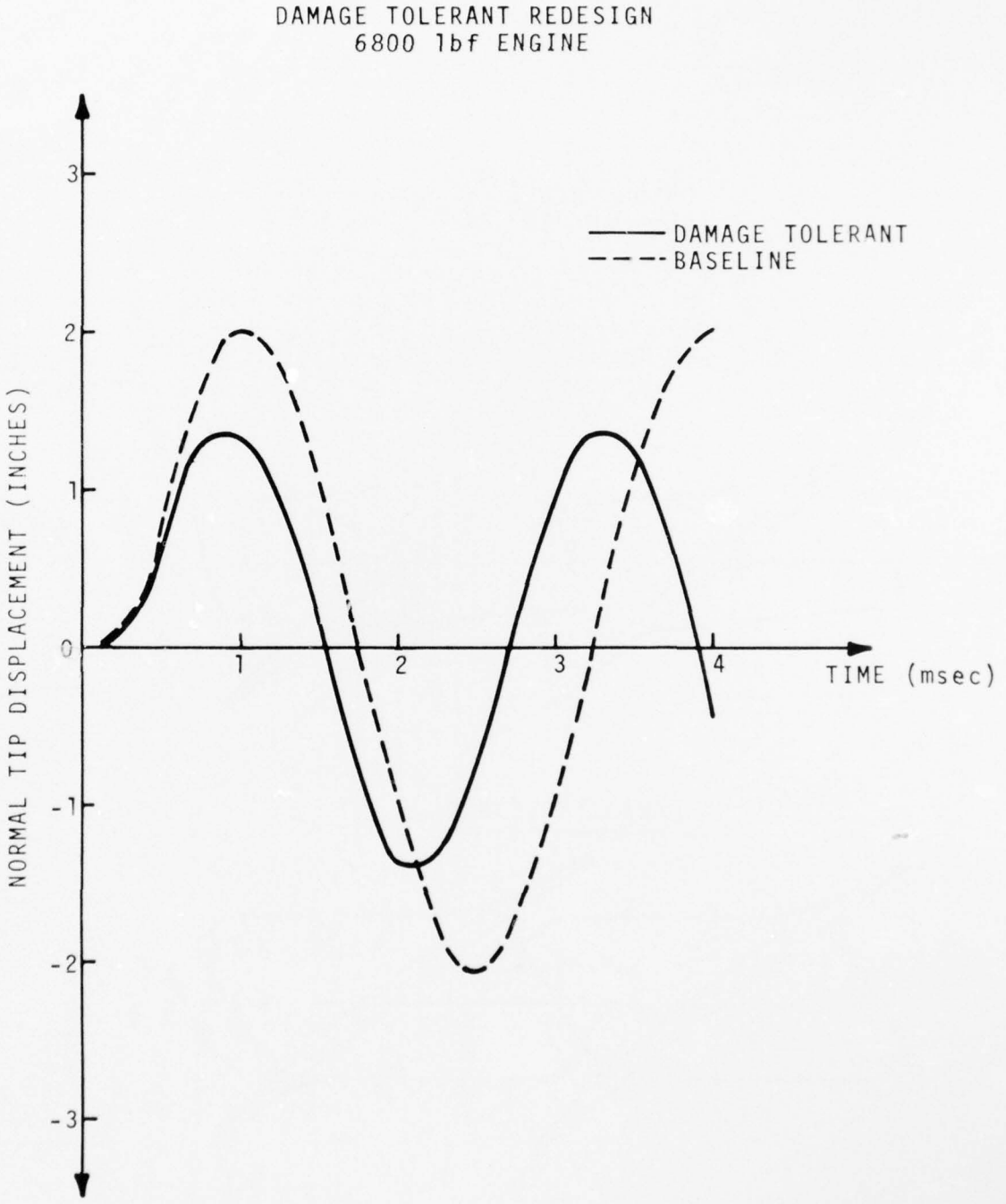

Figure 84. Effect of Redesign on Tip Displacement - 6800 lbf Blade.

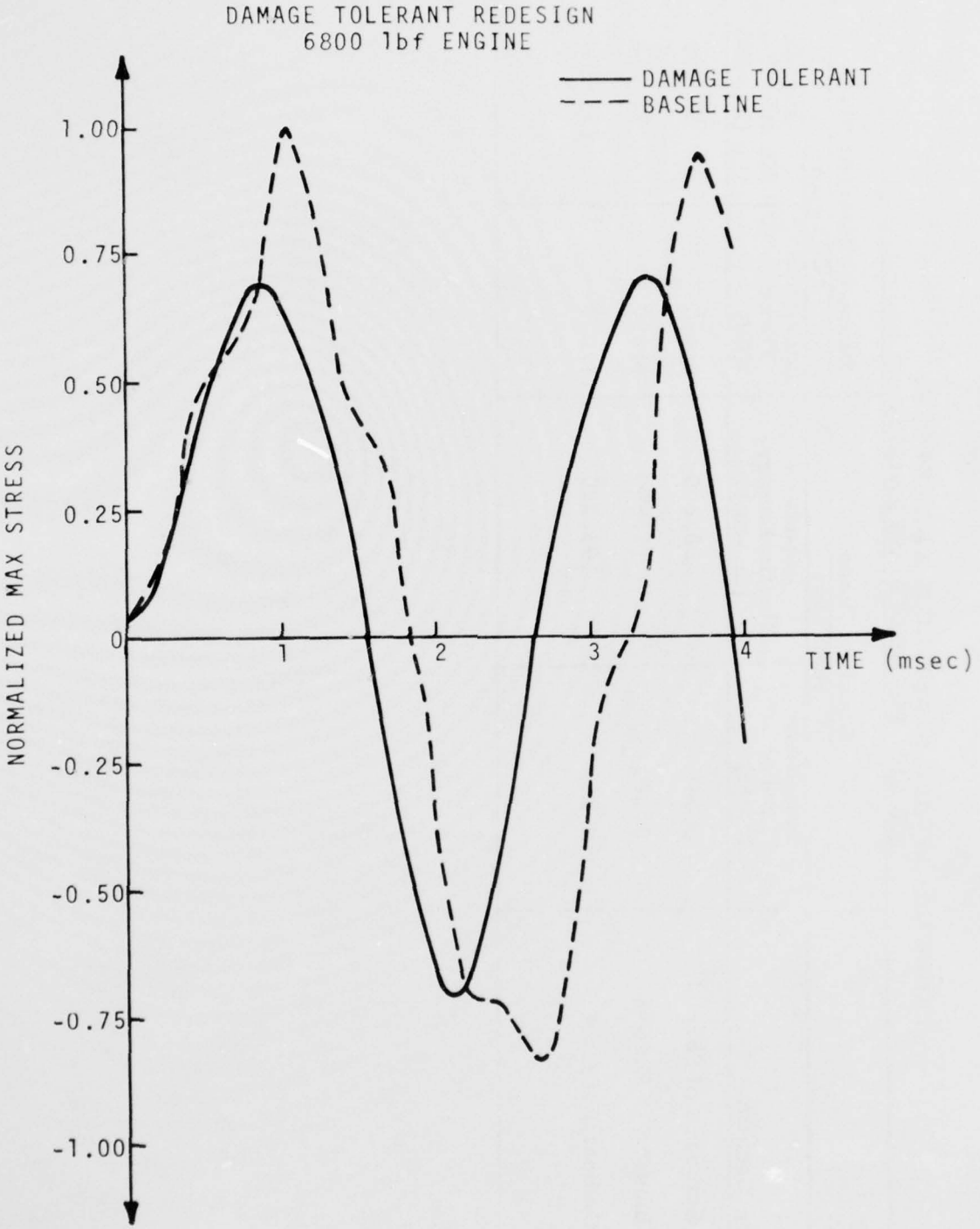

Figure 85. Effect of Redesign on Maximum Stresses - 6800 lbf Blade.

TABLE 22 - SINGLE BLADE LOSS AT TAKEOFF,
6800 LBF THRUST CLASS ENGINE

	Baseline Blade 6880 rpm		Damage-Tolerant Blade 6880 rpm	
Failure Location	Imbalance Force (lbf)	Impact Kinetic Energy (in.-lbf)	Imbalance Force (lbf)	Impact Kinetic Energy (in.-lbf)
0.25-Inch Outboard of Shroud	6,540	58,500	6,480	58,100
0.25-Inch Inboard of Shroud	8,270	71,800	9,090	78,400
0.25-Inch Outboard of Root	14,210	108,300	17,200	131,200

Static and engine running tests confirmed the structural integrity of the damage-tolerant engine, including satisfactory vibration and flutter control by the redesigned shroud. In particular, a full-scale medium-bird ingestion test confirmed the ingestion capability of the damage-tolerant blading. Two 1.5-pound birds striking the shroud region resulted in minor bending of the leading edges struck near the shrouds, with one blade exhibiting a small (1/4-inch) tight spanwise tear at the shroud radius. (A third bird struck the spinner without causing any damage to the spinner, fan, or core engine). See Figure 86. Post-ingestion operation showed essentially no change in engine performance, temperature, or vibration levels.

A performance analysis of the damage-tolerant engine resulted in a take-off thrust penalty of only 1 percent and a TSFC penalty at cruise of only 1 percent from the baseline engine (Refer to Table 23).

These minor engine performance changes have a correspondingly small influence on aircraft operating characteristics as shown in Tables 24 and 25. Maintaining rated cycle temperature for takeoff is seen to result in an increased takeoff distance to clear an obstacle (200 feet) at full weight of approximately 20 feet, or less than 1 percent. Alternatively, the cycle temperature could be increased by 10 degrees for takeoff with no change in aircraft takeoff performance, but with decreased hot-section life.

The structural and performance changes are also seen to have only a minor influence on the total operating costs. Table 26. It is interesting to note that the larger A-2 (reduced wheel speed) design is somewhat more expensive than the damage-tolerant version and still does not have sufficient damage resistance. Consequently, mission analyses were not performed for that configuration.

Damage-Tolerant 1600 lbf Blading

A similar redesign procedure was undertaken for the smaller size machine, but in this case, the unshrouded low aspect ratio baseline blade was thickened rather than the scaled shrouded design due to the better performance and economics of the wide-chord configuration. In particular, the low aspect ratio design allowed removal of the part-span shroud with a corresponding gain in efficiency that more than made up for the reduction resulting from the aspect ratio change. At the same time, the increased hub/tip radius ratio reduced the tip speed, which further reduced the noise level - a prime requisite for the business aircraft market.

Shroud Strikes of Two 1.5 lb Birds

Figure 86. Fan After Medium-Bird Ingestion Test, 6800 lbf Thrust.

TABLE 23 - DAMAGE-TOLERANT ENGINE PERFORMANCE COMPARISON, 6800 LBF THRUST CLASS ENGINE

Damage-Tolerant Versus Baseline Blade		
Rating	Thrust (%Δ)	TSFC (%Δ)
SLS Take-Off (Sea level @ 0kt)	-0.99	+0.73
Initial Climb (100 ft @ 120 kt)	-1.09	+0.97
Max. Cruise (35,00 ft @ 400 kt)	-0.84	+0.97

TABLE 24 - ENGINE MISSION ANALYSIS,
6800 LBF THRUST BASELINE CONFIGURATION

Cruise Altitude (ft)	20,000 Feet			35,000 Feet		
Cruise Mach No.	0.6	0.7	0.8	0.6	0.7	0.8
Take-off Distance (ft)	2180.	2180.	2180.	2180.	2180.	2180.
Time to Altitude (min.)	4.80	4.80	4.80	10.9	10.9	10.9
Avg Rate of Climb (ft/min.)	4170	4170	4170	3210.	3210.	3210.
Cruise Fuel Available * (lb)	8730.	8340.	7840.	9210.	8920.	8680.
Avg Specific Range, Cruise (NM/lb)	0.204	0.176	0.156	0.333	0.308	0.282
Cruise Range (NM)	1780.	1470.	1210.	3090.	2780.	2460.
Cruise Time (hr)	4.82	3,41	2.46	9.07	7.01	5.41
Turbine Inlet Temp., last (° R)	1946.	2126.	2299.	1817.	1965.	2115.

* Allowing for 45 min. fuel reserve at end of cruise gross weight and speed. No allowance for enroute cruise climb.

TABLE 25 - ENGINE MISSION ANALYSIS,
6800 LBF THRUST BIRD -
TOLERANT CONFIGURATION

Crusie Altitude (Feet)	20,000 Feet			35,000 Feet		
Cruise Mach No.	0.6	0.7	0.8	0.6	0.7	0.8
Take-off Distance (feet)	2200.	2200.	2200.	2200.	2200.	2200.
Time to Altitude (min)	4.86	4.86	4.86	11.5	11.5	11.5
Avg. Rate of Climb (ft/min)	4130.	4120.	4120.	3050	3050.	3050.
Cruise Fuel Avaliable* (lb)	8810.	8200.	7640.	9190.	8820.	8610.
Specific Range, Cruise (NM/lb)	0.201	0.175	0.154	0.330	0.305	0.280
Cruise Range (NM)	1770	1430.	1160.	3070.	2730.	2410.
Cruise Time (hr)	4.81	3.33	2.37	9.02	6.86	5.32
Turbine Inlet Temp, last (^{o}R)	1952	2133.	2307.	1823.	1967.	2122.

* Allowing for 45 min. fuel reserve at end of cruise gross weight and speed. No allowance for cruise climb.

TABLE 26 - DAMAGE-TOLERANT ENGINE COST COMPARISON
6800 LBF THRUST CLASS ENGINE

Cost	COSTS IN DOLLARS/HOUR PER ENGINE				
	Baseline $/hr	Damage tolerant $/hr	(%Δ)	A-2 Low Wheelspeed $/hr	(%Δ)
Amortized Cost (1)					
Engine	13.48	13.50	(0.15)	13.55	(0.50)
Airframe	40.44	40.50	(0.15)	40.65	(0.50)
Sub Total	53.92	54.00	(0.15)	54.19	(0.50)
Fuel Cost @ 46 cents/gal	59.87	60.05	(0.29)	- - -	(2)
Direct Maintenance Cost					
Material	9.95	9.96	(0.10)	- - -	(2)
Labor	2.72	2.72	(-0.07)	- - -	(2)
Sub Total	12.67	12.68	(0.06)	- - -	- -
Total Operating Cost	126.47	126.72	(0.20)	- - -	- -

(1) 10 percent residual @ 15 years - - 2000 Hours/Year

(2) Simulations for fuel and DMC not made

Totals may not check due to rounding. The above costs are estimates and should be used only for comparisons with the baseline design.

Because of the absence of the shroud, the allowable damage limits were based on the values of the 6800 lbf engine tests between the shroud and tip region only since this gives a better representation of the blade and support conditions of the smaller machine.

A straightforward spanwise linear thickening procedure was specified from hub to tip with the t_{max} increase varying from 30 percent at the hub to 17 percent at the tip. The leading edge radius was doubled at the hub, increasing to four times at the tip. Similar thickening modifications were incorporated in the airfoil section, tending to produce again a thicker, more blunt, forward region. Figure 87 shows the predicted damage levels of the thickened blade compared with the baseline. Best judgement of the allowable damage and failure damage limits are sketched-in based on the corresponding 6800 lbf engine ingestion tests. It is expected that the redesign will provide adequate damage tolerance to satisfy the 1.5-pound bird FAR ingestion requirements. Additional thickening, if required, should be minor.

In addition, the transient bending response of the damage-tolerant design was compared with that of the low aspect ratio baseline blade, again for a 1.5-pound bird impact under FAR ingestion conditions. See Figures 88 and 89. The thicker blade shows approximately 25- and 20-percent reductions in tip displacement and maximum stress values, respectively.

It should be pointed out that the absolute value of peak stress in this new blade is 61 percent greater than that of the damage-tolerant 6800 lbf blade (which successfully sustained two 1.5-pound bird strikes with only minor damage at the shroud); but, this value is also 32 percent lower than that calculated for the baseline blade when it sustained a blade failure (shown previously in Figure 27). The limiting stress as determined by actual impact tests is not available at this time, so that further modification to this design may still be required, either by additional thickening or through the use of a pinned-root or protective device.

When running at the 100-percent design speed, the centrifugal stresses in the root of the redesigned blade are moderate (45 ksi maximum at 1/3 chord, 30 ksi average). Aerodynamic bending stresses are reduced somewhat due to the increased bending stiffness of the heavier design. Standard vibration/flutter checks confirm that all dynamic excitation requirements are satisfied without recourse to part-span shrouds.

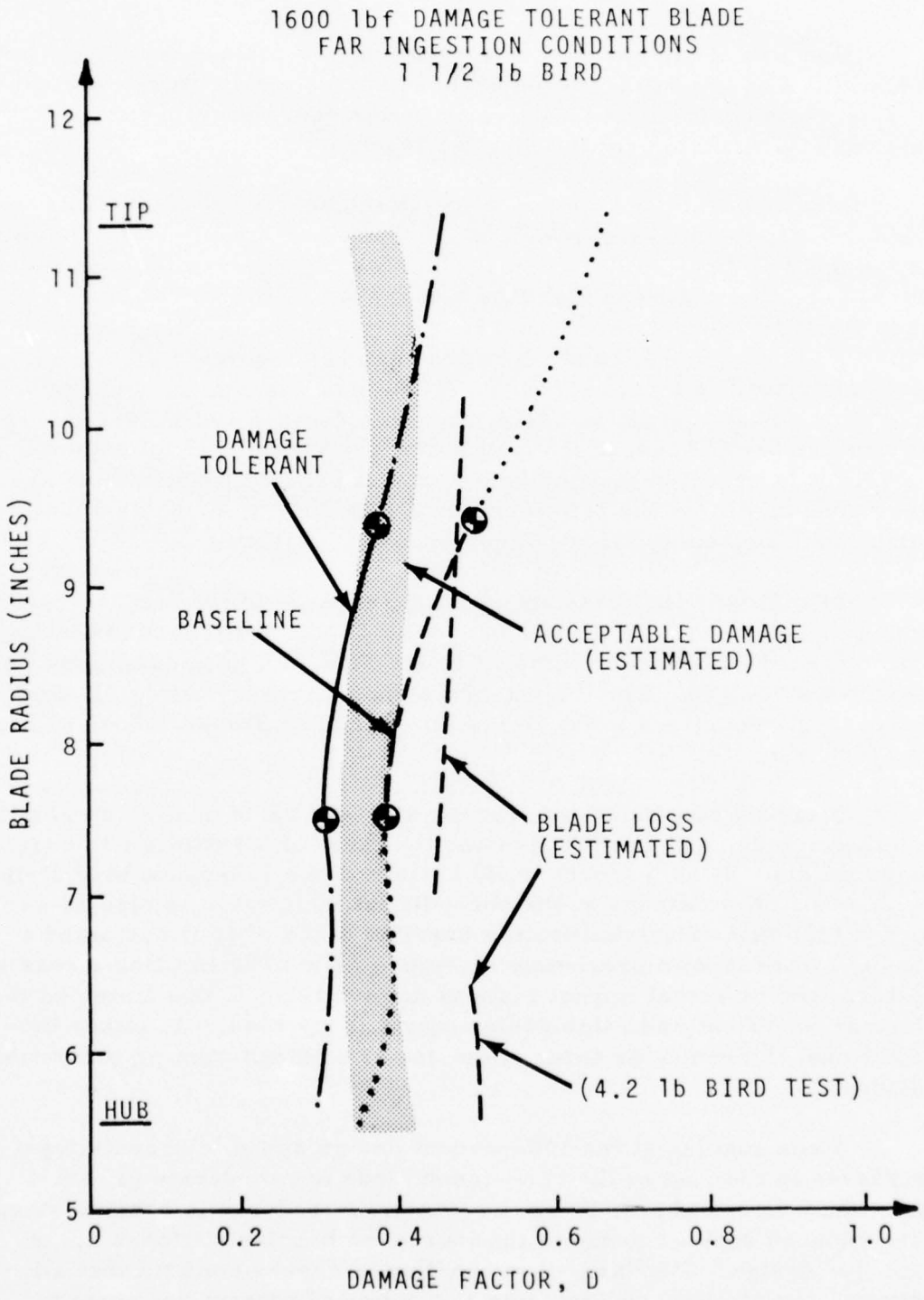

Figure 87. Redesign of Damage Factor Limits - 1600 lbf Blade.

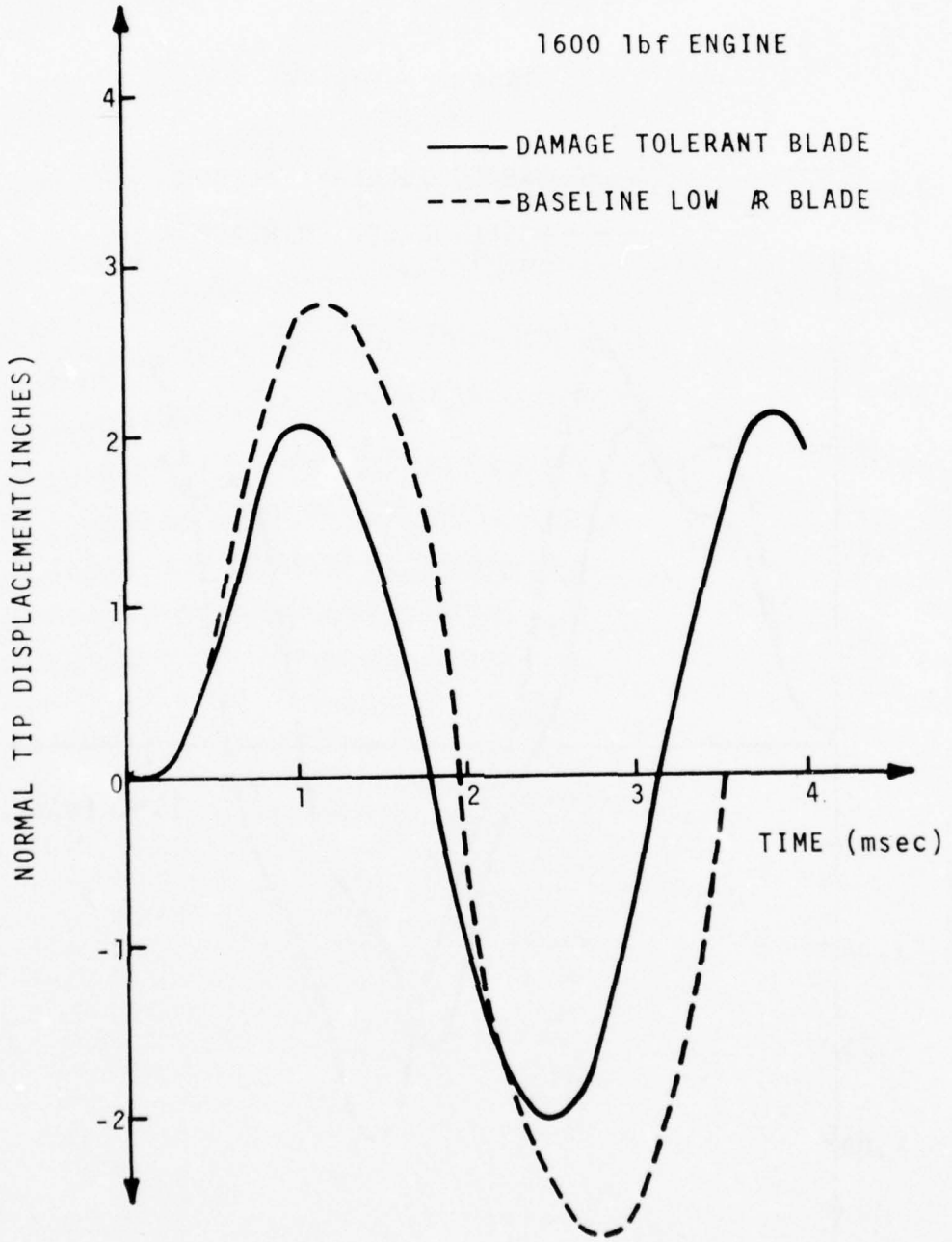

Figure 88. Effect of Redesign on Tip Displacement - 1600 lbf Blade.

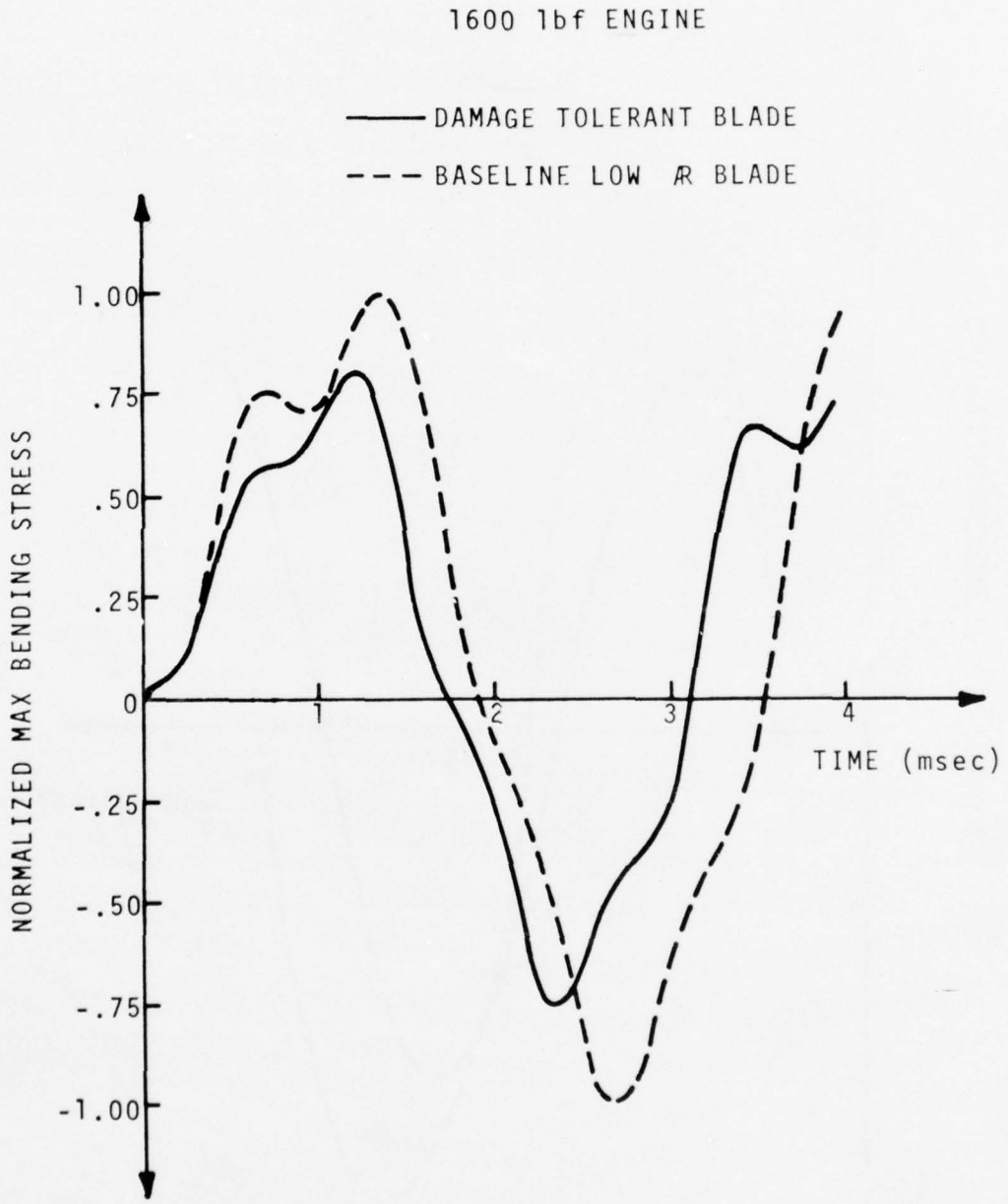

Figure 89. Effect of Redesign on Maximum Stresses - 1600 lbf Blade.

A summary of the rotor and containment ring weight requirements for three of the lower thrust class blades is shown in Table 27. The additional weight penalties incurred in strengthening the low aspect ratio baseline blade is seen to be reasonably low.

Performance comparisons show a modest degradation in thrust and SFC caused by the added damage-resistance of the strengthened blade. (Refer to Table 28). The bird-tolerant design, however, still showed a performance gain over the shrouded baseline version.

Mission comparisons listed in Table 29 show that the flight characteristics of the damage-tolerant engine are essentially the same as those of the (low aspect ratio) baseline and that there is an improvement over the scaled (shrouded) baseline engine .

In line with the performance evaluations, similar conclusions can be drawn about costs. (Refer to Table 30). The damage-tolerant blade imposes a small cost penalty on the (thin) wide-chord baseline design but is still not as expensive as the shrouded baseline engine.

TABLE 27 - SUMMARY OF ROTOR AND CONTAINMENT RING WEIGHT REQUIREMENT
1600 LBF THRUST CLASS ENGINE

	Baseline Scaled Blade (10,340 rpm)		Baseline Low AR Blade (9850 rpm)		Damaged-Tolerant Blade (9850 rpm)	
Failure Location	Imbalance Force (lbf)	Impact Kinetic Energy (in. - lbf)	Imbalance Force (lbf)	Impact Kinetic Energy (in.-lbf)	Imbalance Force (lbf)	Impact Kinetic Energy (in. - lbf)
.25 inch outboard of shroud	1363	6866	- -	- -	- -	- -
.25 inch inboard of shroud	1873	9068	- -	- -	- -	- -
.25 inch outboard of root	3133	13,450	7693	34,190	9323	41,220
Rotor Weight Change (%)	-39.0		0		+14.0	
Containent Ring Weight Change (%)	60.0		0		+24.0	

TABLE 28 - DAMAGE-TOLERANT ENGINE PERFORMANCE COMPARISON, 1600 LBF THRUST CLASS ENGINE

Rating	Scaled Baseline Blade (Shrouded)		Damage-Tolerant Low Aspect Ratio Blade	
	Thrust (%Δ) *	TSFC (%Δ) *	Thrust (%Δ) *	TSFC (%Δ) *
SLS Takeoff (Sea Level @kt)	-1.59	+1.62	- -0.32	+0.27
Initial Climb (100ft @ 115 kt)	-1.76	+1.48	-0.24	+-.22
Max. Cruise (25000 ft @ 350 kt)	-2.03	+1.79	-0.45	+0.30

* Based on Low Aspect Ratio Baseline Blade

TABLE 29 - DAMAGE - TOLERANT ENGINE MISSION COMPARISON, 1600 LBF THRUST CLASS ENGINES

Parameters	Scaled Baseline		Low Aspect Ratio Baseline		Damage-Tolerant Design	
Cruise Altitude (ft)	25,000		25,000		25,000	
Cruise Mach No.	0.60	0.65	0.60	0.65	0.60	0.65
Take-off Distance (ft)	2610.	2610.	2570.	2570.	2580.	2580.
Time to Altitude (min)	12.1	12.1	11.8	11.8	11.8	11.8
Avg. Rate of Climb (ft/min)	2060.	2060.	2130.	2130.	2120.	2120.
Cruise Fuel Available * (lb)	1700.	1700.	1680.	1680.	1670.	1670.
Avg. Specific Range, Cruise (NM/lb)	0.793	0.713	0.808	0.727	0.805	0.724
Cruise Range (NM)	1340.	1210.	1360.	1220.	1340.	1210.
Cruise Time (hr)	3.72	3.09	3.76	3.12	3.71	3.08
Turbine Inlet Temp, last (° R)	2319.	2450.	2309.	2439.	2311.	2441.

*Allowing for 45 min. fuel reserve at end of cruise gross weight and speed. No. allowance for enroute cruise climb.

TABLE 30 - DAMAGE-TOLERANT ENGINE COST COMPARISON, 1600 LBF THRUST CLASS

COST IN DOLLARS/HOUR PER ENGINE					
Costs	Scaled Baseline		Low Aspect Ratio Baseline	Damage-Tolerant Low Aspect Ratio	
Amortized Cost (1)	$/hr	(% Δ)	$/hr	$/hr	(% Δ)
Engine	2.10	(-0.47)	2.11	2.12	(+0.47)
Airframe	6.30	(-0.63)	6.34	6.36	(+0.32)
Sub Total	8.40	(-0.59)	8.45	8.47	(+0.24)
Fuel Cost @ 46 cents/gal	16.66	(-1.40)	16.43	16.48	(+0.28)
Direct Maintenance Cost					
Material	1.66	(-0.60)	1.67	1.68	(+0.60)
Labor	2.92	(0)	2.92	2.92	(0)
Sub Total (DMC)	4.58	(-0.22)	4.59	4.59	(0)
Total Operating	$29.64	(-0.54)	$29.48	$29.55	(+0.24)

(1) 10% residual @ 15 Years - - 2000 Hours/Year

Totals may not check due to rounding. The above costs are estimates and should be used only for comparisons with the baseline design.

3.0 ADVANCED MATERIALS - TASK II

GENERAL

A similar design procedure was followed in Task II to facilitate design of fan/compressor blades for improved bird-impact tolerance through the application of advanced materials.

The major incentive for the use of fan/compressor blades of advanced materials is to reduce engine and airframe weight. For example, a composite boron/aluminum blade would weigh approximately 60 percent of an equivalent titanium blade, while a graphite/epoxy version would weigh one-third of a titanium blade. Additional weight savings would result from the lighter disks, shafts, bearings, etc. permitted for the support of the lighter blades.

Performance benefits are possible as well because high-stiffness and high-strength materials permit the use of thinner and higher aspect ratio blading without resorting to shrouds for controlling flutter or vibration. Greater safety may also be realized, especially with composite blading, since failed composite blades would tend to disintegrate, thereby resulting in less secondary damage and easier containment.

Design analyses of composite fan blades were performed following the methodology presented in Task I for standard isotropic, titanium blades; that is, "short-time" analysis by the local damage criteria relation, followed by the "long-time" structural response analysis provided by the transient impact finite-element program. For the local damage analysis, an equivalent composite shear strength was used for comparisons with the shear strength of titanium blades. For the blade motion study, equivalent isotropic tensile and shear modulii were used.

CANDIDATE FAN BLADE MATERIALS

The basic structural requirements for fan blade materials are that they be lightweight with high stiffness and high strength. Present fan engines are constrained in so far as that specific values of stiffness and strength are very much the same for all orthodox materials (Table 31).

The lightest structural material, magnesium, has exceptionally low stiffness ($E = 6.5 \times 10^6$ psi). It also has very low erosion resistance - an important consideration for practical fan applications. Aluminum ,

TABLE 31 - TYPICAL SPECIFIC PROPERTIES OF LIGHTWEIGHT MATERIALS

Material	Density ν, ($lb/in.^3$)	Specific Stiffness E/ν ($in. \times 10^6$)	Specific Strength σ/ν ($in. \times 10^6$)
Magnesium	0.063	102.	0.5 - 0.6
Aluminum	0.10	105.	0.5 - 0.6
Titanium	0.16	100.	0.6 - 0.8
Steel (Stainless)	0.28	107.	0.5 - 0.7
Beryllium	0.066	640.	0.7 - 0.8
Epoxy	0.050	15.	0.2 - 0.3

which is somewhat better on both these counts, was originally and widely used in the forward, low-temperature stages of compressors. Steel blades, originally used for only the aft, high-temperature stages, are now typically used for the forward compressor stages as well, due mainly to their better erosion resistance.

To date, candidate light weight metal systems for fan blades are limited to titanium because of its all-round satisfactory properties. It is 40 percent lighter than steel but has the same, or better, strength. The stiffness is only one-half that of steel, but it is still 60 percent better than aluminum. Its erosion resistance (and bird tolerance) has also been adequate for fan applications. Ti-6Al-4V is the most common alloy for most production applications but some use has been made of Ti-8Al-1MO-1V which has a slightly higher modulus (and lower resistance to stress corrosion cracking).

Beryllium would be a very attractive material for fan blades because of its low density and abnormally high stiffness ($E = 42 \times 10^6$ psi). Its brittleness and lack of toughness, however, has so far precluded its use as a practical fan blade material.

Efforts directed towards the development of advanced composite material arise because lightweight reinforcing fibers, which are available commercially, have specific stiffness and strengths that are 5 to 10 times higher than orthodox materials. (Refer to Table 32).

For fan blade applications, the most effective reinforcing fibers are seen to be graphite and boron (or borsic) because of their very high stiffness and strength. Glass and steel fibers cannot be expected to provide additional stiffness but can provide additional strength. The intermediate stiffness of Kevlar makes it attractive as an auxiliary fiber in hybrid designs to smooth the load transfer from the very high modulus graphite or boron fibers to the low modulus carrier materials.

Using high-stiffness/high-strength fibers to reinforce a base material produces properties that are considerably different in the longitudinal and transverse directions. This anisotropy enables the designer to optimize the stiffness and strength in different areas of the blade. Material mechanical properties are, therefore, not strictly bulk values but vary sharply between and within the lamina making up a blade cross-section. Combinations of uniaxial and equivalent isotropic properties are typically used for preliminary design studies with the material near the root tending towards the uniaxial and that near the

TABLE 32 - TYPICAL SPECIFIC PROPERTIES OF LIGHTWEIGHT REINFORCING FIBERS

Fiber	Density γ (lb/in.^{3})	Specific Stiffness E/γ (in. x10^6)	Specific Strength σ/γ (in. x10^6)	Diameter (in. x10^{-3})
KEVLAR	0.047	350.	7.0	0.47
Graphite	0.060	650.	4.7	0.3
Beryllium	0.066	640.	2.8	5.0
E Glass	0.092	115.	3.3	0.4
S Glass	0.090	165.	6.0	0.4
Boron	0.095	630.	4.8	4., 5.6, 8.
Borsic	0.096	600.	4.2	4.2, 5.8
Steel	0.28	107	1.07	2.

mid-span tending towards the isotropic. The spanwise properties near both the tip and leading edge may in fact be somewhat worse than the isotropic, since, typically, ±45 degrees lamina predominates in these regions. Tables 33 and 34 list typical engineering design properties of reinforced epoxy, aluminum, and titanium laminates. (References 23 through 27).

The uniaxial properties of a graphite or boron reinforced epoxy laminate are seen to be sufficiently high when the fibers are aligned in the direction of the load but deteriorate very rapidly when the fibers are oriented at an angle to the load. This condition exists because at off-angles the low shear stiffness and strength of the epoxy matrix does not adequately transfer the load between fibers and between lamina. At 90 degrees to the load, the fibers still tend to stiffen the matrix, but they also act as stress raisers and so tend to reduce the transverse strength of the lamina.

The equivalent isotropic property listings show that the specific stiffnesses and strengths of graphite and boron reinforced epoxy are still superior to titanium and would, therefore, be structurally suitable for fan blade applications. These material combinations have not been successful in practice, however, because of their low erosion resistance and susceptibility to impact damage. Protective coatings are called for to correct the erosion problem, while more compatible shear stiffness and strength properties(for example, such as those provided by auxiliary fibers of Kevlar or by a metallic matrix) would be required to improve the impact damage resistance. It would also appear that shear reinforcement (for example, through the use of steel mesh or staples) could be used to help distribute local impact loads to neighboring fibers and lamina.

It is also seen that the equivalent isotropic properties of both beryllium and boron reinforced aluminum are superior to unreinforced titanium, so that either of these composites should be suitable for fan blades from a structural point of view.

A similar situation exists for boron reinforced titanium composites.

Good shear properties are a particular concern of fiber reinforced blading materials, not only to provide a smooth transfer of centrifugal forces between fibers and lamina, but also to facilitate the distribution of impact loads applied normally to the fiber directions. A comparison of the specific shear stiffnesses of candidate composite materials is shown in Table 35. When considering centrifugal loading, the graphite/

TABLE 33 - TYPICAL PROPERTIES OF REINFORCED EPOXY (50% VOLUME RATIO)

Property	KEVLAR		E Glass		S Glass		Graphite		Boron (Borsic)		Steel	
	uni	iso	uni	iso	uni	iso	uni	iso	uni	iso	uni	iso
Density, ν (lb/in.^{3})	0.050	0.050	0.070	0.070	0.070	0.070	0.055	0.055	0.070	0.070	0.180	0.180
Tensile Modulus, (Span) E_1 (psi x 10^6)	11.	4.0	6.0	3.0	9.0	4.0	22.	13.0	30.0	12.0	17.	7.
Tensile Modulus (Chord) E_2 (psi x 10^6)	0.8	4.0	1.5	3.0	1.6	4.0	1.7	13.0	2.2	12.0	1.6	7.
Shear Modulus, G_{12} (psi x 10^6)	0.3	2.5	0.5	1.6	0.6	2.0	0.65	3.6	0.68	4.4	0.63	3.
Tensile Strength (Span) σ_1 (ksi)	190	40	150.	40.	160.	45.	110.	60.	185.	75.	200	95.
Tensile Strength (Chord) σ_2 (ksi)	4.	40.	6.	40.	6.	45.	4.	60.	10.	75.	15	95.
Shear Strength τ_{12} (ksi)	8	13.	11.	35.	12.	40.	12.	45.	13.	45.	20	55.
ε Fract	2.8%		7.0%									

TABLE 34 - TYPICAL PROPERTIES OF REINFORCED METALS (50% VOLUME RATIO)

Property	Beryllium/Aluminum		Borsic/Aluminum		Boron/Titanium	
	uni	iso	uni	iso	uni	iso
Density ν (lb/in.^{3})	0.091	0.091	0.098	0.098	0.113	0.113
Tensile Modulus, (Span) E_1 (psi x 10^6)	21.	18.	33.	21.	40.	33.
Tensile Modulus, (Chord) E_2 (psi x 10^6)	17.	18.	21.	21.	30.	33.
Shear Modulus, G_{12} (psi x 10^6)	7.	7.	12.	13.	12.	14.
Tensile Strength (Span) σ_1 (ksi)	75.	55.	180.	80.	150.	70.
Tensile Strength (Chord) σ_2 (ksi)	77.	55.	15.	80.	45.	70.
Shear Strength τ_{12} (ksi)	35.	40.	20.	55.	60.	55.

TABLE 35 - ISOTROPIC SHEAR PROPERTIES OF COMPOSITES

	Ti	S glass/Ep (Ratio)*	Gp/Ep (Ratio)*	B/Ep (Ratio)*	B/Al (Ratio)*	B/Ti (Ratio)*
G_{12}/ν (inx10^6)	37.3	28.6 (0.768)	72.7 (1.95)	62.9 (1.69)	132.7 (3.56)	123.9 (3.33)
G_{12}/E_{11}	0.373	0.5 (1.34)	0.308 (0.826)	.367 (0.984)	0.619 (1.66)	0.424 (1.14)
$\tau 12/\nu$ (inx10^6)	0.40	0.57 (1.45)	0.82 (2.05)	0.64 (1.61)	0.56 (1.40)	0.49 (1.22)
$\tau 12/\sigma_1$	0.50	0.89 (1.78)	0.75 (1.50	0.60 (1.20)	0.69 (1.38)	0.79 (1.57)

* - With respect to Ti

epoxy composite is the best of the resin systems studied, while the boron/aluminum composite is the best of the metal systems.

A measure of a material's ability to transfer shear loads that is more suitable to impact considerations is the compatibility of the shear and tensile modulii, G/E. Based on this parameter, the S glass/epoxy looks best in the resin system, with both graphite and boron reinforced epoxy composites not performing as well as titanium.

Boron reinforced aluminum is again best in the metal systems and should, in fact, perform somewhat better than titanium,at least up to the point of shear failure of the aluminum matrix. Since the shear strength of aluminum is only one-half that of titanium, additional shear strength reinforcement(with staples or wire mesh) may be required to raise the failure level.

COMPOSITE FAN/COMPRESSOR BLADE APPLICATIONS

In the early 1960's,Lycoming explored the use of lightweight compressor blades made of glass fibers and epoxy. Although these composites were not successful because of their excessive flexibility, the technology was later expanded to the design and fabrication of graphite fiber/epoxy fan blades suitable for use in a small turbofan powerplant employing Lycoming's T53 engine as the core. By the mid 1960's, however, industry-wide evaluation of such blades found them to be deficient in their resistance to rain erosion and bird ingestion. These problems still prevent graphite/epoxy fan blades from entering production.

Accordingly, the major effort of the research and development programs conducted since that time has been directed towards improvement of impact tolerance and, in particular, to bird ingestion. Attempts to improve bird-impact resistance of epoxy blades have included modifications to the lamina layup techniques and the incorporation of different size fibers. Hybrid designs made of combinations of graphite and boron fibers augmented with Kevlar and glass fibers have also been investigated, as has the use of various styles and combinations of monolayer tapes and woven cloth. Boron/epoxy shells applied over titanium and stainless steel cores have been manufactured and tested. Leading-edge protection using nickel plates, steel wire mesh, and steel staples has also been tried. Polyimide resins have been introduced in lieu of epoxy because of their greater stiffness and strength. (References 28 through 32). All resin-based blade designs tested to date, however, have been deficient in their tolerance to bird-impact damage.

Resin - matrix reinforcement techniques have been extended to metal matrices because of their higher stiffness and strength properties, as well as their greater resistance to impact and erosion. Metal matrix technology has been carried to the point where high-temperature materials suitable for the turbine section have been achieved; but for fan applications, the alloys studied are typically aluminum and titanium. Although the principal fibers used for fan applications have been boron or borsic, some work using graphite fibers has been done.

Aluminum matrix components are produced either by diffusion - bonding two layers of aluminum foil around the fiber layer or by plasma-spraying aluminum powder on the fibers. The composite tape is then cut to the dimensional shape, the pre-forms are layed up to achieve the necessary thickness and mechanical properties, and the assembly is diffusion-bonded to shape in a closed die.

Titanium matrix composites are produced in the same fashion, but the diffusion bonding of this material requires higher temperatures and pressures that generally require the use of borsic fibers to prevent excessive reactions between the matrix and fibers.

Although the development of metal matrix composites has not been as extensive as the resin-reinforced systems, several programs have been conducted on fan/compressor blade applications. Adequate mechanical properties to withstand the loads imposed under normal operating conditions have been shown. Impact tests indicate that these blades are less resistant to foreign object damage than current titanium blades but suggest that they might meet flight requirements. Some flight tests are being conducted using intermediate fan or compressor stages where the possibility of large objects reaching the composite blades is small compared to the first stage. (References 33 to 38).

A promising application of a metal matrix composite, described by Troha and Swain (Reference 39), uses the high stiffness properties of a borsic/titanium composite inlay to stiffen an existing titanium fan blade for improved flutter resistance. This approach was proposed in lieu of increased airfoil thickness or the use of part-span shrouds.

COMPOSITE DAMAGE CRITERION

In order to determine composite-material impact characteristics in a form suitable for the design and evaluation of composite blades, the analytic damage model (Equation 1) was refined to include the shear strength contribution of the embedded fibers. An equivalent shear strength relationship was developed for use in the criterion to account for the strength, size, and amount of fibers in each ply and their orientation from the radial direction. A concentration factor was also introduced to account for the matrix strength reduction which can be caused by the embedded fibers.

The composite's equivalent shear strength is calculated according to

$$\tau_Q = F_S / h(d_Q + w) \qquad (13)$$

where dq and w are the bird diameter and slice width determining the spanwise and chordwise extent of the shear area supporting the impact (Figure 90). The thickness, h, is taken as the sum of the ply thicknesses at the impact site. The shear force function becomes

$$F_S = \Sigma \Delta h \left\{ d_Q \left[N_f \tau_f \sin\alpha + V_1 \tau_m^* / K_1 \right] + w \left[N_f \tau_f \cos\alpha + V_2 \tau_m^* / K_2 \right] \right\}$$

and summed over all plies at the impact site. The thickness of each ply is calculated from the fiber diameter, D_f, and fiber volume ratio, v_f according to

$$\Delta h = \frac{D_f}{2} \sqrt{\frac{\pi}{N_f}}$$

AD-A044 203 AVCO LYCOMING DIV STRATFORD CONN F/G 21/5
IMPROVED RESISTANCE TO ENGINE BIRD INGESTION.(U)
MAR 77 H B KAEHLER DOT-FA76WA-3806
UNCLASSIFIED FAA/RD-77-55 NL

3 OF 3
AD
A044203

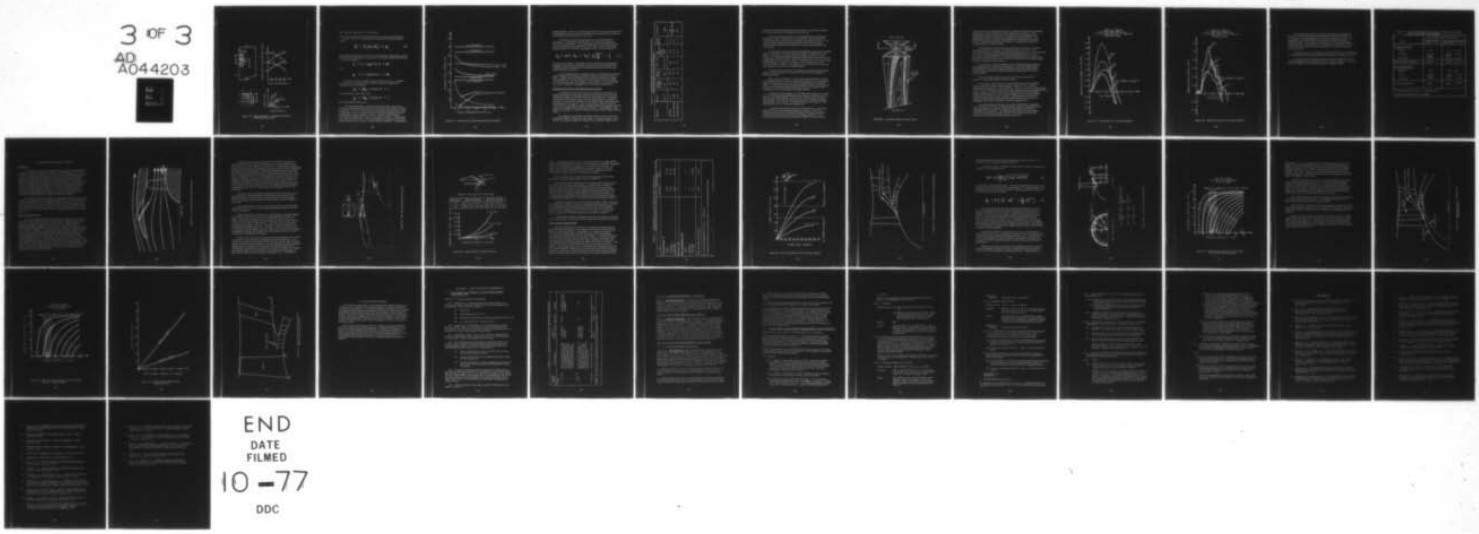

END
DATE
FILMED
10-77
DDC

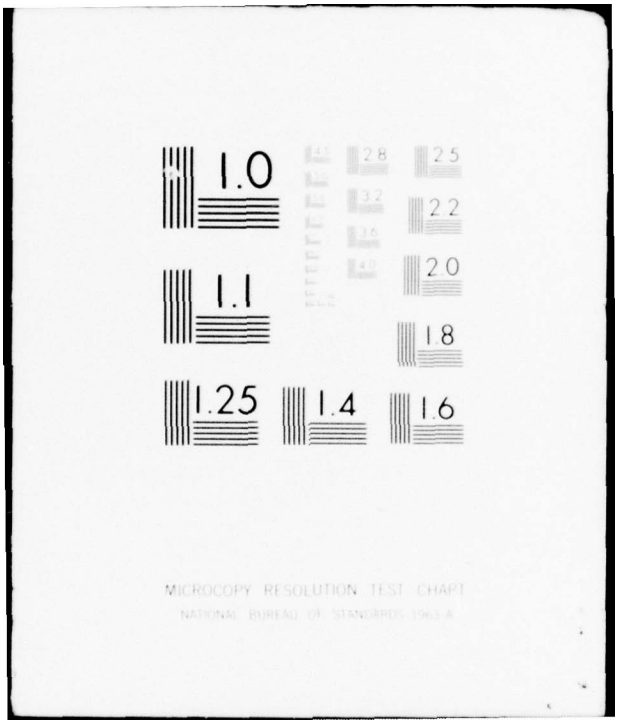
1.0
1.1
1.25
1.4
1.6
2.8
2.5
3.2
2.2
3.6
2.0
4.0
1.8
MICROCOPY RESOLUTION TEST CHART
NATIONAL BUREAU OF STANDARDS-1963-A

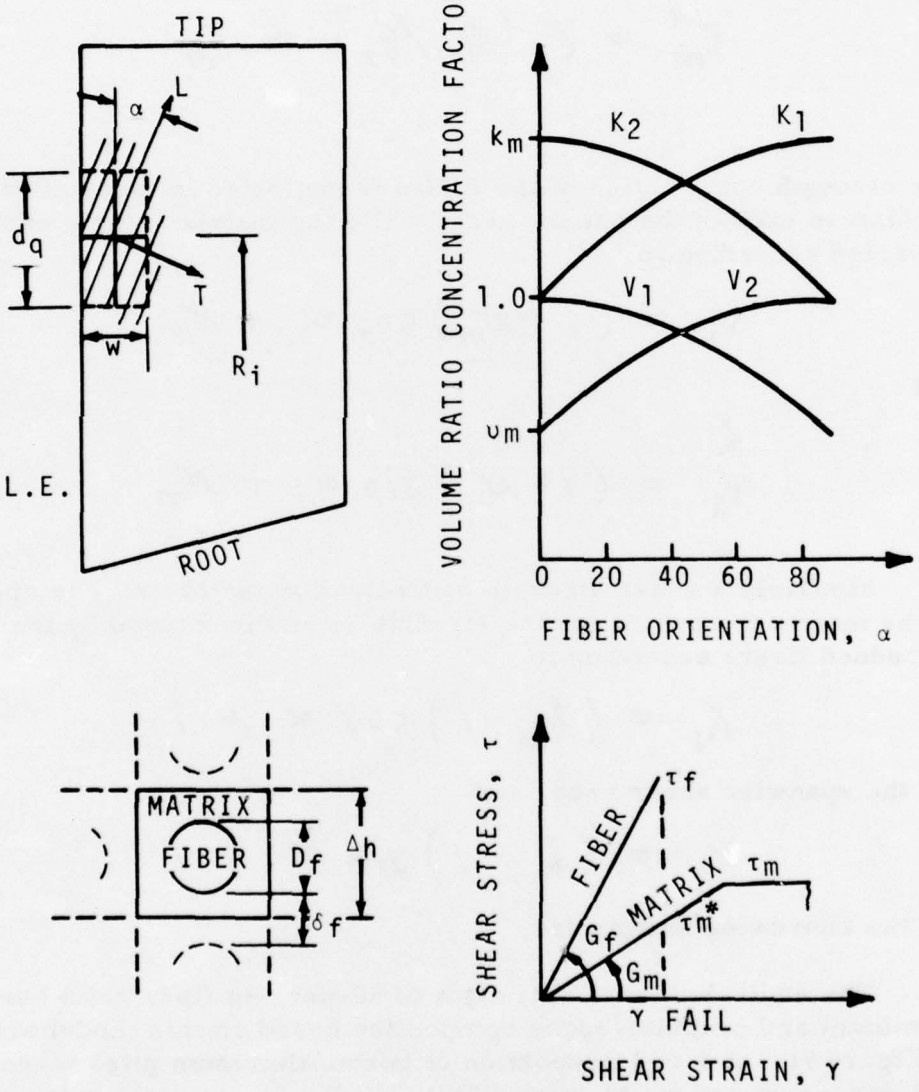

Figure 90. Equivalent Shear - Strength Parameters of the Composite Blade.

for a uniform rectangular array of fibers.

The shear strengths of the fibers and matrix material are denoted by τ_f and τ_m and, assuming the matrix fails at the fiber failure strain,

$$\tau_m^* = \tau_f \left(G_m / G_f \right) \leq \tau_m \qquad (15)$$

The strength contribution of the fibers is neglected in those plies running parallel to each of the shear areas, while the matrix volume contribution is varied according to

$$V_1 = (1 - \nu_m) \cos \alpha + \nu_m$$

and

$$V_2 = (1 - \nu_m) \sin \alpha + \nu_m$$

Similarly a shear strength concentration factor, k_m, is applied to the matrix to account for the strength reduction caused by the embedded fibers according to

$$K_1 = (k_m - 1) \cos \alpha + 1$$

for the spanwise shear area, and

$$K_2 = (k_m - 1) \sin \alpha + 1$$

for the chordwise shear area.

The equivalent shear strength of 50-percent fiber ratio boron/aluminum and graphite/epoxy composites based on this model are shown in Figure 91. A 1 to 1 proportion of boron/aluminum plies taken in the ±45 degree directions to approximate the laminate orientation near the leading edge is seen to perform nearly as well as solid titanium - providing the concentration factor in the matrix is small. If large concentrations of stress occur, the boron/aluminum composite has inferior impact resistance to a similar graphite/epoxy composite. The graphite/

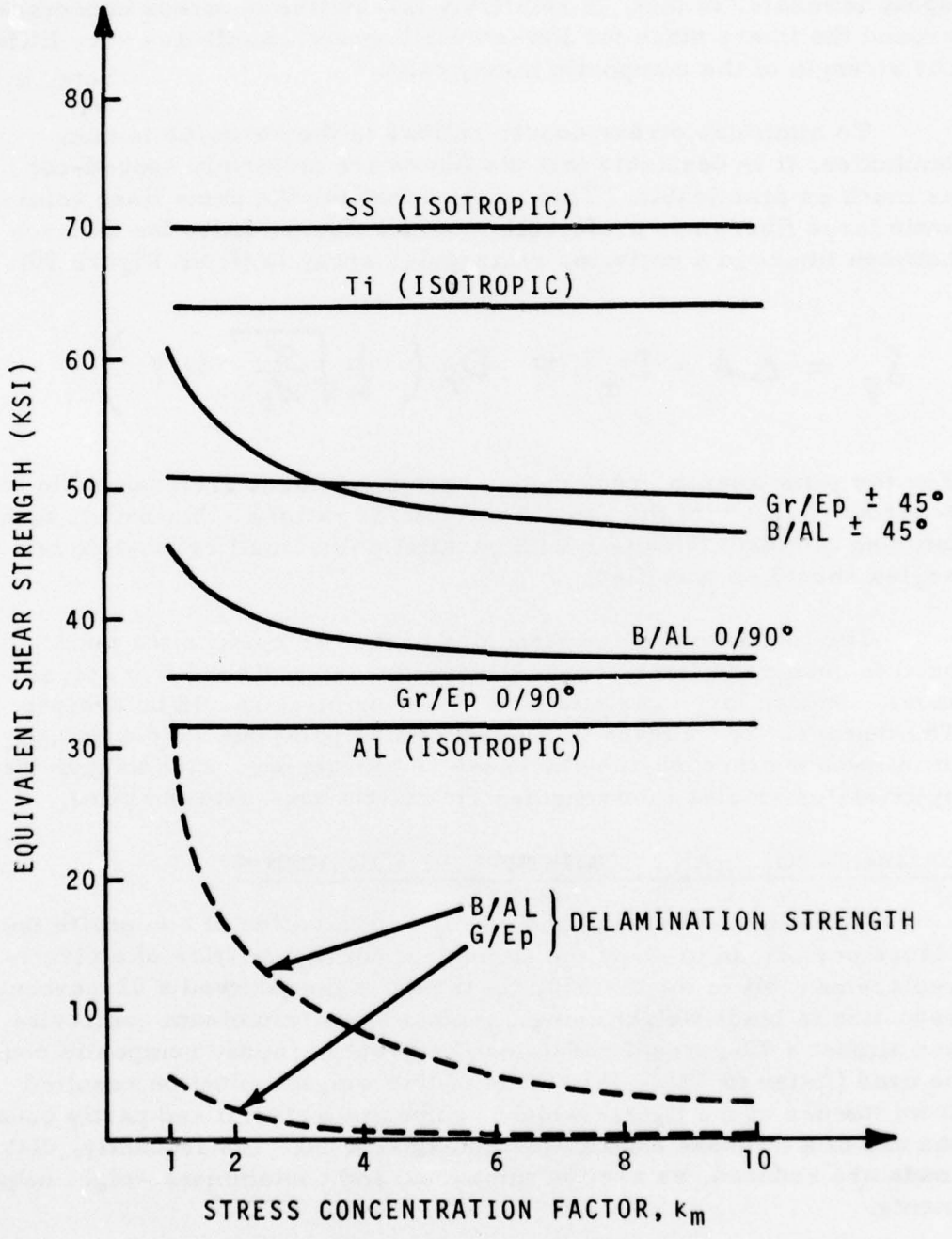

Figure 91. Comparison of Composite Equivalent Strength.

epoxy laminate, in fact, is relatively insensitive to stress concentrations around the fibers since the low-strength epoxy contributes very little to the strength of the composite in any case.

To minimize stress concentrations in the boron/aluminum laminates, it is desirable that the fibers are uniformly spaced-out as much as practicable. This implies that for the same fiber volume ratio large fibers are preferable to small fibers, since the distance between fibers in a uniform, rectangular array is (from Figure 90)

$$\delta_f = \Delta h - D_f = D_f \left(\frac{1}{2}\sqrt{\frac{\pi}{v_f}} - 1 \right) \qquad (16)$$

For the same reason, rectangular arrays of fibers are preferable to hexagonal arrays (of the same fiber volume ratio) so that rather than building laminate thickness with parallel plies, small cross-bracing angles should be specified.

The low delamination strengths of the two composites point out the need to design the laminate for gradual transfer of load from layer to layer. Sudden large variations in ply orientation should be avoided. The delamination curves in Figure 91 also point out the desirability of introducing through-the-thickness reinforcement, such as provided by rivets or staples, to strengthen the matrix bond between plies.

DAMAGE-TOLERANT COMPOSITE BLADE DESIGN

A preliminary stress and vibration evaluation of composite fan blades, performed to study the structural characteristics of a direct-replacement blade for the 6800 lbf thrust engine, showed a 42-percent reduction in blade weight using a typical boron/aluminum composite and almost a 70-percent reduction if a graphite/epoxy composite could be used (Refer to Table 36). Part of this weight reduction resulted from the use of the lighter weight composite material and partly because the use of a midspan shroud was not considered. Consequently, disk loads are reduced, as are the imbalance and containment weight requirements.

The reduction of average centrifugal stresses in the root of the composite blades is substantial and results in far higher safety factors than for the titanium blade; this implies that composite blades can be

TABLE 36 - COMPOSITE DIRECT REPLACEMENT BASELINE BLADE COMPARISON, 6800 LBF THRUST ENGINE

Material	Density ($lb/in.^3$)	Tensile Strength at Root (ksi)	Blade Weight (lb)	Disk Load ($lb \times 10^3$)	Avg Centrigual Stress at Root (ksi)	Safety Factor	Frequency (cps)
Titanium	0.16	128.	.725	606.	32.0	4.0	160 (230 Shrouded)
Boron/Aluminun	0.098	155.	.419	323.	18.4	8.4	230
Graphite/Epoxy	0.055	95.	.321	177.	10.2	9.3	209

designed to provide better performance either by increased tip speed or by increasing the chord length towards the tip.

The first bending frequency of an unshrouded boron/aluminum replacement blade matches that of the shrouded titanium blade and so should provide a similar level of flutter and vibration control. The graphite/epoxy replacement blade does not quite reach this level, indicating that additional thickening (or increased chord length) may be required.

The damage criterion analysis also indicates a reduction in damage tolerance because of the lower equivalent shear strength of the composite. Assuming an equivalent shear strength of 45.0 ksi can be achieved in a boron/aluminum composite in the impact area near the tip leading edge (from Figure 91), then a 19-percent increase in the damage factor (Equation 1) would be expected. A 42-percent increase in thickness would therefore be required to provide the same degree of local damage resistance as a titanium blade.

The lower equivalent shear strength of the graphite/epoxy would require a somewhat greater increase in thickness for comparable damage tolerance.

Based on these results, a 1.42 scaled boron/aluminum version of the damage-tolerant titanium blade would appear to be a reasonable minimum requirement for a successful damage-tolerant composite blade. The airfoil thickness and chord length would be scaled directly; the number of blades would be reduced by the same factor (to 28) to maintain the same airfoil shape and stage solidity.

A typical laminate design for this blade would consist of a center core with the plies aligned along the span direction (zero degrees) to take the centrifugal loading, an outer cover with the fibers oriented ±45 degrees to the span to provide the necessary torsional stiffness and strength, and a number of intermediate plies to smooth the load transfer from cover to core (See Figure 92).

To enhance the laminate structural characteristics, the center plies can be oriented to approximately ±13 degrees, which will significantly increase the torsional stiffness of the core while still maintaining some 90 percent of the zero degree stiffness. This procedure also improves the dimensional stability of the blade and

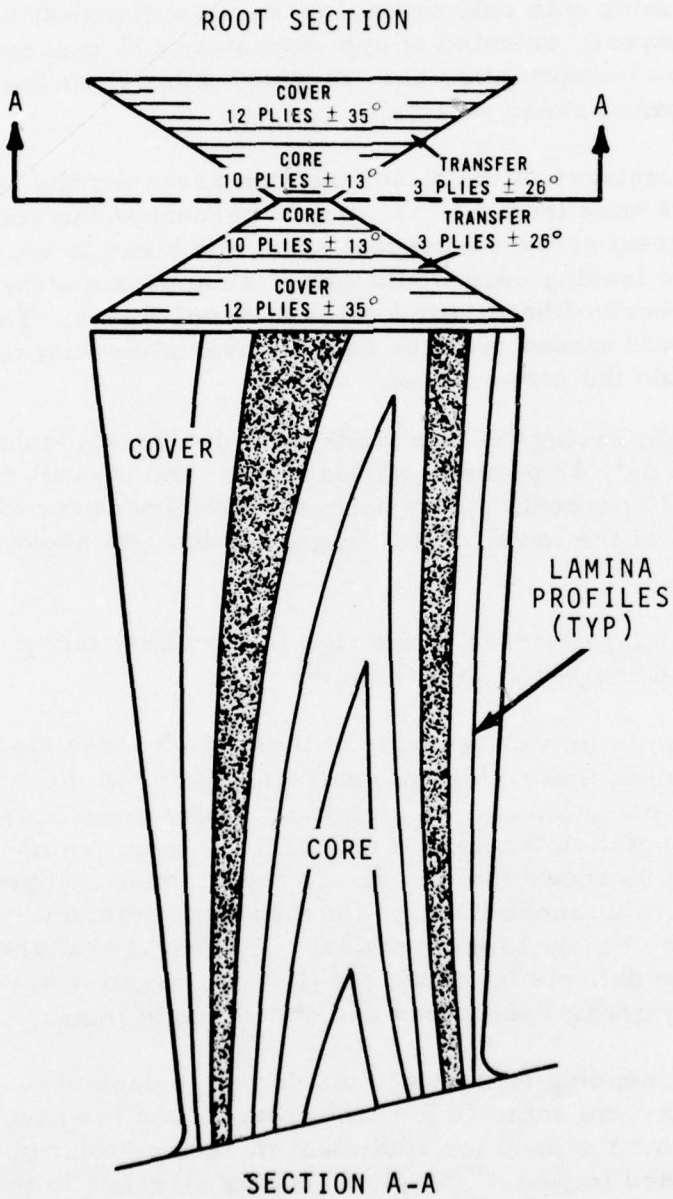

Figure 92. Composite Blade Laminate Layout.

minimizes stress concentrations and the residual stresses incurred during manufacture, both of which may cause separation of the plies. The cover plies can also be oriented at ± 35 degrees to provide substantial spanwise stiffening with only minor losses in torsional stiffness. The intermediate layers, oriented at approximately ± 26 degrees minimizes the fiber angles between plies and thereby minimizes the formation of high interlamina shear strains.

The percentages of the airfoil section areas for the core, transfer and cover plies vary from 63, 11, and 26 percent at the root, to 37, 19, and 44 percent at the 60-percent span; and blend to 30, 21, and 49 percent at the tip. The leading edge would comprise approximately 12 cover plies of 4-mil boron fibers, (or 6 plies of 8-mil fibers). The impact area near the tip would extend over the full 20 cover plies with the transfer plies lying just outside the contact area.

The weight savings of this blade over the damage-tolerant titanium blade would be only 12 percent per blade; but the overall disk loading is reduced by 30 percent, partly because there are fewer blades and partly because of the lower center of gravity brought about by removal of the shrouds.

The centrifugal stress in the root is very low, being only 55 percent of the damage-tolerant titanium blade.

The dynamic impact behavior of these blades was also evaluated using the transient finite-element analysis, again for the 1.5-pound bird tip-strike conditions. For simplicity, equivalent isotropic material properties were specified throughout the blade. Inspection of the tip displacement plots of Figure 93 shows that the direct replacement composite blades deflect considerably more than the (unshrouded) titanium baseline blade, mainly because of their lower inertias. The damage-tolerant boron/aluminum blade deflects less than the titanium baseline because of its proportionately greater thickness and chord length (mass).

The peak bending stresses in the direct replacement composites are very similar and some 30 percent greater than the titanium baseline, again pointing out the need for additional thickening for equivalent resistance to bird impact. The peak bending stresses in the damage-tolerant boron/aluminum blade, however, are some 30 percent less than in the titanium baseline blade (See Figure 94).

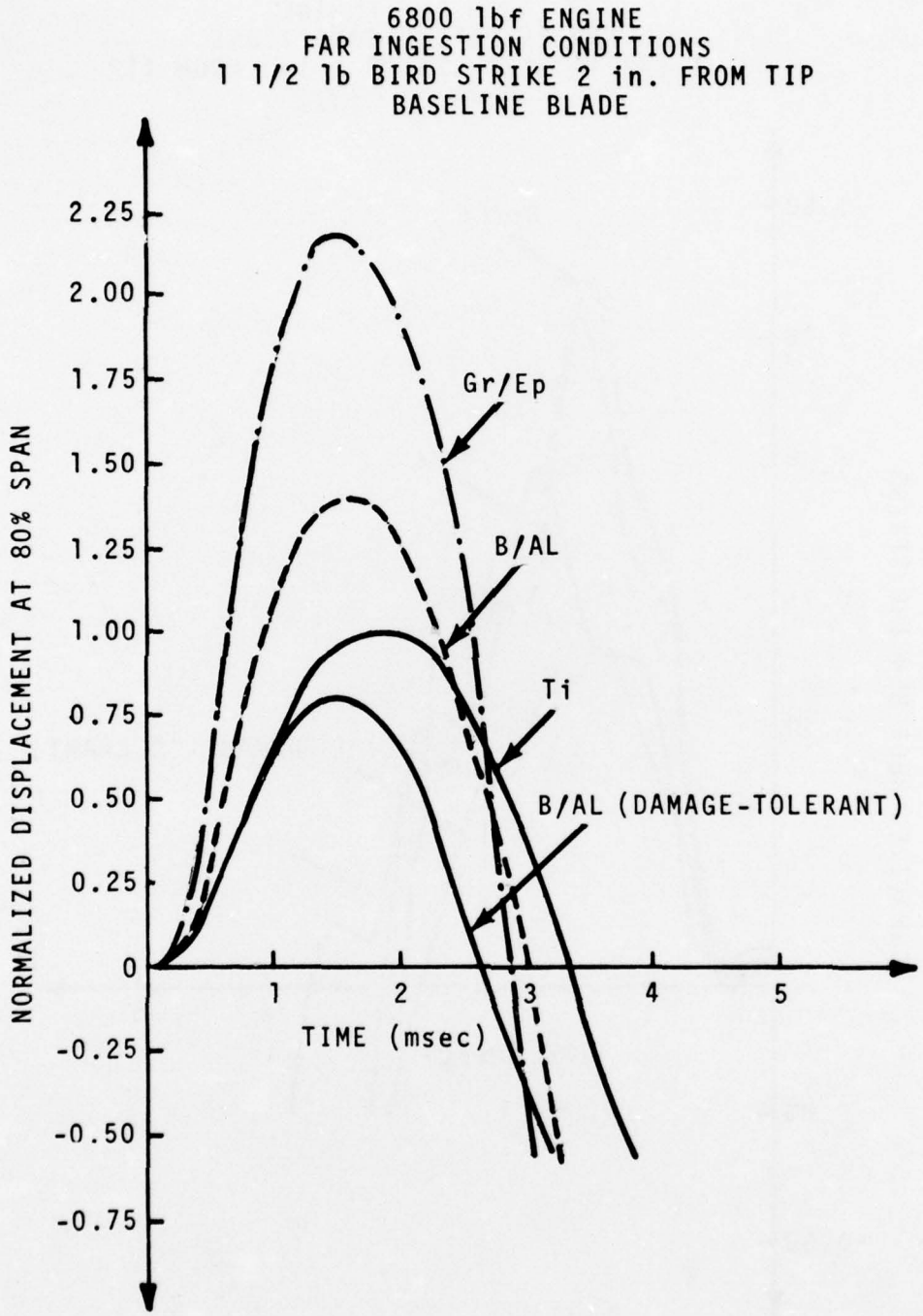

Figure 93. Tip Deflections of Composite Blades.

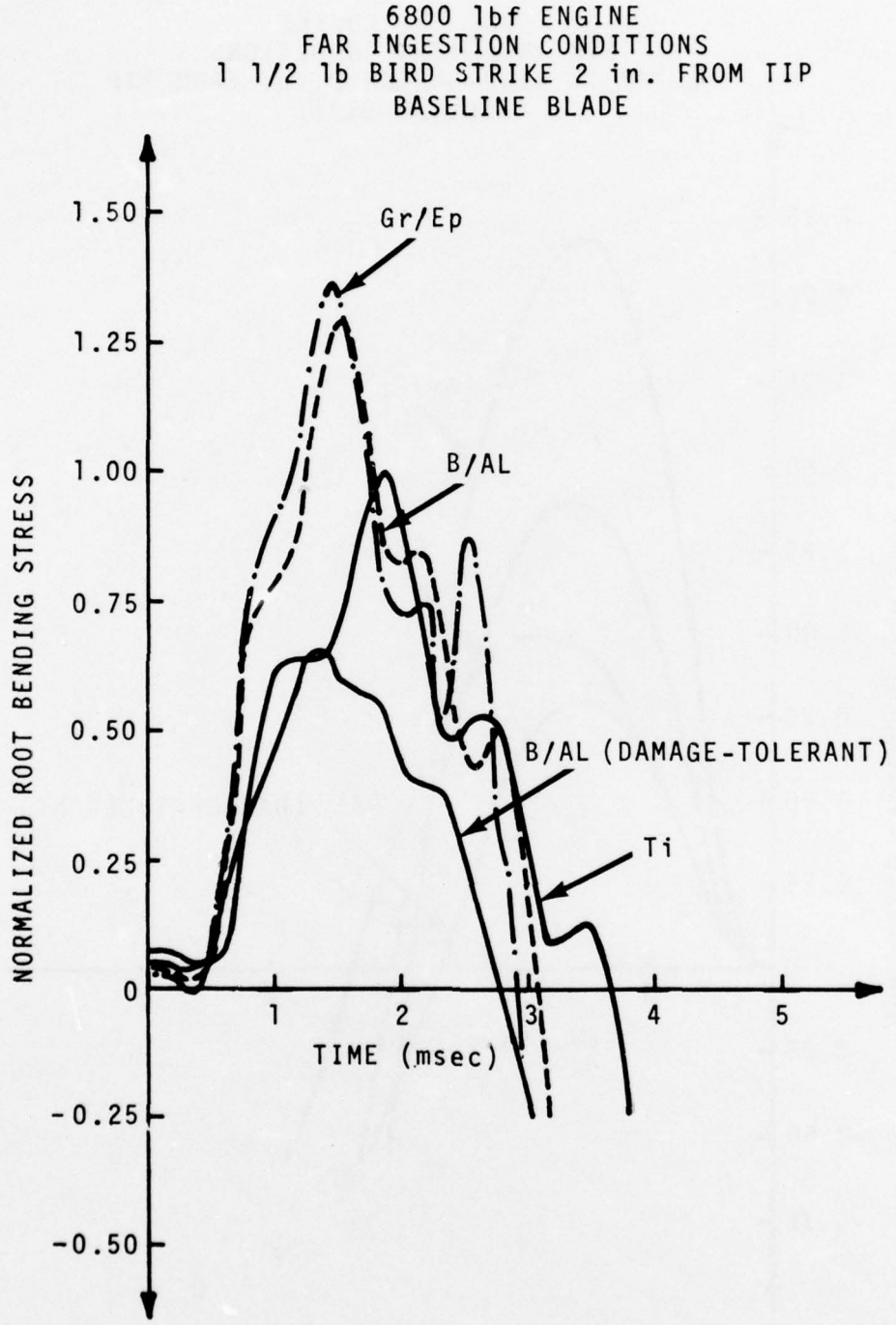

Figure 94. Maximum Stresses in Composite Blades.

An aerodynamic analysis of the damage tolerant composite configuration at the design point indicates that an efficiency increase of 1.6 percent can be anticipated over the damage-tolerant titanium rotor, assuming the composite blade surface quality is equal to that of a machined blade. This increase is made up of a 2.0-point gain due to shroud removal combined with a 0.4-point loss due to the wider chord. The efficiency gain at SLTO operation would be 1.4 percent over the titanium version.

The lower aspect ratio composite design should also be less sensitive to inlet disturbances and also should provide greater freedom from stall.

The estimated cost differences between the boron/aluminum and titanium damage tolerant configurations are shown in Table 37. A 73-cent per hour reduction is anticipated using the composite blades.

TABLE 37 - COST COMPARISON OF DAMAGE - TOLERANT BLADES , 6800 LBF THRUST CLASS ENGINE

Costs	Costs in Dollars/Hour per Engine	
	Titanium Blades $/hr	Boron/Aluminum Blades $/hr (% Δ)
Amortized Cost (1)		
Engine	13.50	13.33 (-1.24)
Airframe	40.50	40.42 (-0.19)
Sub Total	54.00	53.76 (-0.46)
Fuel Cost @ 46 cents/gal	60.05	59.86 (-0.32)
Direct Maintenance		
Material	9.96	9.96 (0.)
Labor	2.72	2.69 (-1.14)
Sub Total	12.68	12.37 (-0.24)
Total Operating Cost	126.72	125.99 (-0.58)

(1) 10% Residual @ 15 years - - 2000 Hour/Year

Totals may not check due to rounding.

4.0 PROTECTIVE DEVICES - TASK III

GENERAL

An alternate approach to strengthening the engine to withstand bird strikes is to provide a protective device to prevent ingestion of a bird, or at least to prevent an ingested bird from striking a sensitive engine part. The use of such protective devices is more practical in small engine applications where the weight and size penalties of building ingestion damage-tolerance into the engine becomes more costly. No attempt was made to determine the engine size cross-over point at which protective devices would be required. Based on the preceding studies, however, it appears that the 1600 lbf thrust size is still of a sufficient size to warrant strengthening of the engine - for example, by thickened wide chord blades - but engines of smaller size may need some inlet protection to supplement the basic engine's ingestion capability.

Two design techniques promising to safeguard only the most critical regions of the engine were investigated in this task. The first consists of a series of deflector doors arranged circumferentially around the inlet to protect only the tip region of the fan blades - the more sensitive region. The second relocates the core splitter so as to protect the supercharger and core engine from bird debris after its passage through the hub region of the fan.

FAN TIP PROTECTION

The preceding analysis and ingestion test results have shown that the outer region of the fan blade is most sensitive to bird impact, while the inboard region near the hub is quite capable of withstanding bird impact with minimal damage. In particular tip strikes on the unshrouded wide-chord blades proposed for the smaller-size engines should be prevented if possible. This indicates that an optimum fan blade protective device would be one which extends inward from the engine cowl, protecting only the outer portions of the blades and leaving the inner portion unprotected. (See Figure 95). By providing the device with retractability so that it can be deployed only in the critical take-off and initial climb flight regimes (where most strikes occur), performance and cost penalties need not be incurred during the cruise phase of flight. The outer cowl is also provided with doors that act in parallel with the inner doors to provide a continuous airflow to the fan tips during the period when the inner doors are deployed.

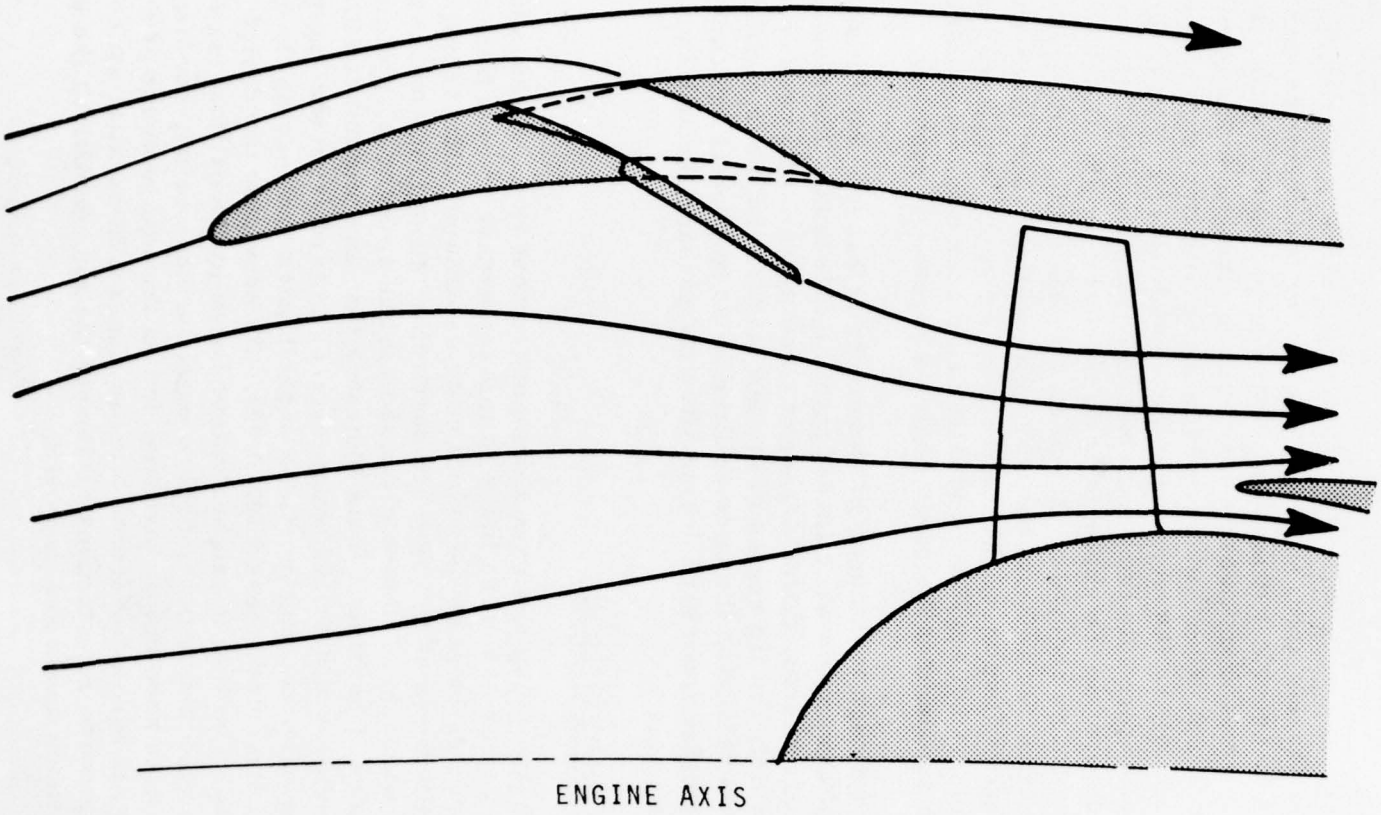

Figure 95. Fan Tip Protection Device Schematic.

The blade-tip protection design that was studied consisted of 12 inner deflector doors, each approximately 9 x 9 inches and hinged at the forward end. (See Figure 96). Each door is controlled by a single fluid actuator to allow some flexibility and to provide a means of absorbing a portion of the normal kinetic energy without detrimental door damage. The deflectors are positioned 9.5 inches in front of the fan, which with the full actuated angle of 18 degrees, shields the blading from tip to mid-span. Although the deflector can be positioned closer to the fan to provide more reliable protection, it increases the risk of aerodynamic disturbances entering the fan and also tends to increase noise. The circumferential gap between doors can be minimized by allowing the doors to overlap the internal I-beam structure that bridges the door flowpath and mechanically connects the forward and aft positions of the cowl assembly.

The outer doors are either mechanically linked to the inner doors or, preferably, actuated automatically by the pressure differential between the inner and outer flows. Similar blow-in doors have been used successfully in airline operations with several types of engines in past years.

This design tends to minimize the icing problems associated with past protective devices, in that conventional means of inner-duct anti-icing are available.

Engine performance penalties are also minimized with this design. At the start of the take-off run and up to approximately 40 knots, the blow-in door feature is expected to provide additonal airflow to the engine, thereby improving the inlet performance, since at these speeds the inlet is still smaller than optimum. The inlet total pressure loss will gradually increase, however, reaching an estimated one-percent at the initial climb speeds of 115 - 120 knots. When the deflectors are retracted for the other flight regimes, their effect on engine performance is negligible, and the only effect on aircraft flight performance would result from the weight of the system.

Impact forces normal to the surface of a fully deployed door, shown in Figure 97, are a function of ingestion velocity and bird size. The forces are moderate and readily controlled using standard material gage thicknesses and design procedures. The resulting design does not impose length or diameter penalties on the engine pod; but the weight of the mechanism is estimated at 70 pounds for the 6800 lbf thrust-class engine. The podded weight for this machine is approximately 1900 pounds, so that the overall aircraft weight penalty amounts to 3.7 - percent per

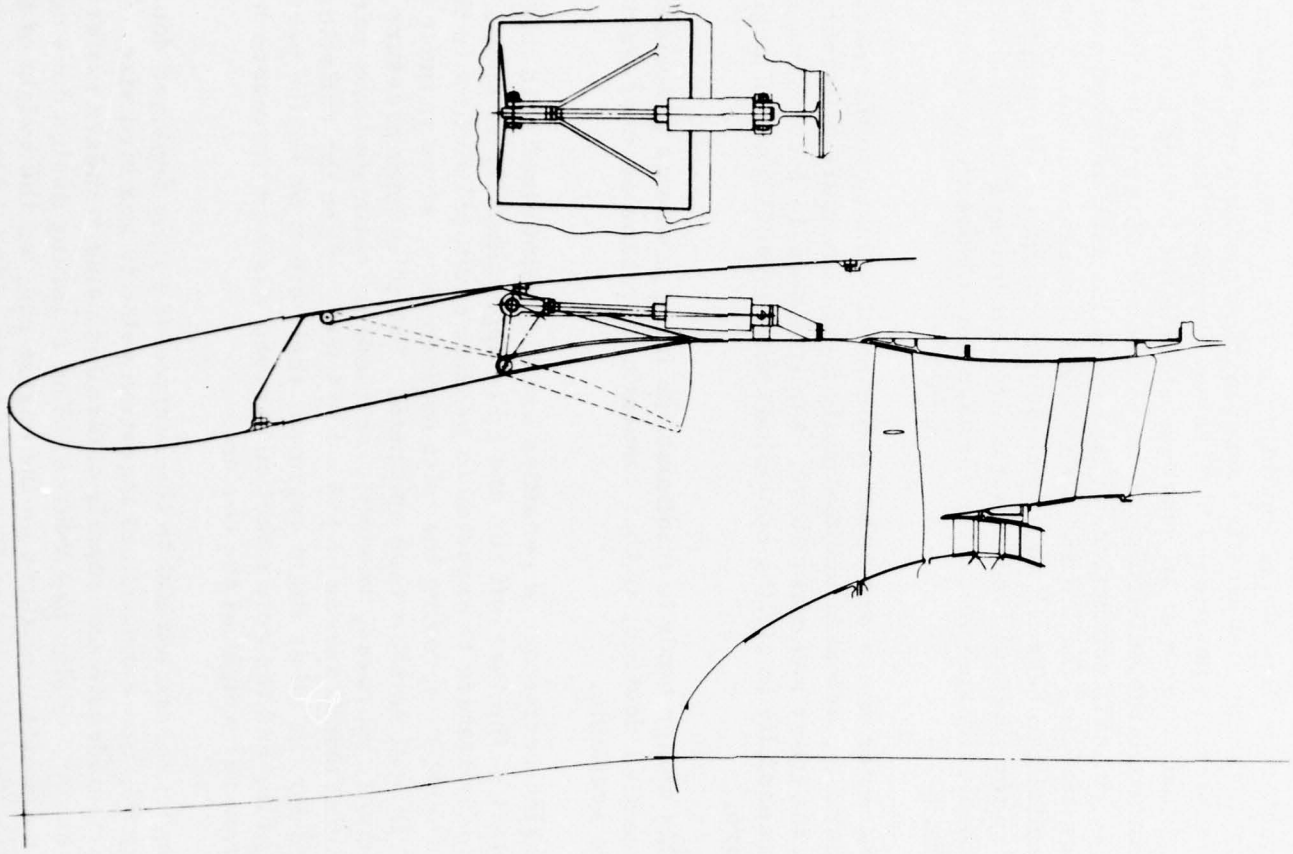

Figure 96. Fan Tip Protection Device Layout.

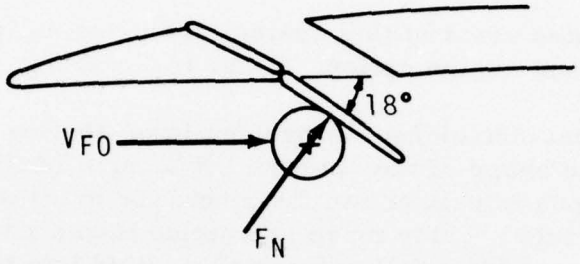

FORCES @ FAR INGESTION CONDITIONS

BIRD SIZE	6800 lbf ENGINE	1600 lbf ENGINE
3 oz	381 lbf @ 100 kts	308 lbf @ 90 kts
1 1/2 lb	2193 lbf @ 120 kts	2014 lbf @ 115 kts
4 lb	7560 lbf @ 160 kts	6645 lbf @ 150 kts

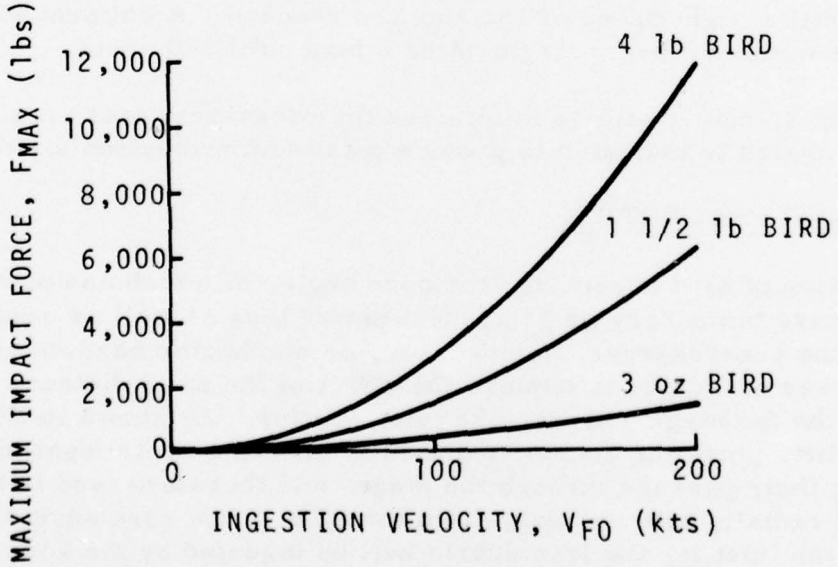

Figure 97. Impact Forces on Deflector Door.

engine. When applied to the smaller thrust machine, the weight penalty will be considerably greater on a percentage basis since the door thickness, actuators, and attachment weights, etc., will not scale directly. In either case, however, aerodynamically optimum engines of reduced weight and increased efficiency could be used to compensate for the added nacelle weight and take-off performance penalty.

The estimated costs of this system are marginally greater than the damage-tolerant engine option. Refer to Table 38.

An additional consideration involved in protecting the blades from bird impact is the shape of the spinner. A blunt spinner designed to breakup a bird upon impact and to distribute the mass over a large annular region would provide more protection than a smoothly blended shape that tends to guide a full unfragmented bird into the stage. The force of such a collision on a blunt spinner is transferred directly to the main bearing mount that typically has more than adequate strength to withstand the impact of a 1.5-pound bird at the FAR ingestion speeds.

As shown in Figure 98, the more blunt the spinner shape, the greater its ability to fragment a bird for subsequent safe passage into the fan. Bird fragmentation is not predicted for the FAR take-off conditions, however, since even for a 90-degree impact, the onset of breakup will not occur until a flight speed of 155 knots is reached. A uniform 45-degree cone would not begin fragmenting a bird until 220 knots.

A blunt spinner that also minimizes the cross-sectional area having small cone angles is indicated to provide maximum protection for the fan.

CORE ENGINE PROTECTION

Ingestion of bird debris into the core engine of a turbofan powerplant can cause temporary or permanent power loss as well as causing damage to the supercharger, compressor, or combustor hardware. This study was conducted to explore the effect of the axial distance separating the fan stage and the core inlet splitter. As shown in Figure 99, bird debris particles become exposed to the fan's centrifugal force field during their passage through the stage and, therefore, tend to be centrifuged radially outward away from the inlet to the core engine. The further aft the inlet is, the less debris will be ingested by the core engine. It would also appear that, on the average, the heavier particles of a fragmented bird - having more resistance to acceleration by the air velocity - would tend to leave the rotor at a lower axial velocity than the lighter particles and so tend to centrifuge more into the bypass stream.

TABLE 38 - COMPARISON OF FAN-TIP PROTECTION SYSTEM COST, BASED ON THE 6800 LBF THRUST CLASS DAMAGE-TOLERANT ENGINE

Cost	Cost Changes Dollar/Hr	(% Δ)
Amortized Cost (1)		
Engine	0.060	(+0.44)
Airframe	0.205	(+0.51)
Sub Total	0.265	(+0.49)
Fuel Cost (2)	0	
Direct Maintenance Cost		
Labor	- - -	- - -
Material	- - -	- - -
Sub Total	0.01	(+0.08)
Total Operating Cost Change	0.275	(+0.23)

(1) 10-percent Residual @ 15 Years - - 2000 Hr/Yr

(2) Mission simulations not performed because of assumed negligible differences

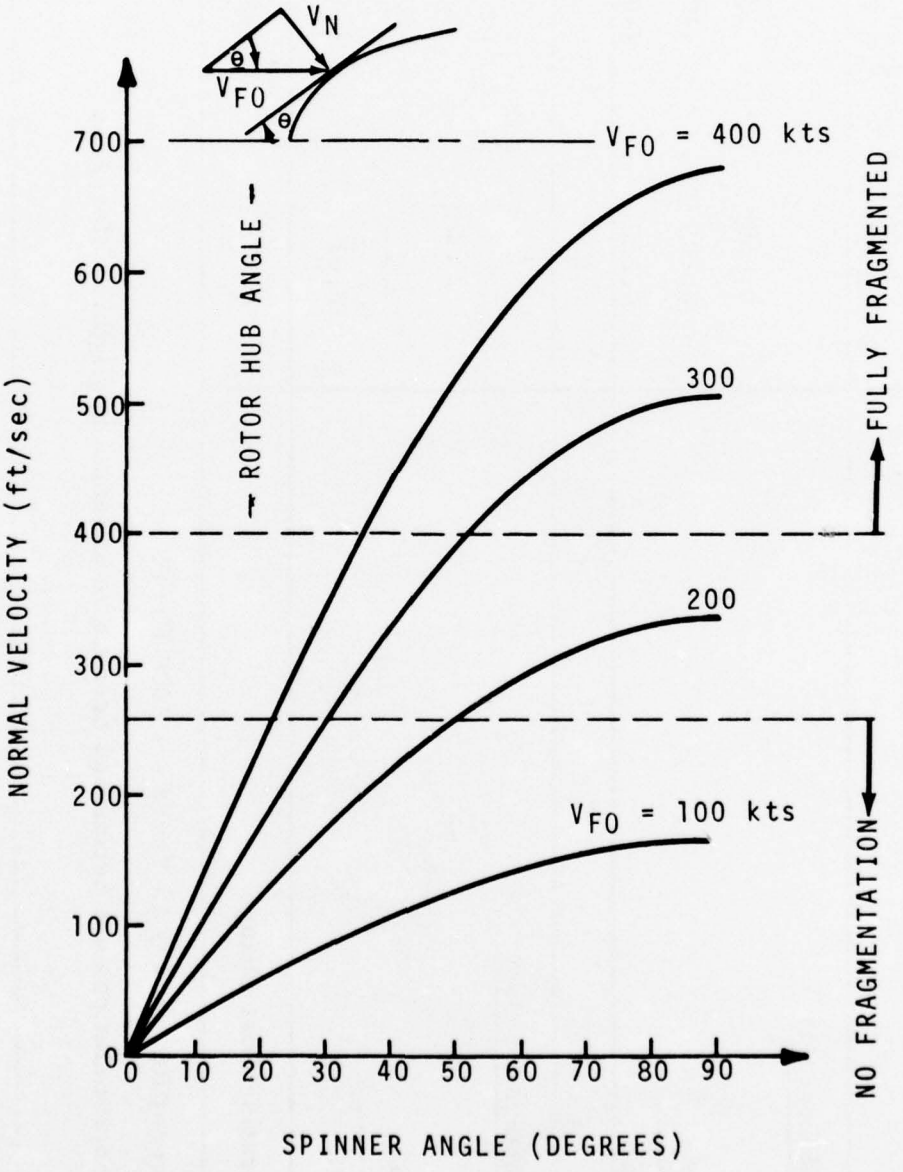

Figure 98. Bird Fragmentation Due to Spinner Impact.

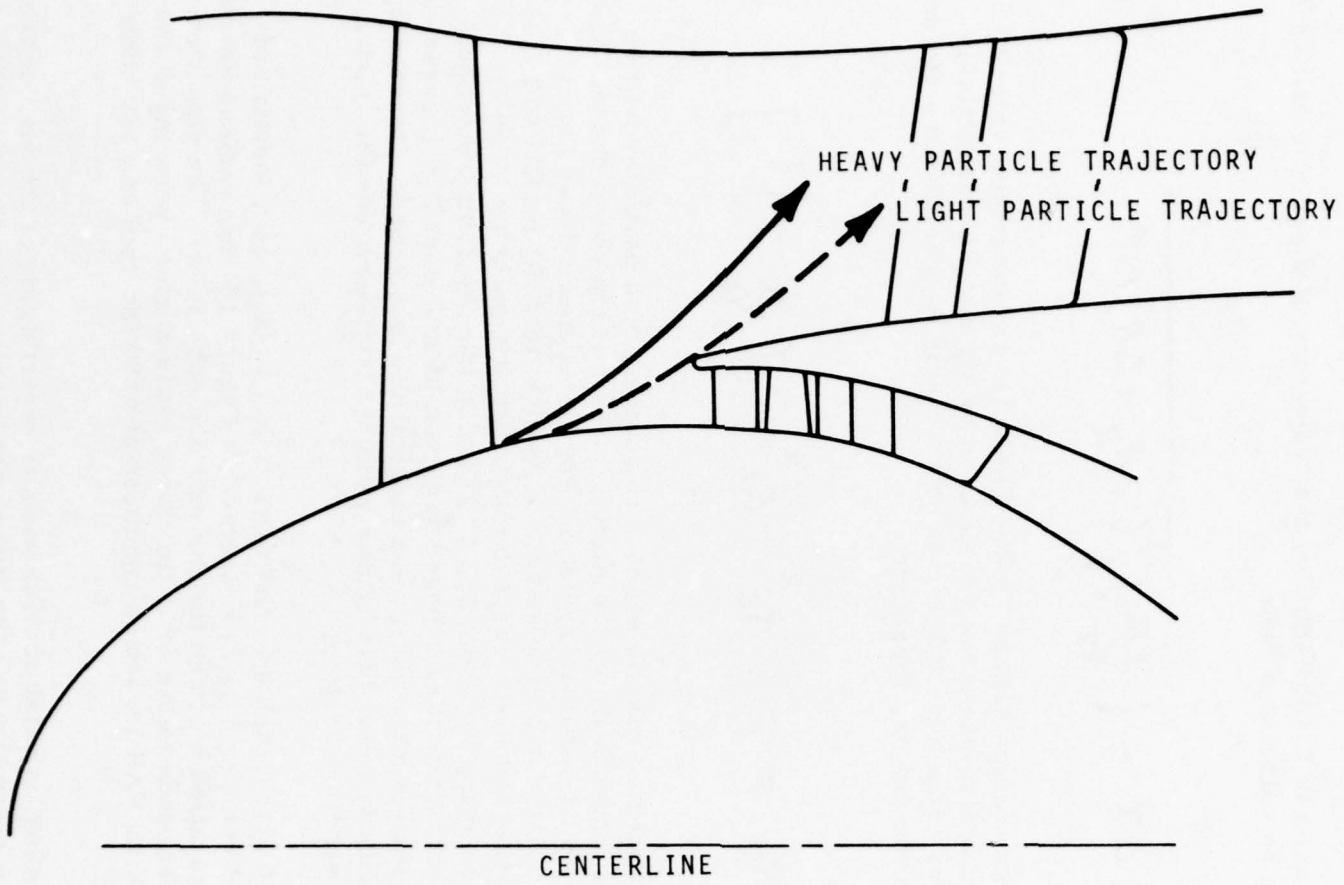

Figure 99. Centrifuging of Bird Particles Leaving Fan Stage.

The debris that does enter the inlet, therefore, would tend to be comprised more of the smaller lighter particles.

It is seen in Figure 100 that the trajectory of a particle exiting from the hub can be calculated from

$$\Delta X = \left(\frac{V_A}{V_T}\right)\sqrt{(2R_H + \Delta R)\Delta R} \qquad (17)$$

for any given radius change, ΔR. The axial and tangential velocity components of the bird particles are denoted by V_A and V_T respectively. The exposed area of an inlet splitter of outer radius R_S positioned a distance X aft of the fan exit is, therefore,

$$A_X = \pi\left[R_S^2 - R_H^2 - \left(\frac{V_T}{V_A}\cdot X\right)^2\right] \qquad (18)$$

It is expected that on average the exiting bird particles will be accelerated tangentially by the airfoil to the full fan wheel speed, V_W. Because the bird particles are some 900 times more dense than air, however, it also seems reasonable to assume that the airfoil will not fully accelerate the bird debris axially from it's entering velocity V_{FO}, to the exiting air velocity, V_e. It can then be seen from Equation 18 that the amount of exposed area can be decreased by increasing the separation distance and/or the tangential wheel speed. Decreasing the axial velocity (or splitter outer radius) also decreases the inlet area exposed to debris ingestion.

A plot of the exposed inlet area ratio (A_X/A_i), as a function of debris axial velocity V_A, is presented in Figure 101 for various amounts of axial separation between the fan exit and core inlet. The condition shown corresponds to the 6800 lbf thrust class engine operating at the 1.5-pound bird FAR ingestion condition of 6880 fan rpm and 120 knots flight speed.

Assuming no axial acceleration or centrifuging of the bird debris during its passage through the rotor, the baseline design has 85 percent of the inlet area exposed to ingested material. Extending the fan

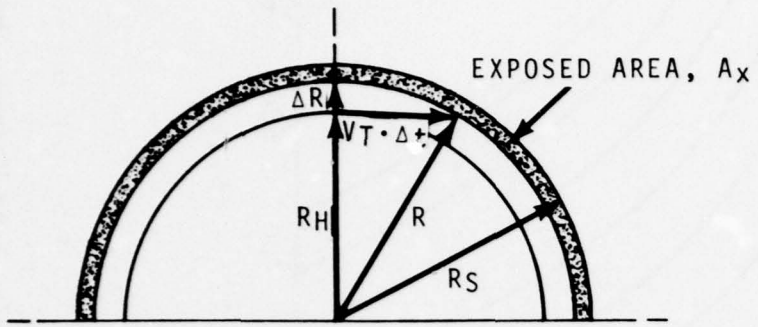

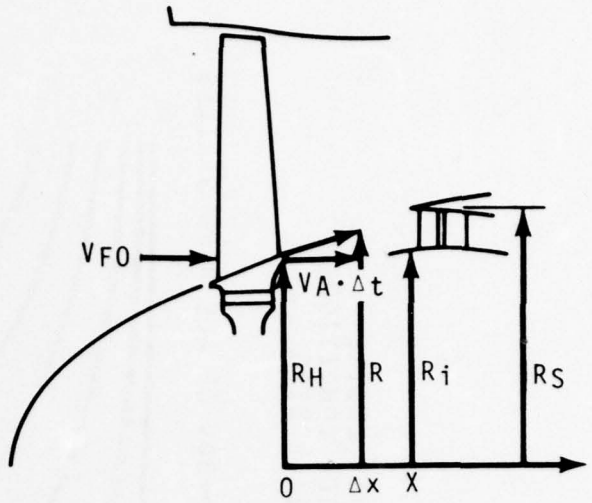

$$R_H^2 + (V_T \cdot \Delta t)^2 = R^2$$

$$\Delta X = V_A \cdot \Delta t$$

$$\Delta X = \frac{V_A}{V_T}\sqrt{R^2 - R_H^2} = \frac{V_A}{V_T}\sqrt{(2R_H + \Delta R)\ \Delta R}$$

$$A_X = \pi\left[R_S^2 - R_H^2 - \left(\frac{V_T}{V_A} \cdot X\right)^2\right]$$

$$A_i = \pi[R_S^2 - R_i^2]$$

Figure 100. Particle Trajectory Parameters.

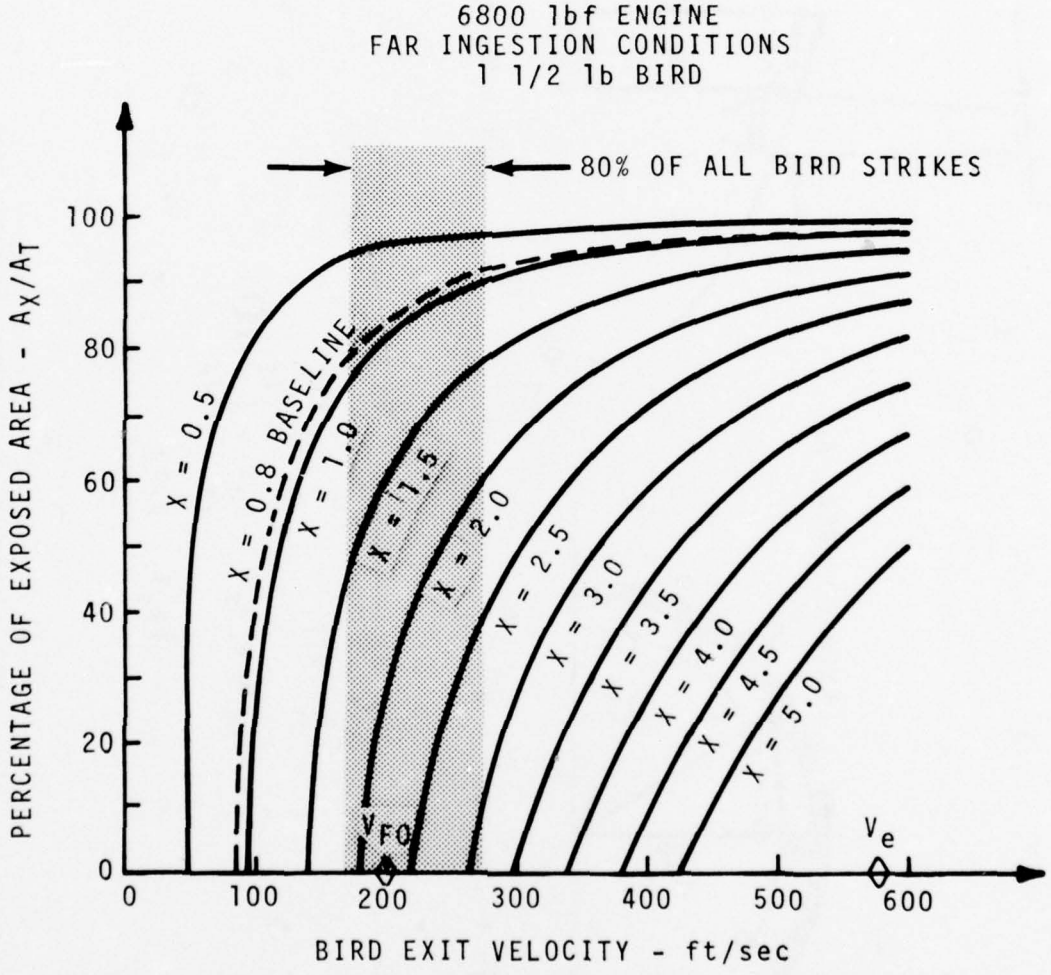

Figure 101. Exposed Core Inlet Area Versus Bird Exit Velocity 6800 lbf Engine.

an additional 1.5 inches would provide complete protection for the core engine. A more reasonable, but still conservative assumption would be that 25-percent acceleration is obtained with effective centrifuging starting near the rotor 3/4 chord (approximately 0.8-inch forward of the exit). For these conditions, the calculated exposed area is 80 percent; an additional 1.9 inches would be required for complete protection of the core engine. Figure 102.

A similar plot for the low aspect ratio 1600 lbf thrust class turbofan is presented in Figure 103 for the 1.5-pound bird FAR ingestion condition. Assuming again that 25-percent acceleration is obtained (from 194 to 257 ft/sec), with effective centrifuging also starting at the rotor 3/4 chord, then the analysis predicts that all of the bird debris would just centrifuge out over the splitter so that complete protection of the inlet would be obtained with the baseline design.

The weight penalties for these two engines are shown in Figure 104 as a function of added axial spacing. The weight penalty per inch is seen to be modest with respect to engine weight.

These results indicated that quite small length and weight increases can yield considerable benefits to core engine inlet exposure. Increased fan-to-supercharger cascade distance can also provide additional noise benefits.

It should also be noted from Equation 18 that the amount of debris entering the core engine may also be reduced by minimizing the splitter outer radius, R_S Figure 105. This option would be specially beneficial if no supercharging stages were present as in the 1600 lbf thrust baseline turbofan so that supercharger penalties resulting from reduced wheel speed would not be incurred.

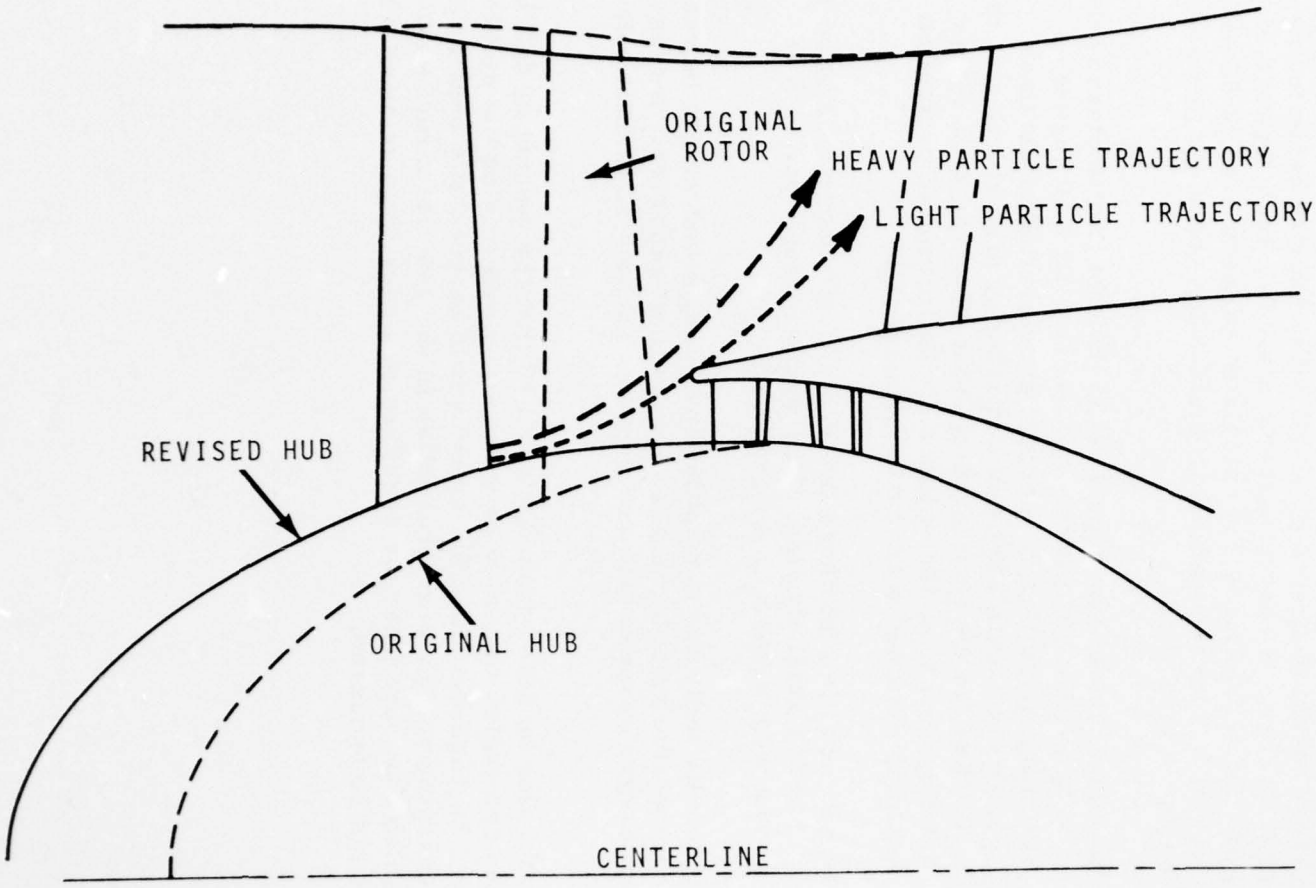

Figure 102. Extended Fan Stage Configuration - 6800 lbf Engine.

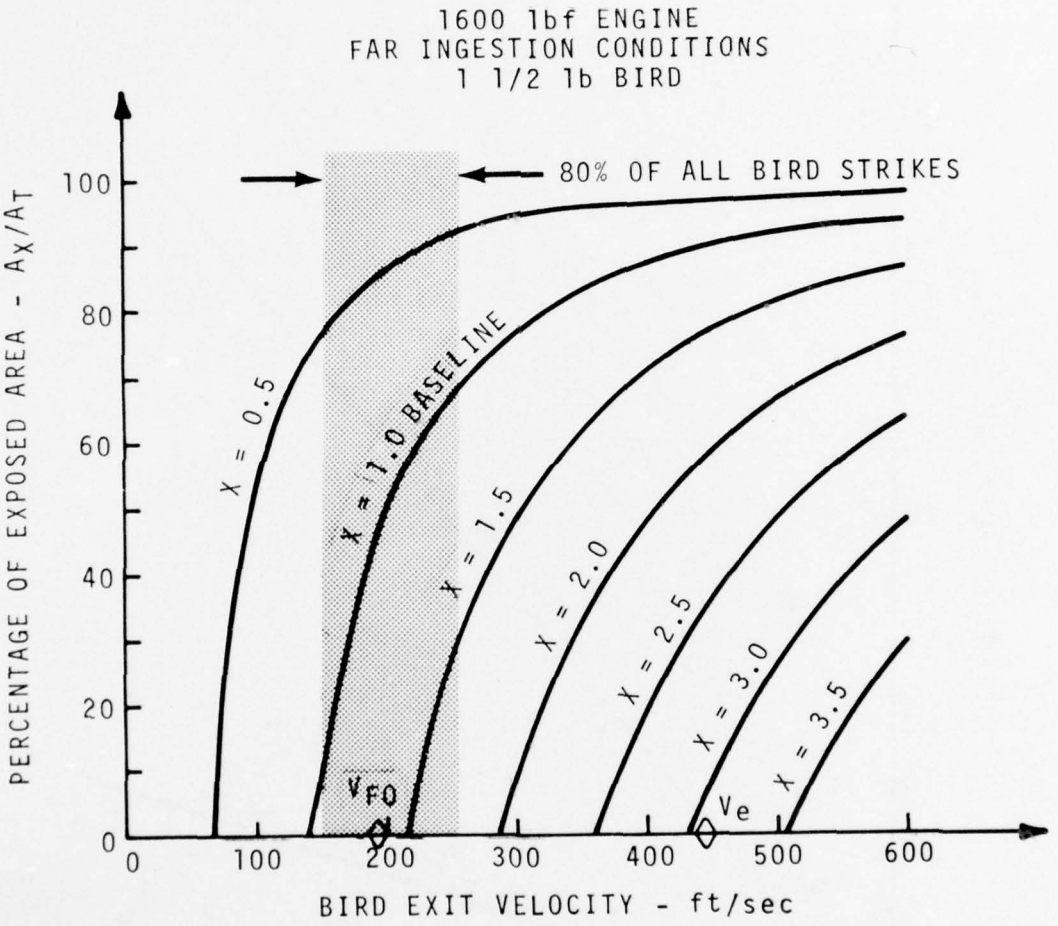

Figure 103. Exposed Core Inlet Area Versus Bird Exit Velocity - 1600 lbf Engine

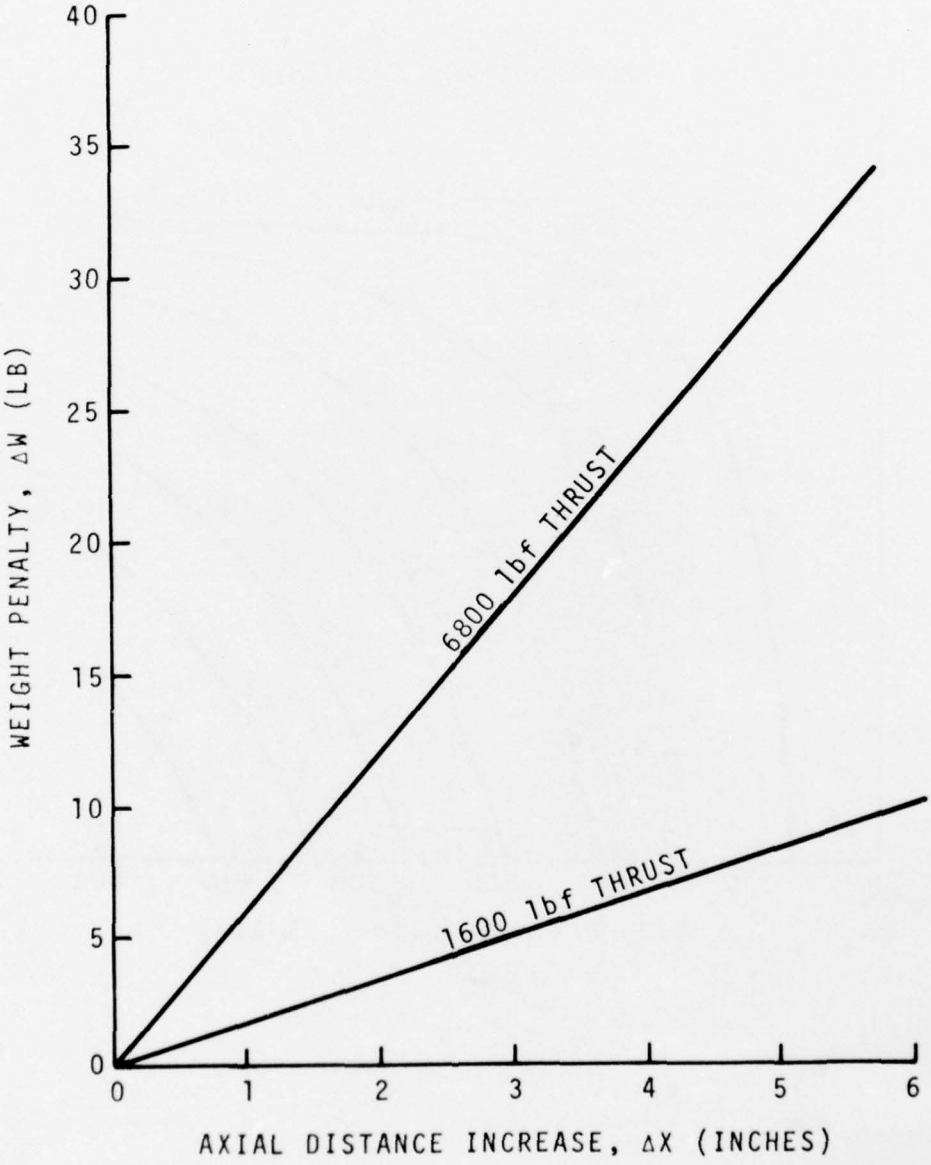

Figure 104. Weight Penalty Versus Axial Distance Increase.

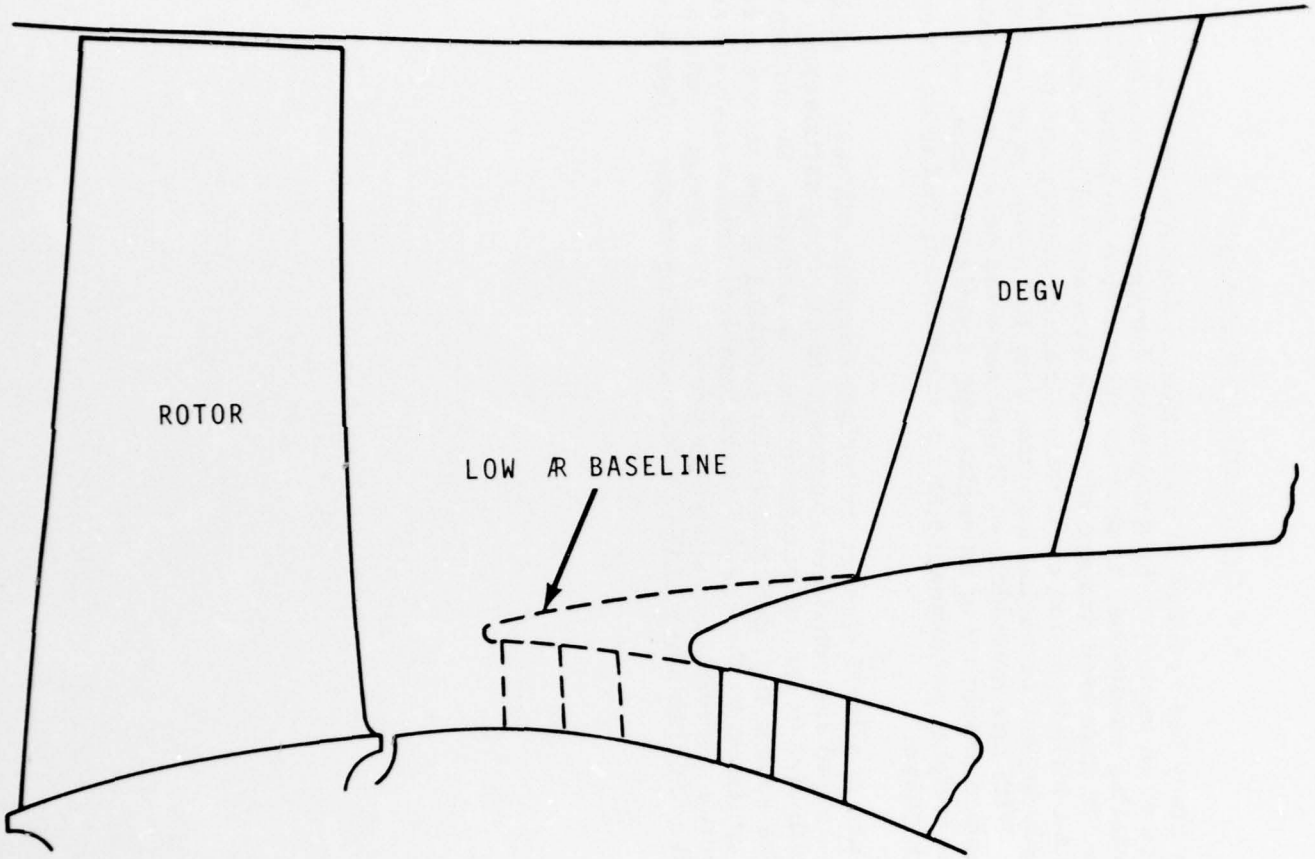

Figure 105. Reduced Inlet Radius Configuration - 6800 lbf Engine Reduced Inlet.

5.0 CONCLUDING REMARKS

This study has resulted in a practicable design method to assess the resistance of an engine-to-bird ingestion damage at various engine/aircraft operating conditions, to provide quantitative guidelines for modifying an engine for improved damage tolerance with special reference to meeting the FAA bird-ingestion certification requirements, and to extend existing blade impact or engine ingestion data to the design of new untested designs. With this methodology, it now becomes possible to maximize the bird ingestion capability of an engine with some confidence, while minimizing its weight, performance,and cost penalties, and to do so early in the design phase.

The use of a local damage criterion, coupled with test correlations, provides a rapid and consistent approach to ensuring satisfactory compliance with bird-ingestion requirements. In addition, the influence of the various engine and flight parameters making up the criterion relation, augmented by the results of the transient impact analysis and the post-ingestion performance analysis, provides the designer with a quantitative understanding of the factors affecting engine safety and reliability.

APPENDIX A. BIRD INGESTION REQUIREMENTS

A 1. FAR. PART 33-6, FEDERAL AVIATION REGULATION 31 OCTOBER 1974

FAR 33.77 FOREIGN OBJECT INGESTION

(a) Ingestion of a 4-pound bird, a piece of tire tread, or a broken rotor blade, under the conditions set forth in paragraph (f) of this section, may not cause the engine to

(1) Catch fire

(2) Burst (penetrate its case)

(3) Generate loads greater than those specificed in 33.23, or

(4) Lose the capability of being shutdown.

(b) Ingestion of 3-ounce birds, 1-1/2 pound birds, or mixed gravel and sand, under the conditions set forth in paragraph (f) of this section, may not cause more than a sustained 25 percent power or thrust loss or require the engine to be shut down.

(c) Ingestion of water, ice, or hail, under the conditions set forth in paragraph (f) of this section may not cause a sustained power or thrust loss or require the engine to be shut down.

(d) For an engine that incorporates a protective device, compliance with this section need not be demonstrated with respect to foreign objects sought to be ingested under the conditions set forth in paragraph (f) of this section, if it is shown that -

(1) Such foreign objects are of a size that will not pass through the protective device.

(2) The protective device will withstand the impact of the foreign objects; and

(3) The foreign object or objects stopped by the protective device will not obstruct the flow of induction air into the engine.

(e) In showing compliance with paragraphs (a) and (b) of this section, the engine need be tested by ingesting only that foreign object specified in paragraph (a) of this section which the applicant shows has the most severe effect on the engine and by ingesting the mixed gravel and sand specified in paragraph (b) of this section and either the 3-ounce birds or the 1-1/2-pound birds, as specified in paragraph (f) of this section.

(f) The prescribed foreign object ingestion conditions are provided in Table A-1.

TABLE A - 1. FOREIGN OBJECT DAMAGE INGESTION CONDITIONS

Foreign Object	Test Quantity	Speed of Foreign Object	Operation	Ingestion
Birds				
3-oz size	One for each 50 $in.^2$ of inlet area or fraction thereof up to a maximum of 16 birds. 3-oz bird ingestion not re-required if a 1-1/2-lb bird will pass the inlet guide vanes into the rotor blades.	Liftoff speed of typical aircraft	Takeoff	In rapid sequence to simulate a flock encounter
1-1/2-lb size	One for the first 300 $in.^2$ of inlet area, if it can enter the inlet, plus one for each additional 600 $in.^2$ of inlet area or fraction thereof up to maximum of 8 birds.	Initial climb speed of typical aircraft	do.	do.
4-lb size	One if it can enter the inlet	Maximum Climb Speed	Maximum Cruise	Aimed at critical area

NOTE: Ice, hail, water, gravel/sand, tire tread requirements not shown

A 2. U. S. ARMY REQUIREMENTS, AV-E-8593B

4.5.20 Bird Ingestion Test. An engine substantially identical (as approved by the Government) to the endurance test engine shall be subjected to a bird ingestion test. One bird shall be ingested for each 50 square inches of inlet area (and fraction thereof). The birds shall weigh 2.0 ounces to 2.4 ounces and shall be ingested while the engine is operating at intermediate power at conditions simulating a flight speed of 100 knots true airspeed.

A 3. U.S. NAVY REQUIREMENTS, MIL-E-8593A

4.6.4.4 Bird Ingestion Test. The test engine shall be subjected to a bird ingestion test conducted in such a manner as to verify the requirements of 3.2.5.6.1. The birds shall be ingested in a random sequence, dispersed over the inlet area, to simulate an encounter with a flock. If approved by the Using Service, synthetic "birds" may be used for testing. The contractor shall specify in the pretest data the critical target areas for each bird size and the procedure to be used for bird ingestion. High speed photographic coverage of the inlet is required during the ingestion test. The test will be considered to be satisfactorily completed when , in the judgement of the Using Service, the performance criteria of 3.2.5.6.1 have been met and there is no evidence of major structural damage which could cause the engine to fail.

A 4. U. S. AIR FORCE REQUIREMENTS, MIL-E-5007D

3.2.5.6 Environmental Ingestion Capability

3.2.5.6.1 Bird Ingestion. When required by the Using Service the engine shall be capable of ingesting the number and different sizes of birds at the bird velocity and engine speed as described below. Under the conditions of a, b, and c, no failures shall result which will cause shutdown of the engine although some damage to the engine parts may occur. No engine flameout will occur and the engine shall recover to the operating condition that existed prior to bird ingestion within the time specified in the engine specification for items a, b, and c. For item d no engine failure shall occur which would result in damage to the aircraft.

a. Birds weighing 2 to 4 ounces (a maximum of sixteen at a time) and birds weighing 2 pounds (one at a time) ingested at a bird velocity equal to the take-off flight speed, with the engine at maximum rated speed.

b. Birds weighing 2 to 4 ounces (a maximum of sixteen at a time) and birds weighing 2 pounds (one at a time) ingested at a bird velocity equal to the cruise flight speed with the engine at maximum continuous speed.

c. Birds weighing 2 to 4 ounces (a maximum of sixteen at a time) and birds weighing 2 pounds (one at a time) ingested at a bird velocity equal to the descent flight speed with the engine at an associated engine speed.

d. Birds weighing 4 pounds ingested at a bird velocity based on the most critical flight speed with the engine at maximum rated speed.

e. The number of birds to be ingested shall be based on the area at the fan/compressor face. The number of birds to be ingested shall be one 2 or 4 ounce bird for each 50 square inches, or for each fraction larger than 50 percent thereof, one 2 pound bird for each 225 square inches, or for each fraction larger than 50 percent thereof, and one 4 pound bird for each 400 square inches, or for each fraction larger than 50 percent thereof. The birds shall be ingested in random intervals, and randomly dispersed over the engine inlet area. If any of the above sizes of birds cannot pass through the inlet, that portion of the requirement shall not be applicable.

A 5. BRITISH CIVIL AIRWORTHINESS REQUIREMENTS, BCAR SECTION 3

Chapter C3-4 - Type Tests for Turbine Engines for Aeroplanes

20 BIRD STRIKES (see C3-4 App., 4) The Board shall be satisfied that no hazardous condition can arise to the aeroplane as a result of the engine struck by a bird or birds except where the Board agrees that the engine installation in a particular aeroplane is such that the engine cannot be struck by birds. Compliance with this requirement shall be shown in accordance with 20.2 and 20.3.

NOTE: Where the Board is satisfied that the engine cannot be struck by birds and compliance with this requirement is not established, the engine approval will be endorsed accordingly.

20.1 General

20.1.1 Where a retractable guard is fitted, compliance with the requirements shall be established with the guard in position. Unless it is also established that the requirements are met with the guard retracted, the engine approval will be endorsed to the effect that compliance with the requirements has only been established with the guard in position.

20.1.2 Where a fixed guard is fitted, compliance with the requirements shall be established with the guard in position.

20.2 Strikes by Large Birds (see C3-4 App., 4.1). It shall be established that when the front of the engine is struck by a large bird in the conditions of 20.2.1, no hazardous condition can arise to the rest of the aeroplane as a result of the damage that may

be caused.

NOTE: For the purpose of this requirement complete loss of power is not considered to be a hazard.

20.2.1 Conditions

Weight of Bird. (a) Impact against front of engine: at least 4 lb.

(b) Ingestion into engine: at least 4 lb unless a lesser weight provides a more critical case for the engine, bearing in mind its characteristics such as intake size.

Number. One.

Speed. The maximum true air speed which a representative type of aeroplane in which the engine is likely to be installed, is expected to achieve in normal operational service up to an altitude of 8,000 feet.

20.3 Strikes by Medium Sized and Small Birds (see C3-4 App., 4.2). It shall be established that when the front of the engine is struck by a number of medium sized birds in the conditions of paragraph 20.3.1, or small birds in the conditions of 20.3.2 there is no unacceptable immediate or ultimate loss of engine performance, no serious increase of engine operating temperatures or deterioration of engine handling characteristics, over the full range of engine operating conditions, and no dangerous physical damage.

NOTE: If the loss of engine performance is found to exceed 25% the engine may not be suitable for installation in some types of aeroplane.

20.3.1 Conditions (Medium Sized Birds)

Weight of Bird. Approximately 1.5 lb. (e. g. seagull).

Number. One for the first 300 sq. in. of a representative intake area, plus one for each additional 1,000 sq. in. with a maximum of ten.

Speed. The maximum true air speed which a representative type of aeroplane, in which the engine is likely to be installed, is expected to achieve during the climb immediately after take-off.

Duration of Ingestion. Not greater than one second.

20.3.2 Conditions (Small Birds)

Weight of Bird. 2 to 4 oz. (e.g. starlings).

Number. One for the first 50 sq. in. of a representative intake area plus one for each additional 50 sq. in. with a maximum of 16.

Speed. The maximum true air speed which a representative type of aeroplane, in which the engine is likely to be installed, is expected to achieve during the climb immediately after take-off.

Duration of Ingestion Not greater than one second.

20.3.3 If birds lodge in the engine intake and adequate indication of this condition is provided to the flight crew by the instrumentation listed as necessary by the engine constructor (in accordance with C3-2, 3.4.2) then either:-

(a) it shall be established by direct measurement that the blade stresses are not so high as to cause blade failure before a landing can be made, or

(b) a test in accordance with C3-4, App., 4.2.2 (a) will be required.

20.3.4 If the birds lodge in the engine intake and no adequate indication of this condition will be available to the flight crew, then it shall either:-

(a) be established by direct measurement that the blade stresses are not so high as to prevent safe operation of the aeroplane until the next visual inspection of the engine intake, or

(b) a test in accordance with C3-4, App., 4.2.2 (b) will be required.

CHAPTER C3-4
APPENDIX

4 BIRD STRIKES (see C3-4, 20).

4.1 Strikes by Large Birds (see C3-4, 20.2). Acceptable methods of meeting the requirements of C3-4, 20.2 are detailed in the paragraph 4.1.

4.1.1 In the condtions of C3-4, 20.2.1 either (a) or (b) of this paragraph 4.1.1,

(a) (i) Tests in the conditions of C3-4, 20.2.1 (a) during which the engine need not be running and the test may be completed on a static rig.

(ii) Tests in the conditions of C3-4, 20.2.1 (b) during which the engine should be running at Maximum Take-off Power conditions.

(b) Adequate evidence from experience of bird strikes on engines agreed by the Board to be of comparable size, design, construction and performance, obtained during development or during operation.

4.1.2 The methods employed in accordance with 4.1.1 should be supplemented, where necessary, by specific evidence on-

(a) the effect of the bird strike on appropriate engine components, e. g., entry guide vanes, front bearing housing,

(b) the compressor casing strength relative to multiple blade failures and the possiblity of blades compacting, and

(c) the strength of the engine structure and main shafts relative to the unbalance and excess torque likely to occur.

NOTE: Should evidence reveal the possibility of consequential damage, e.g., shaft fracture or engine fire, the Board may require additional tests.

4.2 Strikes by Medium Sized and Small Birds (see C3-4, 20.3). Acceptable methods of meeting the requirements of C3-4, 20.3 are detailed in this paragraph 4.2

4.2.1 Either:-

(a) Tests in the conditions of C3-4, 20.3.1 (for medium sized birds) and C3-4, 20.3.2 (for small birds) on an engine running at Maximum Take-off Power conditions.

NOTES: (1) For engines in which the airflow is divided so that not all the flow passes through the central or "core" engine, and where it is accepted that the effect of bird strikes occurring on the blading outside the "core" engine flow cannot affect the functioning of the "core" engine (e.g. by debris entry, surge, flame-out etc.) the test may be divided into two parts.

(i) The "core" engine should be treated as in (a), the number of birds being calulated from the ratio of "core" flow area to main intake area. A deliberate effort should be made to cause the birds to enter the "core" engine by representative firings, although it is accepted that some "core" engines may be self-protecting.

(ii) The fan or bypass stages may then be tested separately, if desired on a suitable rig. If it can be demonstrated from a limited number of separate shots that no significant damage or performance loss is occurring (and taking into account possible bearing and shaft loads arising from a full ingestion) results from such a reduced number of ingestions, without restriction as to timing, would be acceptable.

(2) If, in any of the medium sized bird tests, the birds have passed into the areas of the engine under test without lodging, the prescribed small bird tests may be waived. In cases where engines have been shown to be self-protecting against medium birds (e.g. by momentum separation) such results cannot necessarily be considered as applicable to small birds.

(3) If after any of the tests it is found that significant damage has occurred, further evidence or other running may be required to show that C3-4, 20.3 is complied with,

or (b) Adequate evidence from experience of bird strikes of appropriate weight on engines agreed by the Board to be of comparable size, design, construction, performance and surge margin, obtained during development or during operation.

4.2.2

(a) Should it be elected to show compliance with C3-4, 20.3.3 (b) the appropriate test of 4.2.1 (a) should be continued with the engine running at Maximum Continuous Power conditions for a period of one hour.

(b) Should it be elected to show compliance with C3-4, 20.3.4 (b) the appropriate test of 4.2.1 (a) should be continued with the engine running at Maximum Continuous Power conditions for a period of 5 hours.

NOTE: It is acceptable for the periods of running prescribed in 4.2.2 (a) and (b) to be preceded by a stop for an inspection, if desired.

REFERENCES

1. Crop, H. and Kerstens, G. A., BIRD HAZARDS TO AIRCRAFT, A Literature Survey, TDCK 56961, The Netherlands 1971, (N71-30128).

2. Neal, C. L., FOREIGN OBJECT INGESTION, NASA File, North Carolina Science and Technology Research Center, Bibliography No. 3026, December 1972.

3. Scott, C. L. and Wooten, R. C., Jr., A REVIEW OF PUBLICATIONS ON THE BIRD-AIRCRAFT STRIKE HAZARD, AFWL-TR-74-11, March 1974, (AD 775731).

4. Blokpoel, H., BIRD HAZARDS TO AIRCRAFT, Clark, Irwin and Co. Ltd, Canada, 1976.

5. Horeff, T., DEVELOPMENT OF A PROTOTYPE TURBINE ENGINE INLET DEVICE FOR PROTECTION AGAINST BIRD INGESTION, Proc. World Conf. Bird Hazards to Aircraft, Kingston, Ontario, September 1969.

6. Metcalf, J. M., DEVELOPMENT OF A TURBINE ENGINE INLET DEVICE FOR PROTECTION AGAINST BIRD INGESTION, Vought Aeronautics Division, LTV Aerospace Corp., 1969.

7. Dickey, T. A. and Dobak, E. R., THE EVOLUTION AND DEVELOPMENT STATUS OF THE ALF502 TURBOFAN ENGINE, SAE Paper No. 720840, 1972.

8. Myers, A. and Pease, E., LYCOMING LTS101 - LOW COST TURBINE POWER IN THE 600 HORSEPOWER CLASS, SAE Paper 730911, 1975.

9. Jensen, J. E., THE BALLISTIC DAMAGE CHARACTERISTICS AND DAMAGE TOLERANCE OF WING STRUCTURAL ELEMENTS, ASTM STP 486, 1971.

10. Goldsmith, W. and Lyman, P. T., THE PENETRATION OF HARD STEEL SPHERES INTO PLANE METAL SURFACES, Journal of Applied Mechanics, ASME, December 1960.

11. Levin, E., INDENTATION PRESSURE OF A SMOOTH CIRCULAR PUNCH, Quarterly Applied Math, Vol. 13 No. 2, 1955.

12. Shield, R. T. and Drucker, D. C., THE APPLICATION OF LIMIT ANALYSIS TO PUNCH-INDENTATION PROBLEMS, Journal of Applied Mechanics, December 1953.

13. McNaughton, I. I. and Perfect, D. A., BIRD IMPACT ON OFFSET ENGINE INTAKES, Royal Aircraft Establishment Technical Report 72048, March 1972.

14. Burch, G. T. and Avery, J. G., AN AIRCRAFT STRUCTURAL COMBAT MODEL, Technical Report AFF D1-TR-70-116 Air Force Systems Command, Wright-Patterson Air Force Base, Ohio, November 1971.

15. Allcock, A. W. R. and Collin, D. M., THE DEVELOPMENT OF A DUMMY BIRD FOR USE IN BIRD STRIKE RESEARCH, NGTE Aeronautical Research Council, CP No. 1071, London, 1969.

16. Mitchell, J., SOME THOUGHTS ON FORCES ASSOCIATED WITH A BIRD STRIKE, NRC Field Note No. 24, January 1965.

17. Mitchell, J., MORE THOUGHTS ASSOCIATED WITH A BIRD STRIKE, NRC Field Note No. 37, March 1966.

18. THE NASTRAN THEORETICAL MANUAL, NASA SP-221, September 1970.

19. Salus, W. L., Ip, C. and Van Derlinden, J. W., DESIGN CONSIDERATIONS OF ELASTIC-PLASTIC STRUCTURES SUBJECTED TO DYNAMIC LOADS, Astronautics and Aeronautics, July 1971.

20. Manningham, D., ATM: A TECHNIQUE FOR EXTENDING TURBINE ENGINE LIFE, Business and Commercial Aviation, June 1976.

21. Brennan, T. S., Taylor, R. N., and Steinart, A. G., COST ESTIMATING TECHNIQUES FOR ADVANCED TECHNOLOGY ENGINES, SAE Paper 700271, 1970.

22. Sallee, G. P., ECONOMIC EFFECTS OF PROPULSION SYSTEM TECHNOLOGY ON EXISTING AND FUTURE AIRCRAFT, NASA Report CR-134645.

23. ADVANCED COMPOSITES DESIGN GUIDE, AFML. WPAFB, 1973 (AD 916679).

24. COMPOSITE MATERIALS: TESTING AND DESIGN, ASTM STP 546, 1973.

25. FOREIGN OBJECT IMPACT DAMAGE TO COMPOSITES, ASTM STP 568, 1975.

26. FATIGUE OF COMPOSITE MATERIALS, ASTM STP 569, 1975.

27. COMPOSITE RELIABILITY, ASTM STP 580, 1975.

28. Weil, J. D. D., APPLICATIONS OF ADVANCED MATERIALS, *Aircraft Engineering*, July 1968.

29. Goatham, J. I., DESIGN CONSIDERATIONS FOR LARGE FAN BLADES, SAE Paper 690387, 1969.

30. Premant, E. J. and Stubenrauch, K. R., IMPACT RESISTANCE OF COMPOSITE FAN BLADES, NASA CR-134515, 1973.

31. Steinhagen, C. A. and Salemme, C. T., IMPACT RESISTANCE OF CURRENT DESIGN COMPOSITE FAN BLADES TESTED UNDER SHORT-HAUL OPERATING CONDITIONS, NASA CR-134533, 1973.

32. Ciepluch, C. C. and Hanson, M., QUIET, CLEAN SHORT-HAUL EXPERIMENTAL UTW COMPOSITE FAN BLADE PRELIMINARY DESIGN TEST REPORT, NASA CR-134846, 1975.

33. Goodwin, V. L. and Herman, M., BERYLLIUM WIRE-METAL MATRIX COMPOSITE PROGRAM, AD 853869, 1969.

34. Moore, J. J. et al, TITANIUM-STEEL COMPOSITE MATERIALS, 2nd International Conference on the Strength of Metals and Alloys, Pacific Grove, Calif., September 1970.

35. Weeton, J. W., DESIGN CONCEPTS FOR FIBER-METAL MATRIX COMPOSITES FOR ADVANCED GAS TURBINE ENGINES, ASME Paper 70-GT-133, 1970.

36. Sattar, S. A., Stargardter, H., and Randall, D. G., DEVELOPMENT OF JT8D TURBOFAN ENGINE COMPOSITE FAN BLADES, J. Aircraft, August 1971.

37. Schulz, W. J., Mangiapane, J. A. and Stargardter, H., DEVELOPMENT OF BONIC-ALUMINUM COMPOSITE FAN BLADES FOR SUPERSONIC TURBOFAN ENGINES, ASME Paper 71-GT-96, 1971.

38. Carlson, R. G., FAILURE PROCESSES IN METAL MATRIX COMPOSITES, AFML-TR-74-15, 1973.

39. Troha, W. and Swain, J., COMPOSITE INLAYS INCREASE FLUTTER RESISTANCE OF TURBINE ENGINE FAN BLADES, ASME Paper 76-GT-29, 1976.